# COATED MICRONEEDLES AND MICRODERMABRASION FOR TRANSDERMAL DELIVERY

A Dissertation
Presented to
The Academic Faculty

By

Harvinder Singh Gill

In Partial Fulfillment
Of the Requirements for the Degree
Doctor of Philosophy in Bioengineering

Georgia Institute of Technology

August, 2007

Coated Microneedles and Microdermabrasion for Transdermal Delivery

Dr. Mark R. Prausnitz, Advisor
School of Chemical and Biomolecular Engineering
*Georgia Institute of Technology*

Dr. Mark Feinberg, Co-advisor
School of Medicine and Department of Microbiology and Immunology
*Emory University*

Dr. Mark Allen
School of Electrical and Computer Engineering
*Georgia Institute of Technology*

Dr. Niren Murthy
Department of Biomedical Engineering
*Georgia Institute of Technology*

Dr. Peter Hesketh
School of Mechanical Engineering
*Georgia Institute of Technology*

Dr. Robert Swerlick
Department of Dermatology
*Emory University*

Date Approved: July 5, 2007

An important part of invention today is being able to discover the problem.

**Jerome Lamelson**
*Inventors at work*, Kenneth A. Brown (1988),
Redmond, Washington, Tempus Books of Microsoft
Press, p. 126.

Dedicated to my mother Amarjit Kaur and my father Bahal Singh Gill, who have always valued education, integrity and perseverance.

## ACKNOWLEDGEMENTS

This research has been inspired and supported by numerous people. I would like to take this opportunity to thank all of them.

My doctoral advisor, Dr. Mark Prausnitz has been a great influence on my research as well as my outlook towards a career in academia. His positive thinking, excitement about research, ability to find collaborative opportunities, and passion for excellence has been a great source of motivation. I am thankful to him for his guidance, easy accessibility, for providing growth opportunities and his willingness to work with me on last minute items and technical submissions. If given the opportunity to choose anew, I will again select him as my advisor.

My co-advisor Dr. Mark Feinberg has helped my foray into the exciting world of immunology. I am extremely thankful to him for his guidance and support during my research. I am also thankful to him for encouraging me to participate in his lab's group meetings to help me to learn about the field along the way. Even after he left academia, he continued to advise me and took time out of his busy schedule to accommodate my questions and requirements. His guidance and support during my research have been immensely helpful.

I would like to thank Dr. Mark Allen for his guidance on microfabrication and granting access to his lab for the use of lasers.

I would like to give special thanks to other members of my thesis committee (Dr. Peter Hesketh, Dr. Niren Murthy and Dr. Robert Swerlick) for their intellectual support, encouragement and guidance.

I would like to acknowledge and thank Dr. Donald Denson for his contribution and support during the pain study research. He provided valuable input on the design and analysis of the pain study experiments.

I would like to thank Dr. Silvija Staprans for her guidance, support and encouragement on the microdermabrasion project. Without her support the research on microdermabrasion would have been difficult. I would also like to thank Dr. David Garber for his guidance and help. He has always found time to discuss my immunology-related questions. I am thankful to Samantha Andrews for her help with histology in cutting the hundreds of sections related to the microdermabrasion project. I also acknowledge and thank colleagues in the microdermabrasion project team: Dr. Ifor Williams, Dr. Frances Priddy, Dr. Senthilkumar Sakthivel, Dr. Andrew Fedanov, Dr. Seth Yellin and Judy Mathew, for their support with the microdermabrasion project.

At the Hope Clinic, Emory University, I had the pleasure to work with Dr. Walter Orenstein. I am thankful to him for his support during my experiments at the Hope Clinic.

I would like to thank Dr. Jack Orkin, Stephanie Ehnert, Christopher Souder and Lenox Franker of the veterinary and animal-care staff at the Yerkes National Primate Research Center for the care and preparation of monkeys for microdermabrasion experiments.

I would like to thank Dr. Matti Sallberg for the opportunity to visit his lab at the Karolinska Institute in Sweden. It was a wonderful opportunity to meet colleagues in Sweden and learn immunology first hand, for which I thank Jonas Soderholm. Their warmth towards me and my wife during our trip to Stockholm will always be cherished. I acknowledge the support of the Nerem International Travel Award, which funded majority of this trip.

I learnt a lot through my collaborations with: Dr. Richard Compans, Dr. Ioanna Skountzou and Dr. Joshy Jacob at Emory University; Dr. Audra Stinchcomb and Stan Banks at the University of Kentucky; Dr. A.J. Welch and Oliver Stumpp at the University of Texas, Austin. I thank all of them for the exchange of ideas and work on the collaborative projects.

I would like to thank Bradley Parker, Jeffrey Andrews and Dennis Brown for help with machine shop related work; Richard Shafer, Dr. Shawn Davis, and Ed Birdsell for helpful discussions regarding laser operation; Dr. Jung-Hwan Park for additional helpful discussions and deposition of silicon dioxide on microneedles. I am thankful to Dannae Rowe (MACtac Technical Products) for providing the medical foam tapes used in the microneedle patch fabrication.

I would like to thank my current and past fellow lab members, Samantha Andrews, Ying Liu, Prerona Chakravarty, Jyoti Gupta, Dr. Daniel Hallow, Josh Hutcheson, Dr. Jason Jiang, Yeuchun Kim, Jeong Woo Lee, Dr. Jung-Hwan Park, Samirkumar Patel, Dr. Robyn Schlicher, Sean Sullivan, Dr. Vladimir Zarnitsyn, Dr. Pavel Kamaev, Dr. Wijaya Martanto, Dr. Young Bin Choy, Dr. Ping Wang and Dr. Shawn Davis. I would also like to thank my undergraduate collaborators: Autumne, Shane Bechler, Merin Zachariah, Brett Burris and Youn Kim for their laboratory help.

I would like to thank Donna Bondy for her patience and help with all the office work especially laboratory orders. I will miss her butterscotch cheesecake for my birthday and Thanksgiving dinners. I would like to thank Mureen Mittler at Emory University for her help and support during my research at the Vaccine Research Center. I acknowledge the support of the administrative staff at the Parker H. Petit Institute for Bioengineering and Bioscience, Wallace H. Coulter Department of Biomedical Engineering and the Interdisciplinary Bioengineering Graduate Program at Georgia Tech; with a special thanks to Chris Ruffin, Patricia Fowler and Beth Bullock. I would like to thank the funding agencies NIH and NSF for funding my research.

I would like to thank my mother Amarjit Kaur and my father Bahal Singh Gill for their love, support and constant encouragement. They have always found joy in my big and small achievements. I would also like to thank my elder brother Arvinder Singh Gill who has always shown faith in me and without his support, I would not have had the

courage to venture so far from home to pursue my doctoral degree; my kid sister Rupinder Tur for being a joy to be with and for constantly pushing me to do better; my sister-in-law PrabhAmrit Pal Gill for her support and encouragement; and my brother-in law Mandeep Singh Tur for his support. I also fondly acknowledge my nephew Ekam Singh Gill who has been a constant source of joy and whose questions have inspired me as only a child can inspire, and my niece Reet Kaur Tur for being the sweetest two year old. I would also like to thank my mother-in-law Radha Muthiah and sister-in-law Preethi Muthiah for their support.

And finally I would like to thank my dear wife, Priya Gill. She has been a constant companion during my doctoral research, supporting me, encouraging me, cooking for me and loving me. I could not have expected more from her. She has smiled away my many late nights and weekends at lab; she has shared my setbacks and the glorious results; she has been a true friend and companion; and without her personal sacrifices, this work would not have been complete.

## TABLE OF CONTENTS

## LIST OF TABLES

## LIST OF FIGURES

# NOMENCLATURE

| | |
|---|---|
| $\gamma_{l,v}$ | Liquid-vapor surface energy |
| $\gamma_{s,l}$ | Solid-liquid surface energy |
| $\gamma_{s,v}$ | Solid-vapor surface energy |
| $^{51}Cr$ | Radioactive chromium isotope |
| ANOVA | Analysis of variance |
| BSA | Bovine serum albumin |
| CCD | Charge coupled device |
| CMC | Carboxymethylcellulose |
| CTL | Cytotoxic T lymphocyte |
| DMEM | Dulbecco's modified eagle's medium |
| DNA | Deoxyribonucleic acid |
| ELISA | Enzyme-linked immunosorbent assay |
| FCS | Fetal calf serum |
| GRAS | Generally recognized as safe |
| HCV | Hepatitis c virus |
| HEPES | (4-(2-hydroxyethyl)-1-piperazineethanesulfonic acid ) |
| HIV | Human immunodeficiency virus |
| IACUC | Institutional animal care and use committee |
| IRB | Institutional review board |
| $K_{o/w}$ | Octanol-water partition coefficient |
| MVA | Modified vaccinia Ankara |
| OCT | Optimum cutting temperature compound for histology |
| PECVD | Plasma enhanced chemical vapor deposition |

| | |
|---|---|
| PEG | Polyethylene glycol |
| PFU | Plaque forming units |
| PLGA | Polylactic-co-glycolic acid |
| PVP | Polyvinylpyrrolidone |
| $\theta$ | Contact angle |
| RNA | Ribonucleic acid |
| RSD | Relative standard deviation |
| USP | United states pharmacopeia |
| VAS | Visual analogue scale |

## SUMMARY

The major hurdle in the development of transdermal route as a versatile drug delivery method is the formidable transport barrier provided by the stratum corneum. Despite decades of research to overcome the stratum corneum barrier, limited success has been achieved. The **objectives** of this research were to develop and characterize two different strategies to overcome the stratum corneum barrier for transdermal delivery of biopharmaceuticals and vaccines. In the first strategy, coated microneedles (sharp-tipped, micron-sized structures) were developed to enable delivery of drugs directly into the skin by bypassing the stratum corneum barrier. In the second strategy, instead of bypassing the barrier, microdermabrasion was used to selectively abrade stratum corneum with sharp microparticles for topical drug application.

**Coated microneedles**

For developing painless microneedles, the first detailed study was performed to characterize the effect of microneedle geometry on pain caused by microneedle insertions in human volunteers. This study demonstrated that microneedles are significantly less painful than a 26-gage hypodermic needle and that decreasing microneedle length and numbers reduces pain.

Next, the first in-depth study of microneedle coating methods and formulations was performed to (i) develop a novel micron-scale dip-coating process, (ii) test the breadth of compounds that can be coated onto microneedles, and (iii) develop a rational basis to design novel coating formulations based on the physics of dip-coating.

Finally, a plasmid DNA-vaccine was coated onto microneedles to immunize mice, to provide the first evidence that microneedle-based skin immunization can generate a

robust in vivo antigen-specific cytotoxic-T-lymphocyte response using similar, or lower, DNA doses on microneedles as when using the gene gun or intramuscular injection.

**Microdermabrasion**

We demonstrated for the first time that microdermabrasion in monkeys and humans can selectively, yet completely remove the stratum corneum layer. Using a mobile mode of microdermabrasion, an increase in the number of treatment passes led to greater tissue removal. Furthermore, topical application of Modified Vaccinia Ankara virus after microdermabrasion induced virus-specific antibodies in monkeys.

In conclusion, both coated microneedles and microdermabrasion were developed to enable delivery of biomolecules into the skin, indicating their potential for transdermal delivery of a wide range of biopharmaceuticals and vaccines.

# CHAPTER 1: INTRODUCTION

## 1.1 SPECIFIC AIMS

Delivery of drugs into the body is often achieved through passive diffusion or active transport across body surfaces. The oral route utilizes the gastrointestinal surface for this purpose. While the oral route is convenient and relatively safe, in many instances it is ineffective, for example due to poor drug absorption or when the patient is unconscious and therefore is unable to ingest the medication (Ansel, Allen et al. 1999). As an alternative, hypodermic needles, which are more versatile are often used to inject drugs into the body. However, the pain (Hamilton 1995; Hanas 2004; Deacon and Abramowitz 2006) and safety risks due to transmission of blood borne pathogens like HIV and hepatitis B virus from accidental needle pricks or unsafe injection practices (Kane, Lloyd et al.; Hauri, Armstrong et al. 2004; Pruss-Ustun, Rapiti et al. 2005), make hypodermic needles unpopular.

The skin is another body surface that can be used to transport drugs into the body for both systemic delivery and immunizations. The bed of capillaries located just beneath the epidermal layer is conducive to systemic drug delivery (Braverman 1997; Cevc and Vierl 2007) from topically applied drugs. Furthermore, the epidermal dendritic cells (Langerhans cells), dermal dendritic cells and the epidermal keratinocytes (Babiuk, Baca-Estrada et al. 2000) provide immunological capability to the skin to enable generation of robust immune responses. However, only small and lipophilic molecules have been effectively delivered across the skin via transdermal patches because the skin's top most layer called the stratum corneum provides a formidable transport barrier (Naik, Kalia et al. 2000; Prausnitz, Mitragotri et al. 2004). Many physical and chemical approaches have been tested to enhance transdermal drug delivery, but limited clinical impact has been achieved from these methods (Prausnitz, Mitragotri et al. 2004).

Recently, micron-sized sharp-tipped structures called microneedles have been developed to enhance transdermal drug delivery by creating micro-pores in the stratum corneum (Henry, McAllister et al. 1998). Other variations of microneedles like drug coated, drug encapsulated or hollow microneedle configurations have also been tested (Prausnitz 2004). Despite the attractiveness of coated microneedles, a detailed investigation of the coating process has not been performed.

Another approach to deliver biopharmaceuticals into the skin may involve the full-thickness removal of stratum corneum so that topically applied drugs may easily diffuse into the skin. Microdermabrasion is an FDA approved method currently used to treat scars and acne by partially abrading the stratum corneum (Spencer 2005). The microdermabrasion process has potential to remove the full-thickness of the stratum corneum layer, yet no study has demonstrated this.

Accordingly, the objectives of this research were to develop and characterize (i) drug coated microneedles and (ii) microdermabrasion for transdermal drug delivery. The following specific aims were designed to achieve these objectives.

**Specific Aim 1**: Determine the effect of microneedle design and geometry on pain in human volunteers.

**Specific Aim 2**: Design, develop and characterize microneedle coating process and formulations.

**Specific Aim 3**: Determine the ability of DNA vaccine-coated microneedles to generate a cellular immune response in vivo.

**Specific Aim 4**: Investigate the effect of microdermabrasion parameters on the ability of full-thickness removal of stratum corneum in vivo in humans and monkeys.

The outcomes of this doctoral research have potential to significantly impact mass immunizations by providing safer and less painful alternatives to hypodermic needle-based immunizations. On a broader scale, this research will advance the field of transdermal drug delivery by enabling delivery of hydrophilic molecules and large molecular weight compounds including proteins, DNA and other biotherapeutics through the skin. At a more basic level, results from this research will promote understanding of coatings of micro-structures and the effects of microdermabrasion on skin.

## 1.2 THESIS OUTLINE

Background information relevant to this research can be found in Chapter 2. Each specific aim is then described in its own separate chapter: Chapter 3 (Specific Aim 1), Chapter 4 (Specific Aim 2), Chapter 5 (Specific Aim 2, continued), Chapter 6 (Specific Aim 3) and Chapter 7 (Specific Aim 4). Each chapter on the specific aims is complete in itself and the relevant materials and methods pertaining to the specific aim are included in the chapter. Overall conclusions of this research are presented in Chapter 8 and the recommendations for future work are provided in Chapter 9. Supporting material for different specific aims is provided in the appendices.

# CHAPTER 2: BACKGROUND

## 2.1 SKIN ANATOMY AND VASCULATURE

Skin is the largest organ in the human body covering about 18,000 $cm^2$ of surface area. Its primary function is to prevent entry of harmful substances into the human body and to reduce loss of internal body-water to the surroundings. Structurally, the skin consists of three main layers, the outermost stratum corneum, the middle viable epidermis and the innermost dermis (Figure 2.1). The stratum corneum is about 10-20 μm in thickness and is made of dead, polyhedral, non-nucleated, protein-rich cells called corneocytes. The corneocytes are about 0.5 μm thick and 40 μm in diameter, and about 15 layers of corneocytes stack one above the other in a staggered arrangement to produce a compact layer. The space between the corneocytes is filled with lipids forming a tortuous path in between the protein rich corneocytes. Thus, two domains exist in the stratum corneum, the protein-rich corneocyte domain embedded in an intercellular lipid-rich domain (Figure 2.2) (Schaefer and Redelmeier 1996).

The viable epidermal layer is 50-100 μm thick and is primarily made up of live keratinocytes, which continuously differentiate into corneocytes and replenish the stratum corneum layer above. In addition pigmented melanocytes and special dendritic cells called the Langerhans cells are also found in the epidermis. Langerhans cells are potent antigen presenting cells and are believed to initiate the immune response upon the entry of pathogens through the skin (Babiuk, Baca-Estrada et al. 2000; Partidos, Beignon et al. 2002; Partidos, Beignon et al. 2003). Vascular network is absent in the epidermis. Nutrient exchange occurs by passive diffusion from the lower dermal layer through the interstitial fluid, which constitutes about 15% of the total volume of the epidermis (Schaefer and Redelmeier 1996).

The dermis is 1-2 mm thick and forms the major bulk of the skin. Dermis is made up of collagen fibers and elastin, which provide toughness and elasticity to the skin. The

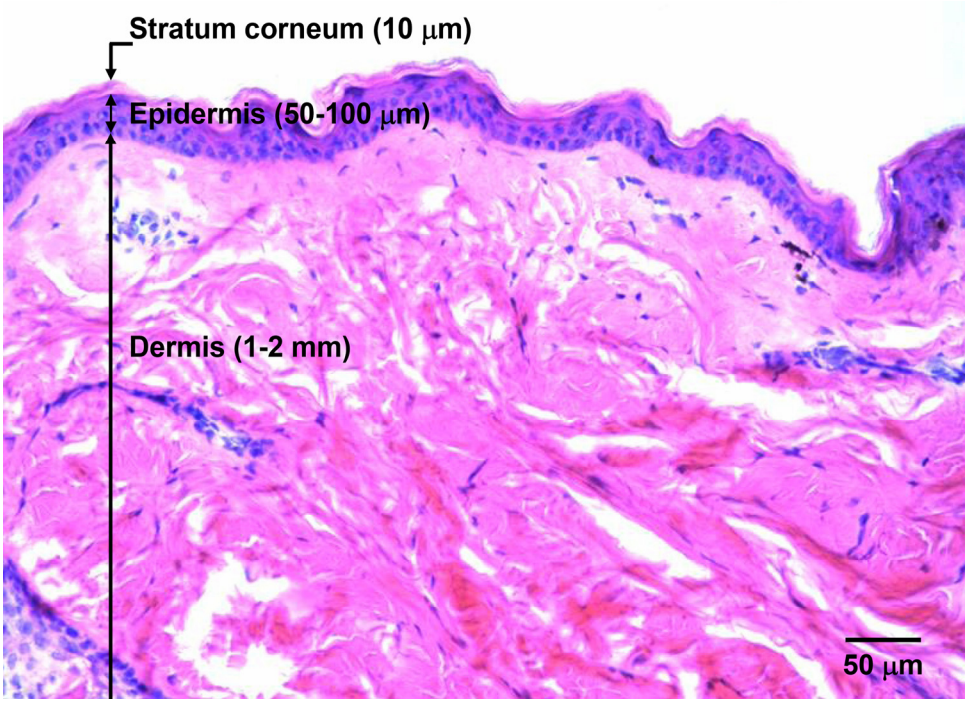


**Figure 2.1. Skin anatomy**. Histological section of monkey skin stained with hematoxylin and eosin showing the three layers of the skin: outermost stratum corneum (SC), middle viable epidermis (Ep) and the innermost dermis (De).

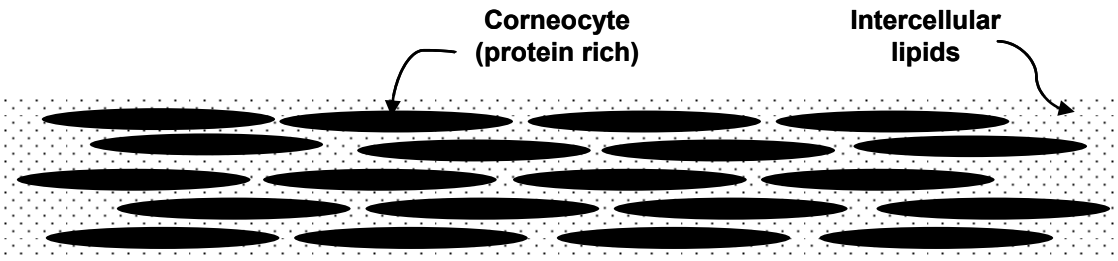


**Figure 2.2. Protein and lipid rich domains of stratum corneum**. A schematic of the stratum corneum layer showing the protein-rich corneocyte domain and the lipid-rich intercellular domain.

cellular components of dermis include fibroblasts, dermal dendritic cells and macrophages. The fibroblasts regulate collagen production while the dendritic cells and macrophages mediate immune responses.

The dermis has a dense vasculature to facilitate nutritional and heat exchange, and to regulate the immune response. This vasculature is organized into two major horizontal plexus (i.e. networks), one situated at the dermal-subcutaneous junction, and the other in the papillary dermis near the epidermal-dermal junction. The two horizontal networks are connected by ascending arterioles and descending venules. The upper plexus gives rise to dermal capillary loops that form a hairpin loop in the dermal-epidermal papillae (Figure 2.3). Majority of the vasculature resides in the upper plexus about 0.1 mm deep into the skin. This network provides an attractive target for systemic transdermal drug delivery, and also plays a role in the clearance characteristic of topically applied drugs (Schaefer and Redelmeier 1996; Braverman 1997).

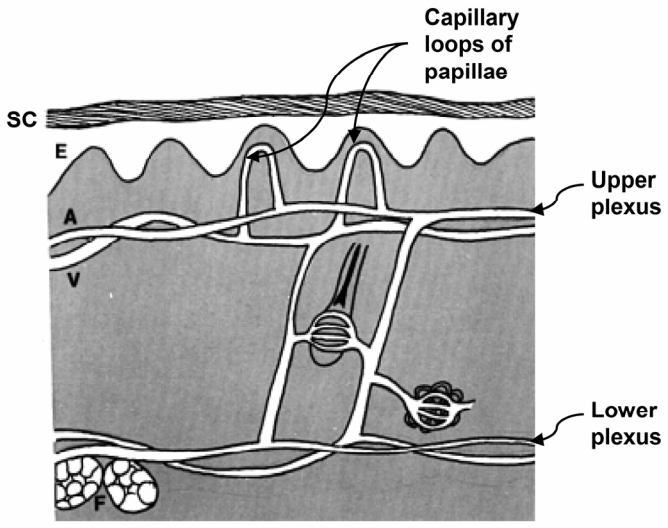


**Figure 2.3. Vascular layout of skin**. A schematic showing the upper and the lower vascular plexus of the skin interconnected with ascending arterioles and descending venules. The capillary loops of the dermal papillae arise from the upper plexus. SC: stratum corneum; E: epidermis; A: arteriole; V: venule; F: subcutaneous fat. Modified from (Braverman 2000)

## 2.2 BARRIER PROPERTY OF THE SKIN

Majority of the skin's permeability barrier comes from just the top 10-20 μm thick stratum corneum layer. The stratum corneum's unique lipid-rich and protein-rich domain structure forms the basis of this tough barrier property. To understand the nature of this barrier to transport, the stratum corneum structure may be considered analogous to a 'mortar and brick' structure, with the intercellular lipids mimicking the mortar and the corneocytes the bricks. Only the lipid-rich domain forms a continuous phase. To permeate through the stratum corneum, any substance must generally either diffuse through the tortuous lipid-rich phase taking the intercellular diffusion pathway, or must take the transcellular route and diffuse through both the protein-rich corneocyte domains and the intervening lipid-rich domains (Figure 2.4). Because the lipid-rich phase forms the continuous phase, it is expected to be the preferred route of diffusion. Available evidence supports this hypothesis because lipophilic molecules with octanol-water partition coefficients between 10 and 1000 show higher permeability through the skin, while the hydrophilic molecules show very poor permeability. In addition, extraction of the lipid phase from mouse skin by acetone treatment has shown an increase in transepidermal water loss, supporting the hypothesis that the lipid phase is a major contributor of skin permeability barrier (Schaefer and Redelmeier 1996).

The protein-rich phase of corneocytes is also important in maintaining the barrier function. The presence of corneocytes disrupts the otherwise continuous lipid-rich phase and creates a tortuous path for diffusion by increasing the diffusive path length by 50-100 fold making the diffusion process even slower (Schaefer and Redelmeier 1996).

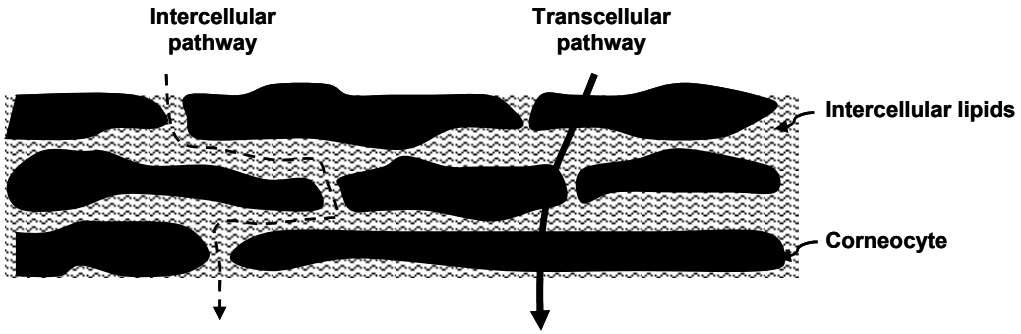


**Figure 2.4. Diffusion pathways through the stratum corneum**. A schematic showing the intercellular and the transcellular diffusion pathways through the stratum corneum.

## 2.3 TRANSDERMAL DRUG DELIVERY

The goal of transdermal drug delivery is to enable transport of drugs into the systemic circulation through the skin surface. Because of the unique nature of stratum corneum's barrier to transport, compounds with the following physicochemical and formulation characteristics have been experimentally found to be favorable for passive diffusion through the stratum corneum (Naik, Kalia et al. 2000):

(i) Aqueous solubility: > 1 mg/ml

(ii) Lipophilicity : $10 < K_{o/w} < 1000$ , where $K_{o/w}$ is the octanol-water partition coefficient

(iii) Molecular weight: < 500 Da

(iv) Dose deliverable: < 10 mg/day

Because of the narrow class of drugs that can passively diffuse through the stratum corneum, currently there are just close to 16 drugs available in the form of transdermal patches from the whole compendium of therapeutic drugs (Center for Drug Evaluation and Research 2007) .

To increase the range of drugs that can be delivered through the skin, a number of chemical and physical approaches have been investigated. Various solvents and

surfactants have been used as chemical enhancers to increase drug permeabilities through the stratum corneum either by improving solubility, fluidizing the lipid-rich domain or by disrupting the lipid-rich domain (Karande, Jain et al. 2005) . Skin irritation limits the use of strong chemical enhancers, and this method has only shown limited successes. Physical enhancement methods like iontophoresis (Nair, Pillai et al. 1999; Pillai, Nair et al. 1999) and electroporation (Prausnitz, Edelman et al. 1995; Banga and Prausnitz 1998; Prausnitz 1999) based on electrical energy, sonoporation based on ultrasound effects (Mitragotri and Kost 2004), thermoporation based on radiofrequency excitation (Sintov, Krymberk et al. 2003; Birchall, Coulman et al. 2006), and high velocity jets based on kinetic energy (Schramm and Mitragotri 2002) have also been investigated. These methods are generally limited to a special class of substances, for example, iontophoresis is applicable only to charged species; and/or require the use of power and equipment, which generally adds expense and complexity to the method (Prausnitz, Mitragotri et al. 2004).

## 2.4 MICRONEEDLES FOR TRANSDERMAL DRUG DELIVERY

Micron-sized needles – microneedles - were developed as a hybrid between hypodermic needles and transdermal patches to eliminate the pain associated with hypodermic needles, and yet, facilitate delivery of a wide range of therapeutic agents through the skin, including proteins, DNA and other biopharmaceuticals.

Microneedles have been used in four different ways for transdermal drug delivery (Prausnitz, Mikszta et al. 2005):

(i) *"poke-and-patch"*: creation of micron-sized holes in the stratum corneum by piercing solid microneedles into the skin to allow topical application of drugs.

(ii) *"coat-and-poke"*: insertion of drug coated microneedles into the skin for drug dissolution into the skin.

(iii) *"poke-and-release"*: encapsulation of drug within solid microneedles to enable rapid or controlled release upon microneedle insertion into the skin.

(iv) *"poke-and-flow"*: injection of drug through hollow microneedles into the skin.

### 2.4.1 Poke-and-patch

The first demonstration of the ability of microneedles to enhance permeability of the skin was done by poking solid, silicon microneedles into skin in vitro (Henry, McAllister et al. 1998). Delivery of compounds including calcein, insulin, bovine serum albumin (BSA) and latex nanoparticles as big as 100 nm in diameter has been demonstrated with up to 10,000 fold permeability enhancement of the skin (McAllister, Wang et al. 2003; Park, Allen et al. 2005; Teo, Shearwood et al. 2005) (Figure 2.5 A-C). In addition, delivery of plasmid DNA and lipid-polycation-plasmid DNA has also been shown in vitro. Bioactivity was shown using β-galactosidase after delivering it into ex-vivo human skin kept viable in culture (Chabri, Bouris et al. 2004; Birchall, Coulman et al. 2005) (Figure 2.5 D).

Blood glucose reduction was shown in hairless rats, demonstrating bioavailability of insulin after its topical application on skin treated with stainless steel microneedles (Martanto, Davis et al. 2004) (Figure 2.5 E). Similarly, delivery of antisense-oligonuletides has also been shown in hairless guinea pigs. Combination of iontophoresis with microneedle pretreatment resulted in 100 fold enhancement of antisense-oligonucleotide delivery over iontophoresis alone (Lin, Cormier et al. 2001).

Using a related blunt-tipped device called the microenhancer array, strong immune response has been generated in vivo against hepatitis B, anthrax and Japanese encephalitis (Mikszta, Alarcon et al. 2002; Dean, Alarcon et al. 2005) (Figure 2.5 F). In all cases the antigen was first applied on the skin and the microenhancer array was

rubbed on the skin to mechanically scrape the stratum corneum and perturb the barrier to allow the uptake of the antigen.

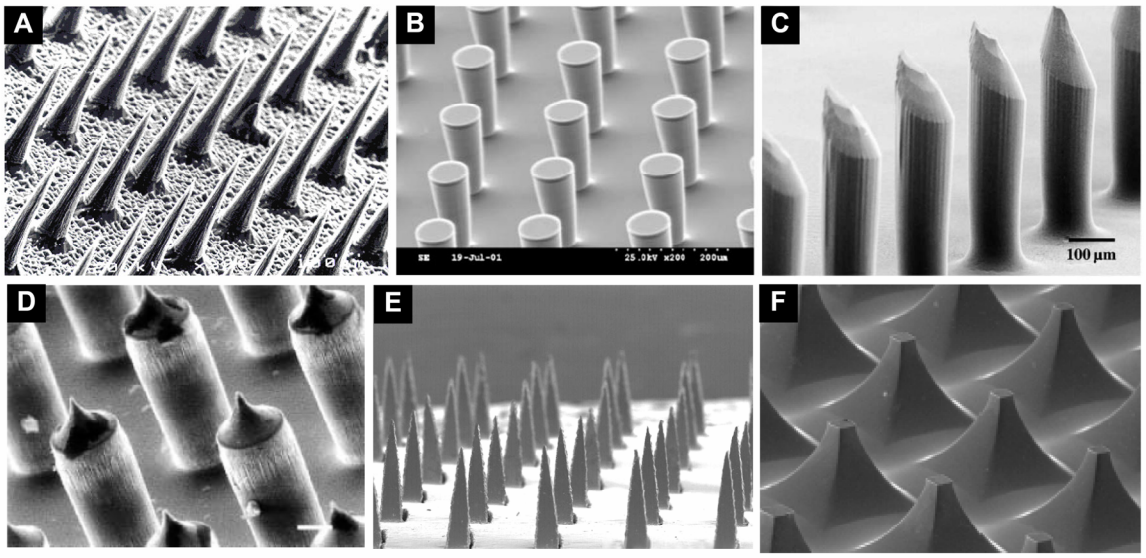


**Figure 2.5. Representative solid microneedles used in poke-and-patch approach**. (A) Sharp tipped, conical, silicon microneedles 150 μm long with a base diameter of 80 μm (Kaushik, Hord et al. 2001; Mikszta, Sullivan et al. 2005). (B) Blunt tipped, cylindrical, silicon microneedles 150 μm long with a base diameter of 80 μm (Teo, Shearwood et al. 2005). (C) Bevel tipped, cylindrical, polyglycolic acid microneedles 600 μm long with a base diameter of 100 μm and a tip diameter of 10 μm (Park, Allen et al. 2005). (D) Sharp tipped, cylindrical, silicon microneedles 150 μm long with a base diameter of about 50 μm (Chabri, Bouris et al. 2004). (E) Sharp tipped, tapered, stainless steel microneedles 1000 μm long with a base width of 200 μm and a thickness of 50 μm (Martanto, Davis et al. 2004). (F) Blunt tipped, pyramidal, silicon microenhancers 150 μm long used to scrape the skin (Mikszta, Alarcon et al. 2002).

### 2.4.2 Coat-and-poke

Drug coated microneedles have been used to deliver drugs and antigens in vivo. Desmopressin coated microneedles were used in hairless guinea pigs to show up to 85% bioavailability (Cormier, Johnson et al. 2004) (Figure 2.6 A-B). In the same animal model, strong immune response against ovalbumin has also been generated after delivery of ovalbumin from coated microneedle arrays made of titanium (Matriano, Cormier et al. 2002; Widera, Johnson et al. 2006).

In another approach, microporous calcium phosphate was coated onto acupuncture needle tips and filled with trehalose to help stabilize proteins (Shirkhanzadeh 2005).

In a different approach, the microneedle substrate was coated rather than the microneedles. The substrate coating functioned as a drug reservoir to deliver drug through the pores created in the skin by the microneedles. Using this method, in vitro delivery of calcein and BSA was shown from chitosan coatings on the microneedle substrate (Xie, Xu et al. 2005) (Figure 2.6 C). This method may also be considered a variation of the poke-and-patch approach with the drug reservoir attached to the substrate of the microneedle array.

Coated microneedles have also been used to deliver pilocarpine and other model compounds into rabbit eye in vivo (Jiang, Gill et al.).

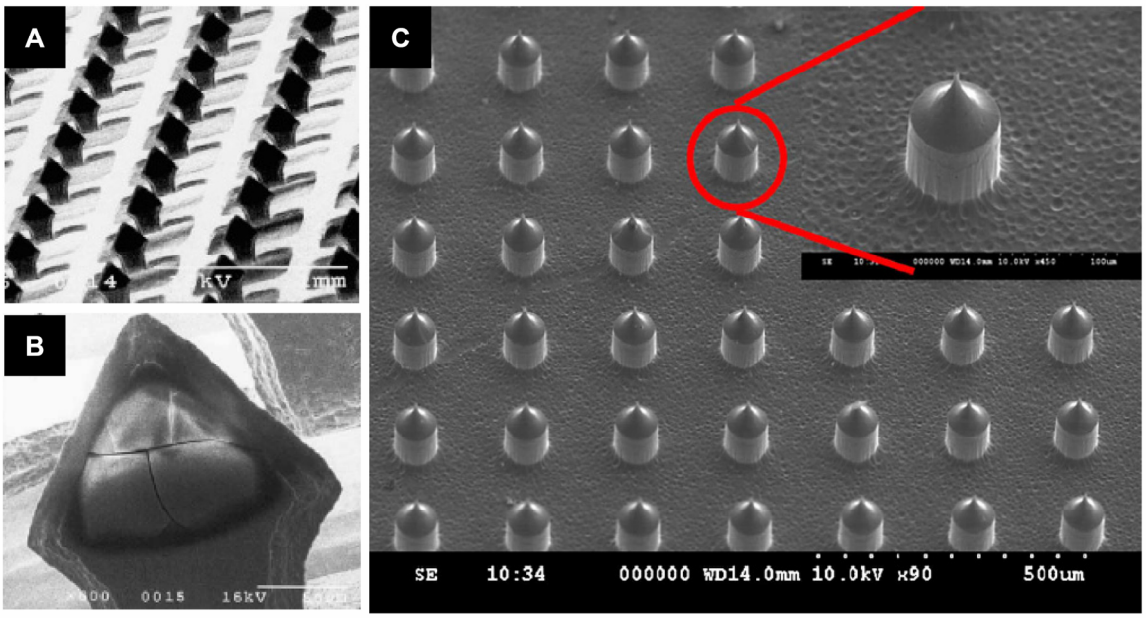


**Figure 2.6. Representative solid microneedles used in coat-and-poke approach**. (A,B) Desmopressin coated, sharp tipped, arrow-head shaped, titanium microneedles 200 µm long, 170 µm wide at the arrow head and 35 µm thick (Cormier, Johnson et al. 2004). (C) Sharp tipped, cylindrical, silicon microneedles 130 µm long with 80 µm base diameter used to apply drug filled chitosan coating on the base (Xie, Xu et al. 2005).

### 2.4.3 Poke-and release

Instead of coating drugs onto microneedles, the drug can also be encapsulated in the matrix of the microneedles, and released by its dissolution or degradation in the skin. Based on this approach, sodium salicylate and ascorbate-2-glicoside was encapsulated in maltose needles. Rapid dissolution of maltose microneedle in less than 5 min was shown in human skin in vivo (Miyano, Tobinaga et al. 2005) (Figure 2.7 A). Similarly, erythropoietin (Ito, Yoshimitsu et al. 2006) and insulin delivery (Ito, Hagiwara et al. 2006) was shown in mice skin in vivo with millimeter scale needles made of a dissolvable matrix of dextrin.

Instead of rapid release, the matrix can be designed to provide a controlled release. Microneedles made from a biodegradable polymer, polylactic-co-glycolic acid (PLGA) have been fabricated to encapsulate calcein, BSA and microparticles (Figure 2.7 B-C). Controlled release over hours to months was demonstrated in vitro depending on the encapsulation formulation (Park, Allen et al. 2006). These needles can be easily incorporated into a small-sized patch for convenient application (Figure 2.7 D)

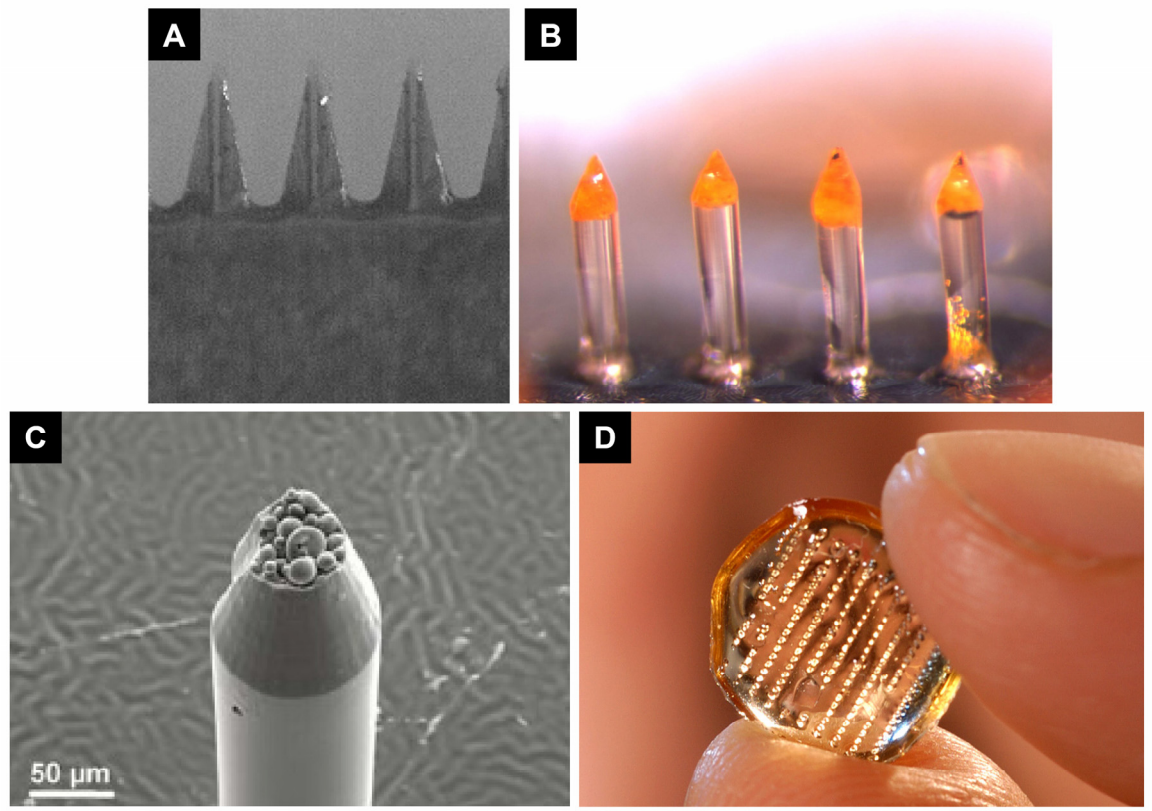


**Figure 2.7. Representative solid microneedles used in poke-and-release approach**. (A) Maltose microneedles 500 µm long encapsulating 10 wt% calcein as a model drug (Miyano, Tobinaga et al. 2005). (B) Bevel tipped, cylindrical PLGA microneedles 600 µm long encapsulating calcein within their tips (Park, Allen et al. 2006). (C) PLGA microneedle with its tip chipped to expose microparticles encapsulated inside the microneedle (Park, Allen et al. 2006). (D) A complete 20 × 10 array of polymer microneedles made of PLGA (Park, Allen et al. 2006).

### 2.4.4 Poke-and-flow

Hollow microneedles have been fabricated using silicon, metal and glass as the materials of construction. Using hollow microneedles, insulin and diclofenac was delivered to rats in vivo (Gardeniers, Luttge et al. 2003; McAllister, Wang et al. 2003) (Figure 2.8 A). Another study demonstrated microneedle injection of methyl nicotinate in human subjects using silicon hollow microneedles (Sivamani, Stoeber et al. 2005) (Figure 2.8 B). Microneedle injections have been precisely made in the epidermis and into the dermis at controlled depths, which can be useful dermatological, vaccine and research purposes (Wang, Cornwell et al. 2006).

Additional research into the fluid dynamics of injection into the skin has helped to show that the primary resistance to microinjection into the skin does not reside in the microneedles, but it is offered by the tissue (Martanto, Baisch et al. 2005). Partial retraction of inserted microneedles has been shown to increase the injection flow rates by up to 10 fold (Martanto, Moore et al. 2006b) (Figure 2.8 C). Mechanistically, retraction allowed the skin to regain its uncompressed state and increased the skin fluid conductivity as compared to its compressed state that was created during microneedle insertion (Martanto, Moore et al. 2006a). Insulin delivery has also been shown in vivo using passive diffusion through hollow microneedles (Davis, Martanto et al. 2005) (Figure 2.8 D).

Using small hypodermic needles measuring 1 – 3 mm in length, mice and rabbits have been vaccinated against anthrax (Mikszta, Sullivan et al. 2005) and non-human primates against Japanese encephalitis (Dean, Alarcon et al. 2005). Dose sparing of vaccine for influenza virus and strong immune response has been shown in rats upon delivery of either a whole inactivated influenza virus, a trivalent split-virion human vaccine, or a plasmid DNA encoding the influenza virus hemagglutinin (Alarcon, Hartley et al. 2007) (Figure 2.8 E-F).

Hollow microneedles have also been used for diagnostic applications like withdrawing blood (Tsuchiya, Nakanishi et al. 2005) and extracting interstitial fluid for glucose monitoring (Smart and Subramanian 2000). Microneedles have also been modified to perform microdialysis for continuous medical monitoring (Zahn, Trebotich et al. 2005).

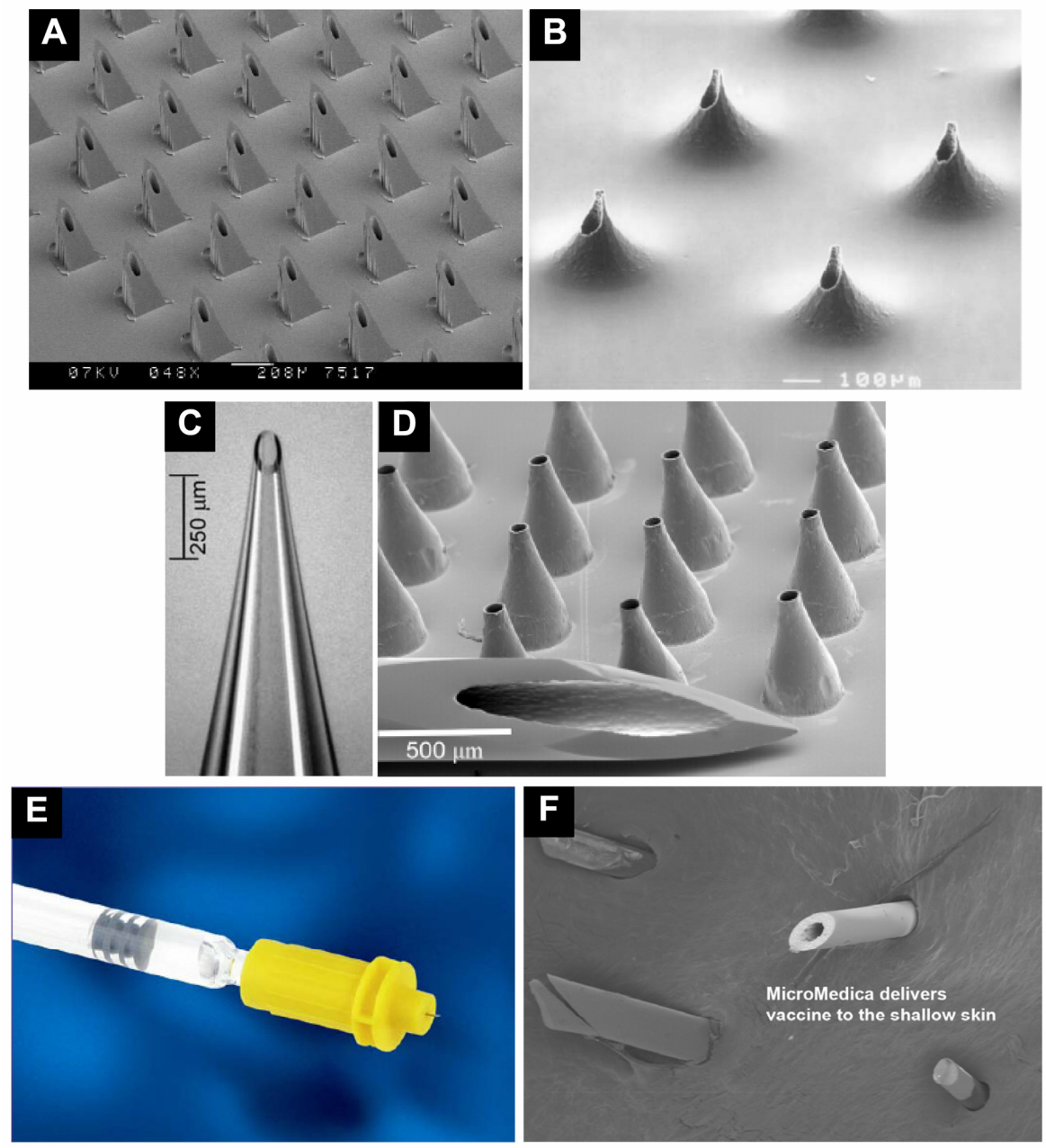


**Figure 2.8. Representative hollow microneedles used in poke-and-flow approach**. (A) Hollow, silicon microneedles 350 µm long with a 70 µm-wide bore (Gardeniers, Luttge et al. 2003). (B) Hollow, silicon microneedles 200 µm long with a lumen diameter of 40 µm (Sivamani, Stoeber et al. 2005). (C) Hollow, glass microneedle with a tip opening effective radius of 30 µm (Martanto, Moore et al. 2006b). (D) Hollow, metal microneedles 500 µm long shown next to a 27-gauge hypodermic needle (Davis, Martanto et al. 2005). (E) Hollow, metal microneedle 2 mm long assembled onto a hypodermic syringe and (F) pierced through swine skin (Mikszta 2003).

## 2.5 ELECTROPOLISHING

Because microneedles are often made of metals and have micron sized dimensions, mechanical methods of polishing will not be suitable to clean the surfaces. Therefore, electropolishing is of interest for metal microneedle fabrication. Anodic dissolution of metal to produce deburred, bright and passivated metal surfaces is called electropolishing. Electropolishing can clean and polish the microneedle surfaces and sharpen the microneedle tips. To electropolish a metal, a direct positive current is applied to it with an appropriate cathode and an electropolishing solution (Landolt 1987). Cardiovascular stent is an example of a medical device that is electropolished to improve its surface finish (Figure 2.9).

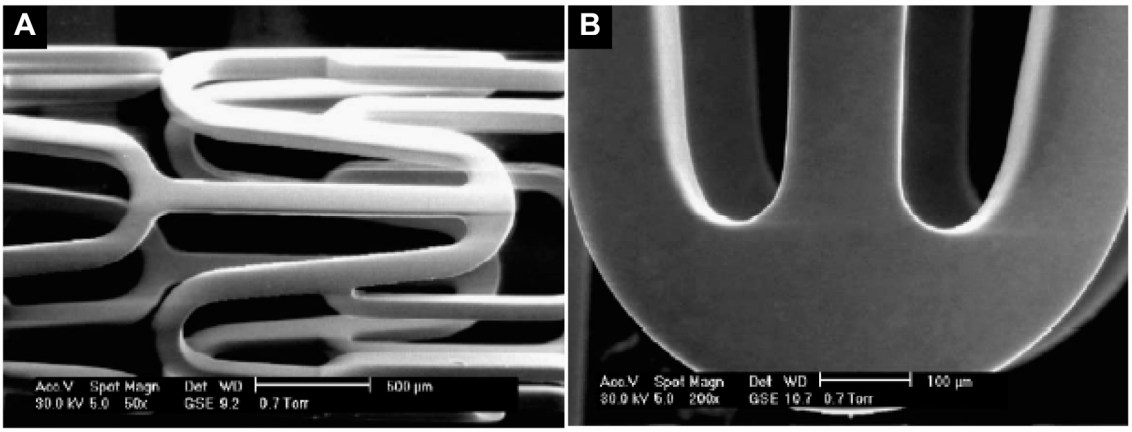


**Figure 2.9. Electropolished cardiovascular stent**. Example of a cardiovascular stent electropolished to produce a smooth and bright surface: (A) entire stent and (B) outer surface (Raval, Choubey et al. 2004).

Electropolishing is thought to occur because of mass transfer limited anodic dissolution of the metal. As the applied voltage across the anode and the cathode increases, the current flowing through the cell increases. However, at a limiting current density the rate of metal ion formation exceeds the rate at which the metal ions can diffuse into the bulk

of the solution and causes the current density to plateau (Figure 2.10 A). At this diffusion controlled stage, an anodic film gets formed, comprising of a saturated metal ion layer and a thin salt film adjacent to the metal surface. This anodic film has a higher electrical resistance than the bulk of the solution and can therefore control the erosion of the anodic metal surface. Because the anodic film has a regular thickness, the raised peaks of the surface roughness features of the metal protrude more into the anodic film and provide a path of lower resistance to the flow of current (Figure 2.10 B). Thus, the peaks get eroded faster than the valleys and lead to the electropolishing effects of deburring and a bright finish of the metal surface (Hahn and Marder 1988; Datta, Vega et al. 1992).

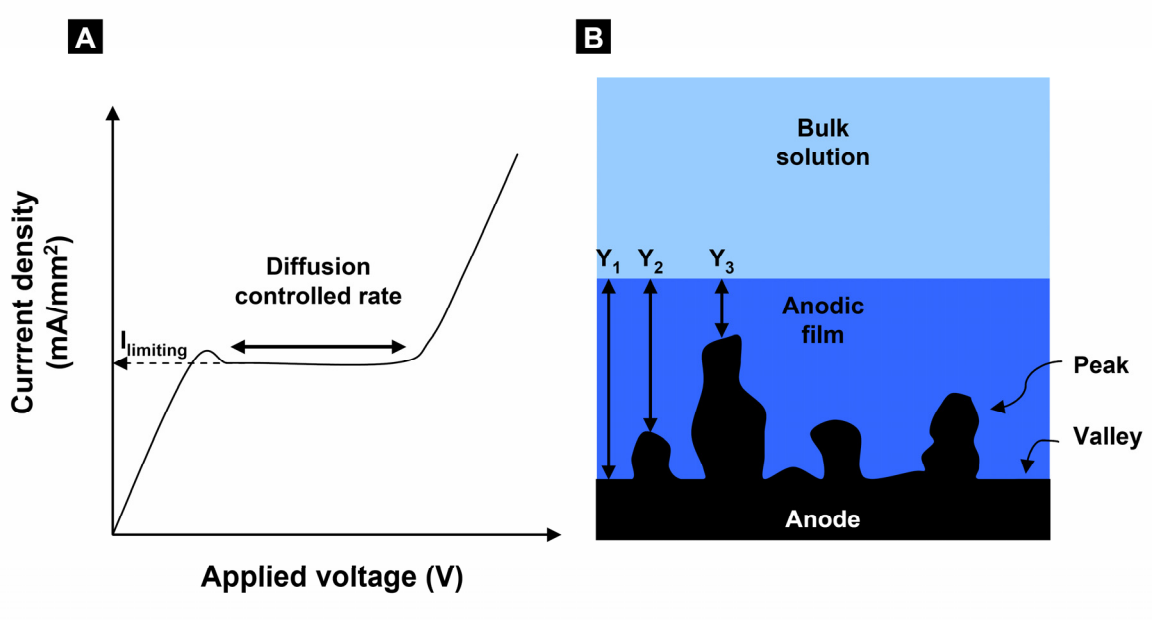


**Figure 2.10. Mechanism of electropolishing.** (A) Polarization curve of a standard electropolishing system showing the current plateau at the limiting current – $I_{limiting}$ when the anodic film is formed because of diffusion controlled rate of reaction. (B) A schematic of an anodic surface showing the peaks and valleys of the surface roughness, the anodic film, the bulk solution and the diffusion distances $Y_1$, $Y_2$ and $Y_3$ that the ions have to travel to reach the bulk solution. Lower diffusion distances of the peaks cause them to erode faster than the valleys and produce a deburring effect.

## 2.6 DIP-COATING

Different coating methods are practiced to form solid coatings on surfaces on a macro scale, for example, roll coating, spin coating, slot coating and dip coating (Weinstein and Ruschak 2004). To form drug coatings on microneedles, dip coating is an attractive method because it is a relatively simple method of forming liquid films on a solid substrate for solidification into solid coatings. Conventional batch dip coating processes consist of the following steps (Scriven 1988) (Figure 2.11 A-C ) :

(i) *Immersion*: A solid substrate to be coated is immersed into a container filled with the coating solution.

(ii) *Withdrawal*: The solid substrate is removed from the coating solution at a constant speed. Because of the viscous drag, the withdrawal of the substrate initiates an upward flow in the coating solution at the substrate boundary. The thickness of the liquid film carried by the substrate depends on the balance between the viscous drag force, gravity and surface tension. A high withdrawal velocity and coating solution viscosity and low surface tension lead to thicker liquid films on the substrate.

(iii) *Drainage and evaporation*: After withdrawal, the excess liquid from the substrate is allowed to drain away under gravity. The solvent from the liquid film is then allowed to evaporate to form a solid coating on the substrate. Depending upon the volatility of the solvent, evaporation may begin as soon as the substrate begins to be withdrawn from the coating solution.

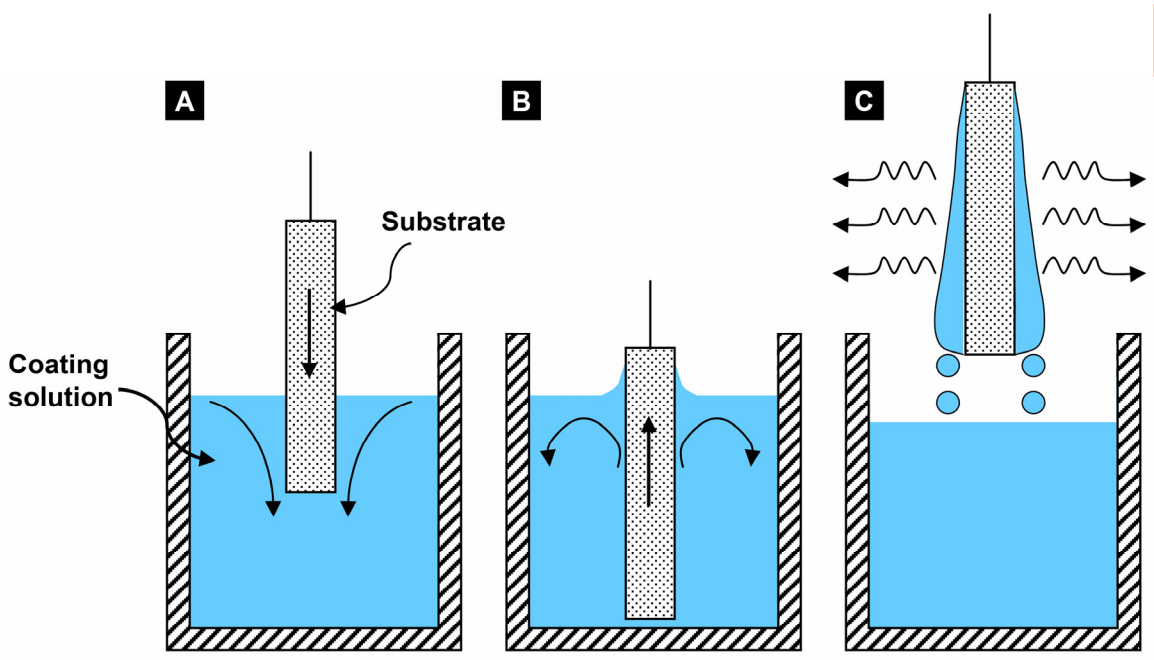


**Figure 2.11. Dip-coating process**. A schematic showing the steps involved in dip coating: (A) immersion of a substrate into a container containing the coating solution, (B) startup of substrate withdrawal from the coating solution, and (C) drainage of excess liquid film and evaporation of the volatile solvent to eventually result in a solid coating.

### 2.6.1 Thermodynamic wetting

To form a uniform solid coating on the substrate, the liquid film must in turn uniformly spread on the solid substrate. Based on the thermodynamics of wetting, the condition for a liquid to completely wet a solid surface can be determined from the Young's equation. The Young's equation reflects a balance of the surface forces acting on a liquid drop lying on a solid substrate (Figure 2.12)

Young's equation : $\cos(\theta) = (\gamma_{s,v} - \gamma_{s,l}) / \gamma_{l,v}$

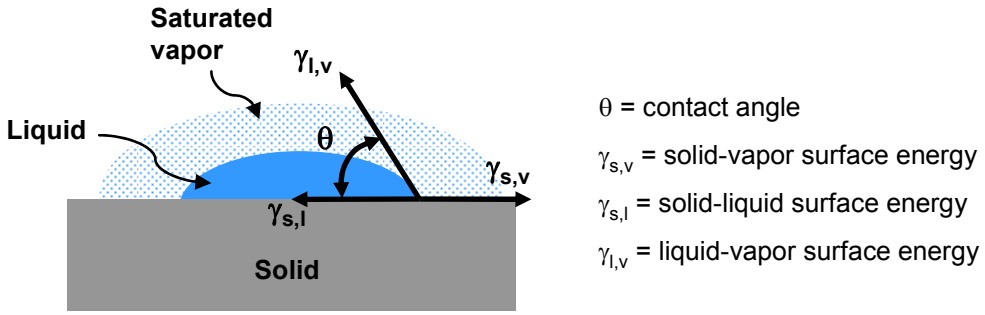


**Figure 2.12. Static thermodynamic wetting**. A schematic of a liquid drop stationary over a solid surface with the associated forces acting on the liquid drop due to the surface energies of the liquid and the solid substrate.

For a liquid to completely wet the solid, the contact angle must be zero. Therefore, based on the Young's equation, the liquid surface tension must be equal or less than the solid surface energy (Stokes, Evans et al. 1997).

### 2.6.2 Dynamic wetting

The thermodynamic criterion of wetting is applicable only to systems at equilibrium. Because the dip coating process is a dynamic process, a uniform liquid film can still be formed on the substrate from liquids that do not completely wet the substrate. This can be achieved by relying on the viscous drag and the inertia of withdrawal of the substrate. Thus, a high velocity of the substrate and a high solution viscosity, which increase the viscous drag force and the inertia of the substrate, can be used to form a uniform liquid film on the substrate even from partially wetting liquids.

Using this method, a solid coating can be formed even from partially wetting liquids by first forming a liquid film on the substrate, and then accelerating the solvent evaporation to solidify it into a solid coating before thermodynamic dewetting can occur.

A high solution viscosity can also aid in this process by resisting dewetting flows (Scriven 1988).

## 2.7 MICRODERMABRASION

Instead of bypassing the stratum corneum layer to deliver drugs across it, the stratum corneum layer can alternatively be selectively removed to deliver drugs topically, to the epidermis beneath it. Microdermabrasion, which uses microparticles to abrade the skin for cosmetic applications like improvement of acne, scars and photoaging (Spencer 2005) has the potential to perform the selective removal of just the stratum corneum. In microdermabrasion, the abrasive action is achieved by impinging aluminum oxide or other abrasive particles on the skin and removing them under vacuum. The particles are irregularly shaped and have sharp edges that can mechanically damage the surface of the skin using the kinetic energy of their motion. Microdermabrasion procedure is performed manually by moving a handpiece on the skin surface. Abrasive particles enter the handpiece under vacuum through a tubing connected to a container filled with clean abrasive particles, and exit through a separate tubing connected to a waste container (Figure 2.13).

Microdermabrasion is used to remodel the skin through a partially known mechanism. Studies have shown that microdermabrasion causes partial abrasion of the stratum corneum, though complete stratum corneum removal is not typically achieved (Spencer 2005). Biological effects like erythema, dermal edema, vasodilation and perivascular inflammation have been reported after microdermabrasion (Freedman, Rueda-Pedraza et al. 2001).

Microdermabrasion also has potential for transdermal drug delivery. Transepidermal water loss in human subjects has been shown to increase significantly 24 h after microdermabrasion (30 g/m$^2$/h) as compared to the baseline value (20 g/m$^2$/h),

which returned to normal levels 7 days later (Rajan and Grimes 2002). A similar result was observed

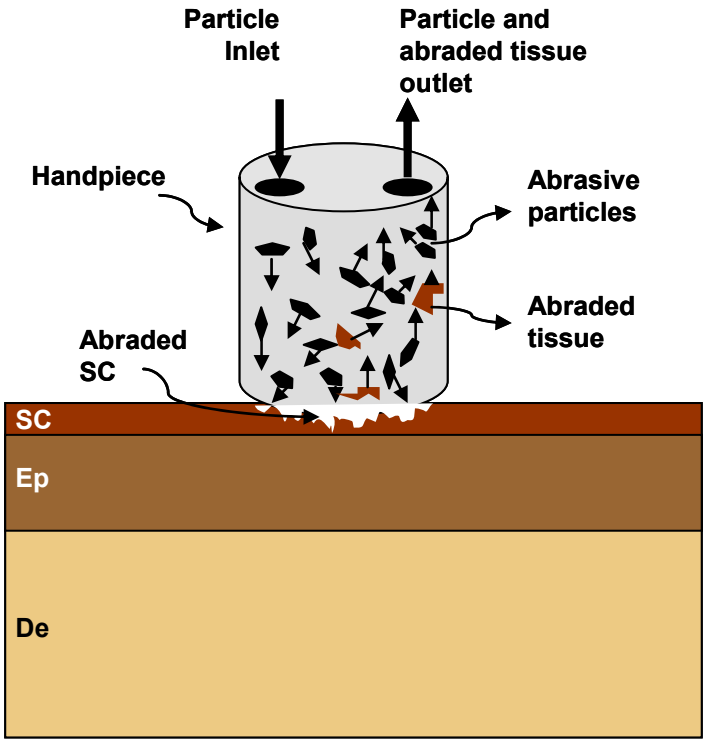


**Figure 2.13. Principle of microdermabrasion**. A schematic of a microdermabrasion handpiece in contact with the stratum corneum (SC) showing the impingement of abrasive particles on to the skin surface leading to its mechanical damage and removal. Ep: epidermis, De: dermis.

in another human study, though the recovery was observed just 1 day later (Song, Kang et al. 2004). Delivery of estradiol was shown through through freshly excised hairless mouse sking using diffusion cells experiments (Fujimoto, Shirakami et al. 2005). In this study majority of microdermabrasion conditions led to only a partial removal of the stratum corneum, and yet demonstrated enhanced delivery as compared to normal skin.

In a related approach called microscission, microparticles were accelerated on to the skin under pressure instead of a vacuum, to create microconduits in the skin of

human subjects. Lidocaine delivery and blood glucose measurement was demonstrated using this approach (Herndon, Gonzalez et al. 2004).

# CHAPTER 3: EFFECT OF MICRONEEDLE DESIGN ON PAIN IN HUMAN SUBJECTS[1]


## ABSTRACT

The purpose of this study was to design microneedles that minimize pain. This study tested the hypothesis that microneedles cause significantly less pain than a 26-gage hypodermic needle, and that decreasing microneedle length and the number of microneedles reduces pain in normal human subjects. Single microneedles with lengths ranging from 480 to 1450 μm, widths from 160 to 465 μm, thicknesses from 30 to 100 μm and tip angles from 20° to 90°; and arrays containing 5 or 50 microneedles were inserted into the volar forearms of ten healthy, human subjects in a double-blinded, randomized study. Visual analog scale pain scores were recorded and compared to each other and to the pain from a 26-gage hypodermic needle. All microneedles investigated were significantly less painful than the hypodermic needle with microneedle pain scores varying from 5 to 40% of the hypodermic needle. Microneedle length had the strongest effect on pain, where a three-fold increase in length increased the pain score by seven fold. The number of microneedles also affected the pain score, where a 10-fold increase in the number of microneedles increased pain just over two-fold. Microneedle tip angle, thickness and width did not significantly influence pain. In conclusion, this study demonstrated that microneedles are significantly less painful than a 26-gage hypodermic needle over the range of dimensions investigated, and that decreasing microneedle length and number of microneedles reduces pain.


[1] This work was done in collaboration with Dr. Donald Denson at the Center for Pain Medicine, Department of Anesthesiology, Emory University

## 3.1 INTRODUCTION

Micron-scaled needles, i.e., microneedles, have been developed as a hybrid approach between transdermal patches and hypodermic needles to overcome the individual limitations of injections and patches, and to create a minimally invasive and less painful method of transdermal drug and vaccine delivery (Prausnitz 2004). A major limitation of hypodermic needles is the pain and risk of infection from bloodborne pathogens. Pain from needle insertion leads to distress and poor patient compliance (Hanas 2004), and in extreme cases can produce needle phobia, which is characterized by fear, anxiety and vasovagal reaction that can lead to fainting or sometimes even death (Hamilton 1995; Nir, Paz et al. 2003; Deacon and Abramowitz 2006). Furthermore, the hazardous practice of needle reuse found predominantly in developing countries puts millions of people at risk. In the year 2000, an estimated 40% of the 16 billion injections administered worldwide were from reused needles, which led to an estimated 21 million, 2 million and 260,000 new cases of hepatitis B, hepatitis C and HIV infections, respectively (Hauri, Armstrong et al. 2004).

To eliminate the pain and risk associated with hypodermic needles, transdermal drug patches have been developed (Prausnitz, Mitragotri et al. 2004). However, transdermal delivery is currently limited in scope because of the formidable transport barrier provided by the stratum corneum (Prausnitz, Mitragotri et al. 2004). Because of this barrier, the 16 drugs that exist as transdermal patches are all small and lipophilic molecules with low dose requirements (Prausnitz, Mitragotri et al. 2004).

In a synergistic approach, microneedles assembled on a patch have been successfully used to deliver a variety of large and hydrophilic compounds into the skin. In vitro delivery of small molecules like calcein and large compounds like proteins, DNA and nanoparticles has been shown (McAllister, Wang et al. 2003; Chabri, Bouris et al. 2004; Gill and Prausnitz 2007b). In vivo delivery has been shown for insulin (Martanto,

Davis et al. 2004) and vaccines, for example, against influenza and hepatitis B (Mikszta, Alarcon et al. 2002; Alarcon, Hartley et al. 2007).

Excitement about microneedles is based in part on the expectation that they cause less pain than hypodermic needles. However, this expectation has not been fully validated. Only one study has formally measured the pain caused by microneedles in human subjects. It found that insertion of 400 microneedles measuring 150 μm in length was painless as compared to a 2-mm deep insertion of a 26-gage hypodermic needle (Kaushik, Hord et al. 2001). In a related study, scraping the skin with microneedle-like structures measuring 50-200 μm in length was similarly found to be painless (Mikszta, Alarcon et al. 2002). However, no study has examined the pain caused by microneedles in detail or determined how microneedle geometry influences pain. Addressing this issue is important because larger microneedles are stronger, can deliver more drug, and are generally easier to handle, but are expected to cause more pain. Design of an effective microneedle drug delivery system that minimizes pain requires a quantitative understanding of the dependence of pain on microneedle geometry.

Therefore, as the first study to examine the relationship between pain and micron-scale trauma to the skin, this study investigated the influence of microneedle design on pain by fabricating microneedles over a broad range of dimensions by varying microneedle length, width, thickness, tip angle and number of microneedles in an array; and comparing the pain they stimulated to a 26-gage hypodermic needle in healthy human subjects.

## 3.2 MATERIALS AND METHODS

### 3.2.1 Fabrication and assembly of stainless steel microneedles

Using methods described in detail previously (Gill and Prausnitz 2007a), microneedle geometries were first drafted in AutoCAD software (Autodesk, Cupertino, CA, USA) and then cut into 50, 75 or 125 μm thick stainless steel sheets (Trinity Brand Industries, SS 304; McMaster-Carr, Atlanta, GA, USA) using an infrared laser (Resonetics Maestro, Nashua, NH, USA). Single, in-plane microneedles (microneedle shafts oriented parallel to the base substrate) were fabricated in different geometries and thicknesses. 'Out-of-plane' microneedles (shafts bent at 90° to the base substrate) were fabricated as two-dimensional arrays after manually bending microneedles perpendicularly out of the plane of their base substrate. To deburr and clean microneedle edges and to make the tips sharp, microneedles were electropolished, washed under running water, dried using compressed air, and stored in air-tight containers until further use.

For insertion into skin, single microneedles were firmly held in slots axially cut through the flat ends of teflon rods (3 mm diameter, McMaster-Carr) and clamped using a one-piece shaft collar (McMaster-Carr). Out-of-plane microneedles were assembled into adhesive patches using methods described in detail previously (Gill and Prausnitz 2007a). Briefly, out-of-plane microneedle arrays were attached to a single-sided medical foam tape (TM9942, MACtac, Stow, OH, USA) and a perforated, double-sided, poly-ethylene-terephthalate carrier tape (63.5 μm thick; T04314A, MACtac) was then attached on top of the array with the microneedles passing through the perforations. The final patch had an adhesive layer surrounding the microneedles to hold the microneedles firmly against the skin after insertion. All the microneedles were assembled in a laminar

flow hood for cleanliness. The final microneedle-teflon rod assemblies were autoclaved and the microneedle adhesive patches were ethylene oxide sterilized (AN 74j, Andersen Sterilizers, Haw River, NC, USA) before use.

### 3.2.2 Pain study design

#### 3.2.2.1 Range of microneedle dimensions

Microneedle length, width, thickness, tip angle (Figure 3.1) and the number of microneedles were independently varied over a wide range to determine their influence on pain in human subjects. The following microneedle dimensions were investigated. Microneedle length: 480, 700, 960 and 1450 μm; microneedle tip angle: 20°, 55° and 90°; microneedle width: 160, 245 and 465 μm; microneedle thickness: 30, 45 and 100 □m; and the number of microneedles: 5 and 50. A 5-mm deep insertion of a 26-gage (outer diameter: 460 μm) hypodermic needle was used as a positive control for comparison with all the different microneedle insertions. The flat tip of a teflon rod pressed against the skin served as a negative control to account for possible pain associated with the teflon rod of the insertion device.

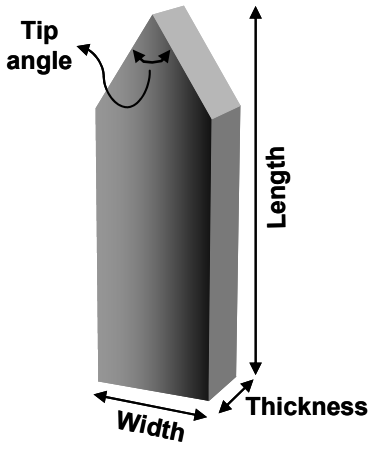


**Figure 3.1. Schematic of microneedle dimensions.** Typical geometry and characteristic dimensions of length, width, thickness and tip angle investigated during the pain study.

Because microneedle dimensions decrease from their AutoCAD design values during the laser cutting and electropolishing steps of the fabrication process, the final dimensions of the microneedles after fabrication were visually measured (n=5 for each dimension configuration) using a stereomicroscope (SZX12, Olympus America, Melville, NY, USA) and a precision micropositioning stage that was equipped with a digital readout display (Boeckeler Instruments, Tucson, AZ, USA). On average, the variability in the dimensions of the fabricated microneedles was low with a mean standard deviation of about 5% (range: 1 to 15%) for all the microneedle geometric parameters.

3.2.2.2 Statistical design

The study was carried out using the within-subject repeated measures design. In this design, all the subjects in a study received identical treatments, which allows for comparisons within the subjects, such that every subject acts as his or her own control (Neter, Kutner et al. 1996). To avoid carryover effects (i.e. influence of previous insertions) caused by too many insertions on a subject during a single session, the study was conducted in two stages. Each stage consisted of 10 subjects. The different

microneedle dimensions to be studied were divided between the two stages. In stage I, the effects of microneedle length and microneedle tip angle were investigated (Table 3.1); and in stage II, the effects of microneedle numbers, thickness and width were investigated (Table 3.1). All insertions were performed in triplicate for every subject.

#### 3.2.2.3 Randomization for bias reduction

To reduce investigator bias and subject preconceived bias to hypodermic needle pain, the subjects and the two investigators performing the study were blinded to the type of microneedle being inserted. Further, the location of insertions on the forearms was also randomized. This was done by stamping rectangular grids of dots onto the subjects' volar forearms using a custom-designed rubber stamp (Dixie Seals and Stamps, Atlanta, GA, USA) to demarcate 40 treatment sites, and then randomly distributing the insertions amongst the treatments sites, with a single insertion per site.

**Table 3.1.** Dimensions of microneedles used in the pain study

| | | Length (μm) | Width (μm) | Thickness (μm) | Tip angle | Number of micronedles |
|---|---|---|---|---|---|---|
| Stage I | Length study | 480 ± 10 | 160 ± 10 | 45 ± 5 | 55° | 1 |
| | | 700 ± 20 | | | | |
| | | 960 ± 20 | | | | |
| | | 1450 ± 10 | | | | |
| | Tip angle study | 480 ± 10 | 160 ± 10 | 45 ± 5 | 20° | 1 |
| | | | | | 55° | |
| | | | | | 90° | |
| | | 960 ± 20 | 160 ± 10 | 45 ± 5 | 20° | |
| | | | | | 55° | |
| | | | | | 90° | |
| Stage II | Number study | 620 ± 20 | 160 ± 10 | 45 ± 5 | 55° | 5 |
| | | | | | | 50 |
| | Thickness study | 700 ± 20 | 160 ± 10 | 30 ± 10 | 55° | 1 |
| | | | | 45 ± 5 | | |
| | | | | 100 ± 5 | | |
| | Width study | 700 ± 20 | 160 ± 10 | 45 ± 5 | 55° | 1 |
| | | | 245 ± 10 | | | |
| | | | 465 ± 10 | | | |
| | Positive* control | 5 mm deep insertion of a 26 gage hypodermic needle | | | | |

* Positive control used in both the stages of the pain study.

3.2.2.4 Volunteer recruitment

Normal human subjects were recruited from the student and staff population at the Georgia Institute of Technology (Atlanta, GA, USA). Allergy to stainless steel was used as the subject exclusion criteria. In addition, individuals conducting research with microneedles were excluded from the study to reduce subject bias. The use of human subjects in the pain study was approved by the Institutional Review Boards at the Georgia Institute of Technology and Emory University. There were three males and seven females (18 to 40 years of age) in each stage of the pain study, with four subjects common to both stages of the study.

3.2.2.5 Insertion protocol

Upon receiving written consent of the subjects, the forearms of the subjects were cleaned using isopropanol swabs (Becton and Dickinson, Franklin Lakes, NJ, USA). Next, the rubber stamp was stamped on the forearms of the subjects. Subjects were then introduced to the use of the visual analog scale (VAS). Throughout the study, the same investigator performed the insertions and the same second investigator performed the pain score measurement.

Insertions were performed manually on the volar forearms of the subjects with a gap of at least 30 s between insertions. All treatment sessions began with the insertion of a microneedle (55° tip angle, 700 μm long, 160 μm wide and 45 μm thick), a negative control teflon rod and a positive control hypodermic needle, in that order, to help the subjects understand the use of the VAS and calibrate their responses to the range of sensations to be encountered. The remaining insertions were then performed according to the randomized sequence for each subject, and pain scores were recorded. Insertion sites were visually examined to note signs of skin reaction. If bleeding was observed after hypodermic needle insertions, a cotton swab dipped in isopropanol was immediately applied to stop the blood flow.

Upon completion of the insertions, the dot-grid was removed using isopropanol swabs. The subjects were contacted after 24 h to check for any adverse sensations or reactions during that period.

3.2.2.6 Measurement of visual analogue pain scores

Each subject was presented with a ruler containing a 100-mm slot with “No Pain” written at the left end and “Worst Pain” at the right end. There were no other markings visible to the subject. Immediately after each insertion, the blinded subjects were asked to move the slider to the place along the slot that best described his or her pain. The

blinded observer recorded the location of the slider along the slot in millimeters, which was visible on the back side of the ruler.

3.2.2.7 Staining of insertion sites

To validate penetration of microneedles into the skin after insertion, three randomly-selected microneedle insertion sites on each subject of stage II of the pain study were stained with gentian violet (2% solution, Humco, Texarkana, TX, USA), a violet-colored topical antifungal agent that preferentially stains sites of microneedle penetration into skin, even after cleaning the skin with isopropanol. To prevent bias during insertion for sites to be stained, the investigator performing the insertions was blinded to the random sites requiring staining. Upon completion of all insertions, images of the stained sites were collected using a digital camera (DMC-TZ3S, Panasonic, Secaucus, NJ, USA).

### 3.2.3 Statistical analysis

VAS pain scores were analyzed for statistical significance using parametric tests on the basis of a previous study, which found no significant differences in conclusions between parametric and non-parametric tests analyzing VAS pain scores, even when the data were not normally distributed (Dexter and Chestnut 1995).

For each subject, average raw VAS pain scores (based on triplicate measurements) for each microneedle geometry were calculated and then normalized to the average raw hypodermic needle pain score to account for the variability in a subject's perception of hypodermic needle pain and thereby provide a common reference point. Because all the negative controls had a VAS score of zero (no pain), no adjustment to the raw VAS scores was necessary to account for pain caused by the microneedle insertion device. The percentage of subjects reporting painless insertions

(i.e., VAS = 0) for each microneedle geometry was also reported. Box plots for raw and normalized VAS pain scores were plotted to show the range and variation of the pain scores across the subjects (Minitab, ver. 15, State College, PA, USA).

To identify if the microneedles and the 26 gage hypodermic needle produce significantly different pain sensations, an omnibus F-test was conducted for each stage of the pain study using the raw (unaveraged) VAS pain scores of all the microneedle configurations and the 26 gage hypodermic needle (repeated measures ANOVA test, NCSS, Kaysville, Utah, USA), where $p<0.05$ was considered statistically significant. When Mauchly's test indicated that the compound symmetry assumption used in this test was invalid, the lower bound F-statistic was calculated and the corresponding corrected p-value was reported. Finally, Tukey's multiple comparison test was used to identify microneedle configurations significantly different in pain level from the hypodermic needle.

To compare pain levels amongst different microneedle designs, the normalized VAS pain scores for each microneedle geometry were statistically tested using the repeated measures ANOVA method (NCSS), where $p<0.05$ was considered statistically significant, followed by Tukey's multiple comparison test.

## 3.3 RESULTS

### 3.3.1 Microneedle fabrication and insertion into skin

Microneedles were fabricated with a range of geometries in order to compare pain between microneedles and a hypodermic needle, and to quantify differences in pain resulting from different microneedle designs. To determine the effect of microneedle geometry, single microneedles of different lengths (Figure 3.2 A), widths (Figure 3.2 B),

tip angles (Figure 3.2 C) and thicknesses (Figure 3.2 D) were fabricated. To study the influence of the number of microneedles, arrays of microneedles with 5 or 50 microneedles were also fabricated (Figure 3.2 E). To facilitate handling, single microneedles (Figure 3.3 A) and arrays of microneedles (Figure 3.3 B and 3.3C) were mounted onto holders.

To verify that microneedles penetrated into the skin, three randomly selected sites on each subject of stage II were stained with gentian violet as described in the Materials and Methods section. This protocol selectively stained sites of skin perforation, as shown in the representative images for a single microneedle (Figure 3.3 D), a microneedle array with 5 microneedles (Figure 3.3 E) and a microneedle array with 50 microneedles (Figure 3.3 F). Analysis of images from all of the stained sites on all subjects indicated successful microneedle penetration into the skin in all cases (data not shown).

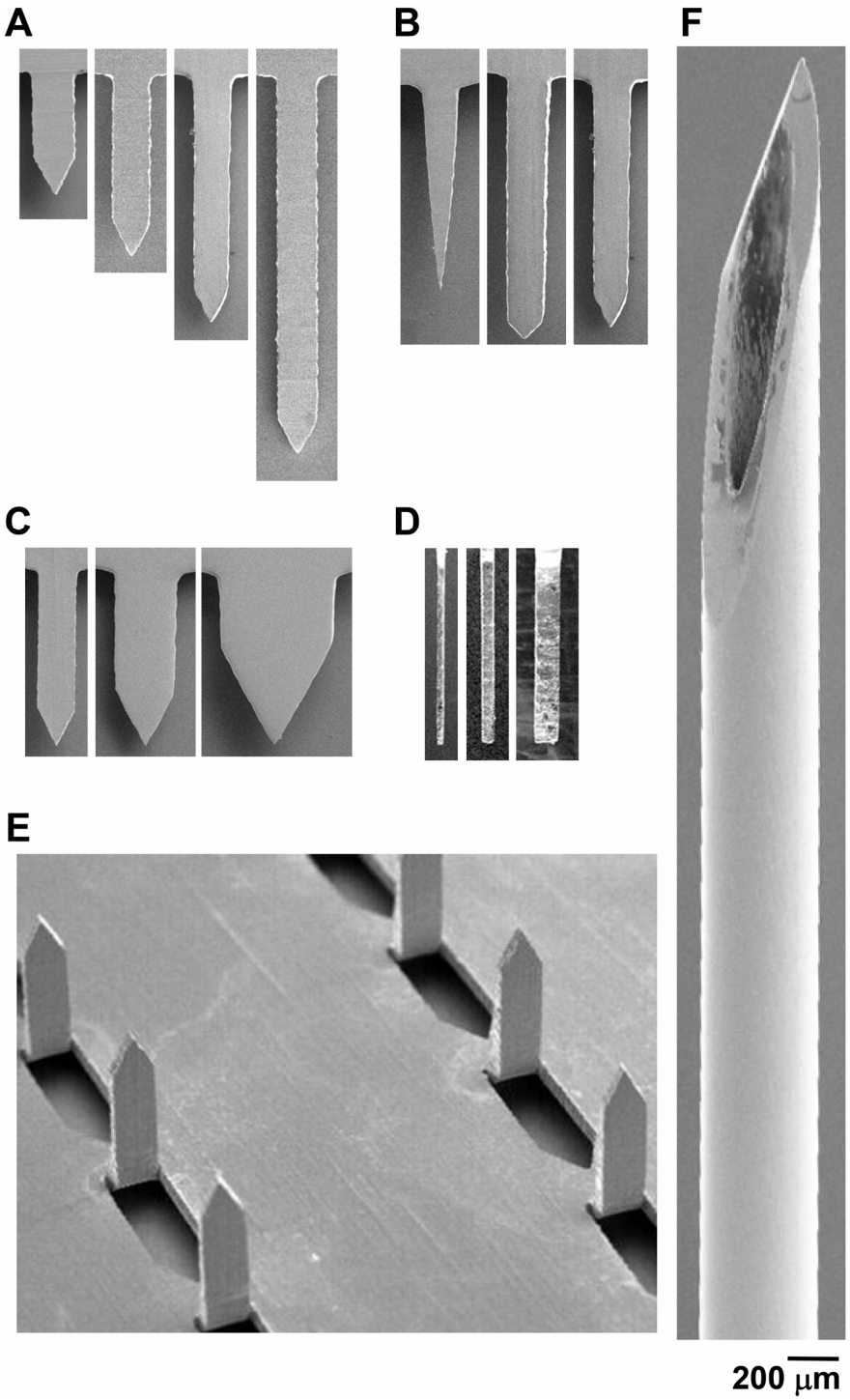


**Figure 3.2. Representative microneedles used for insertion**. Scanning electron microscopy images of microneedles used in the length study (A), tip-angle study (B), width study (C), thickness study (side view) (D) and number of microneedles study (E). A 5 mm-long, 26-gage hypodermic needle was used as a positive control (F). All images are at the same magnification.

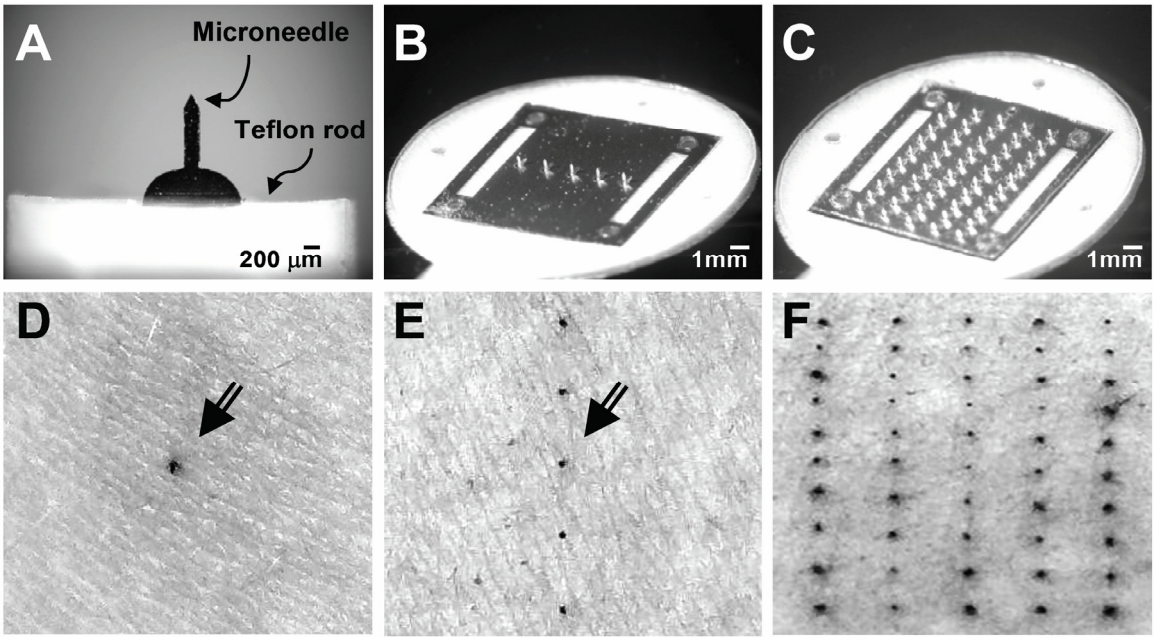


**Figure 3.3. Microneedle devices and stained skin penetration sites**. Brightfield microscopy images of microneedles assembled into devices: a single microneedle affixed to a teflon rod holder (A), a five-microneedle array assembled as an adhesive patch (B) and a 50-microneedle array assembled as an adhesive patch (C). Brightfield microscopy images of the skin surface of human forearms after inserting microneedles and applying gentian violet to stain the sites of microneedle insertion, which demonstrates microneedle penetration into the skin, using: a single microneedle (D), an array of five microneedles (E) and an array of 50 microneedles (F). Arrows in (D) and (E) point to the stained insertion sites.

### 3.3.2 Microneedles vs. 26-gage hypodermic needle

Our next objective was to determine if microneedles cause less pain than a 26-gage hypodermic needle. We compared the pain reported for a hypodermic needle to microneedles over a range of dimensions that varied length (480, 700, 960 and 1450 μm), width (160, 245 and 465 μm), thickness (30, 45 and 100 μm), tip angle (20°, 55° and 90°) and the number of microneedles (5 and 50). A 5-mm deep insertion of a 26-gage hypodermic needle was used as a positive control. Although hypodermic needles are inserted clinically for example, 8 to 12 mm deep during vaccination (2006) and insulin delivery (Hanas, Lytzen et al. 2000; Hanas 2004), we restricted the insertion depth in this study to 5 mm in order to reduce the possibility of bleeding, which could complicate analysis.

Among stage I data, the raw VAS pain scores for microneedles ranged from a minimum of 2±2 mm (mean ± standard deviation) to a maximum of 15±17 mm, whereas the pain score for the hypodermic needle was 39±21 mm. In stage II, the microneedle pain scores ranged from a minimum of 2±2 mm to a maximum of 11±9 mm and the hypodermic needle pain score was 24±16 mm. Based on repeated measures ANOVA, each of the microneedles was found to have a pain score significantly smaller than the hypodermic needle positive control (Tukey's pairwise comparison, $p < 0.05$). These results demonstrate that all the microneedles over a wide range of dimensions investigated in this study were less painful than the 26-gage hypodermic needle.

### 3.3.3 Effect of microneedle length

To study the dependence of pain on microneedle geometry, we hypothesized that increasing microneedle length should increase pain, because pain receptors innervate both the epidermis and the dermis, and longer penetrations should therefore excite more receptors (Oaklander and Siegel 2005). Consistent with this hypothesis, mean pain scores increased with increasing microneedle length, over a range of 2±2 mm for the shortest microneedles (480 μm) to 15±17 mm for the longest (1450 μm) (corrected lower bound p=0.03) (Figure 3.4 A). In addition to calculating mean pain scores, we also tabulated the fraction of subjects who reported each microneedle treatment as completely painless (i.e. VAS pain score = 0). This analysis showed that the frequency of painless insertions decreased with an increase in microneedle length: 30% of subjects reported both the 480 μm and the 700 μm long microneedles as completely painless, whereas just 0% and 10% reported the 960 μm and 1450 μm long microneedles painless, respectively.

Although raw pain scores generally showed variability among subjects, hypodermic needle pain was especially variable, ranging from 7 mm to 63 mm, with a mean value of 39 mm. Because of this large inter-subject variability in pain perception, we re-analyzed the data by normalizing all the microneedle VAS scores from each subject to that subjects's own hypodermic needle control. In this way, all data are presented relative to a common reference pain level that is familiar to most people and of direct relevance to medical applications.

Carrying out a more detailed analysis using these normalized pain scores indicated that the 480 μm long microneedles produced just 5% of the pain of the 26-gage hypodermic needle (Figure 3.4 B). Increasing microneedle length sharply increased pain, such that a three-fold increase in the microneedle length from 480 μm to 1450 μm caused the pain to increase more than seven fold from 5% to 37% (corrected lower bound $p = 0.013$).

Comparing pairwise among the microneedles: (i) increasing microneedle length by at least 700 μm (i.e., 480 μm vs. 1450 and 750 μm vs. 1450 μm) significantly increased pain levels (Tukey's multiple comparison, $p < 0.002$); increasing microneedle length by 480 – 490 μm sometimes increased pain significantly (i.e., 480 μm vs. 960 μm, $p = 0.02$) and sometimes did not (960 μm vs. 1450 μm, $p = 0.38$); and (iii) increasing microneedle length by up to 260 μm (i.e., 480 μm vs. 700 μm and 700 μm vs. 960) did not significant increase pain (Tukey's multiple comparison, $p > 0.1$). This analysis suggests that the threshold for distinguishing differences in pain due to increment in microneedle length was approximately 500 μm .

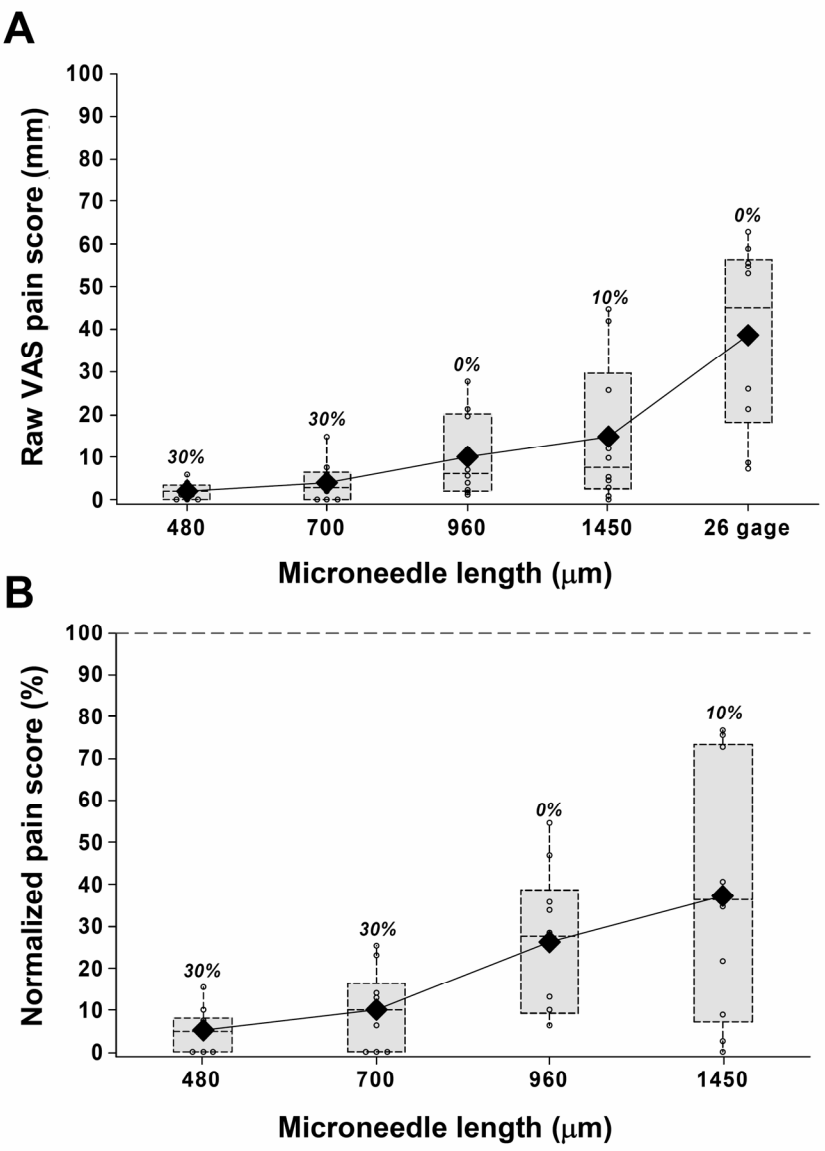


**Figure 3.4. The effect of microneedle length.** Box plots of pain scores after insertion of 480, 700, 960 and 1450 μm long single microneedles (160 μm wide, 45 μm thick and a tip angle of 55°): raw visual analog scale (VAS) pain scores (A) and the normalized pain scores (B), which were calculated as the ratio of the microneedle raw VAS score and the 26-gage hypodermic needle raw VAS pain score for the same subject. The normalized pain score of the hypodermic needle (i.e., 100%) is represented by the horizontal dotted line in (B). The small open circles represent individual data points. Each dotted rectangular box represents the interquartile range (i.e., 25 – 75%) of the pain score for a particular microneedle length, with a horizontal line at the median value. The vertical lines (whiskers) extend from the box boundary to the maximum and the minimum data points within one and a half times the interquartile range. The solid diamonds represent the mean pain scores for each insertion. The numbers above each box present the percentage of subjects who reported the insertions to be painless (i.e., VAS pain score of zero).

### 3.3.4 Effect of the number of microneedles

Drug and vaccine delivery applications will often require multiple microneedles. We hypothesized that increasing the number of microneedles should increase pain, because more sensory nerves would be excited using a larger number of microneedles. Microneedle arrays with 5 or 50 microneedles were used to test this hypothesis. Insertion of a 5-microneedle array caused pain at a low level, corresponding to 10% of the hypodermic needle (Figure 3.5). A 10-fold increase in the number of microneedles to a 50-microneedle array produced a relatively small increase in the pain of just 2.5 fold ($p=0.004$), which corresponded to 25% of the hypodermic needle. The arrays with 5 and 50 microneedles were reported to be completely painless by 40% and 20% of the subjects, respectively.

### 3.3.5 Effect of microneedle tip angle

We next hypothesized that larger tip angles would cause more tissue deformation during microneedle insertion and thereby cause more pain than microneedles with smaller tip angles. To test this hypothesis, we examined microneedles with tip angles of 20°, 55° and 90°, each at two different lengths of 480 μm and 960 μm.

At both microneedle lengths tested, no consistent or statistically significant ($p > 0.12$) relationship was observed between mean pain scores and microneedle tip angle over the relatively large range of tip angles considered (20° to 90°) (Figure 3.6). For the 480 μm long microneedles, the percentage of subjects reporting completely painless insertions decreased with increasing tip angles, but there was no such trend for the 960 μm long microneedles (Figure 3.6). Additional experiments using 960 μm long microneedles at the same tip angles, but with an increased microneedle thickness from

40 μm to 100 μm similarly showed no dependence of pain on microneedle tip angle (data not shown).

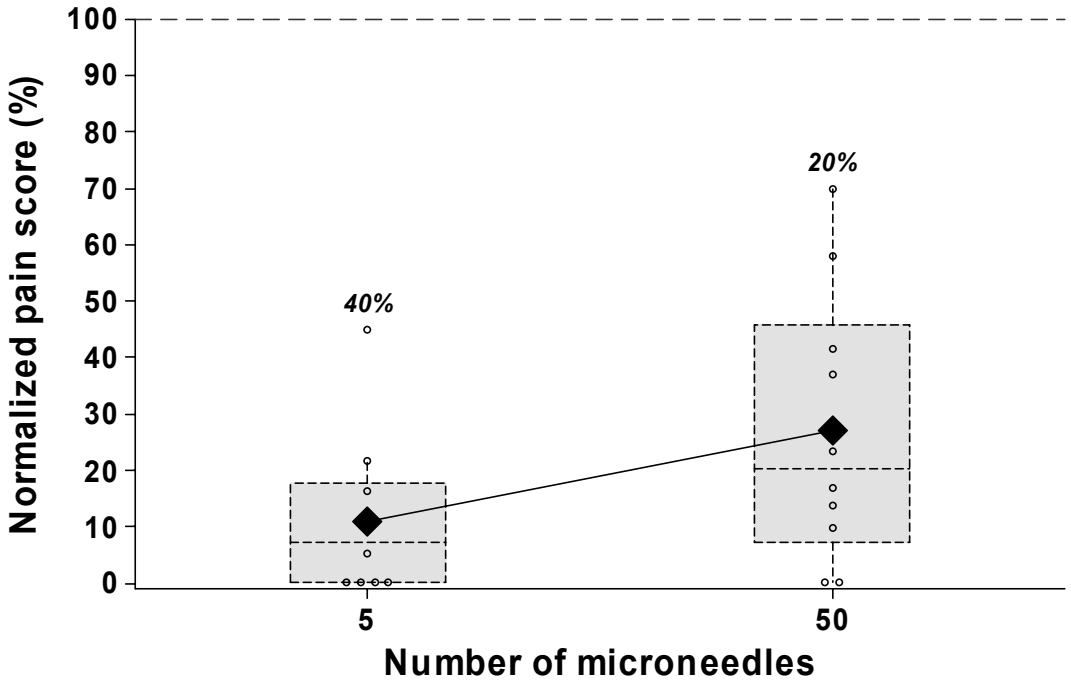


**Figure 3.5. The effect of the number of microneedles**. Box plots of normalized pain scores after insertion of microneedle arrays having 5 and 50 microneedles. All microneedles were 620 μm long, 160 μm wide, 45 μm thick and had a tip angle of 55°.

This finding was contrary to our original hypothesis. To understand this observation, we examined the microneedle tips using high-magnification scanning electron microscopy and found them to be extremely sharp, with a radius of curvature less than 1 μm independent of tip angle. This suggests that pain may correlate with sharpness at the very tip of the microneedle, rather than the overall angle of the tip. A previous study found that the force required for microneedle insertion into skin also

scaled with microneedle tip sharpness (Davis, Landis et al. 2004), which indicates that the force of insertion may correlate with pain. This would be consistent with previous studies involving hypodermic needles, which found that the intensity of pain scales with mechanical workload (area under the force-displacement curve) of hypodermic needle insertion (Egekvist, Bjerring et al. 1999a; Egekvist, Bjerring et al. 1999b). Altogether, these observations suggest a new hypothesis that pain depends primarily on the force of microneedle tip insertion and the depth to which the microneedle tip penetrates into the skin.

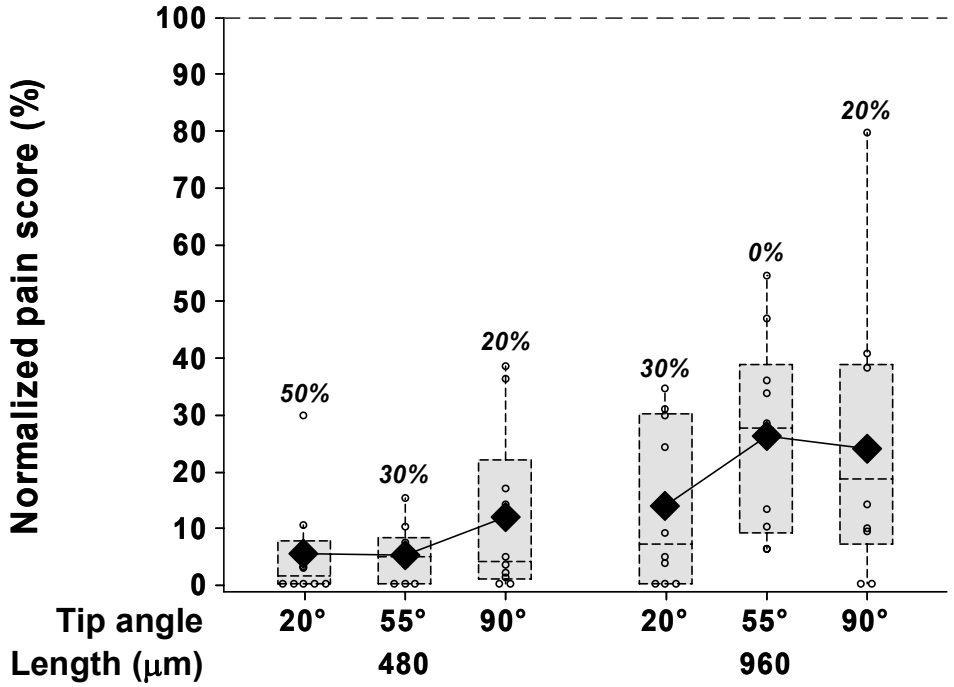


**Figure 3.6. The effect of microneedle tip angle**. Box plots of normalized pain scores after insertion of 480 and 960 μm long single microneedles each with a tip angle of 20°, 55° and 90°. All microneedles were 160 μm wide and 45 μm thick.

### 3.3.6 Effect of microneedle thickness and width

Our last hypothesis was that increased microneedle thickness and width would cause more pain by engaging more pain receptors during insertion. To test this hypothesis, microneedles with thicknesses of 30, 45 and 100 μm and widths of 160, 245, and 465 μm were examined. In contrast to this hypothesis, neither increasing microneedle thickness by more than three fold ($p = 0.6$, Figure 3.7 A) nor increasing microneedle width by almost three fold ($p = 0.30$, Figure 3.7 B) had a significant effect on pain scores.

These observations are, however, consistent with previous reports that pain is independent of needle diameter for lancets with diameters of 800, 400 and 300 μm inserted to a depth of 900 μm (Fruhstorfer, Schmelzeisen-Redeker et al. 1999). They are also consistent with the new hypothesis that pain depends primarily on the force of microneedle tip insertion and not on other features of the microneedle shaft geometry other than length. In contrast, a study of hypodermic needles found that the likelihood of an insertion being painful increased with increasing needle diameter, but also noted that the intensity of those insertions rated as painful was insensitive to needle diameter (Arendt-Nielsen, Egekvist et al. 2006).

### 3.3.7 Skin reaction to insertions

In addition to pain, microneedle insertions into the skin could cause skin irritation. Visual observation of the skin immediately after microneedle insertion revealed highly localized, mild erythema in the form of a light pink dot less than 1 mm across, which was observed at all microneedle insertion sites independent of microneedle geometry. Although this redness could be observed upon direct examination, essentially no cosmetic effect was evident when subjects were viewed from a distance. The erythema

decreased somewhat during the 2 h study period and was self-reported by the subjects to be mostly resolved when they were contacted after 24 h. There were no signs of edema after any microneedle insertions.

The appearance of a tiny droplet of blood (e.g., 1 μl) was observed at the insertion site after some microneedle insertions, especially those involving 1450 μm long microneedles. The shorter microneedles (i.e. 480 and 700 μm) did not result in bleeding.

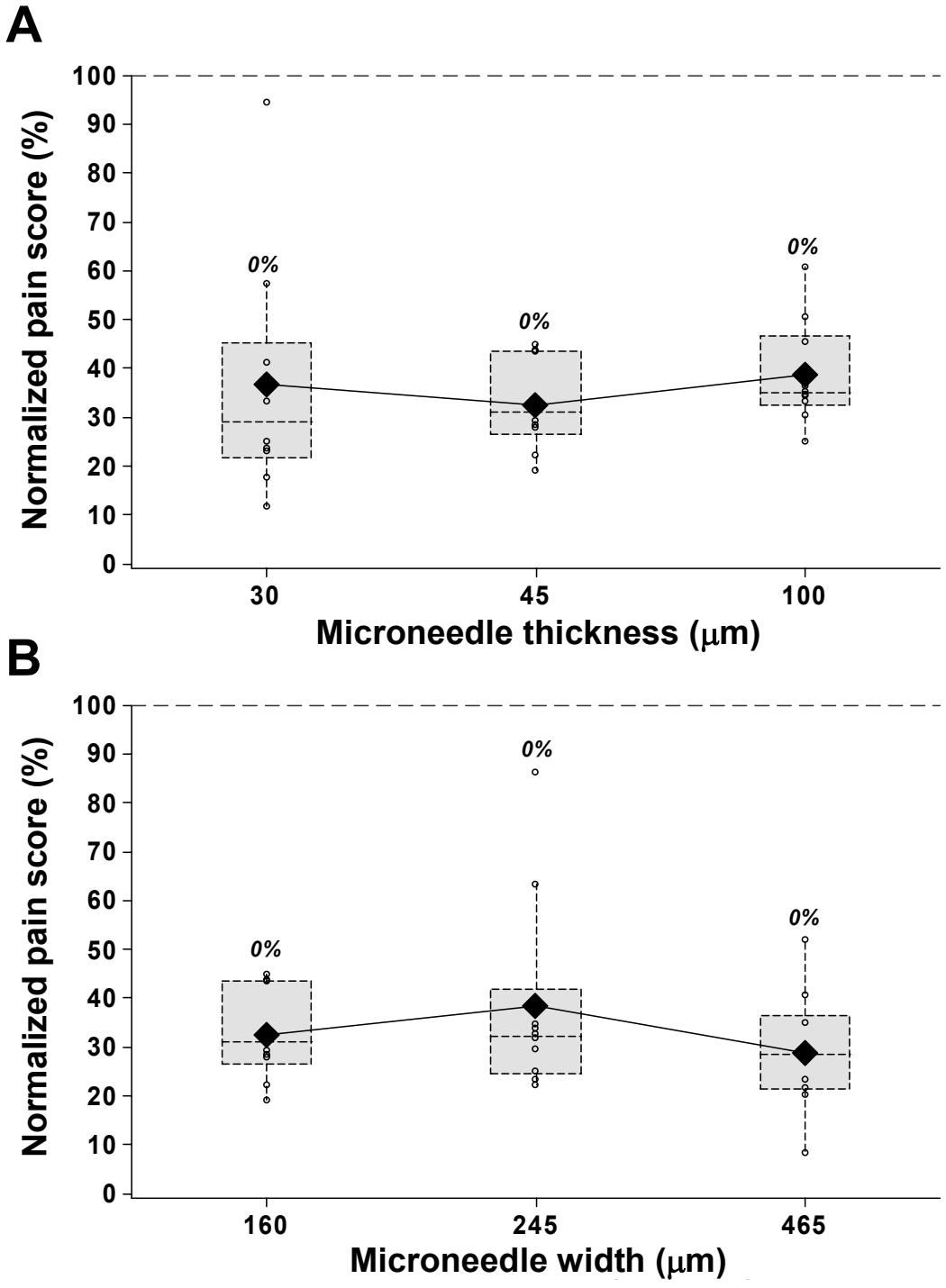


**Figure 3.7. The effect of microneedle thickness and width**. Box plots of normalized pain scores after insertion of 30, 45 and 100 μm thick single microneedles each 700 μm long, 160 μm wide and with a tip angle of 55° (A); and 160, 245 and 465 μm wide single microneedles each 700 μm long, 45 μm thick and with a tip angle of 55° (B).

## 3.4 DISCUSSION

### 3.4.1 Degree of pain reduction

This study shows that microneedles caused significantly less pain than a 26-gage hypodermic needle. Using the shortest microneedles, pain scores were reduced by a factor of 20 compared to the hypodermic needle. Overall, pain scores from the diversity of microneedle geometries considered ranged from 5 to 40%, which was highly significant by statistical analysis. This level of pain reduction could also be significant to reduce needle anxiety and phobia.

Even though the pain reduction reported in this study is considerable, the degree of pain reduction from microneedle-based drug delivery is expected to be still greater. First of all, hypodermic needles are typically inserted 8 to 12 mm deep into the skin (Hanas, Lytzen et al. 2000; Hanas 2004; 2006). In this study, we limited the insertion depth to just 5 mm to minimize bleeding. Because pain is known to depend strongly on device insertion depth, as shown in this study and in the literature (Fruhstorfer, Müller et al. 1995) , the actual pain caused by hypodermic needles in clinical practice is expected to be greater than in this study and thus the relative reduction in pain by using microneedles should also be greater.

In addition, the act of injecting fluid into the skin can itself cause pain, which means that the positive control hypodermic needle insertion used in this study is an even greater underestimate of the pain caused by hypodermic injection. Because solid microneedles do not involve fluid injection for drug delivery, the pain associated with fluid injection would also be eliminated. For these reasons, the relative decrease in pain enabled by the use of microneedles reported in this study is based on a conservative study design. Even greater pain reduction should be expected from drug delivery using solid microneedles as compared to actual hypodermic injections.

It should be noted that this analysis does not take into account pain that could be caused by local irritation by the drug formulation. Solid microneedles deliver a solid drug formulation into the skin, whereas hypodermic injection delivers a liquid drug formulation typically into deeper tissues. These differences may further influence pain in some cases.

### 3.4.2 Microneedle device optimization

Optimization of a microneedle device requires selecting microneedle dimensions and overall design that meets a number of constraints, including minimizing pain, providing sufficient mechanical strength for insertion into the skin, and delivering the required dose in a manner suitable for the target population. To guide optimization that minimizes pain, this study supported the hypothesis that decreasing microneedle length and the number of microneedles reduces pain. It also showed that microneedle tip angle, thickness and width did not have a significant effect on pain score. Altogether, these observations suggested an additional hypothesis that pain depends primarily on the force of microneedle tip insertion and the depth to which the microneedle tip penetrates into the skin, but not on other features of the microneedle shaft geometry besides length. Validation of this new hypothesis requires additional study.

These findings suggest that an optimal microneedle design should involve a small number of short microneedles. Due to the much steeper dependence of pain on microneedle length compared to the number of microneedles, minimizing length should be especially important. For ease of insertion (Davis, Landis et al. 2004) and possible reduction in pain, microneedle tips should also be sharp. Although microneedle thickness, width and tip angle do not appear to affect pain, they do affect microneedle mechanical strength (Davis, Landis et al. 2004; Park, Allen et al. 2005) and therefore need to be considered.

### 3.4.3 Reduction of anxiety and needle phobia

The microscopic dimensions of microneedles may further decrease the perception of pain due to their patient-friendly appearance. It is well known that pain from the use of hypodermic needles can produce poor patient compliance and that needle phobia produces stress, anxiety and vasovagal reaction, which can interfere with treatments that use needles (Hamilton 1995; Nir, Paz et al. 2003; Hanas 2004). Recent research using stress-reducing medical devices involving decorative and aesthetically pleasing syringes has shown significant reduction in needle phobia (Kettwich, Sibbitt et al. 2007). Microneedles should offer similar advantages, due to their small size, inconspicuous profile and ability to be incorporated into Band Aid-like patches that can be aesthetically pleasing and easy to use. Although this blinded study did not assess this aspect of microneedles, we expect microneedle patches to be patient friendly and thereby further reduce anxiety and the perception of pain.

## 3.5 CONCLUSION

This study investigated the influence of microneedle design and geometry on pain and compared it to the pain from a hypodermic needle. Based on statistical analysis of the raw VAS scores, we found that all 18 of the microneedle configurations studied, including lengths up to 1450 μm, widths up to 465 μm, thicknesses up to 100 μm, tip angles up to 90˚, and as many as 50 microneedles in an array, were significantly less painful than a 5-mm deep insertion of a 26-gage hypodermic needle (outer diameter: 460 μm). The shortest (480 μm) microneedles produced pain scores that were 20-fold lower than the hypodermic needle. Further, many microneedle insertions were entirely painless (as much as 50% of the subjects reported VAS scores of zero for the 480 μm

long and 20° tipped microneedle), as compared to the hypodermic needle, for which none of the subjects reported the insertions to be painless.

Analysis of the normalized VAS pain scores of the different microneedle designs showed that microneedle length was the most influential factor affecting pain. A three-fold increase in microneedle length produced more than a seven-fold increase in pain. The number of microneedles was also significant in affecting pain, although less steeply. A ten-fold increase in the number of microneedles increased the pain score only by about 2.5 times, such that the pain score from a 50-microneedle array was still just 25% of the pain caused by a single hypodermic needle. No statistically significant effect was observed due to changes in microneedle tip angle, width or thickness over the range investigated. Altogether, these observations suggested a new hypothesis that pain depends primarily on the force of microneedle tip insertion and the depth to which the microneedle tip penetrates into the skin, but not on other features of the microneedle shaft geometry besides length.

In conclusion, this study demonstrates that microneedles over a wide range of dimensions are significantly less painful than a 26-gage hypodermic needle and that decreasing microneedle length and number of microneedles reduces pain. These findings give insight into the thresholds and parameters that control pain due to micron-scale trauma to the skin and provide a rational basis to optimize microneedle geometry for drug delivery applications that minimize pain.

# CHAPTER 4: COATED MICRONEEDLES FOR TRANSDERMAL DELIVERY[2]


## ABSTRACT

Coated microneedles have been shown to deliver proteins and DNA into the skin in a minimally invasive manner. However, detailed studies examining coating methods and their breadth of applicability are lacking. This study's goal was to develop a simple, versatile and controlled microneedle coating process to make uniform coatings on microneedles and establish the breadth of molecules and particles that can be coated onto microneedles. First, microneedles were fabricated from stainless steel sheets as single microneedles or arrays of microneedles. Next, a novel micron-scale dip-coating process and a GRAS coating formulation were designed to reliably produce uniform coatings on both individual and arrays of microneedles. This process was used to coat compounds including calcein, vitamin B2, bovine serum albumin and plasmid DNA. Modified vaccinia virus and microparticles of 1 to 20 μm diameter were also coated. Coatings could be localized just to the needle shafts and formulated to dissolve within 20 s in porcine cadaver skin. Histological examination validated that microneedle coatings were delivered into the skin and did not wipe off during insertion. In conclusion, this study presents a simple, versatile, and controllable method to coat microneedles with proteins, DNA, viruses and microparticles for rapid delivery into the skin.


[2] This work has been published as: Gill, H. S. and M. R. Prausnitz (2007). "Coated microneedles for transdermal delivery." J Control Release 117(2): 227-237.

## 4.1 INTRODUCTION

Biopharmaceuticals, such as peptides, proteins and future uses of DNA and RNA, represent a rapidly growing segment of pharmaceutical therapies (Walsh 2005). These biotechnology drugs are currently delivered almost exclusively by the parenteral route. The oral route is generally not available, due to poor absorption, drug degradation and low bioavailability. This is problematic, because parenteral administration with hypodermic needles requires expertise for delivery, can lead to transmission of blood borne pathogens due to accidental needle sticks or intentional needle reuse, and causes pain, which results in reduced patient compliance due to needle phobia (Simonsen, Kane et al. 1999; Nir, Paz et al. 2003).

Given these problems, a breadth of research activity has focused on replacing hypodermic needles with alternate drug delivery methods (Orive, Hernandez et al. 2003). Transdermal drug delivery is an especially attractive alternative, because it is usually easy to use, safe, and painless (Barry 2004; Prausnitz, Mitragotri et al. 2004). However, the tough barrier posed by the skin's outer layer of stratum corneum has limited the applicability of this method to drugs that are hydrophobic, low molecular weight, and potent.

Micron-scale needles assembled on a transdermal patch have been proposed as a hybrid between hypodermic needles and transdermal patches to overcome the individual limitations of both injections and patches (Prausnitz 2004; Prausnitz, Mikszta et al. 2005). Microneedles have been shown to be painless in human subjects relative to hypodermic needles (Kaushik, Hord et al. 2001; Mikszta, Alarcon et al. 2002). Unlike transdermal patches, microneedles have been successfully used to deliver a variety of large and hydrophilic compounds into the skin, including proteins and DNA. In vitro skin permeability enhancement of two to four orders of magnitude was observed for small molecules like calcein and large compounds like proteins and nanoparticles (Henry,

McAllister et al. 1998; McAllister, Wang et al. 2003). In vivo delivery has been shown for peptides, such as insulin and desmopressin (Cormier, Johnson et al. 2004; Martanto, Davis et al. 2004); genetic material, including plasmid DNA and oligonucleotides (Lin, Cormier et al. 2001; Chabri, Bouris et al. 2004); and vaccines directed against hepatitis B, anthrax and Japanese encephalitis (Mikszta, Alarcon et al. 2002; Dean, Alarcon et al. 2005; Mikszta, Sullivan et al. 2005). Microneedles can be fabricated for these applications by adapting the tools of the microelectronics industry for inexpensive, mass production (Reed and Lyev 2004).

Currently, four different modes of microneedle-based drug delivery have been investigated (Prausnitz 2004; Prausnitz, Mikszta et al. 2005). These modes are: (1) piercing an array of solid microneedles into the skin followed by application of a drug patch at the treated site (Henry, McAllister et al. 1998; Martanto, Davis et al. 2004); (2) coating drug onto microneedles and inserting them into the skin for subsequent dissolution of the coated drug within the skin (Cormier, Johnson et al. 2004); (3) encapsulating drug within biodegradable, polymeric microneedles followed by insertion into skin for controlled drug release (Park, Allen et al. 2006); and (4) injecting drug through hollow microneedles (Zahn, Talbot et al. 2000).

Among these approaches, coated microneedles are attractive for rapid bolus delivery of high molecular weight molecules into the skin, and can be implemented as a simple ‘Band-Aid’-like system for self-administration. Further, storing drugs in a solid phase as a coating on microneedles may enhance their long-term stability, even at room temperature. Consistent with this expectation, desmopressin coated onto microneedles maintained 98% integrity after 6 months storage under nitrogen at room temperature (Cormier, Johnson et al. 2004). Coated microneedles are also especially attractive for vaccine delivery to the skin, because antigens can be released in the skin to target epidermal Langerhans cells and dermal dendritic cells for a more potent immune

response (Babiuk, Baca-Estrada et al. 2000). As a demonstration of this, a strong immune response in guinea pigs was shown against ovalbumin, a model antigen delivered from coated microneedles (Matriano, Cormier et al. 2002).

Despite the attractiveness of coated microneedles, a detailed investigation of the coating process has not been published. In this study, we therefore wanted to develop a microneedle coating process that elucidated issues involved in coating microneedles and to identify the breadth of applicability of coated microneedles by determining the different kinds of molecules and particles that can be coated and delivered into the skin. This study was guided by identifying essential characteristics needed for the microneedle coating process to achieve precise dose control, safety, and the ability to coat sensitive biological molecules. The coating process should: (1) make a uniform coating as opposed to a patchy coating to provide reproducibility and dosage control, (2) limit deposition only onto microneedles and not on the base substrate for tight dosage control and minimizing drug loss during coating, (3) avoid high temperatures to maintain drug integrity, (4) use aqueous coating solution to prevent denaturing of proteins and other biological molecules, (5) achieve high drug loading per microneedle to maximize drug dosage, (6) provide good adhesion of the coating to the microneedle to prevent wiping off on the skin during insertion and (7) have rapid, or otherwise controlled, dissolution kinetics in the skin for bolus, or sustained, release.

Among the various coating processes, such as dip coating, roll coating and spray coating (Bierwagen 1992), dip coating is particularly appealing for coating microneedles because of its simplicity and its ability to coat complex shapes. A dip-coating process typically involves dipping and withdrawing an object from a coating solution, after which a continuous liquid film adheres and dries on the object's surface, leaving behind a uniform coating. However, dip coating has been developed to coat macroscopic objects mostly by submerging them completely within the coating solution. Because surface

tension becomes dominant on the micron scale (Beebe, Mensing et al. 2002), conventional dip-coating methods have difficulty controlling coating of specified sections of micron-dimensioned structures, especially when those structures are closely spaced. This study sought to addresses these limitations by developing a micron-scale, dip-coating process to coat microneedles with uniform and spatially controlled coatings using methods applicable to a breadth of drugs and biopharmaceuticals.

## 4.2 MATERIALS AND METHODS

### 4.2.1 Microneedle fabrication

#### 4.2.1.1 Laser cutting

Using methods described previously (Martanto, Davis et al. 2004), microneedles were cut from stainless steel sheets (Trinity Brand Industries, SS 304, 75 μm thick; McMaster-Carr, Atlanta, GA, USA) using an infrared laser (Resonetics Maestro, Nashua, NH, USA). The desired microneedle shape and dimensions were first drafted in AutoCAD software (Autodesk, Cupertino, CA, USA). Using this design, the infrared laser was operated at 1000 Hz, 20 J/cm$^2$ energy density and 40% attenuation of laser energy to cut microneedles. A total of three passes were required to completely cut through the stainless steel sheet. A cutting speed of 2 mm/s and air purge at a constant pressure of 140 kPa was used. Microneedles were either prepared as individual rows of needles ('in-plane' needles) or as two-dimensional arrays of needles cut into the plane of the stainless steel sheet and subsequently bent at 90° out of the plane ('out-of-plane' needles).

#### 4.2.1.2 Cleaning and bending microneedles

Laser-cut stainless steel microneedle arrays were manually cleaned with detergent (Alconox, White Plains, NY, USA) to de-grease the surface and remove slag and oxides deposited during laser cutting, which was followed by thorough rinsing in running water. To prepare 'out-of-plane' microneedles, microneedles cut into stainless steel sheets were first manually pushed out of the sheet using either forceps or a hypodermic needle (26 gage, ½ inch long, Becton Dickinson, Franklin Lakes, NJ, USA) while viewing under a stereo microscope (SZX12, Olympus America, Melville, NY, USA), and then bent at 90° angle with the aid of a #9 single-edged razor blade.

#### 4.2.1.3 Electropolishing

To deburr and clean microneedle edges and to make the tips sharp, microneedles were electropolished in a solution containing glycerin, ortho-phosphoric acid (85%) and water in a ratio of 6:3:1 by volume (Fisher Scientific, Fair Lawn, NJ, USA). Electropolishing was performed in a 300 ml glass beaker at 70°C and a stirring rate of 150 rpm. A copper plate was used as the cathode, while microneedles acted as the anode. The anode was vibrated at a frequency of 10 Hz throughout the electropolishing process using a custom built vibrating device to help remove gas bubbles generated at the anodic surface during electropolishing. A current density of 1.8 $mA/mm^2$ was applied for 15 min to electropolish the microneedles. After electropolishing, microneedles were cleaned by dipping alternately three times in de-ionized water and 25% nitric acid (Fisher Scientific) for 30 s each. This was followed by another washing step in hot running water and a final wash in running de-ionized water. Due to the electropolishing process, the thickness of the microneedles was reduced to 50 μm. Microneedles were dried using compressed air before storing in air-tight containers until later use.

### 4.2.2 Micro-dip coating

Microneedles were coated with different molecules using a novel micron-scale, dip-coating process and a specially formulated coating solution.

#### 4.2.2.1 Coating solution

The coating solution was composed of 1% (w/v) carboxymethylcellulose sodium salt (low viscosity, USP grade, CarboMer, San Diego, CA, USA), 0.5% (w/v) Lutrol F-68 NF (BASF, Mt. Olive, NJ, USA) and a model drug/biopharmaceutical. The model drugs tested included 0.01% suforhodamine (Molecular Probes, Eugene, OR, USA), 0.01% calcein (Sigma, St. Louis, MO, USA), 3% vitamin B2 (riboflavin-5'-phosphate sodium salt dihydrate, Fisher Chemicals), 1% bovine serum albumin conjugated to Texas Red (Molecular Probes), 0.05% gWiz™ luciferase plasmid DNA (6732 base pairs, Aldevron, Fargo, ND, USA), 2 x $10^9$ plaque forming units per ml of modified vaccinia virus – Ankara (Emory University Vaccine Center, Atlanta, GA, USA), 10% barium sulfate particles (1 μm diameter, Fisher Scientific), 1.2 % 10-μm diameter latex beads (PN 6602796, Beckman Coulter, Miami, FL, USA) and 8.2% 20-μm diameter latex beads (PN 6602798, Beckman Coulter ), all w/v. DNA and virus were made fluorescent by incubating with YOYO-1 (Molecular Probes) at a dye:base pair/virus ratio of 1:5 for 1 h at room temperature in the dark.

#### 4.2.2.2 Coating single microneedles

Single microneedles were dip-coated by horizontally dipping the microneedle into 20-30 μl of coating solution held as a droplet on the tip of a 200 μl large-orifice pipette tip (catalogue number 21-197-2A, Fisher Scientific). The large-orifice pipette tip was mounted horizontally in a clamp and the microneedle was mounted opposite to it on a

manual linear micropositioner (A1506K1-S1.5 Unislide, Velmex, Bloomfield, NY, USA). Immersion and withdrawal of the microneedle into the liquid droplet was performed manually by moving the microneedle while viewing under a stereomicroscope (SZX12, Olympus America).

#### 4.2.2.3 Coating rows of microneedles

In-plane rows of microneedles were dip coated using an in-house designed coating device. The coating device consisted of two parts: (1) the coating solution reservoir and (2) the micropositioning dip coater.

##### *4.2.2.3.1 Coating solution reservoir*

The coating solution reservoir was designed to restrict access of the coating liquid only to the microneedle shaft to prevent contamination of the base. The coating-solution reservoir consisted of two laminated parts: the 'bottom plate' and the 'cover plate', both of which were made of polymethylmethacrylate (McMaster-Carr) (Figure 4.1 A). The bottom plate had a central feeding channel (1 mm deep x 0.5 mm wide) machined into one of its faces, with a through hole drilled across to the other face. This hole acted as the inlet port to fill the channel with the coating solution. The cover plate had five holes (400 μm diameter) drilled into it at the same interval as the microneedles in the in-plane row to be coated. These 'dip-holes' acted as individual dipping reservoirs to coat each of the microneedles in the row. The two plates (bottom and cover plates) were aligned and adhered to each other using solvent bonding with methylene chloride (Fisher Scientific) as the solvent.

#### *4.2.2.3.2 Micropositioning dip coater*

To enable three-dimensional alignment and dipping of microneedle rows into the dip-holes, three linear-micropositioners were assembled on a 6.35 mm-thick, flat, acrylic plate (McMaster-Carr) (Figure 4.1 B). The first micropositioner (x-micropositioner: A1503K1-S1.5 Unislide, Velmex) was used to control the position of the in-plane microneedle row. The other two micropositioners were assembled one on top of the other on the acrylic plate to create a composite y-z motion micropositioner (two A1503K1-S1.5 Unislides, Velmex) that was used to control the position of the coating solution reservoir. The three micropositioners together allowed the alignment of the in-plane microneedle row to the dip-holes. The x-micropositioner was used to horizontally dip the microneedles into and out of the dip-holes. The coating was performed manually while viewing under a stereo microscope (SZX12, Olympus America). Control over the length of the microneedle shaft to be coated was exercised manually using the x-micropositioner. Tolerance for misalignment was included by designing the dip-hole diameter to be twice the width of the microneedles.

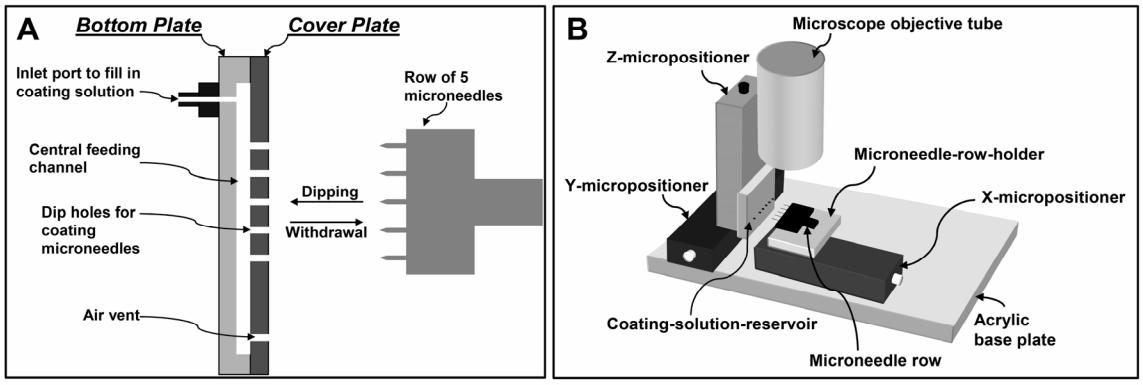


**Figure 4.1. Schematic diagrams of in-plane microneedle row-coating device**. (A) Cross sectional view of the coating solution reservoir showing the microneedles aligned with the dip holes. (B) Isometric projection of the entire device showing the x,y and z-micropositioners used to align the microneedles with dip holes of the coating-solution reservoir. The cylindrical tube represents the stereo-microscope objective, which is used to view the microneedle alignment and coating process facilitating manual control.

4.2.2.4 Coating arrays

Microneedle arrays were dip-coated using a method and dipping device similar to that used to coat in-plane rows of microneedles. The coating-solution reservoir and the microneedle-array holder were pre-aligned opposite to each other on a vertical rod. The cover plate of the coating-solution reservoir contained 50 dip-holes at the same spacing as the microneedles in the array. The coating-solution reservoir was stationary, while the microneedle-array holder could slide up and down the rod. Pins were provided on the microneedle-array holder to position a microneedle array on the holder in alignment with the dip-holes. To coat the microneedles, the microneedle-array holder was manually slid down the rod to dip the microneedles of the array into the 50 dip-holes below.

### 4.2.3 Microneedle patch assembly

Coated microneedle arrays were assembled into transdermal patches containing pressure-sensitive adhesive to adhere to the skin. These patches were fabricated using either multiple in-plane rows of microneedles or individual arrays of out-of-plane microneedles.

4.2.3.1 Microneedle patches from multiple in-plane rows of microneedles

A set of ten in-plane rows of microneedles with each row containing five microneedles were assembled into a patch of 50 microneedles. First, ten slits, each 75 μm wide and 7.7 mm long (i.e. equal to the length of an in-plane row) were laser cut into a 1.6 mm-thick, single-sided polyethylene medical foam tape (TM9716, MACtac, Stow, OH, USA) using a $CO_2$ laser (LS500XL, New Hermes, Duluth, GA, USA). The ten microneedle rows were then manually inserted into each slit from the non-adhesive side of the foam tape and glued to the foam tape using a medical grade adhesive (Loctite 4541, Rocky Hill, CT, USA). The adhesive was allowed to cure for 24 h. A polyethylene

medical foam tape (0.8 mm thick; TM9942, MACtac) was then cut into a disc of 16 mm diameter and affixed onto the dried glue area to provide a cushioned backing to facilitate pressing the patch during insertion.

4.2.3.2 Microneedle patches from complete out-of-plane microneedle arrays

To assemble a microneedle patch using a complete out-of-plane microneedle array, a circular disc of 20 mm diameter was first cut from a 0.8 mm-thick, single-sided medical foam tape (TM9942, MACtac) using the $CO_2$ laser. In the middle of this disc, a rectangular piece of the adhesive release liner equal in dimensions to the periphery of the array (i.e. 12 mm x 12 mm) was cut out using the $CO_2$ laser and peeled off. The stainless steel microneedle array was then attached to this exposed adhesive. The patch at this stage has a release liner-covered adhesive layer around the attached array. To further provide a layer of pressure-sensitive adhesive on the stainless steel surface of the attached array, a double-sided, poly-ethylene-terephthalate carrier tape (63.5 μm thick; T04314A, MACtac) was attached as follows. The poly-ethylene-terephthalate film was first perforated with holes of 400 μm diameter at the same spacing as the microneedles using a $CO_2$ laser. The tape was then slipped over the microneedles using a custom-built alignment device and pressed to stick against the stainless steel substrate without contaminating the microneedles.

### 4.2.4 Imaging and histology

Fluorescence micrographs of coated microneedles and histological skin sections were collected using an Olympus IX70 fluorescent microscope with a CCD camera (RT Slider, Diagnostic Instruments, Sterling Heights, MI, USA). Brightfield micrographs were collected using an Olympus SZX12 stereo microscope with a CCD camera (Leica DC

300, Leica Microsystems, Bannockburn, IL, USA). Digital x-ray imaging to detect barium sulfate was done using the Faxitron MX20 cabinet X-ray (Faxitron X-Ray, Wheeling, IL, USA).

Histological examination of cadaver skin was conducted on frozen sections. Porcine cadaver skin was pierced with microneedles for 1 min, frozen in OCT compound (Tissue-Tek, 4583, Sakura Finetek, Torrance, CA, USA), and cut into 10 μm-thick sections using a cryostat (Cryo-Star HM 560MV, Microm, Waldorf, Germany).

### 4.2.5 In vitro dissolution time and delivery efficiency

Single microneedles (n=3) coated with vitamin B2, calcein or sulforhodamine were inserted into porcine cadaver skin for 10 s or 20 s. Upon removal, these microneedles were imaged by fluorescence microscopy to check for presence of residual coating. To determine the delivery efficiency of coated microneedles, rows of five microneedles coated with vitamin B2 were inserted into pig cadaver skin for 5 min (n=3). The mass of vitamin B2 on the inserted and non-inserted microneedle rows was determined by dissolving the coatings in deionized water through vigorous mixing, quantifying the vitamin B2 concentration in the resulting solution via fluorescence spectroscopy (SpectraMax Gemini, Molecular devices, Sunnyvale, CA, USA), and multiplying the measured concentration by the volume of deionized water used for dissolution to yield the amount of vitamin B2 that was adherent to the microneedles. Similarly, the mass of vitamin B2 left behind on the skin surface during microneedle insertion was estimated by applying tape (Scotch super 33, McMaster-Carr) to the skin surface, removing the tape, dissolving the material removed by the tape in deionized water, and determining the vitamin B2 content by fluorescence spectroscopy. Using a mass balance, the amount of vitamin B2 delivered into the skin was determined by

subtracting the amount remaining on the microneedles and on the skin surface after insertion from the amount originally on non-inserted microneedles.

### 4.2.6 Delivery of molecules and particles

4.2.6.1 Delivery from individual microneedles in vitro

Single microneedles (n=3) coated with calcein were inserted into porcine cadaver skin for 20 s and removed. For particle delivery, barium sulfate particles (1 μm diameter, as determined by scanning electron microscopy, data not shown), or latex beads (10 or 20 μm diameter) were inserted into porcine cadaver skin for 1 min (n=3 single microneedles for each insertion). After removing the microneedles, the skin surface was examined by brightfield microscopy for coating residue. Porcine cadaver skin was then examined histologically to assess the extent of delivery of microneedle coatings into the skin. The use of porcine cadaver skin was approved by the Georgia Institute of Technology Institutional Animal Care and Use Committee (IACUC).

4.2.6.2 Delivery for assembled microneedle patches in vitro and in vivo

For in vitro testing, out-of-plane microneedle arrays (n=3) were coated, assembled into patches and manually inserted into human cadaver skin for 1 min. After 1 min, the patch was removed and visually examined by brightfield microscopy to qualitatively assess the amount of residual coating left on the microneedles. The human cadaver skin was also imaged by brightfield microscopy to assess release and delivery of coatings into the skin. For in vivo analysis, non-coated patches of out-of-plane arrays were sterilized using ethylene oxide and manually applied onto the forearms of human subjects (n=3) for 30 s. Gentian violet (a violet topical antifungal agent, 2% solution, Humco, Texarkana, TX, USA) was then applied on the treated site for 1 min and wiped

away using isopropanol swabs. Gentian violet selectively stained the sites of skin perforation, which identified the sites of microneedle insertion. The use of human subjects was approved by the Georgia Institute of Technology Institutional Review Board (IRB).

## 4.3 RESULTS

### 4.3.1 Fabrication of stainless steel microneedles

Our first objective was to fabricate microneedles with appropriate mechanical properties for reliable insertion into skin and appropriate surface properties for dip-coating with drugs. We selected stainless steel as the microneedle material because it has a well-established FDA safety record, provides good mechanical strength, and can be easily cut using a laser. However, laser-cutting stainless steel produced microneedles with rough edges covered with slag deposits (Figure 4.2 A).

To produce clean, smooth, and sharp microneedle surfaces, we developed an electropolishing technique to remove this slag from the microneedles. Mechanical methods like abrasive cleaning and buffing were difficult to implement without bending or otherwise damaging the microneedles. In contrast, electropolishing utilized a simple, reliable procedure that was effective to remove all of the slag and debris. This approach yielded microneedles with smooth surfaces and very sharp tips (tip radius 0.5 to 1 $\mu$m) (Figure 4.2 B). We believe that electropolishing was especially effective, because current density (i.e., etching rate) is largest at sites of high curvature, which inherently targets sites of surface roughness for removal (Landolt 1987).

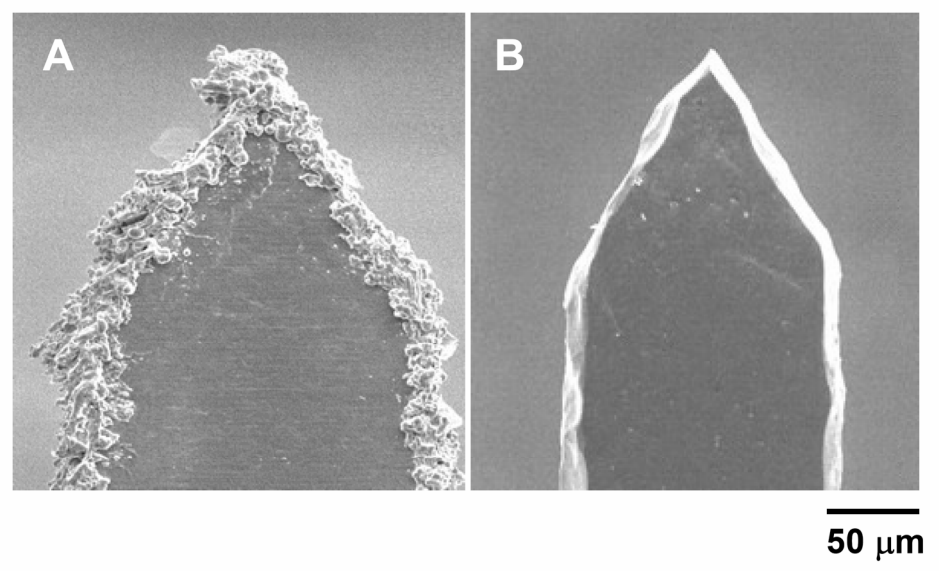


**Figure 4.2. Effect of electropolishing on microneedle surface**. Scanning electron micrographs of: (A) a microneedle tip with slag and debris residue remaining after cleaning with detergent powder and (B) a microneedle tip after electropolishing, resulting in removal of slag and debris, clean edges, and sharp tip.

Laser cutting coupled with electropolishing provides a potentially versatile method to prepare microneedles having a variety of geometries according to the pattern in which the laser is programmed to cut. To assess this versatility in the context of microneedle fabrication, we attempted to laser-cut and electropolish microneedles with increasing geometrical complexity. Using a simpler microneedle design, this process was used to create microneedles of different lengths and widths (Figure 4.3 A). As a more complex design, microneedles were fabricated with small through-holes (which we call 'pockets') of different shapes and sizes in the shafts of these microneedles (Figure 4.3 B). Microscopic examination showed that the inside surfaces of these pockets were smooth and clean. We believe that this is the first report of pocketed microneedles, which can provide protective cavities to transport particles into the skin, as discussed further below. As a still more complex design, we tested the ability of the process to make contoured surfaces in the form of barbs and serrated edges. Although such

surfaces are more difficult to clean, debris was successfully removed with uniform cleanliness and smoothness (Figure 4.3 C). While these needle designs may be useful for improved microneedle retention, cutting or other effects in the skin, they are intended in this study only to demonstrate the capabilities of this fabrication process and have not been optimized for in vivo applications.

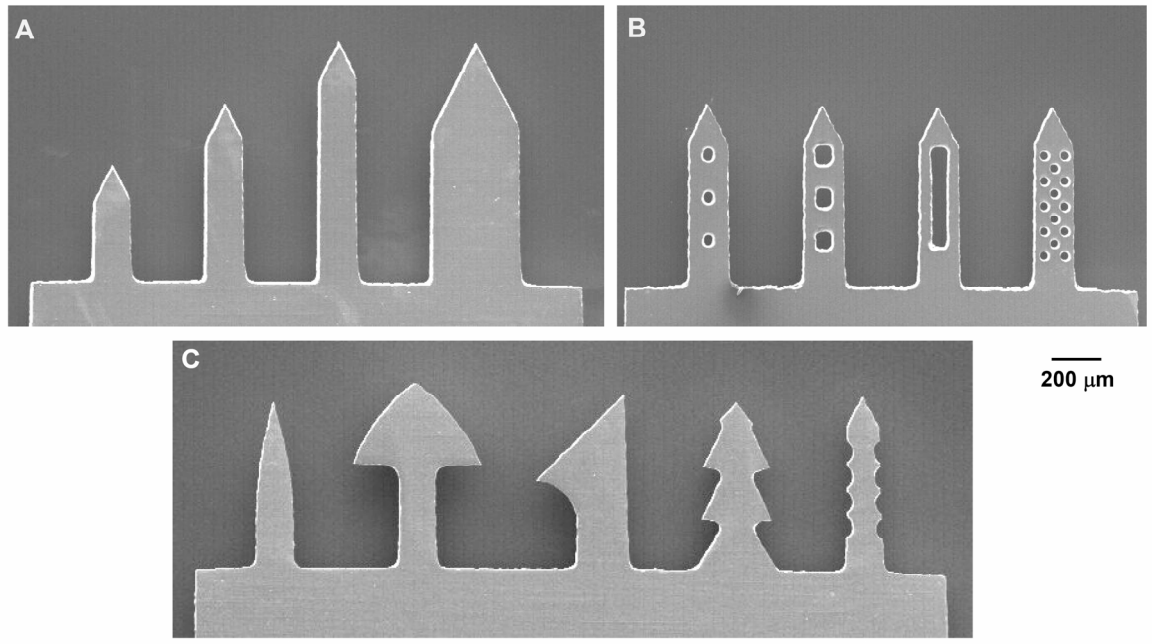


**Figure 4.3. Fabrication of different microneedle geometries**. Scanning electron micrographs of: (A) microneedles having different lengths and widths at a constant tip angle of 55°, (B) microneedles with 'pockets' of different shapes and sizes etched through the microneedle shaft, and (C) microneedles with complex geometries, such as contoured surfaces in the form of barbs and serrated edges.

In addition to fabricating individual microneedles with different shapes, the laser fabrication process was also used to fabricate two different kinds of microneedle arrays in which all needles have the same geometry: (1) in-plane microneedle rows containing microneedles oriented with their axis parallel to the sheet (Figure 4.4 A, a representative in-plane row with five microneedles) and (2) out-of-plane arrays with multiple rows of

microneedles sticking out of the substrate with their axis perpendicular to the substrate (Figure 4.4 C, a representative out-of-plane array with 50 microneedles).

### 4.3.2 Microneedle array patches

To facilitate their insertion and retention into the skin, arrays of microneedles were integrated into adhesive patches. These patches were designed to have a uniform pressure-sensitive adhesive layer on one complete side of the patch intended to contact the skin. The adhesive layer was periodically disrupted via small holes or slits to allow the microneedles to stick out for penetration. The adhesive served to hold the microneedles firmly against the skin by compensating for the mechanical mismatch between the flexible skin tissue and the rigid microneedle substrate, especially in the case of out-of-plane microneedle arrays. Microneedle arrays prepared on the basis of this design are shown for patches of in-plane microneedles (Figure 4.4 B) and out-of-plane microneedles (Figure 4.4 D).

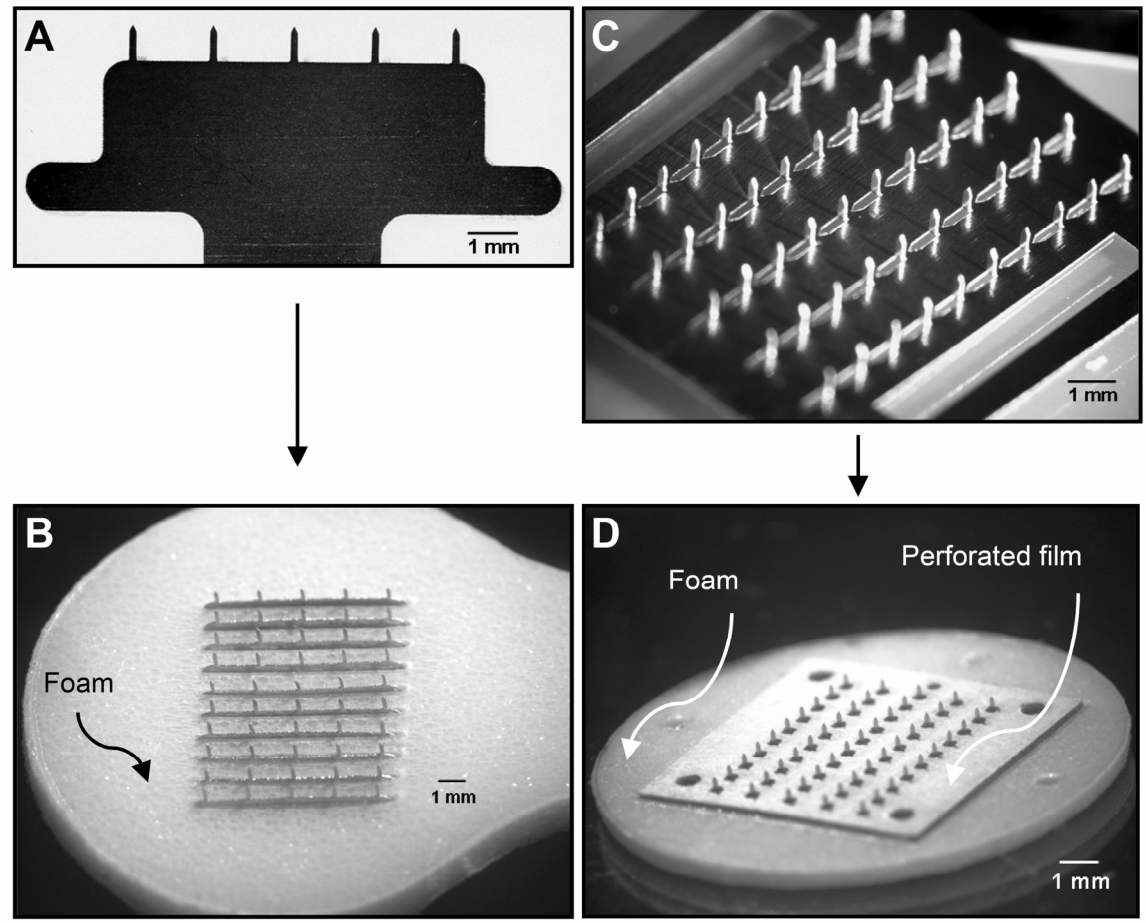


**Figure 4.4. Different types of microneedle arrays and patches**. Brightfield micrographs of: (A) an in-plane row with five microneedles, (B) a 50-microneedle patch after assembly of ten in-plane rows into slits of a foam-tape backing, (C) an out-of-plane microneedle array with 50 microneedles, and (D) a 50-microneedle patch assembled by mounting an out-of-plane array onto a foam-tape backing and then affixing a perforated, double-sided adhesive film onto the base substrate between microneedles.

### 4.3.3 Micro-dip coating of microneedles

Our next objective was to deposit uniform coatings on microneedle shafts. Although the conventional dip-coating process is fairly simple, it is most suitable for macroscopic coatings. Our attempts to achieve micron-scale control over coating by simply dipping and withdrawing microneedles from an aqueous solution resulted in non-uniform coatings with frequent spreading of the solution onto the base substrate. Representative brightfield images of such non-uniform coatings obtained by dipping

microneedles in a 3% (w/v) aqueous solution of vitamin B2 are shown in Figure 4.5 A (single microneedle) and Figure 4.5 B (out-of-plane array).

Based on optimized coating methods developed in other contexts (Schunk, Hurd et al. 1997), reduced surface tension and increased viscosity of the coating solution should improve the coating outcome by increasing the wettability of the microneedle surface and increasing the coating thickness, respectively. In addition to lowering surface tension and increasing viscosity, the ideal excipients had to meet a number of additional specifications. They needed to be water-soluble (for aqueous dipping formulations), FDA-approved as injectable excipients (for safety), solid at room temperature (to convert into a solid coating upon drying) and possess high surfactant or viscosity enhancement activity per unit mass (to minimize the excipient content and thereby maximize drug content in the dry coatings). Sodium salt of carboxymethylcellulose (low viscosity) and Lutrol F-68 NF were found to fulfill these criteria as a viscosity enhancer and surfactant, respectively. After optimization to minimize their concentration in the coating solution, these excipients were found to give uniform coatings at concentrations of 1% (w/v) carboxymethylcellulose and 0.5% (w/v) Lutrol F-68 NF using vitamin B2 as the model compound (Figure 4.5 C).

Further efforts, however, were required to address the problem of microneedle array substrate contamination with coating solution. To address this, we designed a special micro-dip-coating device that covered the dipping solution reservoir with a thin sheet containing micron-sized holes corresponding to the size and position of the microneedles in the array (Figure 4.1). This physical masking eliminated solution contact with the substrate of microneedles. When properly aligned using micropositioners, only microneedles could dip through the micron-sized holes and into the coating solution, which resulted in a controlled micro-dip-coating process.

Using this design philosophy, three different coating devices were built to coat single microneedles, in-plane rows of microneedles, and out-of-plane arrays of microneedles, as described in the Materials and Methods section. These micro-dip-coating devices were able to localize coatings only to microneedle shafts for single microneedles (Figure 4.5 C), out-of-plane arrays (Figure 4.5 D) and in-plane rows (Figure 4.5 E) of microneedles. To further test the ability of this approach to control the length of microneedles getting coated, in-plane rows of microneedles were coated to predetermined lengths of 25%, 50%, 75% and 100% length coverage (Figure 4.5 E). Thus, through the combination of a suitable coating solution and coating device, highly controlled and uniform coatings can be achieved on microneedles. The approach is probably applicable to coating other microstructures as well.

Finally, it is also worth noting that the dead volume of these coating devices was 10 μl for the row-coating device, and 100 μl for the array-coating device. Therefore, only very small coating solution volumes are sufficient to coat microneedles, which is especially important when coating proteins, DNA and other expensive compounds.

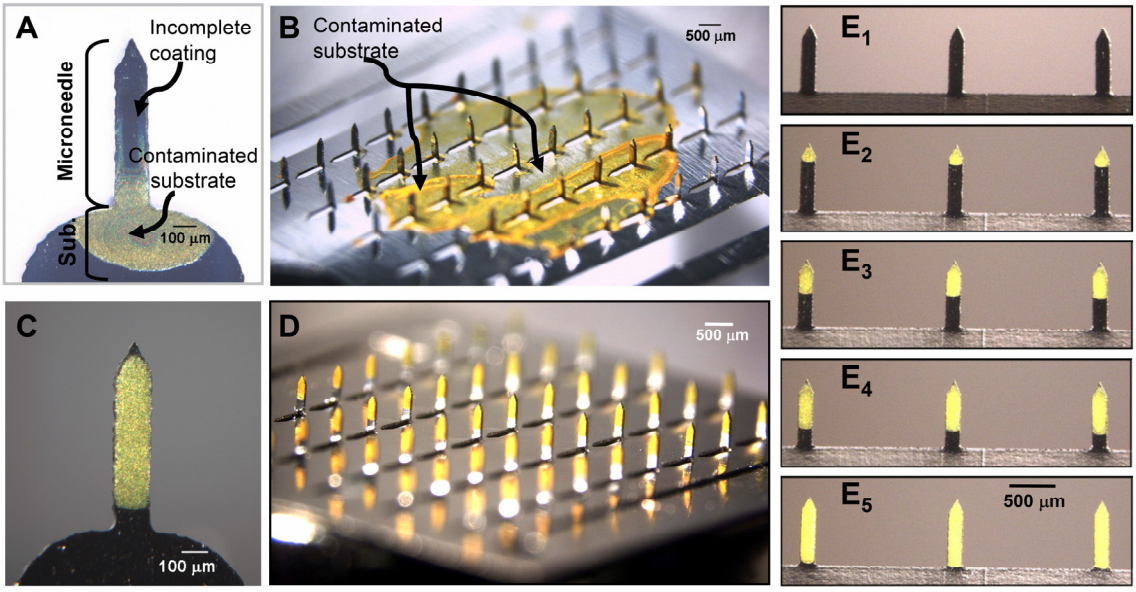


**Figure 4.5. Examples of poor and good microneedle coatings via brightfield micrographs of vitamin B2 coated microneedles.** Poor, non-uniform coatings with base-substrate contamination on: (A) a single microneedle and (B) a 50-microneedle out-of-plane array. Improved coating uniformity and elimination of base-substrate contamination after addition of coating solution excipients and use of a micro-dip-coating device for (C) a single microneedle, (D) a 50-microneedle out-of-plane array, and (E) an in-plane microneedle row. Controlled length segment coverage at ($E_1$) uncoated, ($E_2$) 25% coated, ($E_3$) 50% coated, ($E_4$) 75% coated and ($E_5$) 100% coated, demonstrating spatial control of the microneedle coating process.

### 4.3.4 Coating a large range of compounds

Our next objective was to determine how broadly this approach could be applied to coat different molecules and particles onto microneedles. To study this question, the same coating solution and coating methods were used to reproducibly coat seven different compounds onto microneedles: calcein and vitamin B2 (low molecular weight molecules representative of synthetic drugs), bovine serum albumin and plasmid DNA (high molecular weight biomolecules representative of protein and gene therapeutics), modified vaccinia virus (a virus particle representative of some vaccines), and latex and barium sulfate microparticles (organic and inorganic particles representative of controlled release and other particulate systems). These compounds spanned in size from small molecules (e.g., vitamin B2) to micron-scale particles (e.g., 20-μm latex beads). We

believe this is the first time that coating of microneedles with virus and microparticles has been studied. In all cases, coatings were reproducibly applied onto the microneedles (n=3 single microneedles for each compound). Moreover, the coatings were uniform across the entire microneedle length (representative images shown in Figure 4.6).

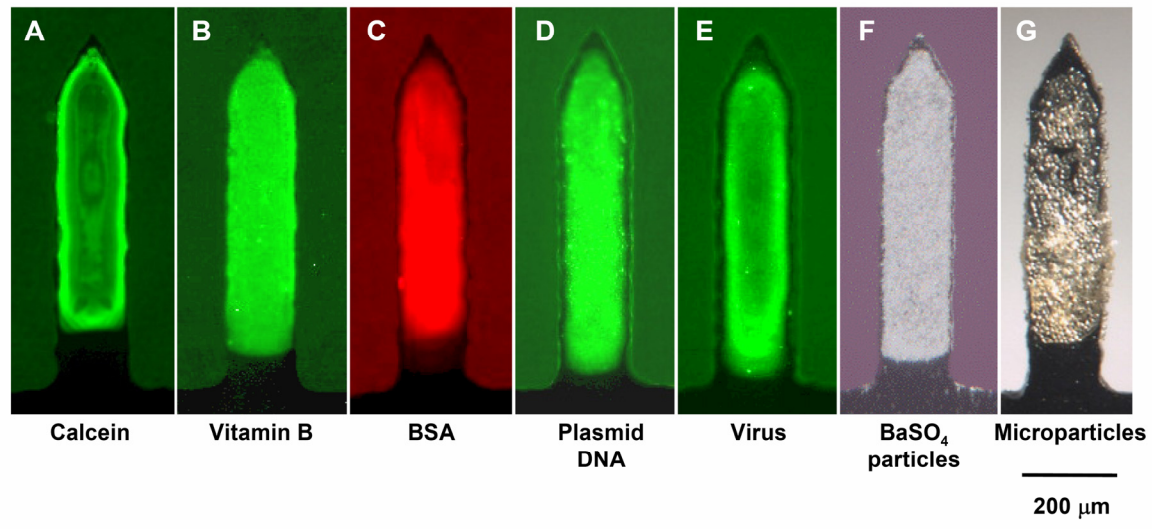


**Figure 4.6. Breadth of molecules and microparticles coated onto microneedles**. Fluorescent or brightfield micrographs of single microneedles coated with: (A) calcein, (B) vitamin B2, (C) bovine serum albumin (BSA) conjugated with Texas Red, (D) plasmid DNA conjugated with YOYO-1, (E) modified vaccinia virus – Ankara conjugated with YOYO-1, (F) 1-μm diameter barium sulfate particles and (G) 10-μm diameter latex particles.

### 4.3.5 Dissolution times and delivery of coated molecules

To determine the dissolution time of coated molecules from microneedles, microneedles coated with vitamin B2 (Figure 4.7 A-*before*) were inserted into porcine cadaver skin. Removal from skin 10-s after insertion showed that most of the coating was removed (data not shown) and 20 s after insertion the microneedle coating was completely removed (Figure 4.7 A-*after*).

To determine if microneedle coatings were being delivered into the skin, as opposed to, for example, flaking off onto the skin surface, calcein-coated microneedles were inserted into porcine cadaver skin. After removing the microneedles and examining the skin surface, no calcein coating residue was observed (data not shown). Examination of histological sections of the skin revealed deposition of calcein along the shaft of the insertion path within the skin (Figure 4.7 B). Together these observations suggest that calcein coated onto microneedles was delivered into the skin without wiping off on the skin surface. Similar results were also observed for sulforhodamine-coated microneedles (data not shown), suggesting that the results are more generally applicable to different molecules.

To further quantify the delivery efficiency of coated microneedles, rows of microneedles coated with vitamin B2 were inserted into pig cadaver skin. A total mass of 7.86 ± 0.3 μg of vitamin B2 was originally coated on these microneedles. After a 5-min insertion of these microneedles into skin, 7.18 ± 0.4 μg (91.4 ± 6 %) of the vitamin B2 was delivered into the skin, whereas 0.17 ± 0.1 μg (2.1 ± 1 %) was found on the skin surface and 0.51 ± 0.2 μg (6.5 ± 2 %) remained adhered to the microneedle surface after removal from the skin. We conclude that these coatings were able to remain adherent during insertion into the skin and then efficiently dissolve off the microneedles within the skin for delivery of greater than 90% of the coated vitamin B2.

### 4.3.6 Delivery of microparticles

It was also of interest to deliver microparticles into the skin, which has not been addressed in previous studies. Delivery of microparticles is challenging, because larger microparticles are more likely to wipe off onto the skin surface during insertion into the skin. To prevent microparticle coatings from wiping off, we hypothesized that faster

insertion (momentum) and seclusion of microparticles within protective cavities in the form of holes or 'pockets' in the microneedles would facilitate carrying microparticles into the skin. To test this hypothesis, we coated microneedles with particles having three different diameters: 1-μm diameter barium sulfate particles, and 10- and 20-μm diameter latex beads. After insertion into porcine cadaver skin at slow speed (0.5 to 1 mm/s), only barium sulfate particles were successfully delivered into porcine skin without wiping off onto the skin surface (Figure 4.7 C).

At higher insertion speed (1 to 2 cm/s), the momentum of the microneedles was able to carry the coating of 10-μm diameter particles into the skin (Figure 4.7 D); however, 20-μm diameter beads were still found predominantly as residue on the skin surface (data not shown). The 20-μm diameter latex particles were successfully delivered into the skin after loading them into the protective cavity of a pocket within the microneedle shaft and delivering at 1 to 2 cm/s (Figure 4.7 E). Therefore, by using appropriate microneedle design and insertion methods, even relatively large microparticles can be delivered into the skin using coated microneedles.

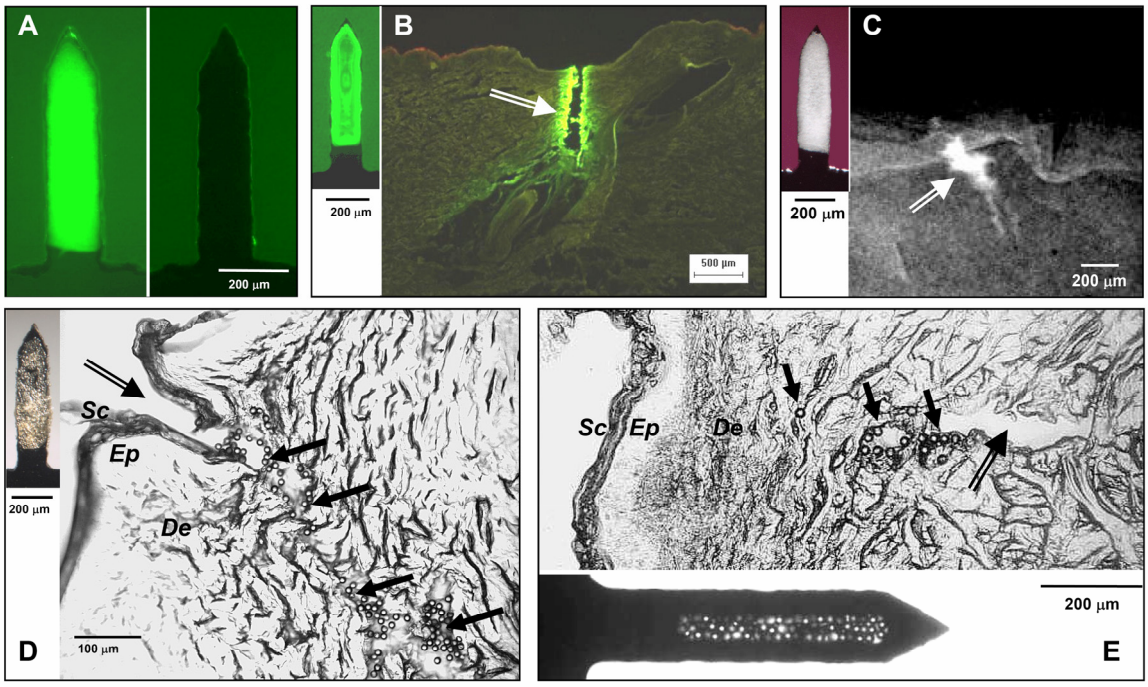


**Figure 4.7. In vitro dissolution and delivery from coated microneedles**. (A) Single microneedle coated with vitamin B2 before and after a 20 s insertion into porcine cadaver skin imaged by fluorescence microscopy. The absence of fluorescence in the image after insertion indicates complete dissolution of the coating in the skin. (B) Histological section of porcine cadaver skin after inserting a calcein-coated microneedle (inset on left) and (C) X-ray micrograph of intact porcine cadaver skin after inserting a barium sulfate-coated microneedle (inset on left). The arrows in (B) and (C) point to the microneedle insertion sites and the bright regions represent calcein and barium sulfate delivery into the skin. The absence of fluorescence on top of the skin suggests that the coating did not wipe off during insertion. (D) Histological section of porcine cadaver skin after inserting a microneedle coated with 10-μm diameter beads (inset on left) and (E) histological section of porcine cadaver skin after inserting a 'pocketed' microneedle containing 20-μm diameter beads (inset at bottom). In (D) and (E), the double lined arrows point to the microneedle insertion sites, while the solid black arrows point to some of the beads delivered into the skin, which appear as tiny circles. The absence of beads on the skin surface indicates that beads did not wipe off during insertion. Sc = Stratum Corneum, Ep = Epidermis, De = Dermis.

### 4.3.7 Delivery from a microneedle array patch

To evaluate the performance of microneedle arrays assembled in a patch, coated microneedle patches (Figure 4.4 D) were inserted into human cadaver skin and non-coated microneedles were inserted into the skin of human subjects. After inserting and removing microneedles coated with Trypan Blue from cadaver skin, surface examination of the treated skin showed an array of blue dots corresponding to sites of microneedle

penetration and coating deposition from the array (Figure 4.8 A). No residue was observed on the skin surface indicating delivery of coatings into the skin.

Although we did not prepare coated microneedles suitable for human use, we did want to evaluate the performance of microneedle patches in human subjects. Out-of-plane arrays containing 50 uncoated microneedles were inserted and removed from the forearms of humans subjects. To determine if microneedles inserted, a solution of gentian violet was applied to the skin to stain sites of microneedle insertion. Complete microneedle insertion was obtained (n=3 subjects, Figure 4.8 B). The subjects reported that insertion of the arrays did not cause discomfort.

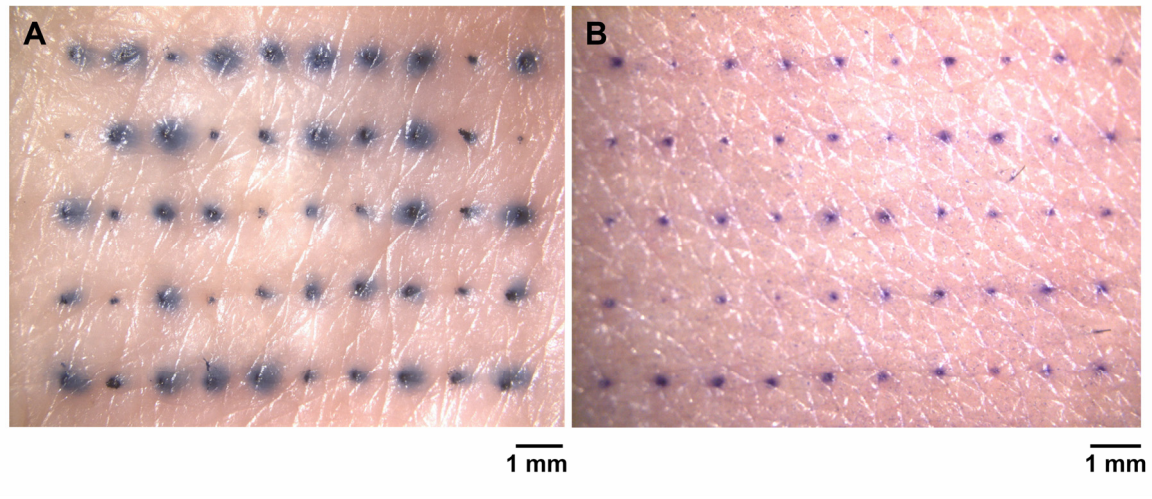


**Figure 4.8. In vitro and in vivo performance of microneedle patches in human skin**. (A) Surface view of human cadaver skin imaged by brightfield microscopy after inserting a 50-microneedle patch dip-coated with trypan blue dye. The 50 dark spots correspond to sites of trypan blue coating delivered and dissolved in the skin from the 50 microneedles in the patch. (B) Skin from the forearm of a human subjected imaged by brightfield microscopy after inserting a microneedle patch containing 50 microneedles and subsequently applying gentian violet to stain the sites of microneedle insertion, which demonstrates microneedle penetration into the skin.

## 4.4 DISCUSSION

This study showed that micro-dip coating provides a versatile technique to coat microneedles with a wide variety of molecules including small synthetic compounds, proteins and DNA. We have also reported for the first time that viruses and a variety of microparticles can be coated onto microneedles. This coating method uses aqueous formulations with FDA-approved excipients at room temperature. Histological examination of skin after insertion of coated microneedles showed successful delivery into the skin within seconds. This detailed study of the microneedle coating process and its breadth of applicability serves to compliment previous studies demonstrating delivery of peptides and proteins to the skin using coated microneedles (Matriano, Cormier et al. 2002; Cormier, Johnson et al. 2004; Widera, Johnson et al. 2006).

### 4.4.1 Microneedle fabrication methods

This study presented fabrication methods to produce microneedles suitable for coating. Although the laser-cutting method could be used with a variety of different metals and other materials, this study employed stainless steel, which is used in many FDA-approved medical devices and is inexpensive. Microneedles were fabricated to have a variety of different geometries. For the first time, we have reported the fabrication of 'pocketed' microneedles (Figure 4.3 B). Pockets provide a protective cavity within the microneedle shaft and were used to deliver particles up to 20-μm in diameter into the skin without wiping off during insertion.

Microneedles with other complex geometries, such as contoured surfaces in the form of barbs and serrated edges, were fabricated and polished to have clean edges and sharp tips (Figure 4.3 C). Some of these shapes can be used to help anchor microneedles within the skin for improved insertion and retention (Matriano, Cormier et al. 2002; Cormier, Johnson et al. 2004); however, they may cause skin damage or pain

upon withdrawal. Microneedles of different lengths and widths (Figure 4.3 A) can be fabricated using this method.

Using a bench-scale apparatus, finished microneedle arrays were cut and polished at a rate of two 50-needle arrays per hour. For large-scale manufacturing, this rate can easily be increased by orders of magnitude by using higher power lasers that can cut more quickly and can be beam-split to cut multiple arrays in parallel using fully automated processes. Use of multiple lasers can increase throughput still further through parallel processing. Likewise, larger and multiple electropolishing baths can increase polishing rates. Finally, the manual process using in this study to bend microneedles for out-of-plane arrays can also be easily automated for mass production.

### 4.4.2 Microneedle coating methods

The success of coated microneedles for drug delivery depends on the ability to reliably coat a controlled drug layer onto microneedles. Our initial attempts to coat microneedles by dipping into an aqueous drug solution resulted in patchy to no surface coverage (Figure 4.5 A). To overcome this difficulty, we formulated a coating solution with increased viscosity and reduced surface tension containing 1% carboxymethylcellulose and 0.5% Lutrol F-68 NF as viscosity enhancer and surfactant, respectively. This enabled complete and uniform coverage of the dipped microneedle surface (Figure 4.5). This coating formulation was shown to be very versatile. Small molecules, macromolecules and microparticles were all applied as uniform coatings (Figure 4.6). The two excipients used to modify the dipping solution have already been approved by the FDA as excipients in injectable formulations, so this coating formulation should also be safe for use in humans.

Another important component of the micro-dip-coating process is the dip-coating device. Simply dipping microneedles into a small beaker containing dipping solution often

resulted in contamination of the microneedle substrate (Figure 4.5 B). Capillary forces are mainly responsible for the rise of the free meniscus along the microneedle shaft to eventually touch the base substrate. This effect is amplified in an array due to the close spacing of the microneedles, which enhances the capillary effect and can lead to bridging of coating solution between adjacent microneedles.

To address these issues, we have developed a dip-coating design that uses dip holes with dimensions similar to that of individual microneedles instead of a large, open coating surface to prevent the meniscus rise and to physically mask the base substrate between microneedles. This design philosophy was incorporated into three different micro-dip-coating devices to coat single microneedles, in-plane rows, and out-of-plane microneedle arrays. Micropositioners were also incorporated into the dipping devices to align microneedles with dip holes. Using these micro-dip-coating devices, coating deposition can be highly controlled to localize only on microneedles and, when desirable, to coat only portions along the shaft of microneedles in a reproducible manner (Figure 4.5 E). In the context of this and other on-going studies, this coating method has been used by us to reliably and reproducibly prepare many hundreds of microneedle devices for in vitro and in vivo drug and vaccine delivery studies.

Concerning the practical use of micro-dip-coating, the devices developed for this study (Figure 4.1) require very small volumes of coating solution, ranging from 10 μl for single microneedles to 100 μl for 50-needle, out-of-plane arrays. The ability to use small reservoirs of coating solution is important, because many experimental and established biotherapeutics are expensive and available only in limited quantity. Another practical issue is that air bubbles were sometimes formed in the dip-coating device, which interfered with the coating process. To prevent this, vent holes were incorporated into the design to release air (Figure 4.1). While coating large numbers of microneedle

devices, evaporation of coating solution from the dipping reservoir sometimes left behind solid deposits that could block the dip-coating holes. To prevent this, the syringe used to fill the dipping reservoir was manually pulsated to mix the coating solution.

### 4.4.3 Delivery from coated microneedles

Delivery from coated microneedles was found to be efficient, where the vast majority of coated drug was deposited in the skin and essentially no residue was found on the skin surface, which suggests high bioavailability. Although efficient, the total amount of drug that can be delivered is constrained by the relatively small surface area of microneedles. Using vitamin B2 as a model drug, we were able to coat up to 2.6 μg of drug per microneedle (750 μm long and 200 μm wide, data not shown). Based on a maximum array size of a few hundred microneedles, we can conclude that hundreds of micrograms up to perhaps 1 mg of drug can be coated onto an array. Therefore, coated microneedles are most suitable for potent drugs, such as therapeutic proteins, DNA and vaccines. Vaccine delivery using coated microneedles is especially attractive, because microneedle-based delivery to the skin can target dendritic cells residing in the epidermis for a more potent immune response. Further, storage and delivery of vaccine in solid-state coatings should increase antigen stability, which may help eliminate the need for cold-chain storage.

## 4.5 CONCLUSION

Motivated by previous results demonstrating coated microneedles to deliver drugs and vaccines to the skin, here we sought to carry out a detailed study examining coating methods and their breadth of applicability. Using laser cutting followed by electropolishing, stainless steel microneedles of different geometries and configurations

were fabricated with sharp tips and clean edges suitable for coating. To facilitate insertion and adhesion to the skin, microneedle patches were developed with pressure-sensitive adhesive surrounding the base of the microneedles.

A novel micro-dip-coating apparatus was designed to control surface tension-driven wicking of coating solution up microneedle shafts and onto the base substrate. A coating formulation was also developed to achieve uniform coating solution deposition on microneedles by using low concentrations of carboxymethylcellulose and Lutrol F-68 NF as excipients to increase viscosity and decrease surface tension, respectively. Using this approach, single microneedles, in-plane rows of microneedles, and out-of-plane arrays of microneedles were coated without contaminating the base and with micron-scale control over the length of the microneedle shaft to be coated. For the first time, organic and inorganic microparticles as well as viruses were coated onto microneedles, in addition to vitamin B2, calcein, bovine serum albumin, and plasmid DNA.

Microneedle coatings dissolved within seconds after insertion into cadaver skin. Successful delivery into skin was achieved from microneedles surface coated with molecules as well as microparticles up to 10 μm in diameter. Using novel 'pocketed' microneedles to mechanically protect coatings during insertion, 20-μm diameter particles were delivered into skin without wiping off onto the skin surface. Integrated patches containing 50-microneedle arrays were also shown to insert into the skin of human subjects and to deliver their coated payload into human cadaver skin. Altogether, this study provides versatile microneedle fabrication and controlled micro-dip-coating methods that enable coating of microneedles using a mild process with FDA-approved excipients with a wide variety of molecules and microparticles for delivery to the skin.

# CHAPTER 5: COATING FORMULATIONS FOR MICRONEEDLES[3]


## ABSTRACT

The purpose of this study was to develop a rational basis for designing coating solution formulations for uniform and thick coatings on microneedles and to identify coating strategies to form composite coatings, deliver liquid formulations, and control the mass deposited on microneedles. To achieve this goal, microneedles were fabricated using laser-cutting and then dip-coated using different aqueous, organic solvent-based or molten formulations. The mass of riboflavin (vitamin B2) coated onto microneedles was determined as a function of coating and microneedle parameters. Coated microneedles were also inserted into porcine cadaver skin to assess delivery efficacy. It was found that sharp-tipped microneedles, including pocketed microneedles, were fabricated. Excipients that reduced coating solution surface tension improved coating uniformity, while excipients that increased solution viscosity improved coating thickness. Evaluation of more than 20 different coating formulations using FDA approved excipients showed that hydrophilic and hydrophobic molecules could be uniformly coated onto microneedles. Model proteins were also uniformly coated on microneedles using the formulations identified in the study. Pocketed microneedles were selectively filled with solid or liquid formulations to deliver difficult-to-coat substances, and composite drug layers were formed for different release profiles. The mass of riboflavin coated onto microneedles increased with its concentration in the coating solution, the number of coating dips and microneedles in the array. Coatings rapidly dissolved in the skin without wiping off on the skin surface. Thus, microneedles and coating formulations can be designed to have a range of different properties to address different drug delivery needs.


[3] This work has been published as: Gill, H. S. and M. R. Prausnitz (2007). "Coating formulations for microneedles " Pharm Res 24(7): 1369-1380.

## 5.1 INTRODUCTION

Conventional transdermal delivery of drugs is limited to small, lipophilic and potent molecules (Prausnitz, Mitragotri et al. 2004). As an alternative approach, microneedles provide a minimally invasive method to create micron-scale pathways into the skin for delivery of small and large molecular weight compounds including proteins, in a manner expected to be safe, painless and cost-effective (Prausnitz 2004; Prausnitz, Mikszta et al. 2005). Microneedles are individual needles or arrays of needles having micron dimensions. They can be fabricated using micromachining tools adapted from the microelectronics industry (Reed and Lyev 2004). Both solid and hollow microneedles have been used in different modes to increase skin permeability by orders of magnitude to deliver large molecular weight molecules and nanoparticles into the skin (Henry, McAllister et al. 1998; McAllister, Wang et al. 2003; Chabri, Bouris et al. 2004). In vivo delivery has been shown for small molecules (Gardeniers, Luttge et al. 2003; Sivamani, Stoeber et al. 2005); peptides, such as insulin (Gardeniers, Luttge et al. 2003; McAllister, Wang et al. 2003; Martanto, Davis et al. 2004) and desmopressin (Cormier, Johnson et al. 2004); genetic material, including plasmid DNA (Mikszta, Alarcon et al. 2002) and oligonucleotides (Lin, Cormier et al. 2001); and vaccines directed against hepatitis B (Mikszta, Alarcon et al. 2002) and anthrax (Mikszta, Sullivan et al. 2005).

An attractive method of transdermal delivery using microneedles involves the use of coated microneedles (Gill and Prausnitz 2007a). This process involves coating a drug formulation onto solid microneedles and inserting them into the skin for subsequent dissolution of the drug within the skin. Coated microneedles have previously been shown to deliver peptides (Cormier, Johnson et al. 2004) and proteins (Matriano, Cormier et al. 2002) into the skin in vivo. Robust immune responses have also been generated in guinea pigs against an ovalbumin model antigen using this approach (Widera, Johnson et al. 2006).

Although, coated microneedles have been used to deliver proteins and drugs into the skin, detailed studies of the coating process itself have not been published. Excipients are known to affect drug stability and activity (Yoshioka and Stella 2002), and therefore a single coating formulation may not be universally applicable to coat all therapeutic compounds and proteins. Therefore, it is desirable to identify a rational basis for designing coating formulations and different coating strategies, which can enable uniform coating of therapeutics with diverse physicochemical properties. To address this, we sought to study the effects of coating methods and formulations, and thereby provide a rational basis for designing microneedles and coating formulations for different applications. The micron length scales of microneedles impose special coating challenges to obtain uniform coatings and to obtain spatial control over the region of the microneedle to be coated. This is largely because the effects of surface tension, capillarity and viscous forces become more prominent at these small length scales. Therefore, in a companion study, we developed a novel micro-dip-coating process that applied uniform coatings with micron-scale control over the length of the microneedle shaft to be coated (Gill and Prausnitz 2007a). Using this device we investigated the range of compounds and molecules that can be coated onto microneedles and found that small molecules, proteins, DNA, viruses and microparticles as large as 10 μm in diameter could be applied onto microneedles as uniform and stable coatings (Gill and Prausnitz 2007a). Coatings were applied not only to the surface of microneedles, but could also be filled into 'pocket' cavities cut into the microneedles.

This study seeks to address the physical chemistry of coating formulations in greater detail to: (i) determine factors that affect coating uniformity and thickness, (ii) develop composite drug coatings to expand the utility of coated microneedles, (iii) deliver liquid formulations using solid microneedles, and (iv) examine the effect of microneedle and coating parameters on the mass of drug coated onto microneedles. To attain these

objectives, we varied the physical properties of the coating solution formulations to control the fluid mechanics of the dip-coating process and the thermodynamics of microneedle surface wetting.

The process of wetting a solid with a liquid under static conditions is described by the Young equation. According to this equation, the contact angle should be zero for the liquid to spread on the solid surface to form a uniform liquid film (Stokes, Evans et al. 1997), which, upon drying, would provide a uniform solid coating on the solid substrate. In a coating process, however, the system is not at rest but in a dynamic state as the microneedle gets dipped into and out of the dipping solution and the gravity and local surface tension gradients cause micro-flows in the liquid film adhering to the microneedle surface. Therefore, the static contact angle is no longer an adequate measure of spreading, and the dynamic equilibrium depends upon: (i) the hydrodynamics of the system, (ii) the physical properties of the coating solution and the solid substrate, and (iii) the rate of evaporation of the solvent (Stokes, Evans et al. 1997). Unfortunately, the complex physics of dynamic wetting is not fully understood, which makes theoretical predictions of coating uniformity and thicknesses difficult (Blake and Ruschak 1997; Stokes, Evans et al. 1997). Therefore, while an understanding of the physics of coating can serve as a guide, the control and optimization of microneedle coatings requires experimental study.

Based on the physics of dip-coating, it is recognized that the dip-coating process consists of two distinct steps generally occurring in sequence: (a) the dipping and withdrawal step, resulting in the formation of a liquid film on the solid substrate, and (b) the drying step, resulting in the conversion of the adherent liquid film into a solid coating (Scriven 1988). In the first step, the formation of the liquid film after dipping and withdrawal is fluid mechanically controlled, such that the thickness of the liquid film formed on the solid substrate depends on the withdrawal speed of the solid substrate

and the physical properties of the coating solution, notably the surface tension and viscosity (Scriven 1988). A faster withdrawal speed of the solid substrate, a higher viscosity of the coating solution, and a lower surface tension of the coating solution tend to produce thicker liquid films. There correspondingly exists a critical speed of withdrawal for each coating solution-substrate combination, below which a liquid film does not form on the substrate because the hydrodynamic force of withdrawal is unable to overcome the forces of gravity and solution surface tension. If the substrate is withdrawn above the critical speed, an adherent liquid film is formed even from thermodynamically de-wetting liquids due to the hydrodynamic drag, which overcomes the opposing forces of surface tension and gravity. However, air entrainment in the liquid film at very high withdrawal speed prevents usage of systems with excessively high critical speed requirements (Scriven 1988; Stokes, Evans et al. 1997).

In the second step involving drying of the adherent liquid film on the substrate, the fate of the entrained liquid film is determined by a complex interaction of the hydrodynamics of the entrained liquid film, the rate of solvent evaporation, and the tendency of the liquid film to attain its thermodynamic equilibrium on the solid surface (Scriven 1988; Kheshgi 1997). Thermodynamically, the deposited liquid film may completely wet the surface, which favors formation of a uniform coating, or, alternatively, may have a tendency to de-wet the surface via a surface tension-driven contraction. In this case, increasing the coating solution viscosity can significantly slow down the de-wetting process and provide the coating solution sufficient residence time on the solid surface to allow for solvent evaporation to form the solid film before de-wetting can occur (Scriven 1988). This kinetic effect, therefore, provides a means to coat devices with liquid formulations that thermodynamically favor de-wetting of the solid surface.

Guided by these physical principles, this study investigated the effect of coating solution surface tension and viscosity, and microneedle surface modification on (i)

microneedle coating uniformity, (ii) the mass of drug coated on microneedles, and (iii) the ability to fill pockets in microneedles with coating solution. The coating solution surface tension was modulated by the addition of surfactants and by using non-aqueous solvents. The coating solution viscosity was also modified to increase the coating thickness in order to coat larger amounts of a model drug onto microneedles.

## 5.2 MATERIALS AND METHODS

### 5.2.1 Fabrication of microneedles

Using methods described in detail previously (Gill and Prausnitz 2007a), microneedle geometries were first drafted in AutoCAD software (Autodesk, Cupertino, CA, USA) and then cut into 75 μm thick stainless steel sheets (Trinity Brand Industries, SS 304; McMaster-Carr, Atlanta, GA, USA) using an infrared laser (Resonetics Maestro, Nashua, NH, USA). To form pockets in microneedles, the desired shapes, dimensions and locations of the pockets on the microneedle shaft were also drafted and then cut together with the microneedles. 'In-plane' microneedles were fabricated as one-dimensional rows of microneedles oriented parallel to their base substrate. 'Out-of-plane' microneedles were fabricated as two-dimensional arrays with microneedles bent perpendicularly out of the plane of their base substrate.

To deburr and clean microneedle edges and pockets, and to make the tips sharp, microneedles were electropolished in a solution containing glycerin, ortho-phosphoric acid (85%) and water in a ratio of 6:3:1 by volume (Fisher Chemicals, Fair Lawn, NJ, USA) by applying 1.8 $mA/mm^2$ of current for 15 min. Microneedles were then washed under running water, dried using compressed air, and stored in air-tight containers until later use.

### 5.2.2 Micron-scale dip-coating

Single microneedles, and arrays of multiple microneedles, were coated with molecules using a micron-scale dip-coating process developed previously (Gill and Prausnitz 2007a). Briefly, a coating solution containing a model drug and, in most cases, a surfactant and a viscosity enhancer was prepared in an aqueous or organic solvent. Microneedles were then dipped into the coating solution held in a dip-coating device. Coatings were formed by dipping just once into the coating solution, unless otherwise specified. The withdrawal speed of microneedles from the coating solution was manually maintained at approximately 2 mm/s to produce solid films and at approximately 0.35 mm/s to fill the pockets with a liquid. The microneedles coated with solid films were allowed to air-dry for at least 24 h before use, whereas the pocketed microneedles filled with liquid were used immediately to minimize liquid evaporation.

### 5.2.3 Coating solution formulations

Aqueous coating solution formulations (w/v % unless otherwise specified) were prepared using DI water according to the following recipes: *Formulation A1:* 0.1% sulforhodamine (Molecular Probes, Eugene, OR, USA). *Formulation A2:* 1% carboxymethylcellulose sodium salt (CMC, low viscosity, USP grade, CarboMer, San Diego, CA, USA), 0.5% Lutrol F-68 NF (BASF, Mt. Olive, NJ, USA), 0.1% sulforhodamine. *Formulation A3*: 52% (w/w) sucrose (Fisher Chemicals), 0.2%(w/w) Tween 20 (Sigma, St. Louis, MO, USA), 0.1% sulforhodamine. *Formulation A4:* 0.5% hyaluronic acid (Sigma), 0.5% Lutrol F-68 NF, 0.1% sulforhodamine. *Formulation A5:* 0.5% xanthan gum (Sigma), 0.5% Lutrol F-68 NF, 0.1% sulforhodamine. *Formulation A6:* 1% sodium alginate (Sigma), 0.5% Lutrol F-68 NF, 0.1% sulforhodamine. *Formulation A7:* 5% polyvinylpyrrolidone (BASF), 0.5% Lutrol F-68 NF, 0.1% sulforhodamine. *Formulation A8:* 52% (w/w) sucrose, 0.5% Lutrol F-68 NF, 0.1% sulforhodamine.

*Formulation A9:* 25% sucrose, 0.1% sulforhodamine. *Formulation A10:* 80% (v/v) glycerol, 20% (v/v) aqueous solution of 0.1% sulforhodamine. *Formulation A11:* 1% CMC, 0.5% Lutrol F-68 NF, 0.2% sodium fluorescein (Sigma). *Formulation A12:* 80% (v/v) glycerol, 20% (v/v) green food dye (Kroger, Atlanta, GA, USA). *Formulation A13:* 80% (v/v) glycerol, 20% (v/v) yellow food dye (Kroger). *Formulation A14:* 80% (v/v) glycerol, 20% (v/v) red food dye (Kroger).

Organic solvent coating solution formulations (w/v % unless otherwise specified) were prepared according to the following recipes: *Formulation O1:* 5% poly(lactic-co-glycolic acid) (PLGA, Absorbable Polymer International, Pelham, AL, USA) in acetonitrile (Fisher Chemicals). *Formulation O2:* 5% polyvinylpyrrolidone, 0.1% curcumin (Fisher Chemicals) in ethanol (Fisher Chemicals). *Formulation O3:* 5% PLGA, 0.03% sulforhodamine in acetonitrile.

### 5.2.4 Coating solution viscosity and contact angle measurement

Viscosity of the aqueous coating solution containing CMC and sucrose was measured using an Ubbelohde type viscometer (viscometer no. 200-c21, Cannon Instrument Company, State College, PA, USA). Static advancing contact angles of the coating formulations containing various excipients were measured on electropolished stainless steel using a VCA 2500 XE contact angle system (AST Products, Billerica, MA, USA). Both the viscosity and the contact angles were measured at room temperature with a sample size of at least n=5 for each solution.

### 5.2.5 Effect of coating solution surface tension and viscosity

To study the significance of surfactants and viscosity enhancers in producing uniform coatings on microneedles, single microneedles (n=3) were dipped in formulations A1, A2 and A3. Aqueous solutions of individual constituents of formulations

A2 and A3 with 0.1% sulforhodamine were also used to evaluate their relative and synergistic effects. Further, to assess the ability of different viscosity enhancers to produce uniform coatings using Lutrol F-68 NF as the surfactant, single microneedles (n=3) were dipped in formulations A4, A5, A6, A7 and A8. Dipped microneedles were air-dried for 24 h and examined by fluorescence microscopy using an Olympus IX70 fluorescence microscope (Olympus America, Center Valley, PA, USA) with a CCD camera (RT Slider, Diagnostic Instruments, Sterling Heights, MI, USA) to assess coating uniformity.

### 5.2.6 Microneedle surface modification

To enable coating of microneedles without the use of excipients in the coating solution, we modified the stainless steel surface properties by depositing silicon dioxide or PLGA. Silicon dioxide was deposited using a vapor deposition method (PlasmaTherm PECVD, Plasma-Therm, St. Petersburg, FL, USA), while PLGA was deposited by dipping the microneedles in formulation O1. Surface-modified microneedles were then dipped into formulation A1, dried, and examined by fluorescence microscopy to assess coating uniformity.

### 5.2.7 Coatings involving hydrophobic molecules, molten coating solutions and pocketed microneedles

To coat hydrophobic molecules, single microneedles (n=3) were dip-coated using formulations O2 or O3. Microneedles dipped in formulation O2 were immersed in water for 15 s and checked for loss of coating from the microneedle surface by fluorescence microscopy. To apply coatings of essentially 100% drug, single microneedles with or without rectangular pockets (400 μm long x 50 μm wide) were dipped in molten liquid solutions of lidocaine (Sigma) at 100°C or polyethylene glycol (MW 1500, Fisher

Chemicals) at 45°C, each containing up to 0.01% (w/v %) sulforhodamine. A hot plate was used as the heat source.

To apply coatings into microneedle pockets, single microneedles (n=3) with a rectangular pocket 400 μm long and 50 μm wide were dipped in formulation A2, A9 or A10. To coat both the microneedle surface and the pockets using formulation A2, a total of 6 dips each separated by 15 s were used. Multiple dips separated by drying intervals enabled filling the pockets with more material as compared to just a single dip. However, for formulations A9 and A10, single dips were used to fill just the pockets. For formulation A9, single dips prevented patchy coatings on the surface that can result from repeated dips and microneedle surface irregularities. For formulation A10, a single dip was sufficient to fill just the pockets, because the coating remained as a liquid phase. After each of these coating procedures, microneedles were air dried for at least 24 h and examined by fluorescence microscopy to assess coating uniformity. However, the liquid-filled pocketed microneedles were used immediately for imaging or insertion into porcine cadaver skin to minimize liquid evaporation.

### 5.2.8 Composite coatings

Single microneedles with or without pockets were sequentially dipped in different formulations to produce composite coatings of multiple molecules. Four different schemes were evaluated. (1) Pocketed microneedles with three circular pockets (90 μm diameter each) were sequentially dipped into different formulations to fill each pocket with a separate solution. This was achieved by first dipping all three microneedle pockets into formulation A12 and then sequentially dipping them into DI water, formulation A13, DI water and formulation A14. At each DI water wash step, the length of microneedle immersed into the wash water and all subsequent dip solutions was

sequentially decreased by one pocket length to retain the formulation filled in the pocket from the previous dip, but cleaning the other pocket(s). (2) Non-pocketed microneedles were dipped into formulation O3 (6 dips) and then into formulation A11 (6 dips). (3) Non-pocketed microneedles were sequentially dipped into formulation A2, O1 and A11. (4) Microneedles with a rectangular pocket (400 μm x 50 μm) were dipped sequentially into formulations A9, O1 and A11. Between sequential dips and after completion of composite coatings, microneedles were air dried and imaged by fluorescence microscopy.

### 5.2.9 Protein coatings

To assess the ability of optimized formulations to coat proteins, fluorescein isothiocyanate-labeled, (i) insulin derived from bovine pancreas (MW= 6 kDa, Sigma) and (ii) bovine serum albumin (BSA) (MW= 66 kDa, Sigma) were coated onto microneedles (n=3). Insulin (0.075% w/v) and BSA (0.15% w/v) were each coated onto single microneedles using excipients of formulations A2, A4 and A6. Microneedles were then air dried and imaged by fluorescence microscopy.

### 5.2.10 Determination of mass in coatings

To modulate the mass of material coated onto microneedles, coating parameters and microneedle parameters were investigated. The coating parameters that were studied included, (i) the concentration of a model drug in the coating solution and (ii) the number of dips during coating, and the microneedle parameters that were investigated included, (i) the number of microneedles in the array and (ii) the ability to selectively fill the microneedle pockets. Riboflavin (vitamin B2, riboflavin-5'-phosphate sodium salt dihydrate, Fisher Chemicals) was used as the model drug in the coating formulations. In-plane rows of microneedles were dipped into a solution containing 1% sodium salt of

CMC, 0.5% Lutrol F-68 NF and a range of riboflavin concentrations. For the study of coating parameter (i), riboflavin was used at 0.01%, 0.1%, 1%, 2%, 3% and 4% concentrations (n=5 rows for each condition) with 6 dips at 15 s intervals between dips. For coating parameter (ii), a 3% riboflavin concentration was used with 1, 3, 6, 12 or 24 dips at 15 s intervals between dips (n=5 rows for each condition). To study microneedle parameter (i), a 3% riboflavin solution was used with out-of-plane arrays having 5 or 50 needles (n=3 arrays for each condition) with 6 dips at 15 s intervals between dips. To investigate microneedle parameter (ii), i.e. the ability of pocketed microneedles to carry the model drug exclusively within the pockets and without coating the surfaces, in-plane rows with five microneedles each having a rectangular pocket (400 μm x 50 μm) were dipped into an aqueous formulation containing 1% or 3% riboflavin and 25% sucrose with 6 dips at 15 s intervals between dips. All coated microneedles were allowed to dry for at least 24 h and imaged by brightfield microscopy using an Olympus SZX12 stereo microscope (Olympus America) with a CCD camera (Leica DC 300, Leica Microsystems, Bannockburn, IL, USA). The mass of riboflavin in the coatings was determined by dissolving the coatings off the microneedles by immersing in DI water and vortexing for 1 min, and then measuring riboflavin concentration by calibration fluorescence spectroscopy (SpectraMax Gemini, Molecular Devices, Sunnyvale, CA, USA; excitation = 450 nm, emission = 534 nm). The mass of riboflavin in the coatings was then calculated by multiplying the riboflavin concentration by the volume of DI water used to dissolve the coatings (typically 1 ml).

### 5.2.11 Microneedle delivery into skin in vitro

Single, non-pocketed microneedles coated with formulation A2 (n=3) and single, pocketed (rectangular pocket - 400 μm x 50 μm) microneedles coated with formulation

A10 (n=3) were each manually inserted into abdominal porcine cadaver skin for 20 s and then removed. Microneedle insertion speed was manually maintained at 0.5 to 1 mm/s or 1 to 2 cm/s for microneedles coated with formulation A2 and A10, respectively. After removing the microneedles, the skin surface was examined by brightfield microscopy for coating residue. The skin was then examined histologically to assess the extent of delivery of microneedle coatings into the skin. The use of porcine cadaver skin has been approved by the Georgia Institute of Technology Institutional Animal Care and Use Committee (IACUC).

### 5.2.12 Microneedle penetration into skin of human subjects

For in vivo analysis, out-of-plane arrays of non-coated microneedles were assembled into adhesive patches (Gill and Prausnitz 2007a), ethylene oxide sterilized, and manually applied to the volar forearms of human subjects (n=3). After removing the microneedle patch, gentian violet (2% solution, Humco, Texarkana, TX, USA) was applied to the treated site for 1 min and then wiped away using isopropanol swabs. Gentian violet selectively stained the sites of skin perforation, which identified the sites of microneedle penetration. The use of human subjects has been approved by the Georgia Institute of Technology Institutional Review Board (IRB).

## 5.3 RESULTS AND DISCUSSION

### 5.3.1 Microneedles for coating and insertion

Stainless steel microneedles with appropriate mechanical properties, sharp tips and clean edges were prepared in different configurations for dip-coating. Microneedles were fabricated as single microneedles without pockets (Figure 5.1 A), single microneedles with three circular pockets each 90 μm in diameter (Figure 5.1 B), single microneedles with a single rectangular pocket measuring 400 μm by 50 μm (Figure 5.1

C), in-plane microneedle rows each containing five microneedles (Figure 5.1 D) and out-of-plane microneedle arrays each with 50 microneedles (Figure 5.1 E). All needles were 700 μm in length, 160 μm in width and 50 μm in thickness. In-plane rows each with five, rectangular pocketed (400 μm by 50 μm) microneedles were also fabricated (image not shown).

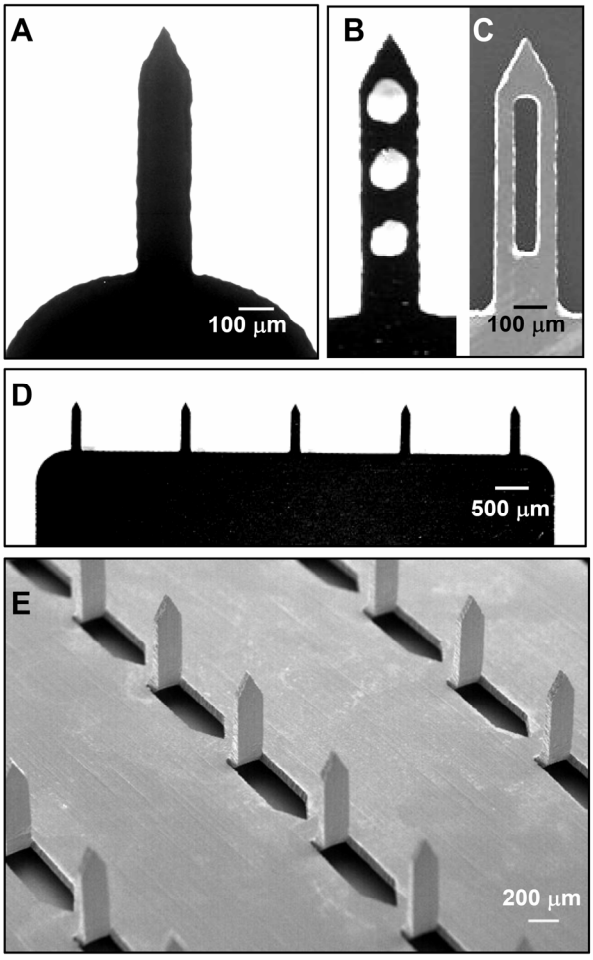


**Figure 5.1. The different microneedle designs used for coating experiments**. Brightfield microscopy image of (A) a single microneedle and (B) a circular-pocketed microneedle. (C) Scanning electron microscopy image of a rectangular-pocketed microneedle. (D) Brightfield microscopy image of an 'in-plane' row of five microneedles attached to a macroscopic base substrate for ease of handling. (E) Scanning electron microscopy image of a section of an 'out-of-plane' array with fifty microneedles.

### 5.3.2 Uniform coatings with spatial control

For dose reliability, it is critical to consistently apply uniform coatings just to the microneedle shafts without contaminating the substrate. Using custom-designed dip-coating devices, microneedles of different configurations including single microneedles, in-plane rows of microneedles and out-of-plane microneedles, were uniformly coated with spatial control over the microneedle length being coated. A representative example of a riboflavin-coated, out-of-plane microneedle array containing 50 microneedles is shown in Figure 5.2 A and a representative magnified view of a single microneedle from the coated array is shown in Figure 5.2 B. The properties of coating solution excipients required to obtain uniform coatings are quantitatively assessed below.

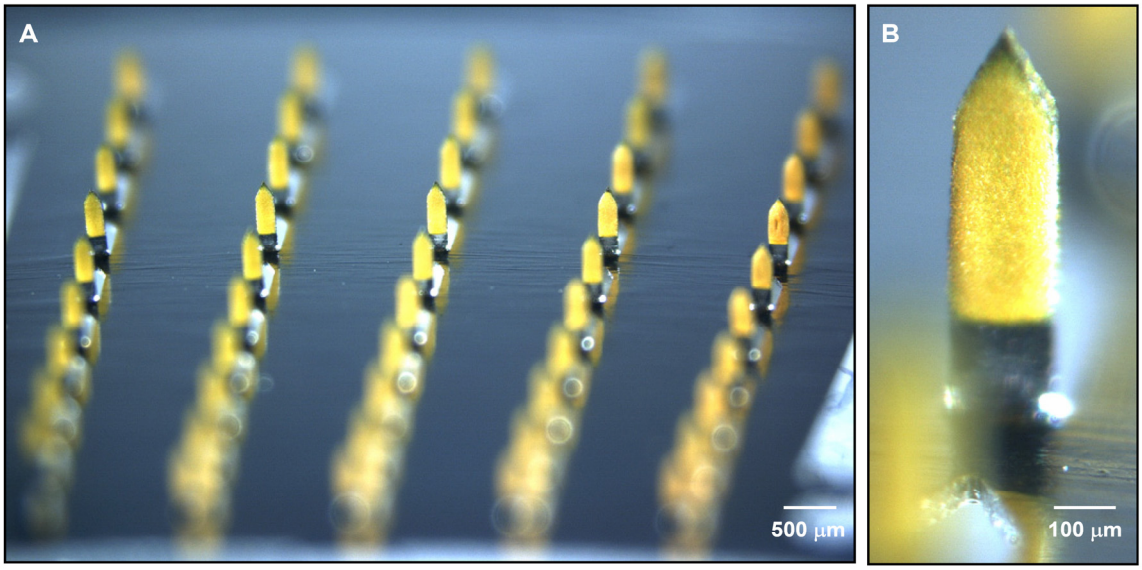


**Figure 5.2. Out-of-plane microneedle array uniformly coated with riboflavin**. Imaging by brightfield microscopy shows (A) uniform coating of microneedle shafts without contamination of the base substrate of an array of 50 microneedles and (B) a representative magnified view of a single microneedle showing the uniform coating.

### 5.3.3 Effect of coating solution surface tension and viscosity

Dose reproducibility and a high drug loading into microneedle coatings are critical for pharmaceutical drug and vaccine delivery applications of coated microneedles. This requires precision deposition of uniform and thick coatings onto microneedle shafts. Control over physical properties and kinetic parameters that affect the thermodynamics and hydrodynamics of dip-coating are expected to result in uniform and thick coatings. The two important physical properties of the dipping formulation that are known to influence the thermodynamics and hydrodynamics of dip-coating are surface tension and viscosity. However, the complex physics of dip-coating is not fully understood to develop theoretical models that can accurately predict the effect of surface tension and viscosity on coating uniformity and thickness, especially at the micron length scales of microneedles. Therefore, we dip-coated microneedles using different formulations to experimentally study their effect on coating uniformity and coating thickness.

First, microneedles were dipped in an aqueous solution containing sulforhodamine as a model drug. This formulation did not produce any coating on the microneedle (Figure 5.3 A). Thermodynamics of wetting dictates that only solutions that can completely wet the substrate i.e. have contact angles that approach zero can produce uniform films on the substrate, but the static contact angle of DI water on electropolished stainless steel was measured to be 47.5 ± 3 degrees. This large contact angle is the result of the aqueous coating solution having a surface tension (72 mN/m at 25 °C) (Lide 2006) much larger than the stainless steel substrate (39.6 $mJ/m^2$) (Zhao, Wang et al. 2007). We therefore added Lutrol F-68 NF, a surfactant, which lowered the coating solution surface tension and thereby decreased the contact angle to 25.9 ± 5 degrees. This produced a uniform, but thin, coating on the microneedles (Figure 5.3 B).

Thicker coatings should increase the drug loading on microneedles. Based on the hydrodynamics of dip-coating, thicker coatings can be obtained by increasing the

coating solution viscosity, because elevated viscosity increases the hydrodynamic drag on the liquid during substrate withdrawal and leads to an increase in the volume of the liquid film that is formed on the microneedle upon withdrawal. Thus, to test the ability of a higher viscosity of the aqueous formulation to produce thicker coatings, CMC, a viscosity enhancer, was added to the aqueous coating solution. The surfactant, Lutrol F-68 NF was not included in the formulation to independently study the effect of the viscosity enhancer. Using a 1% (w/v) aqueous CMC solution (viscosity: 47 ± 0.5 mPa.s) as the coating solution, a thicker coating was produced on the microneedle. However, the coating was localized towards the center, away from the microneedle periphery (Figure 5.3 C). This phenomenon of de-wetting suggested that the high surface tension of the CMC-containing aqueous solution induced contraction of the liquid film on the microneedle during the drying phase.

Finally, we simultaneously modified the surface tension and the viscosity of the coating solution by adding both the surfactant and the viscosity enhancer, which resulted in thick and uniform coatings (Figure 5.3 D). Thus, application of the macro-scale principles of thermodynamics and hydrodynamics of wetting and dip-coating to the micron length scale of microneedles enabled the formation of (i) uniform coatings on microneedles by matching the surface energies of the coating solution and the substrate to promote wetting and (ii) thicker coatings by increasing the viscosity of the coating solution, which increased the volume of the liquid film adhering to the microneedle upon withdrawal from the coating solution. These two criteria form a general basis for designing coating solution formulations to produce uniform coatings on microneedles.

In order to test the generality of these findings, we coated microneedles using another aqueous surfactant-viscosity enhancer system. Based on a previous study (Widera, Johnson et al. 2006), we selected Tween 20 as the surfactant and sucrose as the viscosity enhancer. A similar trend in coating uniformity and thickness was observed

for these aqueous coating solutions. A coating solution containing only Tween 20 (contact angle: 25.3 ± 4 degrees) and sulforhodamine as the model drug resulted in a very thin, but uniform layer on the microneedle surface (Figure 5.3 E), while coating with only sucrose (52% w/w, viscosity: 18.7 ± 0.1 mPa.s) produced a thicker coating which was localized along the center of the microneedle shaft (Figure 5.3 F). Next, combining Tween 20 with sucrose increased the spread of the coatings on the microneedle surface, although the tip still remained uncoated (Figure 5.3 G). Thus, this surfactant-viscosity enhancer combination gave results similar to the Lutrol F-68 NF and CMC combination. Uncoated microneedle tips can slightly decrease the amount of drug coated onto microneedles. However, if this decrease is not significant, the excipients may be acceptable.

### 5.3.4 Choice of excipients for coatings

The previous set of experiments identified two formulations useful for microneedle coatings, both of which utilized excipients categorized by the FDA as safe for parenteral delivery (Kibbe 2000). Optimization among these and other possible coating formulations will depend on drug physicochemical properties and needs of specific applications. For example, the use of CMC as a viscosity enhancer may be preferred over sucrose, because just 1% CMC (w/v) increased viscosity more than twice as much as 52 % (w/w) sucrose. Minimizing excipient concentrations maximizes drug content in the coatings. Comparing the surfactants, Lutrol F-68 may be preferred over Tween 20, because Lutrol F-68, which is solid at room temperature, produced hard coatings, whereas, Tween 20, which is a liquid at room temperature, produced coatings with a waxy texture.

For specific applications, it may be desirable to use other excipients, for example, to avoid unfavorable drug-excipient interactions. Therefore, based on the coating

formulation design criteria established above, we examined the ability of five additional viscosity enhancers in combination with Lutrol F-68 surfactant to produce good coatings. In all five cases, using hyaluronic acid (Figure 5.3 H), xanthan gum (Figure 5.3 I), sodium alginate (Figure 5.3 J), polyvinylpyrollidone (Figure 5.3 K) and sucrose (Figure 5.3 L) as the viscosity enhancers, thick uniform coatings were formed, although the sucrose formulations did not coat the tips, which may be due to the crystallinity and relatively high surface tension of sucrose. Altogether, this suggests that decreasing surface tension and increasing viscosity of the coating solution is a broadly applicable approach to rationally design optimized coating solution formulations.

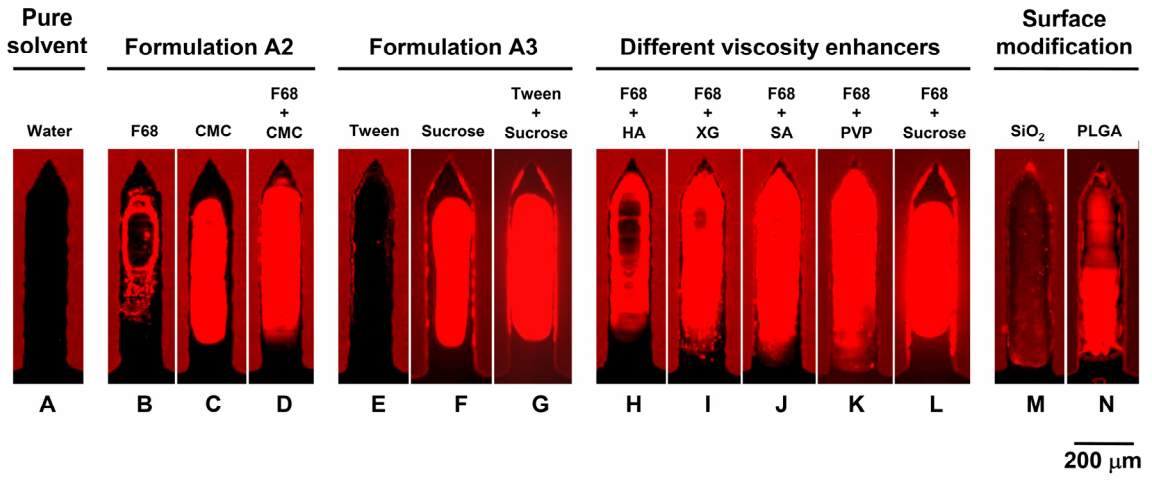


**Figure 5.3. Effect of surface tension and viscosity on coating uniformity on microneedles with sulforhodamine as the model drug.** Fluorescence microscopy images with supplemental brightfield illumination to also view the microneedle outline after dip-coating single non-pocketed microneedles from different formulations. (A) Aqueous coating without excipients (Formulation A1). Based on Formulation A2, (B) coating only with Lutrol F-68 (F68), (C) coating only with carboxymethylcellulose (CMC), and (D) coating with the full formulation. Based on Formulation A3, (E) coating only with Tween 20, (F) coating only with sucrose, and (G) coating with the full formulation. Coating with F68 and (H) hyaluronic acid (HA) (Formulation A4), (I) xanthan gum (XG) (Formulation A5), (J) sodium alginate (SA) (Formulation A6), (K) polyvinylpyrrolidone (PVP) (Formulation A7), and (L) sucrose (Formulation A8). Aqueous coating without excipients (Formulation A1) on microneedle surfaces modified by pre-coating with (M) silicon dioxide ($SiO_2$) and (N) poly(lactic-co-glycolic acid) (PLGA).

### 5.3.5 Surface modification for coating

The addition of excipients may be undesirable for some drugs due to incompatibility between the drug and the excipients, which may lead to loss of drug activity (Yoshioka and Stella 2002). Rather than matching the surface energies of the coating solution and the microneedle surface by lowering the surface tension of the coating solution using a surfactant, we instead raised the surface energy of the stainless steel microneedles by making it more hydrophilic by pre-coating the microneedles with a thin layer of silicon dioxide. Subsequent coating with an excipient-free, aqueous solution of sulforhodamine resulted in a uniform but thin coating (Figure 5.3 M), consistent with coating using appropriately matched surface energies, but inadequate viscosity.

As an additional approach, the stainless steel microneedle surface was pre-coated with PLGA, which also resulted in a uniform, but thin coating using an excipient-free solution (Figure 5.3 N). Although, PLGA provides a hydrophobic surface that does not improve the thermodynamics of the microneedle-coating solution surface energy mismatch, we believe it instead increased surface roughness, which increased the hydrodynamic drag to allow entrainment of a liquid film and reduced the surface tension-induced fluid contraction on the microneedle surface, and thereby increased the residence time for drying of a thin film on the PLGA surface. Although these excipient-free methods produced only thin coatings, surface modification may nonetheless be well suited for coating sensitive protein solutions, since protein solutions are often inherently viscous and can act as self-viscosity enhancers to increase the coating thickness.

### 5.3.6 Coating proteins

To directly assess the ability of optimized formulations to coat proteins, we coated insulin and bovine serum albumin onto microneedles using Lutrol F68 as the surfactant and either CMC, hyaluronic acid or sodium alginate as the viscosity enhancer.

Uniform coatings were obtained on the microneedle shafts for both proteins and all formulations tested (Figure 5.4). These observations are consistent with our previous work (Gill and Prausnitz 2007a), which demonstrated coating of peptides, proteins, DNA, viruses and microparticles. Together, these results suggest that the coating formulations developed in this study may have a broad applicability to coat a range of compounds and microparticles.

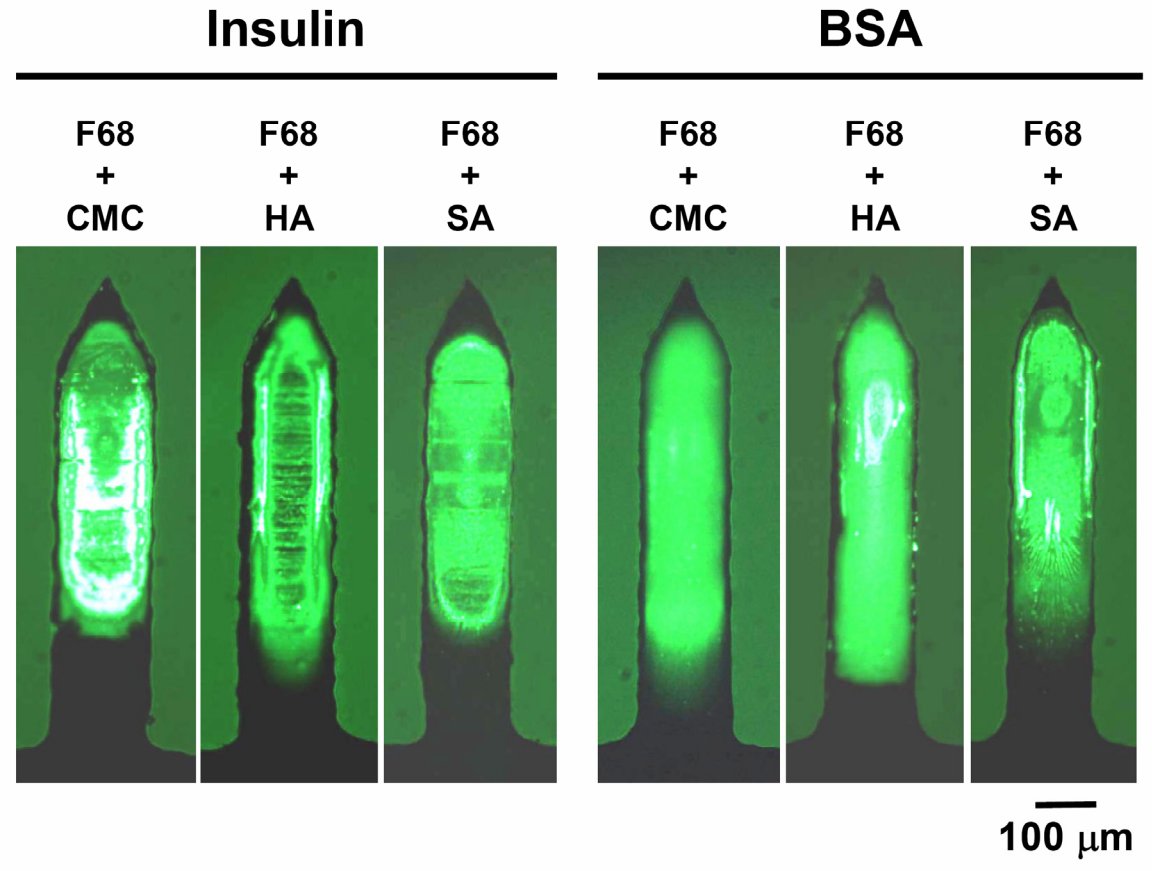


**Figure 5.4. Microneedles with protein coatings**. Fluorescence microscopy images with supplemental brightfield illumination of single non-pocketed microneedles dip coated with fluorescein isothiocyanate-labeled insulin and bovine serum albumin (BSA) using Lutrol F-68 (F68) and carboxymethyl cellulose (CMC) (Formulation A2), Lutrol F-68 and hyaluronic acid (HA) (Formulation A4) and Lutrol F-68 and the sodium salt of alginic acid (SA) (Formulation A6).

### 5.3.7 Coating hydrophobic molecules

Having studied a variety of approaches to coat microneedles from aqueous formulations, we next wanted to investigate coating of hydrophobic molecules. This provided an interesting formulation challenge, because excipients for this application need to be soluble in an organic coating solution solvent as well as soluble in the aqueous environment of the skin for rapid dissolution off the microneedle after insertion. We therefore selected an amphiphilic viscosity enhancer, polyvinylpyrrolidone (PVP), which has good solubility in water and in ethanol, the organic solvent selected for the coating solution. Use of an organic solvent also removed the need to add surfactant, since ethanol already has a low surface tension (21.8 mN/m at 25 °C) (Lide 2006). For this study, curcumin was used as the model hydrophobic drug. Curcumin is also fluorescent, making it easy to visualize the coatings.

Microneedles prepared using this formulation resulted in uniform coatings of the microneedle surfaces (Figure 5.5 A). Consistent with the design, dipping the coated microneedles into DI water for just 15 s completely removed the coatings. Even though curcumin has negligible solubility in water, dissolution of PVP excipient caused the microneedle coating to fall off the microneedle surface (Figure 5.5 B). Using an alternate approach, microneedles were coated using PLGA as the viscosity enhancer from an acetonitrile-based coating solution containing sulforhodamine. This formulation approach also resulted in uniform coatings (Figure 5.5 C). Because PLGA coatings degrade slowly in water, this formulation is envisioned to provide controlled release from coated microneedles left in the skin for an extended period of time.

### 5.3.8 Molten coating solutions

To simplify the coating formulation further, we next wanted to investigate coatings prepared without solvent or excipient. Because many solid drugs can remain

stable above their melting point, microneedles could be coated by dipping them into pure drug as a molten liquid. This method would enable coatings made of 100% drug and therefore result in higher mass loaded per microneedle. To test this idea, both pocketed and non-pocketed microneedles were dip-coated into molten lidocaine. Because the molten lidocaine was very viscous, the resulting coatings were thick and covered the entire surface in both non-pocketed (Figure 5.5 D) and pocketed (Figure 5.5 E) microneedles. As an additional model compound, molten polyethylene glycol (PEG) was coated onto microneedles, which was unable to coat non-pocketed microneedles well (data not shown). This probably occurred because molten PEG has high surface tension (45 mN/m at 70 °C) (Cheboyina, O'Haver et al. 2006). However, molten PEG was able to fill the interior of pocketed microneedles (Figure 5.5 F). These observations show that by using the molten liquid coating approach, drugs can be coated in their pure state on the surface of microneedles and inside microneedle pockets. As another variation, coating microneedles via the molten formulations may provide a way to coat and deliver hydrophobic molecules using molten polymers as a non-volatile solvent, because molten substances like PEG and PVP are known to improve solubility of hydrophobic drugs (Leuner and Dressman 2000).

### 5.3.9 Pocketed microneedles

We next wanted to explore other ways to fill drug formulations into microneedle pockets. Pockets in microneedles can provide a protective cavity that can be exploited to deliver drug formulations that would otherwise be difficult to coat onto microneedles or would wipe off on the skin surface during insertion. The previously successful formulation comprising Lutrol F-68 and CMC was used to coat pocketed microneedles, and was found to coat both the microneedle surfaces as well as fill the pockets (Figure 5.5 G). Thus, the use of formulations with surfactant and viscosity enhancer may provide

a general method to coat and fill pocketed microneedles. However, in some circumstances it may be desirable to only fill the protective pockets without coating the microneedle surfaces. We were able to selectively fill the pockets by (i) removing the surfactant to inhibit surface wetting and increase the critical speed of liquid film formation, (ii) keeping the viscosity enhancer to help retain coating solution within pockets, and (iii) increasing the solids content by using 25% sucrose to help produce a conformal solid layer in the pockets (Figure 5.5 H).

In some cases it may be desirable to store and deliver a drug in liquid solution. Pocketed microneedles offer the further possibility to deliver drug formulations as liquids. In this way, the liquid can be protected from wiping off the microneedle during insertion into skin (see below). Dipping microneedles in a viscous glycerol solution containing sulforhodamine selectively filled the pockets without coating the microneedle surfaces (Figure 5.5 I). Glycerol has a high surface tension (62.5 mN/m at 25 °C) (Lide 2006) and such a high critical speed of liquid film formation that it does not produce liquid films on the microneedle surface. Yet, it is viscous enough to fill the pockets by counteracting the surface tension that tends to collapse the liquid drop formed inside the pocket. To further prevent micron-scale surface roughness from accumulating any liquid drops, microneedle withdrawal from the glycerol solution was done at a slow speed (about 0.35 mm/s). A limitation of this approach, however, is that the liquid in the pockets can evaporate: the glycerol in this example completely evaporated after approximately 24 h at ambient conditions. A similar coating using sulforhodamine dissolved in propylene glycol also selectively filled the pockets, but evaporated more rapidly (data not shown). For extended storage, these liquid filled pockets can be made more stable, for example, by packaging under pressure in a nitrogen atmosphere.

### 5.3.10 Composite coatings

Some therapeutic delivery scenarios may require the application of different drugs from the same microneedle and may require different drug release profiles. To address this scenario, our next objective was to study composite drug coatings as a way to coat multiple drugs on the same microneedle. As a first example, microneedles were prepared to each have three circular pockets. Using the liquid glycerol method to selectively fill pockets, a sequence of dipping and washing steps (see Materials and Methods) was used to fill the upper pocket with a red dye, the middle pocket with a yellow dye and the lower pocket with a green dye (Figure 5.5 J). This “traffic signal” design enabled microneedles with three different model drugs each sequestered in different pockets to avoid drug-drug interactions.

We also explored ways to prepare layered coatings, such that each layer could contain different drugs and could be formulated to have different release kinetics. To have a burst release of a first drug followed by slow release of a second drug, a PLGA layer containing sulforhodamine was overcoated with water-soluble excipients containing sodium fluorescein (Figure 5.5 K). To achieve sequential burst releases separated by a delay, a coating made of water soluble excipients containing sulforhodamine was overcoated with PLGA followed by applying another layer containing water-soluble excipients and sodium fluorescein (Figure 5.5 L). As another double-burst approach, microneedle pockets were selectively filled with water-soluble excipients containing sulforhodamine and covered with PLGA, which was then followed by another layer containing water-soluble excipients and sodium fluorescein (Figure 5.5 M). Dipping these layered composite microneedles into DI water for 1 min caused the exposed water-soluble layers to dissolve, while the PLGA layers and the water-soluble layers beneath them remained intact (data not shown). Variations on these composite coatings

could be tailored to meet drug delivery requirements for complex delivery profiles for single or multiple drugs.

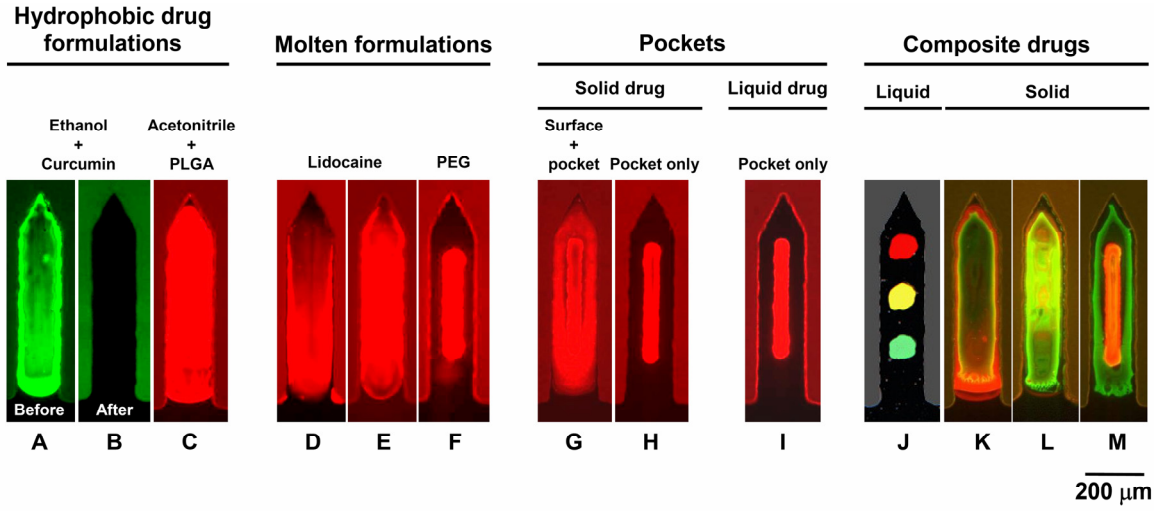


**Figure 5.5. Microneedles with hydrophobic coatings, molten formulation-based coatings, coatings of pocket designs, and composite coatings**. Fluorescence microscopy images with supplemental brightfield illumination to also view the microneedle outline after dip coating single microneedles (non-pocketed unless specified) from different formulations. Coating resulting from Formulation O2, containing polyvinylpyrrolidone and fluorescent curcumin in ethanol solvent (A) before and (B) after dipping in water for dissolution test. (C) Coating resulting from Formulation O3, containing poly(lactic co-glycolic acid) (PLGA) in acetonitrile solvent with fluorescent sulforhodamine. Coating resulting from liquid molten lidocaine containing fluorescent sulforhodamine on (D) non-pocketed microneedles and (E) pocketed microneedles. (F) Coating resulting from liquid molten polyethylene glycol containing fluorescent sulforhodamine. Coatings of pocketed microneedle designs from aqueous solutions of fluorescent sulforhodamine, (G) using Formulation A2 containing carboxymethylcellulose and Lutrol F-68, (H) using Formulation A9 containing sucrose, and (I) using Formulation A10 containing glycerol. (J) Three circular pockets filled with glycerol solution containing a green dye (bottom pocket), a yellow dye (middle pocket) and a red dye (apical pocket) using Formulation A12, A13 and A14, respectively. (K) Two distinct coating layers from sequential dips, first in poly(lactic co-glycolic acid) (PLGA) in acetonitrile solvent with fluorescent sulforhodamine (Formulation O3) and then in an aqueous solution of carboxymethylcellulose, Lutrol F-68 and sodium fluorescein (Formulation A11). (L) Three distinct coating layers from sequential dips, first in an aqueous solution of carboxymethylcellulose, Lutrol F-68 and sulforhodamine (Formulation A2), then in poly(lactic-co-glycolic acid) in acetonitrile (Formulation O1) and lastly in an aqueous solution of carboxymethylcellulose, Lutrol F-68 and sodium fluorescein (Formulation A11). (M) Three distinct coating layers from sequential dips, first in an aqueous solution of sucrose containing fluorescent sulforhodamine (Formulation A9), then in poly(lactic-co-glycolic acid) in acetonitrile solvent (Formulation O1), and lastly in an aqueous solution of carboxymethylcellulose, Lutrol F-68 and sodium fluorescein (Formulation A11).

### 5.3.11 Factors affecting mass in coatings

Because microneedles are small, they are inherently limited to deliver small doses of drug. To determine how much drug could be delivered using microneedles and how to coat microneedles with controlled amounts of drug, we studied the effect of four parameters on the mass of drug coated onto microneedles using riboflavin (vitamin B2) as the model drug. First, two coating parameters were examined, which showed that the concentration of drug in the coating solution and the number of coating dips increased both the mass of drug coated onto microneedles and the thickness of the coating (Figures 5.6 A and B). At the maximum concentration of riboflavin used (i.e. 4%), a mass of 2.6 ± 0.3 μg of riboflavin was coated per microneedle. At the maximum number of dips used (i.e. 24 dips), a mass of 6.4 ± 0.8 μg riboflavin was coated per microneedle. Although we determined that coatings containing up to 1.8 μg riboflavin (i.e. 6 dips) successfully inserted into porcine cadaver skin, thicker coatings may wipe off onto the skin surface during insertion, which would limit their utility. Despite this limitation, these results suggest that a patch about 10 to 20 $cm^2$ in size containing a few hundred microneedles is capable of delivering up to 1 mg of drug.

Changing microneedle design also affected drug coating. For example, increasing the number of microneedles from 5 to 50 did not change the drug mass on each microneedle and therefore proportionally increased the mass on the array approximately ten fold (Figure 5.6 C). This demonstrates the consistency and uniformity of the coatings among the needles of the arrays. Filling drug selectively into pockets reduced the amount of drug per microneedle. For example, filling the pockets with riboflavin using an aqueous formulation containing 3% riboflavin and 25% sucrose enabled loading up to 0.066 ± 0.013 μg per microneedle (Figure 5.6 D). Guided by

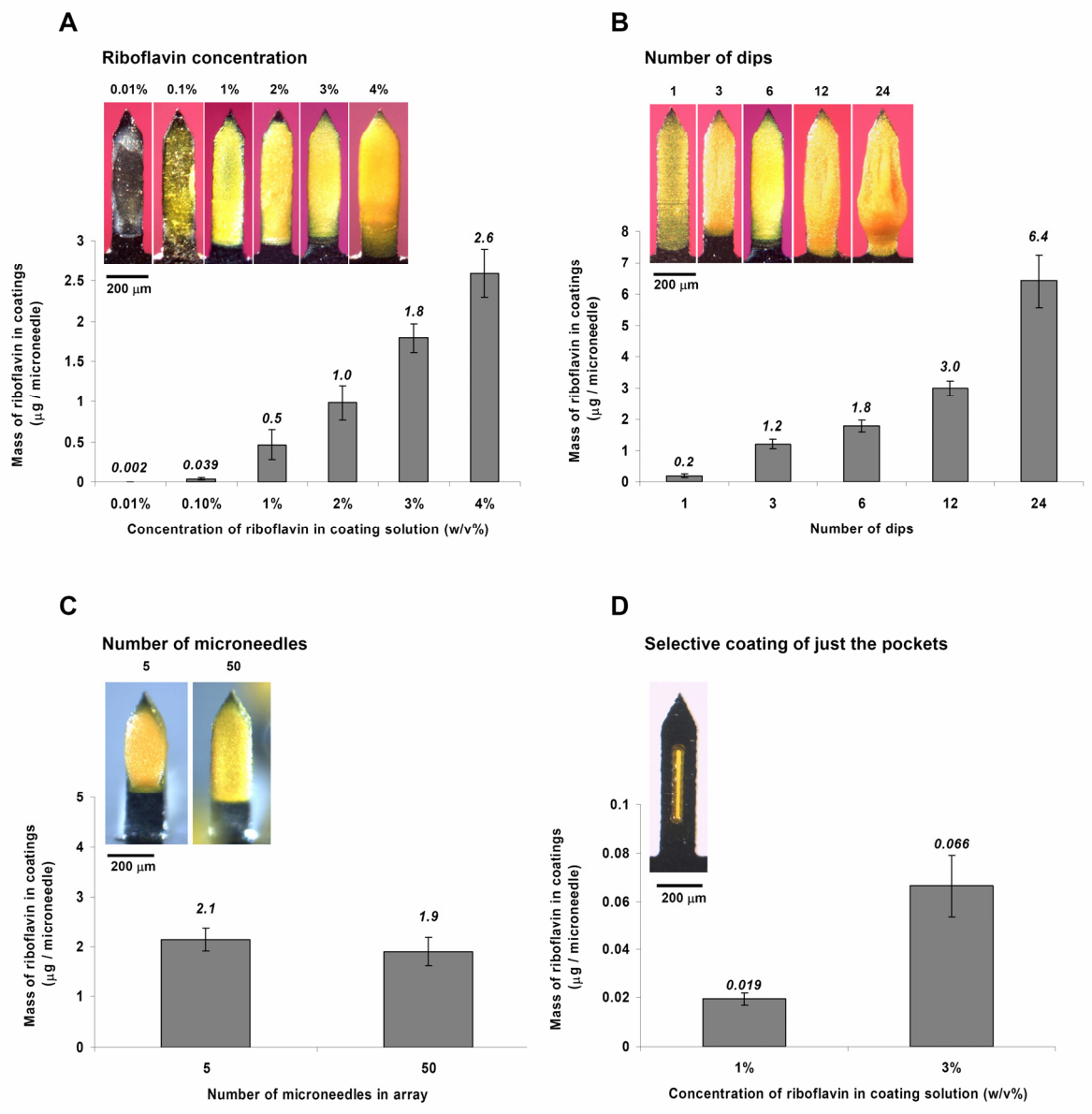


**Figure 5.6. Mass of riboflavin coated on microneedles as a function of formulation and microneedle parameters**. Effect of (A) riboflavin concentration in coating solution, (B) number of coating solution dips, (C) number of microneedles in the array, and (D) riboflavin concentration during selective coating of microneedle pockets. The coatings were done using (A), (B) and (C) Formulation A2, and (D) Formulation A9, with riboflavin as the model drug. Inset images show brightfield microscopy views of microneedles representative of the ones used to generate the data in the graphs.

these relationships, a single coating or microneedle parameter or a combination can be used to coat a pre-determined mass of drug onto microneedles.

As an additional assessment, we studied the reproducibility of controlling the amount of drug coated on to microneedles for drug delivery. While standard deviation bars are shown for the specific experiments in the graphs in Figure 5.6, the average relative standard deviation (RSD) of all the standard deviation bars in Figures 5.6 A, B and C equals 19%. As a comparison, the 'readily acceptable' pass criteria established by the FDA for the manufacture of tablets and capsules is set at RSD ≤ 5% . We expect that since the current microneedle coating process is performed manually, improved control of temperature and humidity in the coating environment, precision in making coating formulations, and automation of the coating process should reduce the RSD to within acceptable limits.

### 5.3.12 In vitro and in vivo insertion into skin

It is important to prepare microneedle coatings that not only adhere to microneedles, but adhere to them during insertion into the skin and then dissolve off within the skin. To assess this, microneedles coated using many of the formulations discussed above were inserted into porcine cadaver skin. Coated microneedles were found to insert into the skin, their coatings did not wipe off onto the skin surface, and the coatings dissolved off the microneedles within less than 1 min and remained in the skin after microneedle removal.

Figure 5.7 A shows a representative result for a non-pocketed microneedle coated with an aqueous formulation of sulforhodamine. The histological section of pig skin after insertion and removal of the microneedle displays the track left in the skin at the site of microneedle insertion and the fluorescence of coated sulforhodamine deposited in the skin. Note the lack of fluorescence on the skin surface consistent with deposition within the skin, and not on the surface. After removal, the microneedle was clean, indicating complete delivery of the coated formulation. No noticeable difference

was perceived in the manual effort required to insert a coated versus an uncoated microneedle into porcine cadaver skin.

Through a companion study, quantitative assessment of the percentage of model drug delivered into the skin was made (Gill and Prausnitz 2007a). It was found that after a 5-min insertion of riboflavin coated microneedle rows with 5 needle shafts, 91 ± 6 % of the riboflavin was delivered into the skin, whereas 2 ± 1 % was found on the skin surface and 7 ± 2 % remained adhered to the microneedle surface after removal from the skin.

Figure 5.7 B shows a representative result for a pocketed microneedle filled with a liquid, glycerol-based formulation of sulforhodamine. As proposed, the pocket protected and carried the liquid formulation into the skin for subsequent and rapid release within the skin. Microneedle insertion speed affected the tendency of the liquid in the coatings to wipe off on the skin surface. Low insertion speeds (0.5 to 1 mm/s), typically used for inserting microneedles coated with a solid film, led to wiping off of some liquid on the skin surface (data not shown). To prevent this liquid wipe off during insertion, higher insertion speed of about 1-2 cm/s was used, which reduced the contact time between the liquid contained in the pockets and the skin surface, thus preventing liquid wipe off on the skin surface.

As a final assessment, we wanted to determine if these microneedles can insert into the skin of human subjects in vivo. Because we did not have IRB approval to use coatings on human subjects, we inserted a non-coated 50-microneedle array into the skin of human subjects. After removing the microneedles, a dye was applied to the skin to stain the sites of microneedle penetration into the skin. Brightfield imaging of the skin surface displayed stained dots that correspond to the insertion sites of all 50 of the microneedles in the array (Figure 5.7 C). Insertion of 50-microneedle arrays into the skin of human subjects elicited mild sensation that was reported to be non-painful.

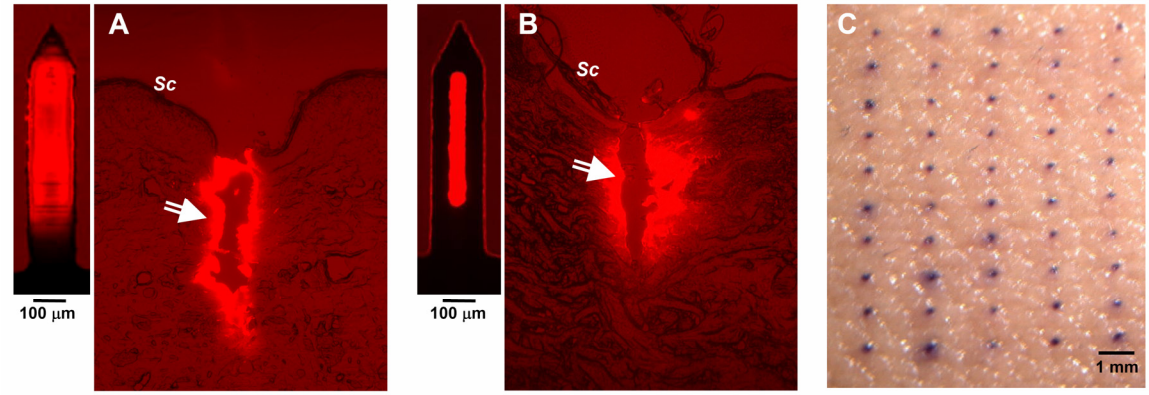


**Figure 5.7. Insertion of microneedles into skin in vitro and in vivo**. Histological sections of porcine cadaver skin after insertion and removal of (A) a non-pocketed microneedle coated with a solid-phase (Formulation A2) and (B) a pocketed microneedle filled with a liquid-phase (Formulation A10). The images exhibit perforations in the skin at the sites of microneedle penetration, which are surrounded by fluorescence of sulforhodamine released from the coatings indicated by the arrows. Images offset to the left show the coated microneedles used at the same magnification. Imaging was done using combined brightfield and fluorescence microscopy. (C) Brightfield microscopy surface image of skin on the forearm of a human subject stained with gentian violet after insertion and removal of an out-of-plane, 50 microneedle patch. The sites of microneedle penetration into the skin are stained by the dye. Sc = Stratum Corneum.

## 5.4 CONCLUSION

Motivated by previous demonstrations of peptide and protein delivery using coated microneedles, this study provides the first detailed examination of the design and control of microneedle coating formulations. First, stainless steel microneedles with or without pockets were fabricated by laser micromachining. Then, microneedle coating solution formulations were designed by recognizing the need to lower solution surface tension (i) to promote good wetting of the microneedle surface and (ii) to decrease the critical speed of film formation, which facilitates retention of a liquid film on the microneedle after dipping. Good surface wetting was achieved through the addition of FDA approved surfactant excipients, the use of organic solvents, and modification of microneedle surface properties. Coating solutions were also designed to increase solution viscosity by using FDA approved viscosity enhancing excipients. Increased viscosity led to increased volume of liquid film adhering to the microneedles and an increased residence time of the adherent liquid film, producing thicker and more uniform

coatings. When selectively filling pockets, increased solution viscosity was helpful, but surface tension was kept high in order to prevent coating of the microneedle surface.

Depending on drug properties, different aqueous, organic and molten coating formulations were used to coat microneedle surfaces and also to incorporate drugs into pockets in solid and liquid phases. Model proteins, insulin and bovine serum albumin, were coated onto microneedles using three different coating formulations, which demonstrates the versatility of this coating approach. Using an amphiphilic excipient, a hydrophobic molecule was also coated from an ethanol-based formulation and released from the microneedle in aqueous medium within 1 min. Composite drug coatings were applied as distinct layers, and to distinct regions on the microneedle, to either segregate different drugs from each other or to facilitate combination of burst and controlled release from the same microneedle.

The mass of a model drug, riboflavin, coated on microneedles was found to increase with its concentration in the coating solution, the number of coating solution dips, and the number of microneedles in the array. These data indicated that up to 1 mg of drug can be expected to be coated on a few hundred microneedles on a patch size of about 10 to 20 $cm^2$. The average relative standard deviation of the current microneedle coating process was found to be 19%, although reduced deviation is expected with automated manufacturing. Microneedle insertion into skin was demonstrated and shown to rapidly release coatings within the skin and not wipe off on the skin surface. Altogether, this study shows that microneedle coating formulations can be designed to have a range of different properties to address a variety of different drug delivery scenarios.

# CHAPTER 6: HEPATITIS C IMMUNIZATION VIA SKIN USING DNA VACCINE-COATED MICRONEEDLES[4]


## ABSTRACT

Although naked DNA-based vaccines have shown promising results in rodents, their effectiveness in humans by a similar intramuscular route is severely limited due to their poor immunogenicity. In contrast, the intradermal route has shown hundreds of fold higher potency, but there is lack of a convenient and inexpensive method of intradermal delivery of DNA vaccines. Recently, microneedles have been developed for painless delivery to the skin, and have been used to show humoral response to conventional viral and protein based vaccines. The hypothesis of this study was that DNA-coated microneedles can be used to elicit an efficient cellular immune response. To test this hypothesis, groups of mice were immunized intradermally, either using microneedles coated with a plasmid encoding the hepatits C virus (HCV) non-structural (NS) 3/4A protein or via the gene gun. The intramuscular route of immunization was also compared. After immunization, i*n vivo* functional NS3/4A-specific cytotoxic T lymphocytes (CTLs) were effectively primed using similar, or lower, DNA doses on microneedles as when using the gene gun or intra muscular injection. A 30-fold lower dose delivered to the skin using coated microneedles produced an in vivo CTL response similar to a 100 μg dose delivered by the intramuscular route. In conclusion, this study showed that microneedle based intradermal delivery of an HCV DNA vaccine has a high potency similar to the gene gun based delivery, while in contrast, the intramuscular route was less potent.


[4] This work was done in collaboration with Dr. Matti Sãllberg and Dr. Jonas Sõderholm at the Division of Clinical Virology, Karolinska Institute, Stockholm, Sweden.

## 6.1 INTRODUCTION

DNA vaccines are attractive alternatives to conventional virus- or protein-based vaccines. Their advantages include: easy manipulation and versatility to express different antigens, rapid and inexpensive mass-production capability, stability at room temperature and the ability to generate both humoral and cellular immune responses (Garmory, Perkins et al. 2005). Plasmid DNA vaccines are therefore considered as good vaccine candidates for a wide variety of pathogenic infections, especially those requiring cellular responses, like HIV, hepatitis C virus (HCV) and malaria (Greenland and Letvin 2007).

However, low potency of DNA vaccines in humans has prevented their use as vaccines in a clinical setting. Few milligram of DNA is typically required to generate a robust immune response in humans (Donnelly, Berry et al. 2003; Graham, Koup et al. 2006). To reduce the dose of DNA required for vaccination, various methods like adjuvants and different routes of delivery are being investigated (Greenland and Letvin 2007). Intradermal immunization has shown about three orders of magnitude potency improvement in humans and non-human primates using gene guns and electroporation (Roy, Wu et al. 2000; Luckay, Sidhu et al. 2007). However, gene guns and electroporation are not attractive for mass vaccinations because they require elaborate vaccination protocols and equipment, and the gene gun typically requires multiple shots to deliver even a few microgram of DNA (Babiuk, Baca-Estrada et al. 2000; Peachman, Rao et al. 2003). Therefore, there is need for a convenient and robust intradermal DNA vaccine delivery method.

Recently, microneedles, which are sharp micron-sized structures that can painlessly penetrate the skin have been used to deliver micro-and macro-molecules (Prausnitz 2004; Prausnitz, Mikszta et al. 2005); genetic material, including plasmid DNA and oligonucleotides (Lin, Cormier et al. 2001; Chabri, Bouris et al. 2004); and vaccines

directed against hepatitis B, anthrax and Japanese encephalitis (Mikszta, Alarcon et al. 2002; Dean, Alarcon et al. 2005; Mikszta, Sullivan et al. 2005) into the skin. Coated microneedles are especially attractive because they are readily coated with uniform coatings of proteins, plasmids and viruses, and can be assembled as 'Band-Aid' like coated microneedle patches for easy self-administration (Gill and Prausnitz 2007a), which is expected to facilitate mass vaccination.

Coated microneedles have been previously used to study the humoral response against a model antigen, i.e., ovalbumin, using ovalbumin-coated microneedles for immunization (Widera, Johnson et al. 2006). However, the ability of coated microneedles to deliver DNA vaccines has not been studied before. Furthermore, only humoral immune responses have been measured from other microneedle-based vaccinations (Matriano, Cormier et al. 2002; Mikszta, Alarcon et al. 2002; Mikszta, Sullivan et al. 2005; Alarcon, Hartley et al. 2007). The ability to prime cellular responses using microneedle-based immunization has not been shown. Therefore, in this study we sought to measure the cellular immune response in vivo after the delivery of a DNA vaccine coated onto microneedles.

Induction of cellular immune responses is an important aspect of developing a therapeutic vaccine against HCV. Cytotoxic T lymphocytes (CTL) are generally thought to play an important role in clearance of the HCV infection by killing HCV infected hepatocyte cells and by secreting antiviral cytokines (Chisari 1997). Recently, DNA immunizations in mice using a low dose of hepatitis C, codon optimized plasmid DNA vaccine, coNS3/4A, administered through a gene gun, produced robust CTL responses (Frelin, Alheim et al. 2003). We hypothesized that an intradermal delivery of this DNA vaccine through DNA-coated microneedles should similarly be able to induce a strong CTL response.

Therefore, in this study, hepatitis C, codon optimized plasmid DNA vaccine, coNS3/4A, was coated onto microneedles and delivered into the skin of mice. CTL response after immunization was measured using chromium release assay and an in vivo tumor challenge assay. Microneedle effectiveness was also compared to gene gun and intramuscular (i.m.) delivery of the DNA vaccine.

## 6.2 MATERIALS AND METHODS

### 6.2.1 Microneedle fabrication and coating

Stainless steel microneedles were fabricated as described previously (Gill and Prausnitz 2007a). Briefly, microneedles were cut from stainless steel sheets using an infrared laser and electropolished to yield sharp, clean microneedles. Microneedles were then uniformly coated with the antigen, i.e., plasmid coNS3/4A, using an in-house developed dip-coating device. The aqueous coating solution consisted of, 1% (w/v) CMC, 0.5% (w/v) F-68 and 4 mg/ml coNS3/4A plasmid. The coating solution excipients, CMC and F-68 were added to modulate the coating solution surface tension and viscosity to obtain uniform coatings; and the high concentration of DNA solution was used to allow coating of a high mass of DNA on the microneedles (Gill and Prausnitz 2007b). The mass of plasmid DNA coated on to microneedles was then determined using UV spectrophotometery, and each row of five microneedles was found to be coated with 1.6 μg of DNA.

Because plasmid coatings were difficult to visualize, the uniformity of coatings was assessed by coating microneedles with a model colored compound, vitamin B2 (Fisher Scientific, Fair Lawn, NJ, USA). The coating solutions for vitamin B2 and the plasmid DNA had identical concentrations of the excipients.

### 6.2.2 Cell lines

The SP2/0-Ag14 myeloma cell line (H-$2^d$) was maintained in DMEM medium supplemented with 10% FCS (Sigma Chemicals, St Louis, MO, USA), 2 mM L-glutamin, 10 mM HEPES, 100 U/ml penicillin, 100 μg/ml streptomycin, 1 mM nonessential amino acids, 50 μM β-mercaptoethanol, and 1 mM sodium pyruvate (GIBCO-BRL, Gaithersburgh, MD, USA). SP2/0-Ag14 cells with stable expression of NS3/4A were maintained in 800 μg geneticin (G418)/ml complete DMEM medium (Frelin, Alheim et al. 2003).

RMA-S cells were maintained in RPMI 1640 medium supplemented with 5% FCS, 2 mM L-glutamine, 100 U/ml penicillin and 100 μg/ml streptomycin. All cells were grown in a humidified 37°C, 5% $CO_2$ incubator.

### 6.2.3 Immunization protocol

The experimental protocol was approved by the ethical committee for animal research at Karolinska Institute. HCV coNS3/4A plasmid DNA was used as the immunization antigen.

To assess the ability to induce CTL activity via microneedle based immunizations, groups of 4-8 week old female C57BL/6 (H-$2^b$) mice (n=4 per group, Charles River, Uppsala, Sweden) were either immunized via gene gun (Bio-Rad Laboratories, Hercules, CA, USA) at a dose of 4 μg/mouse or via microneedles at a dose of 8 μg/mouse (5 microneedles per mouse x 1.6 μg plasmid DNA per microneedle). A third non-immunized group (n=2 mice) of naïve mice served as the negative control.

For in vivo tumor challenge studies, groups of 4–8 week old female BALB/c (H-$2^d$) mice (n=5 per group) were either immunized with DNA coated microneedles (3.2 μg dose per mouse, 2 microneedles x 1.6 μg plasmid DNA per microneedle) or an

intramuscular (i.m.) injection of 100 μg of coNS3/4A in the tibialis anterior muscle. A third non-immunized group (5 mice) served as the negative control.

For coated microneedle-based immunizations, microneedles coated with plasmid DNA were manually inserted into trimmed abdominal or back skin and held for 1 min to allow dissolution of coated antigen into the skin. For gene gun-based immunizations, plasmid DNA was linked to 1-μm diameter gold particles for subsequent immunizations according to protocols supplied by the manufacturer.

### 6.2.4 Detection of NS3/4A-specific CTL activity

Two weeks after immunization, spleen cells from DNA-immunized C57BL/6 mice or naïve mice were resuspended in complete RPMI 1640 medium supplemented with 10% FCS, 2 mM L-glutamin, 10 mM HEPES, 100 U/ml penicillin and 100 μg/ml streptomycin, 1 mM nonessential amino acids, 50 μM β-mercaptoethanol, and 1 mM sodium pyruvate. In vitro stimulation was carried out for 5 days in 25-ml flasks at a total volume of 12 ml, containing $25x10^6$ spleen cells and $25x10^6$ irradiated (2000 rad) syngeneic spleenocytes. The re-stimulation was performed in the presence of 0.05 μM NS3/4A H-$2D^b$ binding peptide, a nine-mer sequence – GAVQNEVTL, corresponding to a NS3 CTL epitope in H-2b mice, synthesized by automated peptide synthesis as described previously (Frelin, Alheim et al. 2003). After 5 days of in vitro stimulation, a standard $^{51}$Cr-release assay was performed. Effector cells were harvested and a 4-h $^{51}$Cr assay was performed in 96-well U-bottom plates in a total volume of 200 μl. A total of $1x10^6$ target cells (peptide-pulsed RMA-S cells) were labeled for 1 h at 37°C with 20 μl of $^{51}$Cr (5 mCi/ml) and then washed three times in PBS. Different numbers of effectors and $^{51}$Cr-labeled target cells ($5x10^3$ cells/ well) were added to wells at effector:target (E:T) ratios of 60:1, 20:1, and 7:1. The level of cytolytic activity was determined after

incubation of effectors and targets for 4 h at 37°C. A volume of 100 μl supernatant was harvested and the radioactivity was measured with a γ-counter.

Results were expressed according to the following formula:

percent specific lysis =(experimental release -spontaneous release)/(maximum release-spontaneous release). Experimental release is the mean counts/minute released by the target cells in the presence of effector cells. Maximum release is the radioactivity released after lysis of target cells with 10% Triton X-100. Spontaneous release is the leakage of radioactivity into the medium of target cells .

### 6.2.5 In vivo functionality of primed NS3-specific CTLs

In vivo challenge of immunized mice with SP2/0 myeloma cell line expressing coNS3/4A was performed according to the method described by Encke et al. (Encke, zu Putlitz et al. 1998). In brief, groups of BALB/c mice immunized once with microneedles or i.m. were injected with $1x10^6$ coNS3/4A-expressing SP2/0 cells subcutaneously into the right flank. The kinetics of the tumor growth was determined by measuring the tumor size through the skin upto day 14 after tumor injection. The mean tumor sizes were compared using the analysis of variance (ANOVA) test.

## 6.3 RESULTS AND DISCUSSION

### 6.3.1 Uniform plasmid coatings

In-plane stainless steel microneedles measuring 700 μm in length and 160 μm in width were fabricated as a row of five microneedles. To ensure dose reproducibility, it is important to achieve a uniform plasmid coating on the microneedles. Because the plasmid coatings were difficult to visualize, the uniformity of coating was first determined

by using vitamin B2 as a model drug. After coating with vitamin B2, all the five microneedles of the row were found to be uniformly coated (Figure 6.1 A). Next, as an indirect method to assess plasmid coating uniformity, the plasmid-coated microneedles were physically scraped to damage the coating and visualize the parts of the microneedle surface coated with the plasmid. This analysis demonstrated that the plasmid was uniformly coated on all the five individual microneedles in the row. A representative single microneedle of the row after scraping is shown in Figure 6.1 B.

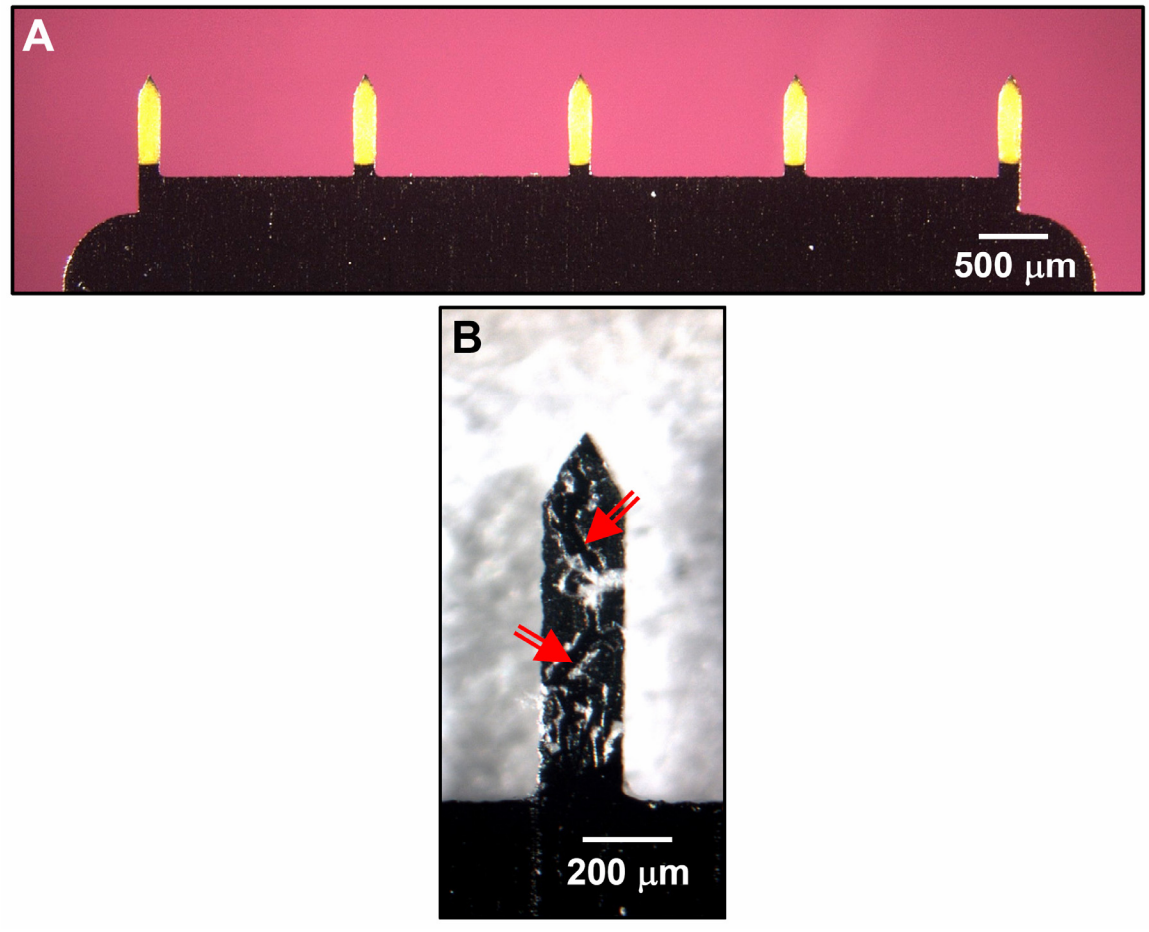


**Figure 6.1. Coated microneedles**. (A) Microneedle row with five microneedles uniformly coated with vitamin B2 as a model drug. (B) Plasmid coating uniformly formed on the microneedle surface and visualized by scraping. Arrows point to exposed stainless steel surface.

### 6.3.2 Priming of NS3-specific CTLs by microneedle delivery

Because CTL responses are important to eliminate hepatitis C and other virus infected cells, we investigated the ability of microneedles to induce a CTL response. From the $^{51}Cr$ release assay it was found that both the microneedle and gene gun immunized mice showed antigen specific cell lysis, while the naïve mice did not show any significant response (Figure 6.2). Even at low effector to target ratios (E/T ratio), significant target cell lysis was observed, indicating a robust immune response from DNA-coated microneedles, comparable to that from the gene gun based immunization.

Previous studies have shown that intradermal delivery of low (≤ 10 μg) doses of the codon optimized NS3/4A DNA plasmid effectively primes NS3-specific CTLs in Balb/c and C57BL/6 mice (Frelin, Ahlen et al. 2004). A single immunization with 4 μg of coNS3/4A using a gene gun primed in vitro-detectable CTLs (Figure 6.2 A). Importantly, a single 8 μg dose of coNS3/4A DNA delivered using microneedles primed a response fully comparable to the gene gun (Figure 6.2 B). The naïve mice did not show a detectable CTL activity (Figure 6.2 C). It has been previously shown that a single i.m. injection of the same low dose also fails to generate a robust CTL response (Frelin 2004). These results collectively indicate that similar to a gene gun, microneedle based Intradermal immunization in mice produces a robust CTL response at low doses, without the use of an adjuvant.

### 6.3.3 In vivo functionality of primed NS3-specific CTLs

An in vitro detection of robust NS3-specific CTLs does not imply that these cells also have a strong CTL activity in vivo. Therefore, we next wanted to conduct a functional in vivo test to measure the ability of the CTLs to kill HCV infected cells in vivo. Because HCV is a noncytolytic virus, a relevant model to characterize this in vivo CTL

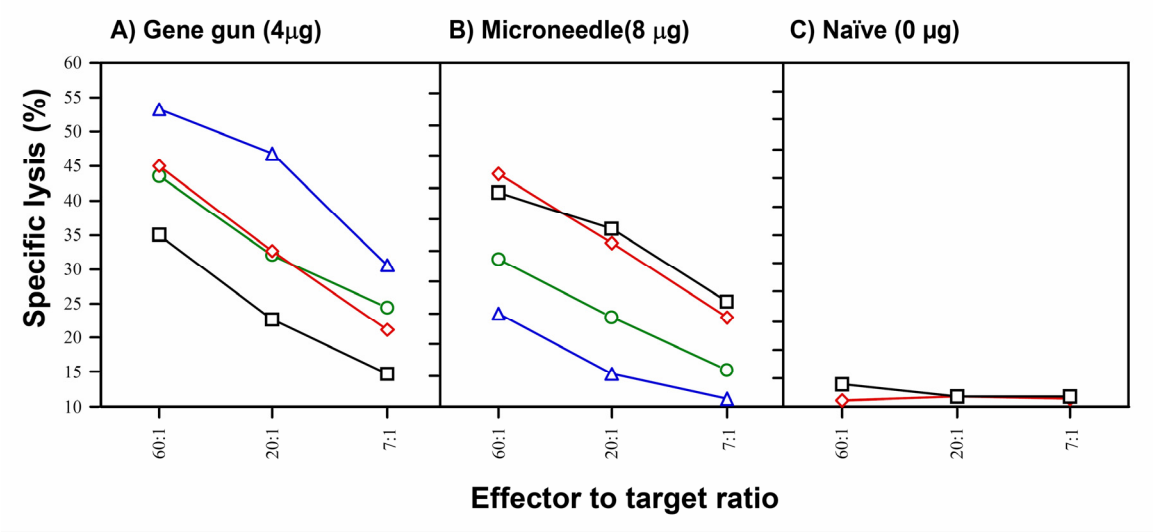


**Figure 6.2. Microneedle based immunization induces antigen specific CTLs, in vitro**. C57Bl/6 mice were immunized once with codon optimized NS3/4A using either (A) microneedles (8 μg dose), (B) gene gun (4 μg dose) or (C) no immunization and sacrificed on week 2. The spleen harvested cells (effector cells, $25x10^6$ cells) were restimulated with a specific NS3 H-$2D^b$ peptide and $25X10^6$ irradiated naive C57Bl/6 spleenocytes cells. On day 5, $5x10^3$ RMA-S cells were loaded with the H-$2D^b$ specific peptide and used as target cells. The specific cell lysis of target cells was then measured at different effector to target cell ratios.

response is to determine the inhibition of tumor growth in vivo, using syngeneic lymphoma cells expressing the viral antigen. This assay is based on the principle that the injected syngeneic tumor cells will continue to grow in mice without in vivo functional CTLs against NS3/4A, but will diminish in size in mice with in vivo NS3/4A specific CTLs. Therefore, BALB/c mice immunized with microneedles or the i.m route were challenged with SP2/0 myeloma cells stably expressing NS3/4A. At day 14, the tumor size reduction was significant ($p < 0.05$) in the microneedle and the i.m. immunized mice (tumor size about 5 mm) as compared to the naïve mice (tumor size about 15 mm) Figure 6.3. It is important to note that a 3.2 μg dose delivered from coated microneedles and a 100 μg dose given i.m. produced similar reduction in tumor size.

These results highlight two significant findings. First, that just 3.2 μg of DNA delivered via coated microneedles could generate CTLs comparable to those generated by an i.m. delivery of 100 μg DNA, and second that the CTLs could produce lytic activity

in vivo, especially of cells endogenously expressing NS3/4A, much like an HCV infected hepatocyte. These results collectively suggest that the CTLs generated should be effective in lysing HCV infected hepatocytes, which also express NS3/4A in vivo.

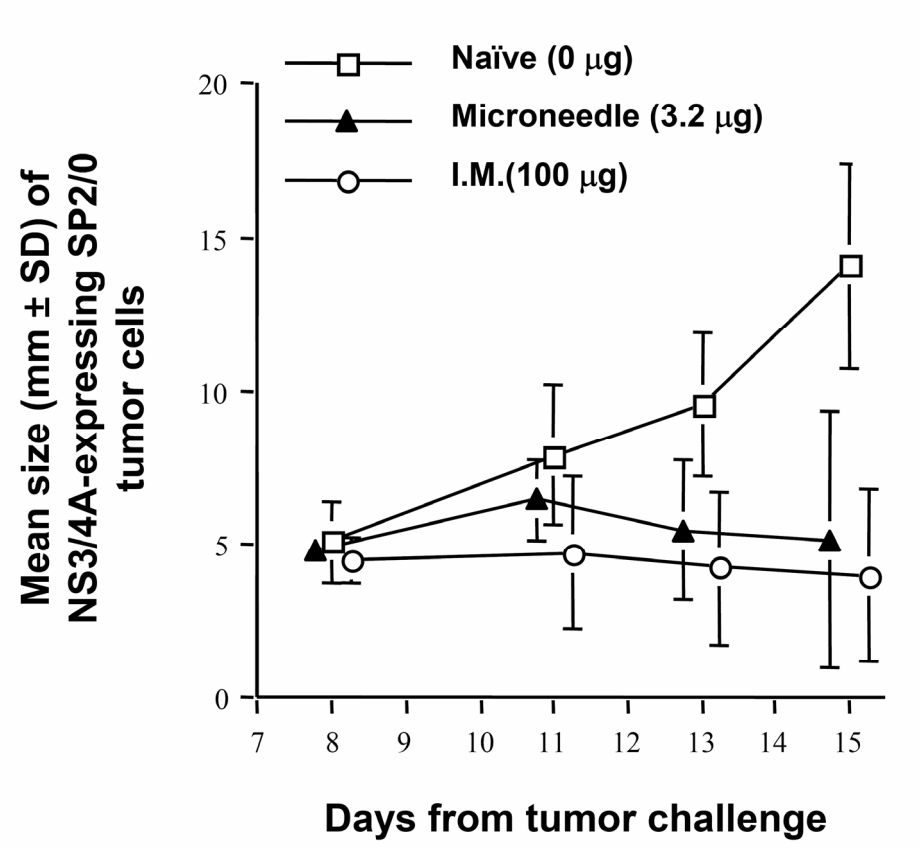


**Figure 6.3. Microneedle immunization reduces tumor size in vivo**. SP2/0 cells (1 x $10^6$) stably transfected with NS3/4A were injected subcutaneously into the flank of naïve and immunized Balb/C mice. After 8 days of injecting the tumor, the size of the tumor was big enough to be measured and it was monitored till 14 days after tumor injection.

### 6.3.4 Implications for microneedle-based plasmid DNA vaccination

Recently microneedles have been coated with DNA for rapid delivery into the skin (Gill and Prausnitz 2007a). The advantages of microneedles are that they cause

minimal discomfort and pain, are expected to be inexpensive and can be easily administered. Therefore, we tested a newly developed DNA based vaccine targeting the hepatitis C virus, a common infection in developing countries and for which no vaccine is yet available. We showed that microneedles were successfully coated with hepatitis C NS3/4A DNA vaccine in a controllable dose of 1.6 μg per row of five microneedles. Although we used multiple insertions of these rows for delivery of 8 or 3.2 μg dose, arrays of microneedles with tens and hundreds of microneedles can be easily fabricated instead, to deliver tens or hundreds of microgram of DNA into the skin in a single microneedle insertion.

Intradermal immunization using the coNS3/4A DNA-coated microneedles resulted in the priming of antigen specific CTLs at low vaccine doses (3 to 8 μg) and without the use of any additional adjuvants. The magnitude and efficiency of the lytic activity of the CTLs primed through microneedle and gene gun was similar. This suggests that these two approaches of intradermal delivery can yield comparable results. This is of significance because gene gun mediated delivery has consistently shown up to 1000 fold higher potency than the i.m. route in larger animal models and phase-I human clinical trials (Fuller, Loudon et al. 2006).

Further, NS3/4A-expressing tumor-cell growth was inhibited in the vaccinated mice unlike in the naïve mice, demonstrating that the CTLs were effective in vivo as well. Importantly, the same level of protection through an i.m. administration required more than 30-fold higher dose of the coNS3/4A plasmid. This is in concurrence with previous observations when high doses (about 100 μg) of NS3/4A administered by a standard i.m. injection were required for a similar effect (Frelin, Ahlen et al. 2004). Also, based on previous work it is known that a low i.m. dose of the DNA in mice does not produce an effective immune response. Thus, microneedles coated with the coNS3/4A plasmid DNA

effectively prime lytic CTLs that are functional *in vivo*, and demonstrated about a 30-fold higher potency.

Microneedles used for coating DNA were about 700 μm in length. From previous skin histology studies we know that coatings from the microneedle surface dissolve in the skin and are delivered into the epidermis and the dermis. Therefore, we expect that different cell populations may have helped in generating a potent immune response. Antigen presenting cells, i.e., the Langerhans cells found in the epidermis and the dermal dendritic cells; and the keratinocytes of the epidermis may all have a role in the immune response (Bos 2005).

In conclusion, the present data suggests that a NS3/4A-expressing DNA plasmid can be effectively delivered through the skin using coated microneedles to elicit a robust CTL response specific for the hepatitis C virus. Similarities between the immune response from coated microneedle- and gene gun-based immunizations suggest that like gene guns, high potency may be achieved in humans through the use of coated microneedles.

## 6.4 CONCLUSION

Microneedles were successfully coated with hepatitis C NS3/4A DNA vaccine in a controllable dose of 1.6 μg per row of five microneedles. Mouse immunization using NS3/4A coated microneedles resulted in antigen specific cytotoxic T-lymphocyte production at low vaccine dose (3 to 8 μg) and without the use of adjuvants. Chromium release CTL assay demonstrated that the CTL response was robust, while the in vivo tumor challenge assay demonstrated that the cytotoxic T-lymphocytes had the ability to recognize and kill cells expressing the antigen, NS3/4A, in vivo. Together, these results show that coated microneedle-based immunization has the potential to be used for

intradermal immunization against hepatitis C. More broadly, this experiment suggests that coated microneedles have the potential to be used for administering DNA vaccines to the skin in a safe and painless manner, and may offer a convenient method for mass immunization in humans.

# CHAPTER 7: SELECTIVE REMOVAL OF STRATUM CORNEUM BY MICRODERMABRASION AS A NOVEL METHOD OF TRANSDERMAL DRUG DELIVERY[5]


## ABSTRACT

This study sought to determine if microdermabrasion can selectively remove full-thickness stratum corneum as a novel method of transdermal drug delivery. Although microdermabrasion has been used for cosmetic treatment of skin for decades, no study has assessed the detailed effects of microdermabrasion conditions on the degree of skin-tissue removal. Therefore, we histologically characterized the skin of rhesus macaques and human subjects after exposure to a range of different microdermabrasion conditions. Using a mobile tip, an increase in the number of treatment passes led to greater tissue removal ranging from minimal effects to complete removal of epidermis, although intra- and inter-subject variability was significant. Of note, these data showed for the first time that selective removal of full-thickness stratum corneum with little damage to deeper tissue could be achieved using microdermabrasion. In the stationary mode of microdermabrasion, selective stratum corneum removal was not observed, but micro-blisters could be seen. Similar tissue removal was observed in human subjects. As proof of concept for drug delivery applications, a model fluorescent drug (fluorescein) was delivered through microdermabraded skin and antibodies were generated after topical application of vaccinia virus in monkeys. In conclusion, microdermabrasion can selectively remove full-thickness stratum corneum with little damage to deeper tissues and thereby enhance transdermal flux and enable epidermal vaccination.


[5] This work was done in collaboration with Dr. Andrew Fedanov, Dr. Senthilkumar Sakthivel, Dr. Ifor Williams, Dr. Seth Yellin, Dr. David Garber, Dr. Frances Priddy, Dr. Silvija Staprans and Dr. Mark Feinberg at Emory University.

## 7.1 INTRODUCTION

This study tested the hypothesis that microdermabrasion can selectively remove full-thickness stratum corneum with little damage to deeper tissues and thereby enhance transdermal flux and enable epidermal vaccination. Although applications to drug delivery are new, microdermabrasion was first introduced in 1985 and has become a popular cosmetic procedure, widely used to treat scars, acne and other cosmetic-dermatologic conditions (Spencer 2005). Mechanistically, microdermabrasion involves impingement of sharp microparticles on the skin surface, which are then removed under vacuum into a waste container along with the abraded skin tissue. Partial-thickness removal of the skin's top-most layer, the stratum corneum, has been demonstrated in microdermabraded skin in human subjects (Spencer 2005). Because stratum corneum provides the primary transport barrier to entry of drugs into the skin, microdermabrasion has been proposed as a method to remove the stratum corneum and thereby enhance transdermal drug delivery (Lee, Shen et al. 2003; Fujimoto, Shirakami et al. 2005).

Transdermal drug delivery is of interest as an alternative to the oral route, which is not suitable for many drugs, especially biopharmaceuticals, due to their poor absorption and degradation in the gastrointestinal tract (Degim and Celebi 2007). Biopharmaceuticals therefore usually require painful injections for their administration. Because the skin has a dense vasculature just 100 μm below the skin surface, the transdermal route offers an attractive alternative for systemic delivery of biopharmaceuticals and other drugs. Furthermore, the Langerhans cells in the viable epidermis are considered an attractive target for vaccine delivery to generate a robust immune response (Partidos, Beignon et al. 2003).

Despite the attractiveness of the skin, the stratum corneum barrier has limited the transdermal route to just 16 FDA-approved drugs, all of which are small and lipophilic molecules that require a low dose (Prausnitz, Mitragotri et al. 2004). To overcome the

transport barrier provided by the stratum corneum two different approaches can be followed: (i) to disrupt or bypass the stratum corneum or (ii) to physically remove the stratum corneum.

In accordance with the first approach, many chemical and physical methods have been investigated, including solvents and surfactants, iontophoresis, electroporation, sonoporation, high velocity jets and particle bombardment methods, and microneedles (Prausnitz, Mitragotri et al. 2004). Based on the second approach, lasers and thermal ablation have been investigated to remove stratum corneum using focused thermal energy (Sintov, Krymberk et al. 2003; Fang, Lee et al. 2004a). This second approach of stratum corneum removal should be highly effective for drug delivery, since it completely removes the transport barrier, but its application has been constrained by the need to develop methods that selectively remove stratum corneum without damaging deeper tissues. In addition, removal of stratum corneum can also expose the keratinocytes of the viable epidermis for direct efficient targeting by drugs, for example by viral vectors for gene therapy of skin diseases (Titeux and Hovnanian 2006).

Various researchers have shown increased permeability of freshly excised animal skin to very low molecular weight compounds (<300 Da) after microdermabrasion, recording a 12-fold increase in delivery of estradiol (Fujimoto, Shirakami et al. 2005), a 25-fold increase for vitamin C (Lee, Shen et al. 2003), and a 15-fold increase for 5-aminolaevulinic acid (Fang, Lee et al. 2004b). These studies have reported thinning of the stratum corneum, but have not demonstrated full-thickness removal of stratum corneum. In contrast to microdermabrasion, which uses vacuum to produce flow of microparticles, a related approach called microscission uses a positive pressure to accelerate and impinge microparticles on the skin. Using this approach, lidocaine delivery and blood glucose measurement was demonstrated in vivo in human subjects

(Herndon, Gonzalez et al. 2004). Of note, neither microdermabrasion nor microscission has been successfully used before to deliver macromolecules or vaccines.

In this study, we propose that selective full-thickness removal of stratum corneum is the key to enabling microdermabrasion to increase skin permeability to macromolecules and vaccines. To identify such conditions and test our hypothesis, we carried out a detailed study of skin histology after microdermabrasion at different conditions. Specifically, microdermabrasion was performed in vivo on the skin of rhesus macaques and human subjects. Multiple skin biopsies were then obtained from the microdermabraded sites and histologically analyzed to assess the effects of microdermabrasion on the different skin layers. In addition, the suitability of microdermabraded sites for drug delivery was assessed in rhesus macaques using sodium fluorescein and modified vaccinia Ankara (MVA) virus as model compounds for a hydrophilic drug and a vaccine, respectively.

## 7.2 MATERIALS AND METHODS

### 7.2.1 Microdermabrasion apparatus

Microdermabrasion was performed using an FDA-approved device (MegaPeel® Gold Series, DermaMed International, Lenni, PA, USA) with disposable microdermabrasion tips having a skin-contacting hole with a 7 mm inner diameter (Figure 7.1 A). The size and morphology of the aluminum oxide particles (DermaMed International) used for microdermabrasion were determined through scanning electron microscopy (LEO-1530, LEO electron microscopy, Cambridge, England). The particles were found to have highly irregular shapes with sharp edges (Figure 7.1 B). The largest dimension of the majority of the particles was between 100 to 200 μm, although a small amount of particulate debris (about 1 μm) was also found.

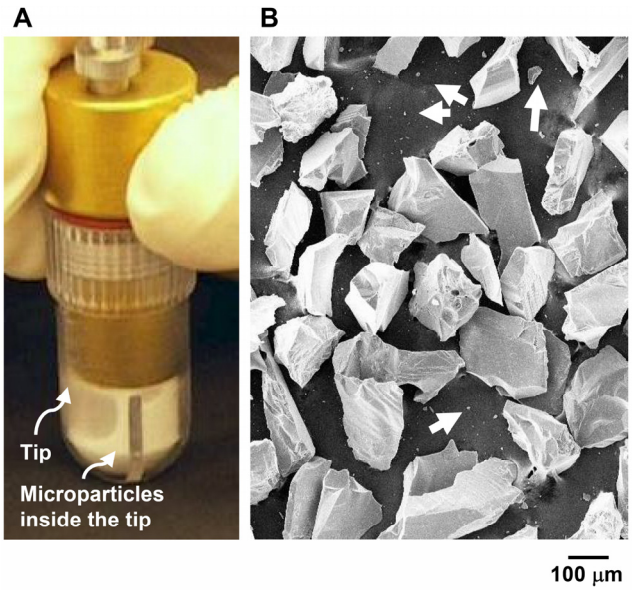


**Figure 7.1. Microdermabrasion tip and particles**. A microdermabrasion tip pressed on a black paper in a stationary mode with aluminum oxide microparticles flowing inside the tip (A), and scanning electron microscopy image of aluminum oxide microparticles with a small population of very small particles (pointed to by white arrows) (B).

To facilitate reliability in the manual microdermabrasion procedure, rectangular stencils (55 x 30 mm) made of polyethylene medical foam tape (TM9716, MACtac, Stow, OH, USA) with slits (40 x 10 mm) precisely cut using a $CO_2$ laser (LS500XL. New Hermes, Duluth, GA, USA) were attached to the skin of rhesus macaques and human subjects. For the mobile tip mode, the tips were moved manually back and forth within the slit of the stencil. The slit width of 10 mm closely accommodated the outer diameter of the microdermabrasion tip and thereby facilitated repeated motion over the same path on the skin. For the stationary tip mode, the microdermabrasion tip was placed directly on the skin surface without the use of a stencil.

### 7.2.2 In vivo rhesus macaque microdermabrasion

Microdermabrasion was performed on the backs of rhesus macaque monkeys (Yerkes National Primate Research Center, Emory University, Atlanta, GA) after trimming the hair and cleaning the skin with ethanol swabs.

For the mobile mode of microdermabrasion, two pressure settings of 25 kPa at 100, 200 and 300 passes and 50 kPa at 10, 30, 50, 80 and 100 passes were each tested in triplicate. Three monkeys were assigned for each pressure level group, and each monkey of the group received all the passes at different skin sites to enable every monkey to act as its own control. One pass is defined as the movement of the microdermabrasion tip from one end to the other on the treated skin site exposed through the stencil slit. The hand-piece was manually moved at a speed of approximately 40 mm/s and the flow rate of microparticles was kept at 70% of the maximum flow rate of the instrument. A vacuum pressure of 50 kPa was selected because it is considered a medium dermabrasion setting by the manufacturer, and this pressure resulted in complete stratum corneum removal in preliminary experiments on porcine cadaver skin (data not shown). A lower vacuum pressure of 25 kPa was also selected to determine the effect of pressure. A non-microdermabraded, but trimmed and ethanol-cleaned section of skin from the back of the monkeys was used as a negative control.

The stationary mode of microdermabrasion was performed by keeping the hand-piece stationary on the skin and exposing the skin to a vacuum pressure of 30 kPa or 50 kPa for 3 s or 6 s each. The treatments were done in triplicate with (n=3 monkeys, each monkey received all the treatments). To facilitate direct comparison between microdermabrasion in the mobile mode and the stationary mode, the equivalent microdermabrasion exposure time in the mobile mode was calculated by dividing the tip

diameter (7 mm) and by the speed of tip movement (40 mm/s) and then multiplying by the number of passes.

A 6 mm skin biopsy was obtained from the center of each microdermabraded and control skin site (mobile mode = center of stencil; stationary mode = center of treated skin), mounted in OCT (Tissue-Tek®, Fisher Scientific, Pittsburg, PA, USA), and frozen in liquid nitrogen for histological analysis. This protocol was approved by the Emory University IACUC.

### 7.2.3 Microdermabrasion of human subjects

Sixteen healthy human volunteers, consisting of 6 males and 10 females aged 19 to 40 years old, were recruited for the study from the general population of Atlanta, GA, USA.

A group of six subjects was exposed to the mobile mode of microdermabrasion at 40 kPa vacuum pressure with seven passes of the hand-piece at a speed of approximately 13 mm/s (i.e., three times slower than that used in monkeys). Two groups of five subjects each were exposed to the stationary mode of microdermabrasion at a vacuum pressure 30 kPa and 45 kPa, respectively, for 3 s each. The flow rate of microparticles was always kept at 70% of the maximum flow rate of the instrument.

For each subject, microdermabrasion was performed on the volar forearm. One forearm was randomly selected for microdermabrasion and the other forearm acted as the negative control. The mobile and the stationary modes of microdermabrasion and the subsequent biopsy collection were performed in a manner similar to that of the monkeys, with the exception that the size of the skin biopsy was 1 mm. This protocol was approved by the IRBs at Emory University and the Georgia Institute of Technology.

### 7.2.4 Histology and microscopy

Skin biopsies embedded in OCT were cut into 10-μm thick sections using a cryostat (Cryo-Star HM 560 MV, Microm, Waldorf, Germany) and mounted onto glass slides (Fisher Scientific). All the skin sections except those from sites exposed to sodium fluorescein were stained with hematoxylin and eosin (H&E). Skin sections were then examined either for removal of skin layers or for delivery of sodium fluorescein using brightfield or fluorescence microscopy, respectively (Nikon Eclipse 600, Nikon, Tokyo, Japan), with a CCD camera (Retiga 1300, QImaging, Surrey, BC, Canada).

### 7.2.5 Histological assessment of skin layers

Quantitative analysis was carried out on biopsies taken from monkeys exposed to mobile-mode microdermabrasion. In this case, 30 consecutive H&E-stained skin sections from the biopsy were scored visually for full-thickness removal of stratum corneum and of viable epidermis. Two investigators independently scored the biopsies by determining the percentage of each tissue layer with full-thickness removal on each slide. Stratum corneum and viable epidermis were each categorized into the intervals 0-25% removal, 26-50% removal, 51-75% removal or 76-100% removal, and scored as 0, 1, 2 or 3, respectively. For example, a skin section with full-thickness removal of stratum corneum on slightly less than half of the slide and with almost all of the viable epidermis intact was scored ‘1’ for stratum corneum and ‘0’ for epidermal removal.

The resulting data were presented in two ways. First, the average score was calculated for each condition to provide a single number that characterized the degree of tissue removal from each layer. To provide additional information about variability, the distribution of scores for each condition was also reported as a histogram.

Qualitative analysis was carried out for the remaining biopsies taken from monkeys exposed to stationary-mode microdermabrasion and all biopsies taken from

humans. In this case, 3 to 5 consecutive sections each were visually assessed for damage and characterized qualitatively.

### 7.2.6 Topical delivery to microdermabraded skin

To assess the ability to deliver drugs through microdermabraded skin, 200 μl of an aqueous solution containing 10 % (w/v) sodium fluorescein (parenteral injection-grade, Akron, Buffalo Grove, IL, USA), was applied topically for 2 h on skin microdermabraded at 25 kPa for 100, 200 and 300 passes, and at 50 kPa for 50 passes (n=3 monkeys). Topical application of the fluorescein solution to a non-microdermabraded skin site was used as a negative control. An 8-mm diameter skin biopsy was collected from each skin site to assess delivery into the skin by fluorescence microscopy of histological sections.

The fluorescein solution also contained 5 μg/ml human MIP-3α protein (360-MP/CF, R&D Systems, Minneapolis, MN, USA) and 1 x $10^9$ plaque forming units (PFUs) of MVA virus, which were added to assess delivery of larger compounds. However, our immunohistochemical staining protocol failed to stain positive controls and, therefore, we have no results concerning delivery of these compounds.

In a separate study, we assessed the delivery of MVA by measuring the immune response from topical application of this model vaccine (Tatsis, Lin et al. 2007) onto microdermabraded skin. The skin of monkeys (n=3) was exposed to  of phosphate-buffered saline containing 6 x $10^8$ PFUs of MVA virus after microdermabrasion at 25 kPa and 10-15 passes as a primary immunization. A booster dose was applied 11 weeks later after microdermabrasion at 50 kPa and 50 passes at a different site on the back of the monkeys. Blood samples were collected 1 day before the primary immunization, 6 weeks after primary immunization and 1 week after the booster dose. The blood

samples were analyzed in triplicate using ELISA to determine the end point titers of the MVA-specific IgG antibodies (Harrop, Ryan et al. 2004).

## 7.3 RESULTS

### 7.3.1 Mobile microdermabrasion in monkeys

7.3.1.1 Qualitative measure

To test the hypothesis that microdermabrasion can selectively remove full-thickness stratum corneum with little damage to deeper tissues, we histologically characterized the skin of rhesus macaques after exposure to microdermabrasion at 50 kPa vacuum pressure as a function of the number of passes across the skin.

Histological analysis showed a broad range of removal effects on the stratum corneum and the viable epidermal layers of the skin, as compared to the untreated skin (Figure 7.2 A). In general, more skin was removed with increasing number of passes. At 10 passes, the stratum corneum and viable epidermis resembled the negative control, exhibiting full-thickness stratum corneum removal only at occasional focal regions (Figure 7.2 B). At 30 and 50 passes, larger areas of the skin were seen to have full-thickness removal of stratum corneum accompanied by little damage to the viable epidermis (Figure 7.2 C and D). At 80 and 100 passes there was almost complete removal of the stratum corneum accompanied by extensive damage to the viable epidermis and some damage to the dermis (Figure 7.2 E and F). In support of our hypothesis selective removal of full-thickness of stratum corneum with little damage to deeper tissues was observed at 30 to 50 passes.

Aluminum oxide particles with diameters less than 5 μm were sometimes observed sticking to the skin after microdermabrasion (indicated by arrows in Figure 7.2 E). Note that most microdermabrasion particles are on the order of 100 μm in size and

that these small adherent particles are from the particulate debris (Figure 7.1 B). Adherent particles were almost always seen after 80 and 100 passes (> 90% of skin sections), but only occasionally present after 10, 30 and 50 passes (< 5% of skin sections). This result may be explained by the observation that body fluid including blood was often observed on the skin surface after 80 and 100 passes, whereas fluid was generally not seen after 10, 30 and 50 passes, although mild to strong erythema was common. We hypothesize that the small particles adhered to the wet skin created after 80 and 100 passes due to surface tension forces.

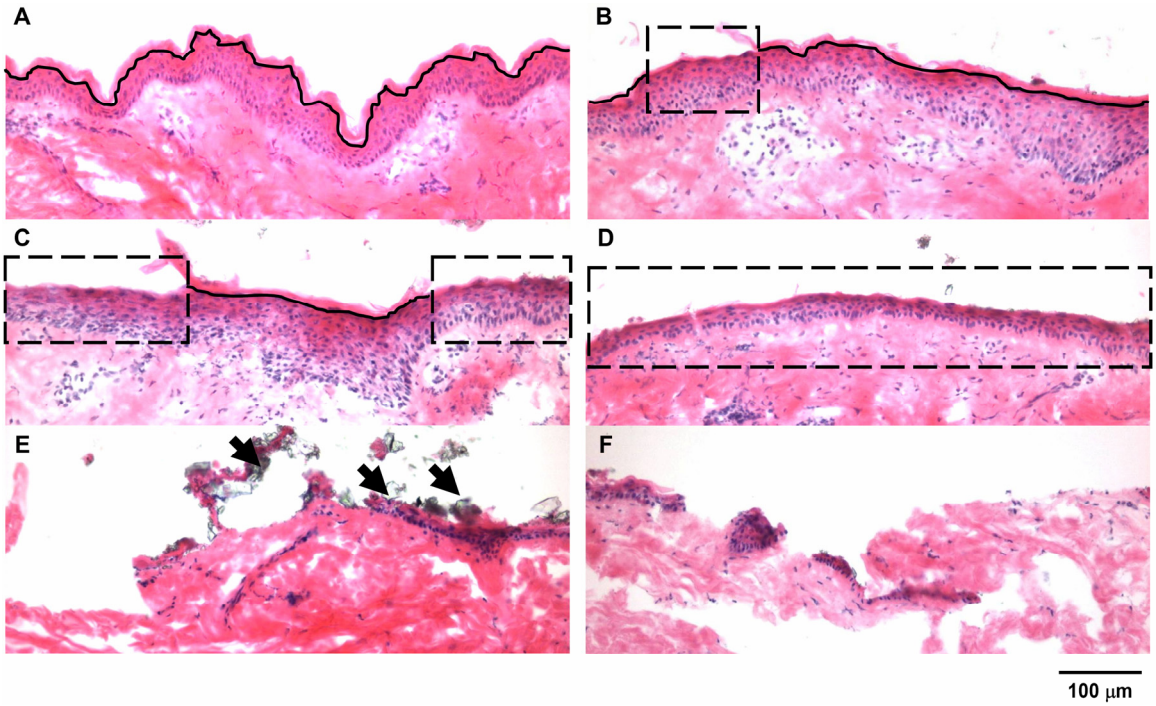


**Figure 7.2. Effect of number of passes on removal of skin layers in monkeys after mobile microdermabrasion**. Brightfield images of H&E stained skin sections from biopsies obtained from an untreated control site (A), and sites exposed to mobile mode of microdermabrasion with 50 kPa vacuum pressure and with 10 passes (B), 30 passes (C), 50 passes (D), 80 passes (E) and 100 passes (F). Solid line indicates intact stratum corneum and is drawn at the junction of the stratum corneum and the epidermis layers, dotted rectangles indicate areas of complete stratum corneum removal, and solid arrows point to residual aluminum oxide particles.

7.3.1.2 Quantitative measure (effect of number of passes)

To quantify the effects of microdermabrasion on skin tissue removal, the extent of full-thickness removal of stratum corneum and of viable epidermis was visually scored on a scale of 0 to 3 (see Materials and Methods section). Based on these scores, the mean tissue removal scores were computed as a function of the number of microdermabrasion passes (Figure 7.3 A). The mean tissue removal scores represent the average fraction of a given skin section from which the full thickness of the stratum corneum or viable epidermis was removed. Further, as a measure of the variability of tissue removal, the distribution of scores for each condition was also reported as a histogram (Figure 7.3 B).

This analysis showed that the extent of full-thickness stratum corneum removal and the extent of full-thickness viable epidermis removal both increased with increasing number of passes, as measured by the mean tissue removal score (ANOVA, $p < 0.05$, Figure 7.3 A) and the frequency of non-zero tissue removal scores (Figure 7.3 B).

Stratum corneum was mostly intact until 30 microdermabrasion passes, at which point 34% of the skin sections, including skin from all three monkeys, had substantial removal of stratum corneum (with a mean tissue removal score of 0.6 ± 0.9), which was accompanied by just 5% of the skin sections exhibiting substantial removal of viable epidermis (with a mean tissue removal score of 0.1 ± 0.4). At 50 passes, 99% of the skin sections had substantial stratum corneum removal (with a mean tissue removal score of 1.7 ± 0.7), which was accompanied by 23% of the skin sections exhibiting substantial removal of viable epidermis (with a mean tissue removal score of 0.3 ± 0.6). At 80 and 100 passes, 99 – 100% of skin sections had substantial stratum corneum removal (with mean tissue removal scores of 2.6 ± 0.6 and 3.0 ± 0.2, respectively), which was accompanied by 92 – 99% of skin sections exhibiting substantial removal of viable epidermis (with means tissue removal scores of 1.9 ± 0.8 and 1.8 ± 0.9, respectively).

These results are consistent with the qualitative analysis above and show that significant stratum corneum removal can be achieved with almost no damage to viable epidermis after 30 passes and that widespread stratum corneum removal can be achieved with low levels of damage to viable epidermis after 50 passes. Although further optimization is needed, these findings suggest that microdermabrasion might be used for transdermal drug delivery at conditions that selectively breach the stratum corneum barrier without causing significant damage to living tissue below.

7.3.1.3 Quantitative measure (effect of vacuum pressure)

To determine the effect of microdermabrasion vacuum pressure on skin tissue removal, microdermabrasion was also performed at 25 kPa. Because vacuum pressure is the driving force for the flow of microparticles, a decrease in the vacuum pressure from 50 to 25 kPa is expected to decrease the microparticle kinetic energy and flow rate. In an attempt to compensate for this, more passes were used at this lower pressure, which yielded full-thickness stratum corneum tissue removal scores of 2.9 ± 0.4, 3.0 ± 0.1 and 2.3 ± 1.1 and viable epidermis tissue removal scores of 2.9 ± 0.4, 3.0 ± 0.1 and 2.3 ± 1.1 at 100, 200 and 300 passes, respectively (histology images not shown). Blood was generally observed following microdermabrasion, and residual particles were also seen on the histology sections. These results suggest that we overcompensated for the expected reduction in efficacy at the lower pressure, because all three conditions led to almost complete removal of both the stratum corneum and the viable epidermis. Indeed, the tissue removal scores at 25 kPa and 100 passes were similar to those at 50 kPa and 100 passes, which suggests that this two-fold change of pressure had less effect than, for example, a two-fold change of the number of passes.

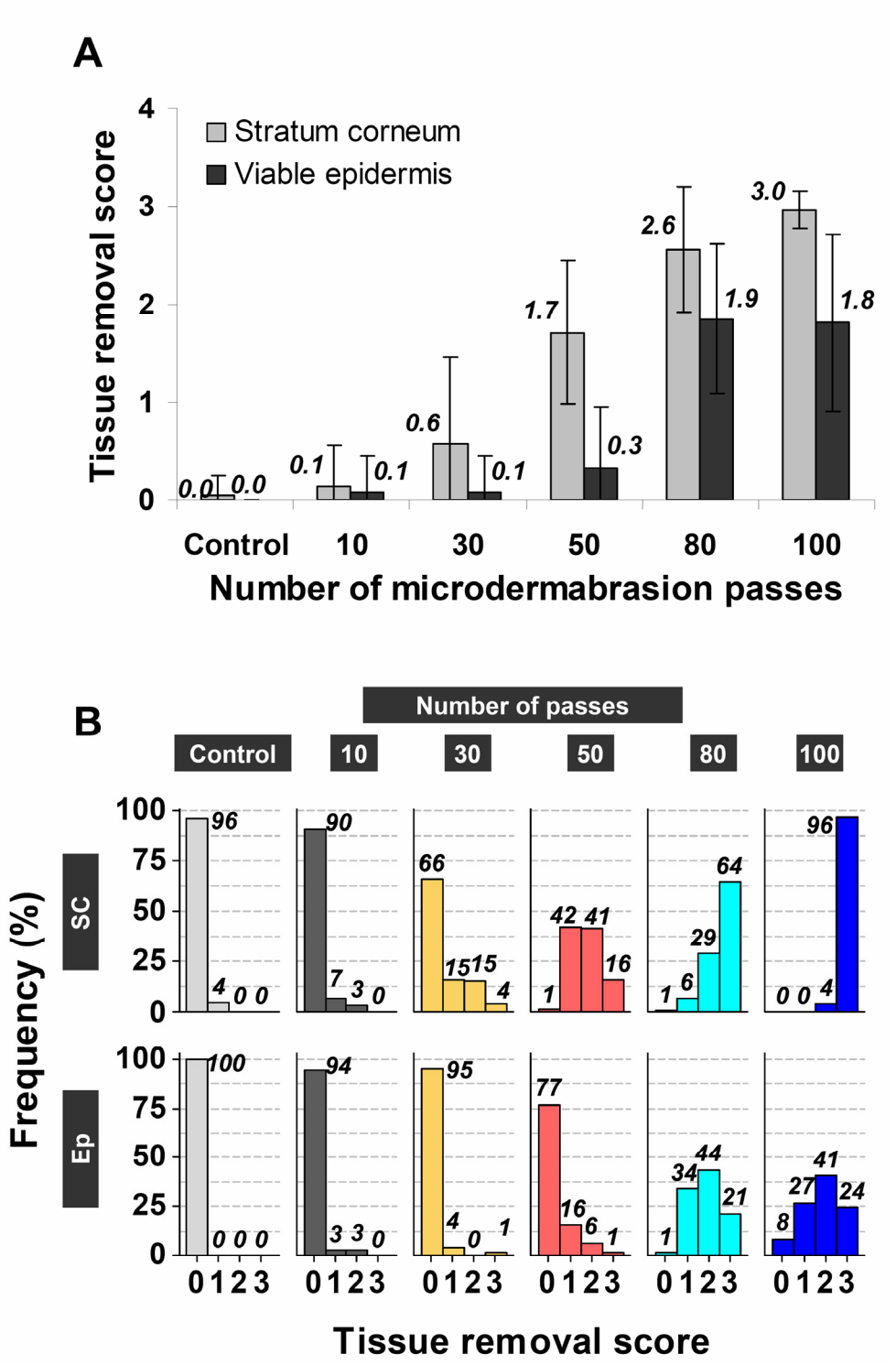


**Figure 7.3. Tissue removal scores of skin layers**. Quantitative representation of removal scores of stratum corneum and epidermis for a control site and sites exposed to different pass numbers at a mobile mode of microdermabrasion of 50 kPa vacuum pressure, as frequency distribution for a total of 180 scores for each site (A), and their means (B). Numbers above the bars represent percent frequency (A) and means (B). Error bars correspond to the standard deviations. SC=stratum corneum, Ep=Epidermis.

### 7.3.2 Stationary microdermabrasion in monkeys

The stationary mode of microdermabrasion is simpler to perform than the mobile mode because the microdermabrasion tip just needs to be held against the skin for a fixed period of time. We therefore characterized the histological effects on skin tissue removal from stationary microdermabrasion to assess its ability to selectively remove full-thickness stratum corneum. Similar to the untreated skin (Figure 7.4 A), the stratum corneum and the viable epidermis were both generally intact following exposure at 30 kPa for 3 s (Figure 7.4 B) and 6 s (Figure 7.4 C). However, using a higher vacuum pressure of 50 kPa with an exposure time of 3 s led to microscopic blisters (separation of viable epidermis from the dermis, indicated by the double-line arrow in Figure 7.4 D) accompanied by partial removal of stratum corneum (Figure 7.4 D), while a 6 s exposure time led to extensive removal of both stratum corneum and viable epidermis (Figure 7.4 E).

For most drug delivery scenarios, blister formation is an unnecessary injury that should be avoided. However, for vaccine delivery applications, blisters may enhance the immune response by recruiting inflammatory cells to the delivery site (Bos 2005).

Residual particles were observed on some histology sections (indicated by single-line arrows in Figures 7.4 C, D and E). Overall, selective full-thickness removal of the stratum corneum was not observed, but was instead mostly accompanied by extensive damage to the viable epidermis.

The mobile and the stationary modes at 50 kPa can be compared by calculating an equivalent exposure time for the mobile-mode procedures (see Materials and Methods). Stationary-mode dermabrasion for 6 s can be compared to mobile-mode dermabrasion at 30 passes and 50 passes, which have equivalent exposure times of 5.3 s and 8.8 s, respectively. While both of these mobile-mode conditions yielded selective stratum corneum removal with little damage to deeper tissues, the stationary-mode

procedure caused extensive epidermal tissue damage. These different responses may be explained by the possibly stronger effects of continuous exposure for 6 s compared to intermittent exposure for a similar amount of time, but broken up into 30 or 50 segments.

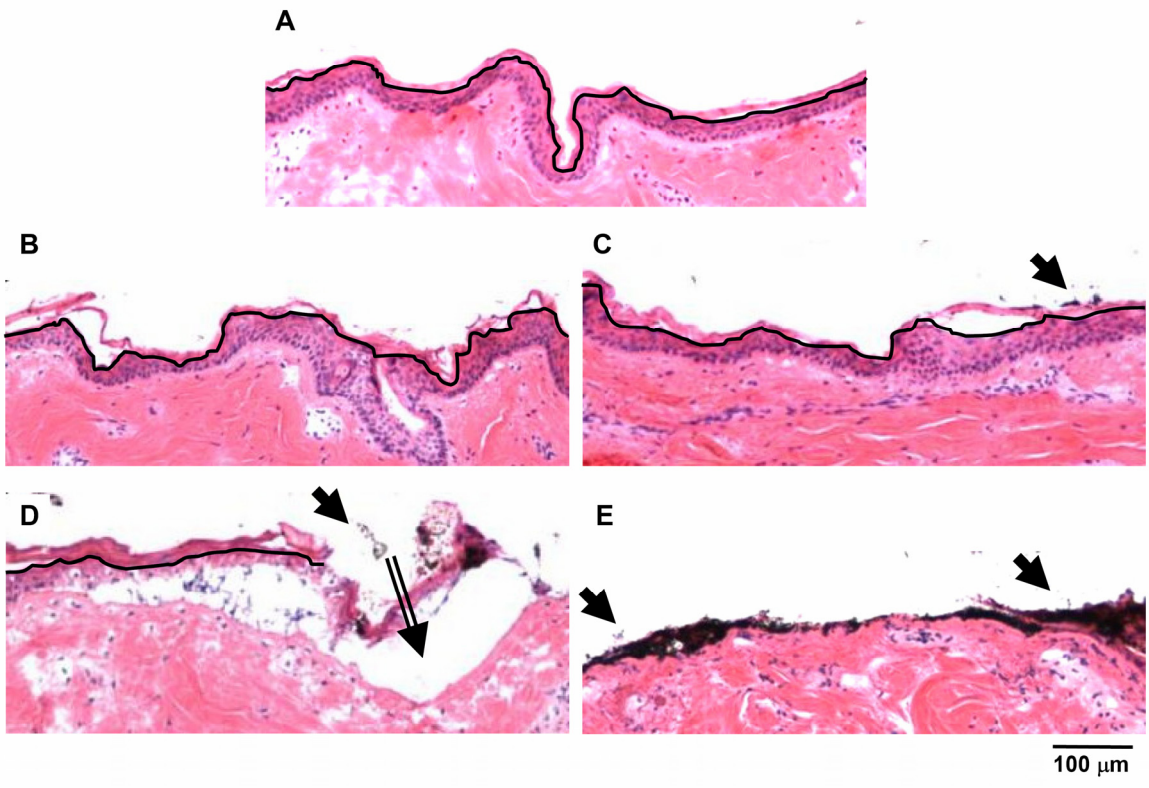


**Figure 7.4. Effect of exposure time and vacuum pressure on removal of skin layers in monkeys**. Brightfield images of H&E stained skin sections from biopsies obtained from an untreated control site (A), and sites exposed to stationary mode of microdermabrasion with 30 kPa vacuum pressure and exposure time of 3 s (B) or 6s (C), and 50 kPa vacuum pressure and exposure time of 3 s (D) or 6s (E). Solid line indicates intact stratum corneum and is drawn at the junction of the stratum corneum and the epidermis layers, solid double lined arrows point to blisters and solid single lined arrows point to residual aluminum oxide particles.

### 7.3.3 Mobile and stationary microdermabrasion in humans

To determine the applicability of these results in rhesus macaques to humans, we carried out an additional study of the mobile and stationary modes of microdermabrasion on the skin of human subjects. As compared to control skin (Figure

7.5 A), selective removal of stratum corneum was observed using a mobile tip at 40 kPa (Figure 7.5 B and C) and blisters were also sometimes seen (Figure 7.5 C). Because the IRB-approved protocol limited the maximum number of tip passes to seven and the vacuum pressure to 40 kPa, we used a slower speed of tip movement to increase the exposure time of microdermabrasion, which may explain the occurrence of microscopic blisters. However, this result validated the ability to selectively remove the stratum corneum in humans similar to that observed in monkeys. Inter-subject variability in full-thickness stratum corneum removal was high and full-thickness removal of stratum corneum was observed in two of the six subjects.

Stationary microdermabrasion performed for 3 s at 30 kPa produced microscopic blisters generally beneath intact stratum corneum (indicated by double-lined arrows in Figure 7.5 D) and at 45 kPa caused extensive removal of both stratum corneum and viable epidermis (Figure 7.5 E). Similar to the observation in monkeys, the stationary mode was unable to produce selective removal of the stratum corneum. Residual particles were also seen on the skin surface (indicated by single-lined arrows in Figures 7.5 D and E).

Despite the occurrence of microscopic blisters, the procedure was well tolerated by the subjects and no visible signs of damage were observed at the treated sites by study personnel. Mild erythema was often present, but no visible damage to the skin or bleeding was seen.

### 7.3.4 Drug and vaccine delivery to monkeys

To test our hypothesis that full-thickness stratum corneum removal can enhance transdermal flux and enable epidermal vaccination, we measured the extent of topical delivery through dermabraded skin. Topical application of sodium fluorescein, a model fluorescent hydrophilic compound, on non-microdermabraded skin resulted in essentially

no detectable delivery across the stratum corneum (Figure 7.6 A). However, application to microdermabraded skin enhanced transdermal flux and delivered fluorescein deep into the dermis (Figure 7.6 B).

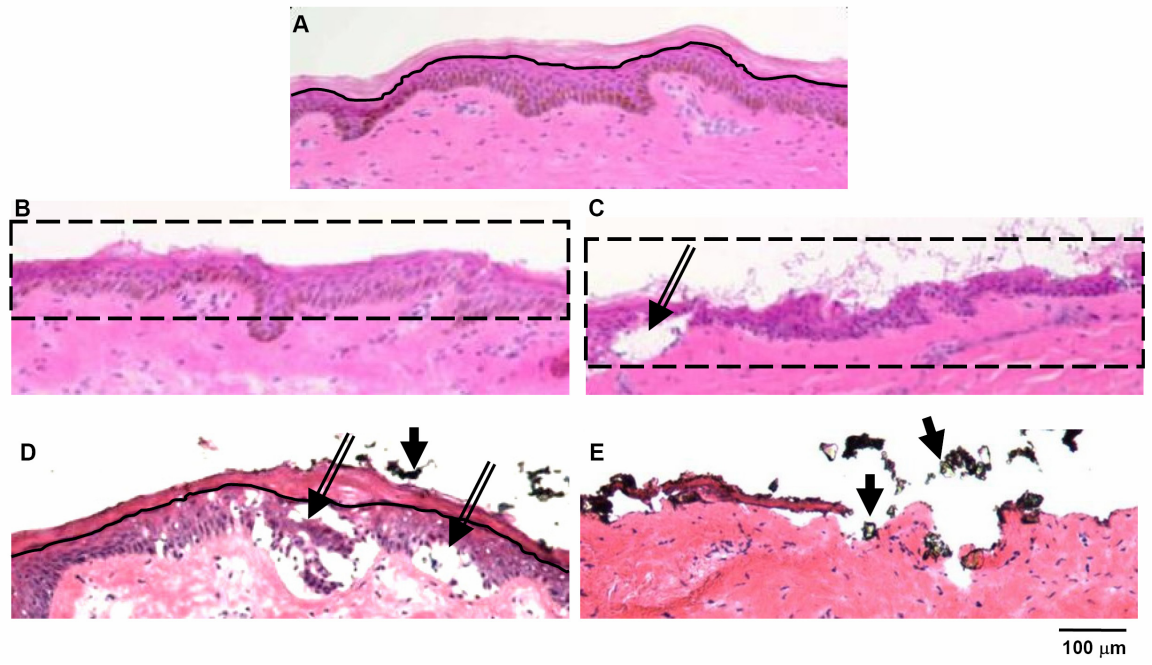


**Figure 7.5. Mobile and stationary mode of microdermabrasion in humans**. Brightfield images of H&E stained human skin sections from biopsies obtained from an untreated control site (A), sites exposed to mobile mode of microdermabrasion with 40 kPa vacuum pressure and 7 passes (B and C), and sites exposed to stationary mode of microdermabrasion with an exposure time of 3 s and a vacuum pressure of 30 kPa (D) and 45 kPa (E). Solid line indicates intact stratum corneum and is drawn at the junction of the stratum corneum and the epidermis layers, dotted rectangles indicate areas of complete stratum corneum removal, solid double lined arrows point to blisters and solid single lined arrows point to residual aluminum oxide particles.

Topical application of MVA, which is a live attenuated virus that serves as a model vaccine, generated virus-specific antibodies measured in the blood after primary immunization (antibody titer: 530 ± 230, $p>0.05$) and a still greater response after the booster dose (antibody titer: 5300 ± 1800, $p<0.05$). This result demonstrates the ability

to deliver viral particles through microdermabraded skin that produce a significant antibody response, which may enable epidermal vaccination.

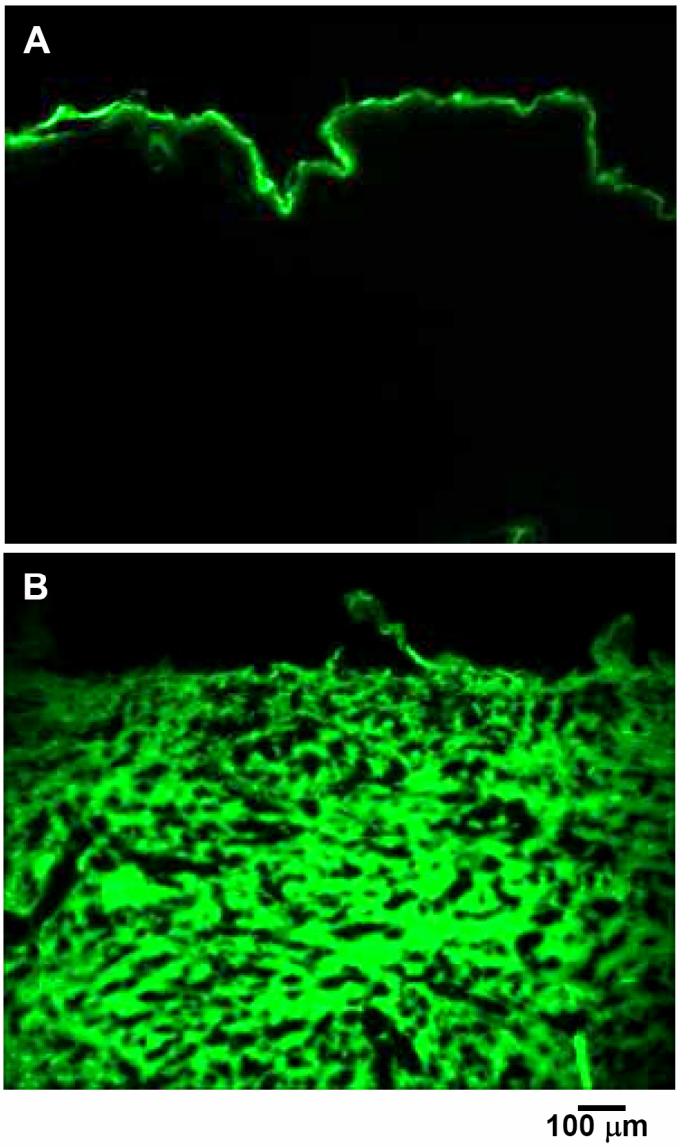


**Figure 7.6. In vivo delivery through dermabraded skin**. Fluorescent images of skin sections obtained from sites topically perfused with a sodium fluorescein solution for 2 h, without microdermabrasion treatment (A) and after mobile mode of microdermabrasion at 50 kPa and 50 passes (B).

## 7.4 DISCUSSION

### 7.4.1 Histological changes in skin layers

Despite widespread use of microdermabrasion in clinical practice, the microscopic changes in the skin that are caused by this procedure have not been studied in detail before. The few studies that have done histologic evaluation of skin after microdermabrasion have reported thinning of stratum corneum at the specific conditions tested (Shim, Barnette et al. 2001; Tan, Spencer et al. 2001). No previous study has documented that microdermabrasion can cause a range of skin tissue removal effects, including selective removal of full-thickness stratum corneum at some conditions and removal of the viable epidermis and formation of micro-blisters at other conditions.

In this study we performed a detailed histologic evaluation over a broad range of microdermabrasion parameters using the skin of monkeys and humans in vivo. In monkeys, 10 passes of microdermabrasion caused thinning of stratum corneum that rarely led to full-thickness stratum corneum removal. This observation is consistent with other reports in humans under conditions representative of conventional cosmetic microdermabrasion (Tan, Spencer et al. 2001; Karimipour, Kang et al. 2005), which typically involves just a few passes (Spencer 2005), although variations in vacuum pressure, microdermabrasion devices and tip designs, speed of tip movement and device operators complicate direct comparisons. For the first time, we have also looked at the effect of larger numbers of passes and have shown that selective full-thickness removal of stratum corneum can be achieved at both 30 and 50 passes.

The effects of microdermabrasion were found to be heterogeneous. Not only was there considerable inter-subject variability, but intra-subject variability was consistently seen at the micron scale. Heterogeneity was generally seen among the 30 consecutive sections collected within a 300 μm interval from each skin biopsy. This variability may be

explained by the stochastic process of particle flight and impingement with the skin during the microdermabrasion process. In human subjects, a greater variability in stratum corneum removal was observed. This variability may be due in part to the fewer (just 3 - 5) sections that were collected for analysis. Given the micron-scale heterogeneity associated with microdermabrasion, future histologic studies would benefit from analyzing a larger number of sections spanning a larger area of the biopsy.

Micro-blisters were sometimes observed after microdermabrasion, especially after stationary microdermabrasion. These micro-blisters may represent an early stage of suction blister formation, which is a well-established technique used to harvest epidermis for transplantation or to study inflammatory reactions and wound healing in skin (Gupta and Kumar 2000). Typically, about 40 kPa vacuum pressure is applied for 1 - 3 h to create blisters measuring 10 - 30 mm in diameter to harvest the epidermis for grafting.

### 7.4.2 Implications for transdermal drug delivery

Microdermabrasion has only recently been investigated for transdermal drug delivery. Previous studies have demonstrated transdermal flux enhancement only for very low molecular weight compounds <300 Da) under conditions that were not shown to remove full-thickness stratum corneum. To deliver larger molecules, biopharmaceuticals and vaccines, removal of full-thickness stratum corneum is probably required. Even small regions (e.g., microns) of full-thickness stratum corneum removal should have a large impact on skin permeability to macromolecules, which are of nanometer dimensions. Such micron-sized “leaks” in the skin barrier have been created using microneedles and shown to increase skin permeability by orders of magnitude (McAllister, Wang et al. 2003).

In this study, we have shown full-thickness removal of stratum corneum from areas with characteristic dimensions of less than 100 μm up to approximately 1000 μm, which depended on microdermabrasion conditions. As a proof-of-concept that microdermabrasion makes skin permeable, we have dramatically increased transdermal delivery of a model drug, fluorescein, and demonstrated a heightened antibody response generated by a model live-virus vaccine. This is the first demonstration of delivery of a molecule larger than 300 Da in size and the first demonstration of delivery of a viral vaccine to generate an immune response by microdermabrasion. These results were enabled by using large numbers of microdermabrasion passes to remove full-thickness stratum corneum, which differs from previous work that has involved much fewer passes that only thinned the stratum corneum.

Overall, these results suggest that microdermabrasion under suitable conditions may be used as a skin pre-treatment followed by subsequent application of a transdermal patch to delivery drugs, biopharmaceuticals and vaccines. Because this process exposes the viable epidermis, gene delivery to epidermal keratinocytes may also be possible through direct application of cell transfection agents.

In a related process called microscission, microparticles were impinged on the skin using a high pressure carrier gas to create 50-200 μm deep microconduits in the skin (Herndon, Gonzalez et al. 2004). Microscissioning is similar to the stationary mode of microdermabrasion, but differs in the use of high-pressure gas rather than vacuum suction to propel the microparticles. Lidocaine delivery and glucose measurements from blood extracted through the microconduits were demonstrated. Because these microconduits were at least 50 μm deep, microscissioning may produce more deep-tissue trauma than microdermabrasion with selective full-thickness stratum corneum removal. The microscissioning procedure was enhance through the additional use of

protective masks with micron-sized openings applied to the skin surface to control the diameter of the microconduits. This use of masks may also be useful as an adjunct to microdermabrasion in order to better control and localize the microdermabrasion effects to smaller skin areas for better cosmetic appearance and decreased tissue trauma.

### 7.4.3 Implications for cosmetic use

Microdermabrasion is presently approved as a class I device by the FDA (Spencer 2005). As a result, phase III clinical trials demonstrating the safety and efficacy of microdermabrasion have not been done. Based on this study in monkeys and human subjects, it is expected that large numbers of passes in the mobile mode should be avoided to prevent full-thickness removal of stratum corneum and, possibly, deeper tissues. Small numbers of passes just removes partial-thickness stratum corneum, which has been documented by previous researchers as well (Karimipour, Kang et al. 2005; Spencer 2005).

The stationary mode of microdermabrasion should also be avoided, because of its tendency to form micro-blisters. Furthermore, topical creams and ointments for cosmetic or other purposes should be used with caution after microdermabrasion, because the stratum corneum thinning may enhance absorption of the topical formulations, leading to increased and possibly adverse effects.

## 7.5 CONCLUSION

Motivated by the need to microscopically characterize the effects of microdermabrasion on skin and the goal to selectively remove full-thickness stratum corneum for transdermal drug delivery, we performed mobile and stationary microdermabrasion on the skin of rhesus macaques and human subjects in vivo. This is

the first detailed study to characterize the effects of microdermabrasion on skin over a broad range of microdermabrasion conditions.

In the monkeys, the degree of skin tissue removal increased with the number of passes in the mobile mode. At 30 and 50 passes, selective full-thickness removal of stratum corneum was observed with little damage to the viable epidermis. At larger numbers of passes, viable epidermis was removed. Using the stationary mode, selective stratum corneum removal was not achieved. Typically, either the stratum corneum and epidermis were both intact, with possible formation of micro-blisters at the dermal-epidermal junction, or the stratum corneum and epidermis were both removed. Similar tissue removal trends were observed in human subjects using both the mobile and stationary modes of microdermabrasion. Finally, delivery of sodium fluorescein and an enhanced antibody response to MVA virus were demonstrated.

Thus, this study demonstrated for the first time that microdermabrasion can selectively remove full-thickness stratum corneum with little damage to deeper tissues and thereby enhance transdermal flux and enable epidermal vaccination.

# CHAPTER 8: CONCLUSIONS

Majority of biopharmaceutical drugs and vaccines continue to be delivered by means of painful and potentially unsafe hypodermic injections. Although the transdermal route is attractive, the stratum corneum layer provides a formidable transport barrier and prohibits delivery of biopharmaceuticals via the skin. In this research we developed and characterized two different approaches, i.e., coated microneedles and microdermabrasion to facilitate painless transdermal delivery of biopharmaceuticals.

**Coated microneedles**

Stainless steel was selected to fabricate microneedles because of its high mechanical strength and known history of use in medical devices. Based on laser cutting and electropolishing a versatile stainless steel microneedle fabrication process was developed. Using this process, microneedles with sharp tips, clean surfaces and complex geometries were fabricated. Novel pocketed microneedles, i.e., microneedles with through-holes in the shaft, were also fabricated. For convenient application of microneedle arrays on the skin, prototype microneedle patches with arrays of microneedles were developed. Pressure-sensitive adhesive was integrated on these patches to: (i) secure the microneedle patch on the skin and (ii) prevent the skin-pierced microneedles from regressing out of the skin due to skin recoil when the force used to apply the patch ceases to exist.

With the goal of optimizing microneedle geometry for minimal pain from insertion, we conducted a pain study in human subjects using microneedles of different dimensions and numbers. A 26-gage hypodermic needle inserted 5-mm deep into the skin was used as a positive control for comparison. Statistical comparison between all the different microneedle dimensions that were investigated (lengths as much as 1450

μm, widths as much as 465 μm, thicknesses as much as 100 μm and as many as 50 microneedles in an array) showed that all microneedles were statistically less painful than the 26-gage hypodermic needle (outer diameter of 460 μm). In addition, many microneedle insertions were rated as entirely painless (as much as half the subjects scored the 480 μm long and 20° tipped microneedle as having zero pain) as compared to the hypodermic needles for which none of the subjects reported the insertions to be painless. Based on this study microneedle length was found to be the most influential factor affecting pain. A three fold increase in microneedle length produced more than a seven fold increase in pain. The numbers of microneedles was also significant in affecting pain, though less steeply. A ten fold increase in the number of microneedles from 5 to 50 increased the pain by just around two and half times. No statistically significant effect was observed due to change in tip angle, width or thickness over the range investigated. This study suggested that microneedle length and numbers are important parameters to optimize to obtain minimally painful microneedle devices for drug delivery.

To produce uniform coatings on microneedles without contaminating their substrate, a novel micro-dip-coating method was designed. The coating device primarily controlled the surface tension-driven rise of coating solution up the microneedle shafts to prevent contamination of the substrate. Based on this design, coating devices were fabricated to coat single microneedles, in-plane microneedles or out-of-plane microneedles. A coating formulation was also developed to achieve uniform films on microneedles. This formulation used low concentrations of carboxymethylcellulose and Lutrol F-68 NF as excipients to increase the viscosity and to decrease the surface tension of the coating solution, respectively. Using the coating devices and the coating formulation, vitamin B2, calcein, bovine serum albumin, and plasmid DNA were coated

onto microneedles. For the first time, organic and inorganic microparticles as well as viruses were also coated onto microneedles. This study demonstrated that a broad range of compounds could be coated on the microneedles. Assessment of the performance of coated microneedles showed that microneedle coatings dissolved within seconds after insertion into cadaver skin. Successful in vitro delivery into skin was achieved for microneedles coated with microparticles up to 10 μm in diameter. Using novel 'pocketed' microneedles to mechanically protect coatings during insertion, 20-μm diameter particles were delivered into skin without wiping off onto the skin surface. Integrated patches containing 50-microneedle arrays were also shown to insert into the skin of human subjects and to deliver their coated payload into human cadaver skin. Collectively these results demonstrated that (i) microneedles coated with drug could be reliably inserted into the skin without drug wiping off on the skin surface, and (ii) the coatings rapidly dissolved off the microneedle surface after microneedle insertion into the skin.

A detailed study of coating formulations was performed to develop a rational basis for designing coating solution formulations for uniform and thick coatings on microneedles, and to identify coating strategies to form composite coatings, deliver liquid formulations, and control the mass deposited on microneedles. Recognizing that lower solution surface tension promotes good wetting of the microneedle surface, FDA-approved surfactants, organic solvents, and microneedle surface modification methods were successfully tested to promote uniform coatings. Use of viscosity enhancers led to thicker microneedle coatings, promoted by increase in the volume of liquid film adhering onto the microneedles after dipping, and an increase in the residence time of this adherent liquid film on the microneedle. Control over coating solution surface tension and viscosity also enabled filling of pockets in microneedle with purely liquid or solid

films. Thus, control over the coating solution viscosity and surface tension enabled predictable uniform coating of microneedle surfaces and/or pockets. Furthermore, a hydrophobic molecule was also coated on microneedles using an ethanol-based formulation. Surfactants were not required in this case because ethanol already has a low surface tension. We further tested the ability to form multi-layered coatings, with each layer consisting of a different drug. Several different drug-layers were successfully coated on top of each other, including first filling pockets with drugs and then overcoating with another film. Such multilayered coatings can facilitate combination of burst and controlled release from the same microneedle. We also investigated quantitatively the mass of drug in microneedle coatings. The mass of a model drug, riboflavin, coated on microneedles was found to increase with its concentration in the coating solution, the number of coating solution dips, and the number of microneedles in the array. Based on this data, up to 1 mg of drug can be expected to be coated on a few hundred microneedles on a patch size of about 10 to 20 $cm^2$. Altogether, microneedle coating formulations can be designed to have a range of different properties to address a variety of different drug delivery scenarios.

Finally, coated microneedle characterization was done in vivo by immunization of mice using hepatitis-C DNA coated microneedles. Antigen specific T-cell response was generated at low vaccine dose (3 to 8 μg) and without the use of adjuvants. Chromium release CTL assay demonstrated that the CTL response was robust in vitro. The in vivo tumor challenge assay demonstrated that the cytotoxic T-lymphocytes also had the ability to recognize and kill cells expressing the immunizing antigen in vivo. This study suggests that DNA-coated microneedles have potential to deliver DNA vaccines into the skin with high potency.

**Microdermabrasion**

Microdermabrasion has potential to selectively, yet completely remove the stratum corneum barrier for topical delivery of biopharmaceuticals. Motivated to determine the effect of different microdermabrasion conditions on skin and to identify conditions for full-thickness removal of stratum corneum, we performed microdermabrasion in vivo in human volunteers and monkeys. Using the mobile mode of microdermabrasion, the degree of removal of the stratum corneum and viable epidermis was found to increase with the number of passes. At 50 passes, selective removal of stratum corneum was observed with little damage to the viable epidermis. Quantitative measurement demonstrated that at 50 passes, at least 25% of the skin was devoid of stratum corneum, and much less of the skin had viable epidermis removed. Under the stationary mode, selective stratum corneum removal was not achieved but micro-blisters (separation of viable epidermis and dermis) were observed. Similar removal trends were observed in human subjects under both the mobile and the stationary modes of microdermabrasion. Finally, delivery of sodium fluorescein and MVA virus was demonstrated after their topical application on microdermabraded skin. An antibody response was detected from the topical delivery of MVA. Thus, in this study, we demonstrated for the first time that microdermabrasion can be used to selectively remove the stratum corneum layer and also demonstrated the ability to deliver model hydrophilic compounds and virus through the microdermabraded skin.

Altogether, the coated microneedle and microdermabrasion studies have shown that both approaches can be used to target the skin for delivery of hydrophilic and large molecular weight compounds including proteins, DNA and viruses. More broadly, both coated-microneedles and microdermabrasion have the potential to enable painless transdermal delivery of biopharmaceuticals and vaccines in a convenient manner.

# CHAPTER 9: RECOMMENDATIONS

Experimental results from this thesis research have demonstrated the ability of coated microneedles and microdermabrasion to deliver hydrophilic and large molecular weight materials in vivo. Microneedles coated with hepatitis C DNA were able to elicit strong T-cell responses in mice. In the case of microdermabrasion, a preliminary experiment with topical application of MVA on the skin of monkeys generated MVA specific antibodies. Based on these promising results and unpublished data, I believe that coated microneedles and microdermabrasion have potential to be developed as transdermal drug delivery methods for application in clinics or for self-administration. Specifically, both these methods have the ability to emerge as safer and largely painless vaccine administration methods suitable for mass immunizations. To fully develop each method for clinical use, I make the following recommendations.

## 9.1 COATED MICRONEEDLES

### 9.1.1 Advancement of microneedle fabrication and coating process

#### 9.1.1.1 Improvement in microneedle fabrication

In this study, microneedles were fabricated from stainless steel using laser cutting. Although laser cutting is very versatile, mass fabrication will be limited by availability of lasers. Because laser machines require large capital investment, other microneedle fabrication methods can facilitate inexpensive large scale fabrication of stainless steel microneedles. Wet etching of stainless steel is one such method. However, because wet etching of stainless steel, and other metals in general is isotropic in nature, fabricating microneedles with sharp tips may be difficult. Electrochemical etching enhances metal removal through use of electrical energy and provides a higher

degree of etch ratio (vertical to lateral etch depth). Therefore, I recommend that a process of electrochemical etching of stainless steel be developed to enable inexpensive mass fabrication of microneedles.

In this study, microneedles were manually bent out of plane of the metal sheet. However, I recommend that an automated mechanism should be developed to bend the microneedles out of their substrate to ensure reproducibility and to achieve vertical microneedles.

Metal microneedles have higher elastic modulus and are mechanically strong to pierce the skin. However, metal microneedles can still be misused for re-use, and also pose a disposal problem, though on a much smaller scale than hypodermic needles. Therefore, I recommend that alternative non-metallic materials, which are mechanically strong and easy to dispose, should be explored for microneedle fabrication for coating applications. An ideal case will be a material that dissolves in the skin along with the drug coated on its surface.

#### 9.1.1.2 Improvement in dip-coating

The microneedle dip-coating process and formulation guidelines developed in this research can allow coating of a broad range of drugs with different physicochemical properties. However, because the dip-coating devices were designed for manual dipping of microneedles into the coating solution, the average variation of the mass coated onto microneedles was 19% relative standard deviation. For many clinical applications this deviation must be decreased. Therefore, I recommend that the dipping process should be automated. This will improve coating reproducibility and lead to a tighter control on the mass coated on each microneedle array.

A further improvement to the dipping process can be made by modifying the coating solution holder. In its current design, the coating solution is filled into the coating

solution holder at the beginning of the coating process. Over time, during the coating process, the coating solution becomes concentrated due to solvent evaporation. Because small holes are used as individual dipping ports for microneedles, deposit of solute can start accumulating on the edges of the holes at high solute concentrations. Partly, this can be addressed by controlling the humidity and temperature of the coating environment. But a more thorough solution will require modification of the coating solution holder to incorporate either a gentle pulsatile movement of the fluid in the solution holder to enhance mixing without pushing the fluid out of the dip holes, or a continuous flow of the coating solution to prevent stagnation. The latter solution can also be designed to have provision for automated sampling and addition of new solution to compensate for evaporation.

#### 9.1.1.3 Prediction of mass in coatings

To control the mass of drug coated onto microneedles, various coating and microneedle parameters can be independently controlled. Because theoretical prediction of the mass coated onto microneedles is difficult, in this research, vitamin B2 was used as a model drug and its mass in the coatings was determined as function of coating and microneedle parameters. However, it is not practical to repeat mass characterization for all the different candidate drugs, especially for expensive biopharmaceuticals. Therefore, I recommend experiments should be performed to determine if mass in the coatings has a functional dependence on some measurable parameter(s) of the coating solution, for example molecular weight of the drug and/or its relative concentration in the coating solution. When the dependence is identified, extensive data should be generated using model compounds and validated against a set of different compounds, including proteins and DNA. Results from these experiments will ultimately allow selection of coating and

microneedle parameters required to produce coatings with a specified mass of drug in them.

#### 9.1.1.4 Assessment of coating safety prior to use in humans

Both CMC and F-68, the two commonly used excipients in this research, are approved by the FDA for parenteral injection. However, before coated microneedles can be used in humans, I recommend that the safety of the coatings should be evaluated in vitro and in vivo.

Some of the potential sources of concern that should be addressed are: thermal degradation of CMC and F-68 or other excipients during the autoclaving process; change in properties of drug molecules due to physical interaction between solutes and drug either in solution or after solidifying on the microneedle surface; long term stability of drug in the coatings; and pyrogenicity and irritation from coated microneedles. Appropriate in vitro and in vivo models should be used to address these concerns.

#### 9.1.1.5 Development of larger arrays

For delivery of compounds with dose in the range of few hundred micrograms, arrays with many hundred microneedles will be required. I recommend that research should be carried out in this direction to design and develop larger solid microneedle arrays. Corresponding modifications in the coating process and technique of array insertion into the skin will also need to be made.

### 9.1.2 Application development

#### 9.1.2.1 Vaccination via regular antigens

I predict that the major impact of coated microneedles will be in the field of vaccination and delivery of biopharmaceuticals. I recommend that in vivo immunization

studies should continue to be performed to characterize the immune responses in more detail and to assess the long term stability of the coated antigens. Based on my experience, CMC and F-68 appear to be good excipients, and can be used to coat most antigens and DNA molecules, either for vaccination or gene therapy.

#### 9.1.2.2 Vaccination through antigens encapsulated in microparticles

Delivery of microparticles encapsulating antigen into the skin may allow combination of prime and boost effects into a single dose, eliminating the need for multiple doses of vaccines. In addition, microparticles can be designed to better interact with the Langerhans cells of the skin by controlling microparticle diameter, to produce a more robust immune response. Because, in this research we have already demonstrated the ability to coat microparticles onto microneedles and their subsequent delivery into the skin, I recommend that microparticle encapsulated antigen based delivery into the skin should be studied in greater detail. This method has potential to decrease the frequency of vaccine administration.

#### 9.1.2.3 Delivery of other compounds

Most compounds with a dose in the range of few hundred micrograms are available for delivery through coated microneedles. Biopharmaceuticals like growth hormones and peptides like desmopressin are few examples. Molten liquid formulations after melting the drug can also enable coating of pure drug onto microneedles, increasing the dose coated on a single microneedle. Further, pocketed microneedles provide a unique way to deliver difficult to coat materials like large particles and liquids, into the skin. All these techniques can be very useful and I recommend that effort should continue to further develop and apply these strategies for delivery of compounds into the skin.

#### 9.1.2.4 Tattoos

Coated microneedles also offer some non clinical applications, for example, for tattoo formation. I hypothesize that microneedle length can be controlled to produce temporary or permanent tattoos. Shorter microneedle lengths because of shallow insertion and deposition into the epidermis may result in temporary tattoos because of clearance of the tattoo dye due to high turnover rate of the epidermis and the stratum corneum. I recommend testing of this hypothesis to ultimately develop self administrable temporary or permanent tattoos based on coated microneedles.

## 9.2 MICRODERMABRASION

In this research, microdermabrasion was demonstrated to selectively remove the stratum corneum layer. I consider the main utility of this method to remove stratum corneum for subsequent transdermal patch application for controlled or bolus drug delivery. Because the stratum corneum will take a few days to grow back (maybe slower when it is occluded by the patch), drug delivery can occur for a longer duration. I recommend the following research direction for microdermabrasion.

### 9.2.1 Process development

#### 9.2.1.1 Modeling of the microdermabrasion process

Microdermabrasion is a complex process with a number of different variables like particle flow rate, vacuum pressure and time of exposure. All these variables can independently affect the microdermabrasion process. It is important to identify which variables are most important in controlling the skin layer removal process and to identify the optimum numerical range of these variables in removing the stratum corneum without deeper damage to the skin. I recommend development of a detailed mechanistic model of microdermabrasion to aid in microdermabrasion process optimization. Such a

model can help guide the selection of optimum operating parameters and their levels. In this thesis a few parameters have been studied, however, a more detailed analysis is required to develop the model in detail.

#### 9.2.1.2 Decreasing heterogeneity

The microdermabrasion process resulted in heterogeneous tissue removal, even though the particle size was small compared to the treated skin area. Heterogeneity in stratum corneum and epidermis removal will cause variations in drug dose administered to different individuals. Therefore, I recommend that effort should be made to reduce the level of heterogeneity. One method to achieve this is by masking the treated skin with an abrasion-resistant mask containing smaller openings. This will allow small and targeted regions of the skin to be abraded. Further homogeneity can be achieved by experimenting with particle size, duration of exposure and other microdermabrasion parameters.

### 9.2.2 Applications

#### 9.2.2.1 Gene therapy, vaccination and biopharmaceutical delivery

I expect the greatest impact of microdermabrasion to be in the field of gene therapy and vaccination through topical delivery to the exposed epidermal keratinocytes. I recommend that in vivo experiments should be performed to investigate these applications in greater detail. In addition, biopharmaceutical delivery after microdermabrasion is another application with good clinical potential. Transdermal patches that control the release of biopharmaceutical compounds can be applied to microdermabraded skin. Therefore, I also recommend conducting in vivo pharmacokinetic studies after topical drug administration on microdermabraded skin. These studies can promote understanding of the change in plasma concentration

profiles, and to estimate the effective time for patch application before the skin starts to heal itself. Transepidermal water loss or skin electrical resistance measurements can further aid in studying the skin's barrier formation kinetics.

# APPENDIX A: PAIN STUDY – EXPERIMENTAL DETAILS AND PAIN DATA

## 1) RANDOMIZATION

To obtain unbiased pain data, the sequence and location of insertion of different microneedles and controls was randomized for each human volunteer. The procedure of randomizations is described below:

**Insertion-sequence randomization**:

1. Each microneedle and control treatment, in triplicate, was given an identifier-label. These labels were then pre-arranged in a column in Microsoft-Excel.
2. Random numbers, equal to the number of identifier-labels were then generated in an adjacent column.
3. The two columns were next sorted in an ascending order based on the random numbers column. This sorting process arranged the random numbers in an ascending order, but led to a random shuffling of the identifier-labels column, resulting in a list of randomized insertion sequence.
4. Steps 2 to 3 were repeated for each volunteer to generate different randomized insertion sequence lists for each volunteer.

**Insertion-location randomization**

A random sequence was also generated to associate each insertion from the insertion sequence list to a unique but random location of insertion on the skin.

1. A rubber stamp with grids of dots was stamped on the forearms of human volunteers. Each square that was formed between the dots was then assigned a unique address. The addresses were numbered 1 through 40 for stage-I of the

study (Figures A.1) and were given rectangular matrix addresses for stage-II of the study (for example, LA-1, LA-2, LA-3, RB-7 etc., Figure A.2).

2. The addresses were then listed in a column in Microsoft Excel and steps 2 and 3 of the insertion-sequence randomization process were performed to randomly shuffle the addresses. In this manner, randomized square-address lists were generated for each volunteer.

Thus, for each volunteer two randomized lists were generated, a randomized insertion sequence list and a randomized address list. Through a sequential pair-wise matching of the two lists, the sequence in which the different insertions were to be made in the skin and the location of insertion on the skin were uniquely identified through this randomized process.

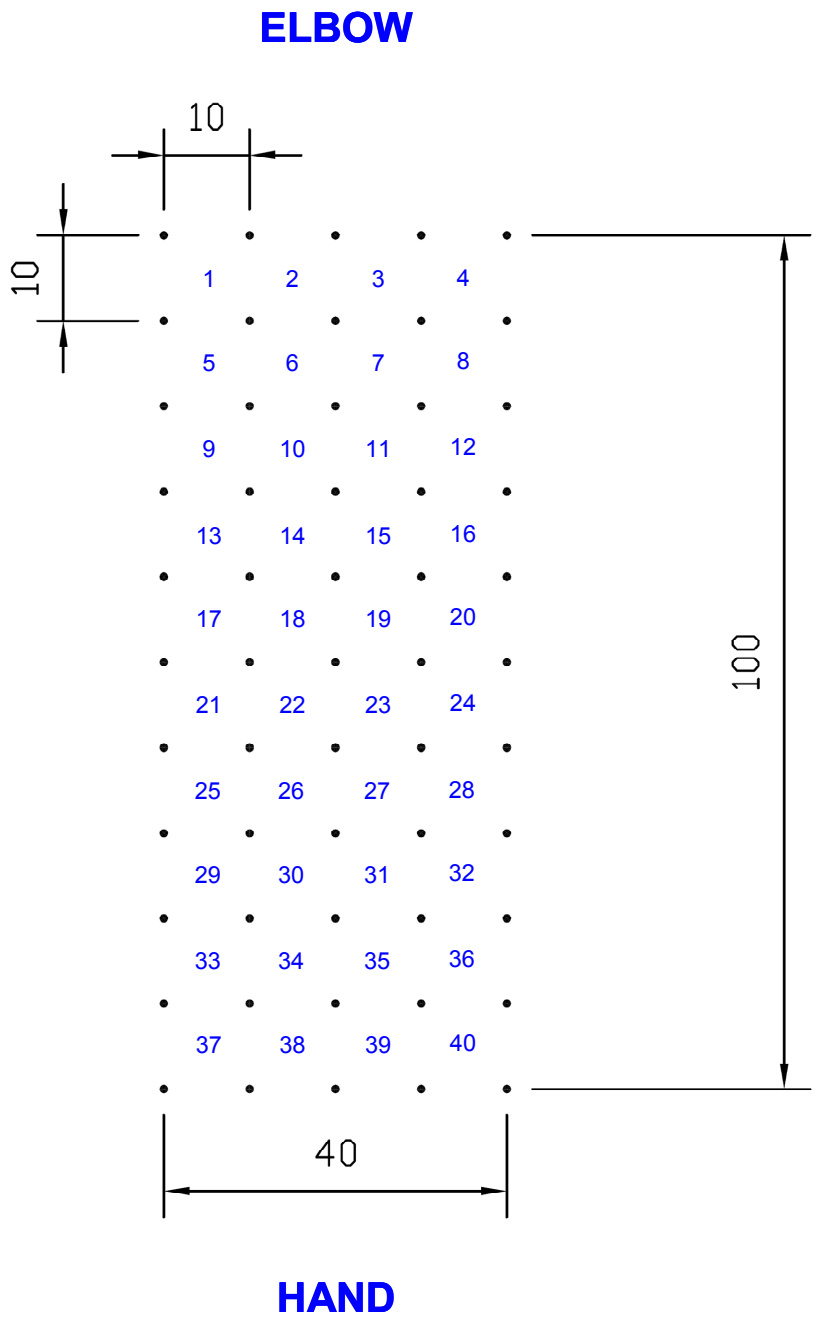


**Figure A.1. Dot pattern used in pain study stage-I**. Design of the dots imprinted on the forearms of human volunteers in stage-I of the pain study. The address associated with each insertion square site is labeled. The numbers were not physically stamped and only served as a tool in randomizing the insertion locations. The dimensions are in mm. 'Elbow' and 'Hand' represent the orientation of the stamp on the forearm.

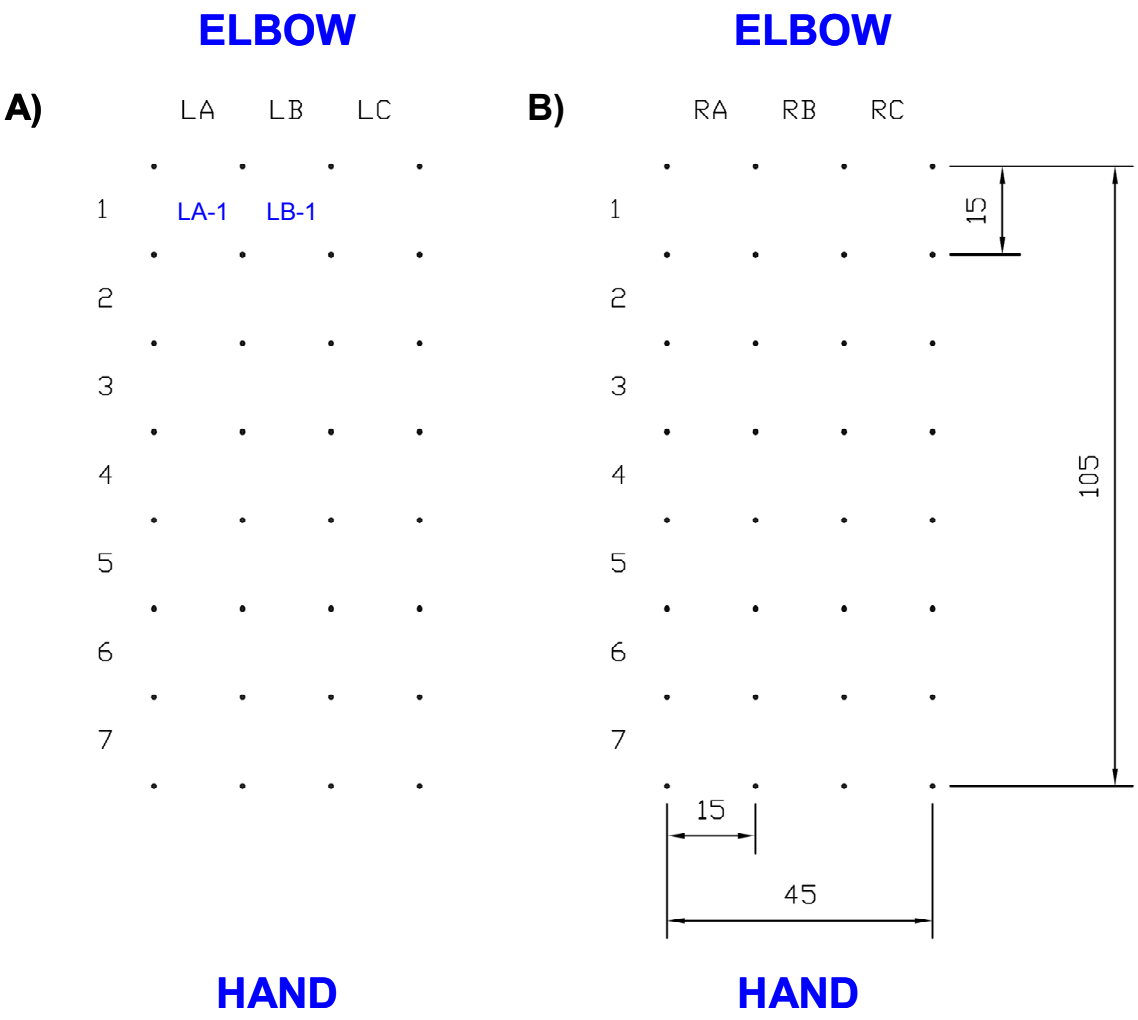


**Figure A.2. Dot pattern used in pain study stage-II**. Design of the dots imprinted on the (A) left and the B) right forearms of human volunteers in stage-II of the pain study. The addresses associated with each insertion square site should be read as a matrix address. Example addresses are labeled as 'LA-1' and 'LA-2' and the remaining addresses should be filled as a combination of the matrix column labels LA, LB, LC, RA, RB and RC, and the row labels 1 to 7. All dimensions are in mm. 'Elbow' and 'Hand' represent the orientation of the stamp on the forearm.

## 2) DEPTH CONTROL OF HYPODERMIC NEEDLE

To reproducibly insert a 26 gage hypodermic needle 5-mm deep into the skin, a sleeve was fabricated that allowed just 5 mm of the hypodermic needle to protrude out (Figure A.3). The sleeve was fabricated by cutting an appropriate length of the tip of the protective sheath that encases a new hypodermic needle in its blister pack.

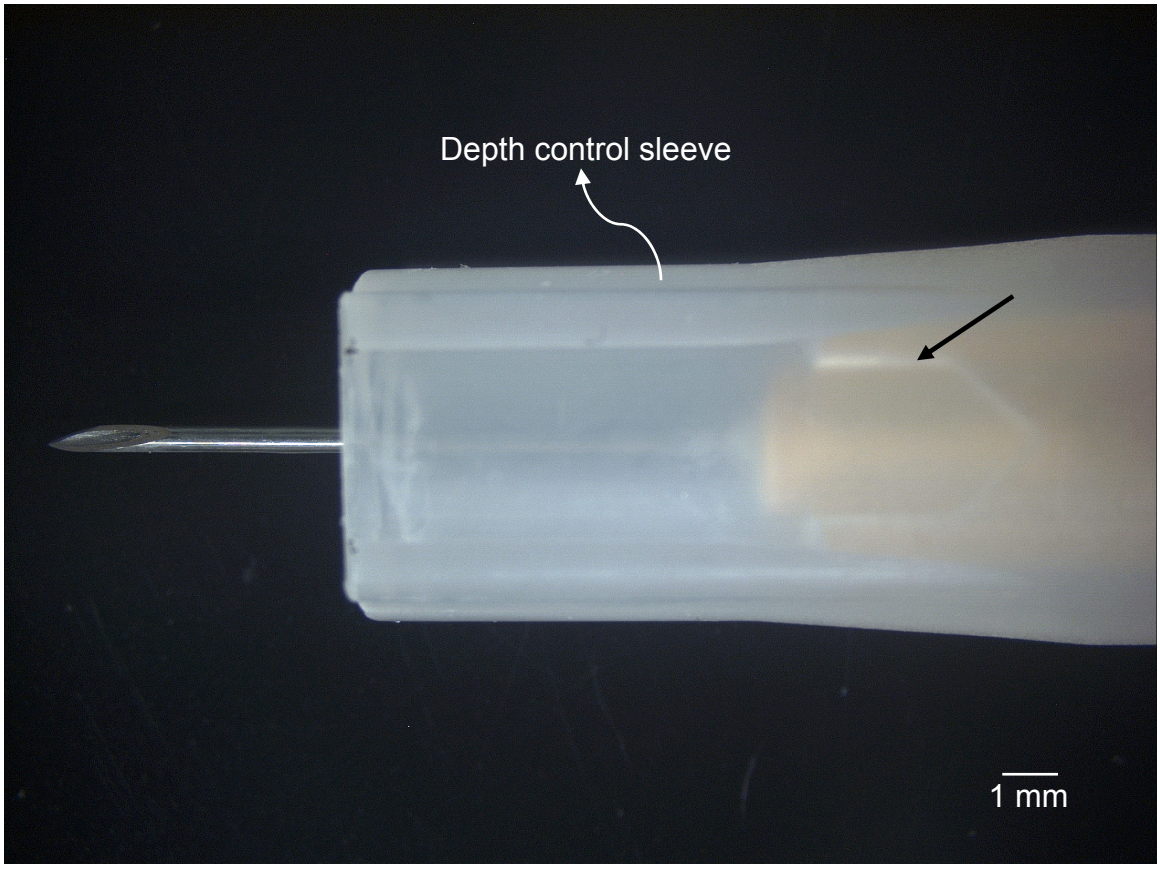


**Figure A.3. Depth control of a hypodermic needle**. A 26 gage hypodermic needle protruding 5 mm from the sheath. The arrow points to the hypodermic needle hub inserted into the sheath.

**3) RAW VAS PAIN SCORE**

After each insertion of the microneedle or the control treatment, human volunteers rated the pain using a visual analog scale (VAS). The side of the scale visible to the human volunteers had “No pain” and “Worst pain” printed at its two ends and was fitted with a movable slider (Figure A.4 A). Human volunteers moved this slider between the two ranges based on their perception of pain after each insertion. The opposite side of the same scale was printed with a number scale (in millimeter units, Figure A.4 B), which the investigators used to numerically quantify the pain from each insertion. This numerical score was reported as the raw VAS pain score, and it was used for analysis of the pain as described in Chapter 3. Raw VAS pain scores of all the human volunteers from different microneedle and control treatments, in triplicate, for stages-I and -II are given in Tables A.1.A, A.1.B, A.2.A and A.2.B.

An example calculation to find normalized pain scores from triplicate raw pain scores is given in Table A.3. The table has four columns. The first column contains the labels of microneedles forming the ‘length study’ group. The second column contains their raw pain scores, the third column contains the average raw pain scores obtained as a mean of the triplicates for each microneedle length, and the fourth column contains the normalized pain scores obtained by dividing the mean raw pain scores of column three with the mean raw hypodermic needle pain score in the column and then multiplying with 100. The mean raw and normalized pain scores for all the ten subjects for the ‘length study’ are given in Table A.4.

A)

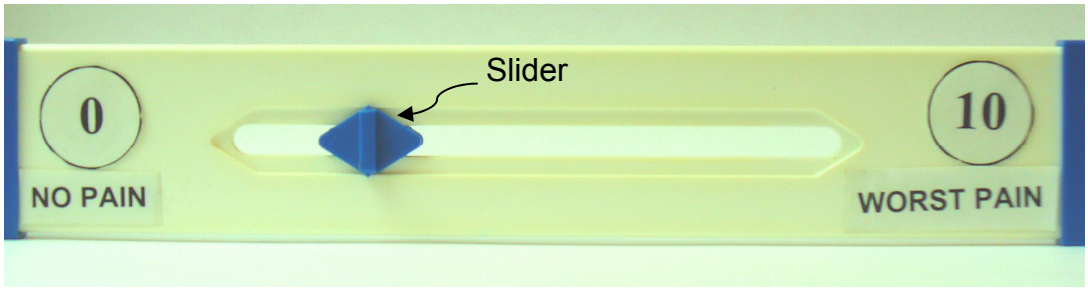


B)

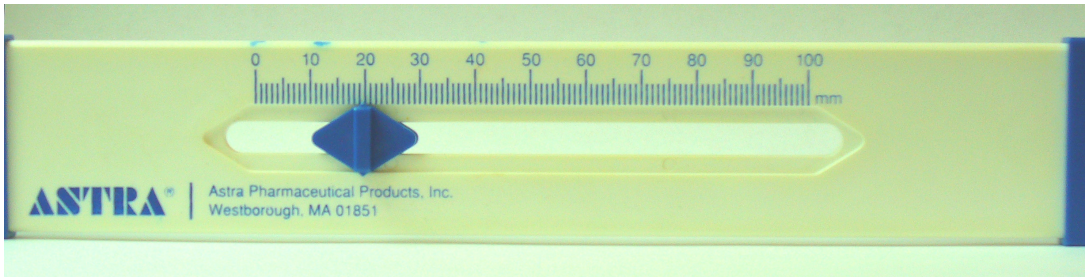


**Figure A.4. Visual analog scale**. The two sides of the visual analog scale used to measure the pain scores, (A) the side visible to the human volunteer and (B) the side visible to the investigator.

**Table A.1.A.** Triplicate raw VAS pain scores for stage – I of the pain study (Volunteers 1 to 5).

| Skin insertion treatment | Raw VAS pain scores | | | | |
|---|---|---|---|---|---|
| | Subject 1A | Subject 2A | Subject 3A | Subject 4A | Subject 5A |
| 20°- 480μm - 1 | 0 | 0 | 5 | 5 | 0 |
| 20°- 480μm - 2 | 0 | 28 | 0 | 3 | 0 |
| 20°- 480μm - 3 | 0 | 25 | 0 | 9 | 0 |
| 20°- 960μm - 1 | 0 | 25 | 5 | 24 | 0 |
| 20°- 960μm - 2 | 0 | 18 | 0 | 3 | 0 |
| 20°- 960μm - 3 | 0 | 10 | 10 | 24 | 0 |
| 55°- 1450μm - 1 | 4 | 30 | 6 | 12 | 0 |
| 55°- 1450μm - 2 | 8 | 77 | 19 | 64 | 3 |
| 55°- 1450μm - 3 | 4 | 27 | 11 | 50 | 0 |
| 55°- 480μm - 1 | 0 | 0 | 10 | 2 | 0 |
| 55°- 480μm - 2 | 0 | 18 | 0 | 5 | 4 |
| 55°- 480μm - 3 | 0 | 0 | 0 | 2 | 0 |
| 55°- 700μm - 1 | 0 | 22 | 0 | 2 | 0 |
| 55°- 700μm - 2 | 0 | 0 | 15 | 7 | 7 |
| 55°- 700μm - 3 | 0 | 23 | 0 | 14 | 0 |
| 55°- 960μm - 1 | 6 | 28 | 5 | 6 | 21 |
| 55°- 960μm - 2 | 4 | 4 | 4 | 8 | 3 |
| 55°- 960μm - 3 | 2 | 51 | 8 | 45 | 8 |
| 90°- 480μm - 1 | 0 | 0 | 0 | 25 | 1 |
| 90°- 480μm - 2 | 4 | 25 | 8 | 0 | 0 |
| 90°- 480μm - 3 | 4 | 0 | 0 | 3 | 3 |
| 90°- 960μm - 1 | 3 | 49 | 4 | 9 | 5 |
| 90°- 960μm - 2 | 6 | 60 | 0 | 28 | 6 |
| 90°- 960μm - 3 | 0 | 32 | 60 | 3 | 0 |
| Hypodermic - 1 | 6 | 84 | 10 | 60 | 46 |
| Hypodermic - 2 | 7 | 40 | 73 | 55 | 20 |
| Hypodermic - 3 | 9 | 53 | 84 | 49 | 46 |
| Teflon rod - 1 | 0 | 0 | 0 | 0 | 0 |
| Teflon rod - 2 | 0 | 0 | 0 | 0 | 0 |
| Teflon rod - 3 | 0 | 0 | 0 | 0 | 0 |

*Note: Dimension pairs refer to microneedle 'tip-angle in degrees'-'length in microns''. The trailing numbers -1,-2 and -3 refer to triplicates for each insertion. Use Table 3.1 to determine the remaining microneedle dimensions and the appropriate groups for 'Length study' and 'Tip angle study'.*

**Table A.1.B.** Triplicate raw VAS pain scores for stage – I of the pain study (Volunteers 6 to 10).

| Skin insertion treatment | Raw VAS pain scores | | | | |
|---|---|---|---|---|---|
| | Subject 6A | Subject 7A | Subject 8A | Subject 9A | Subject 10A |
| 20°- 480μm - 1 | 4 | 0 | 0 | 0 | 0 |
| 20°- 480μm - 2 | 4 | 4 | 0 | 0 | 0 |
| 20°- 480μm - 3 | 3 | 2 | 0 | 0 | 0 |
| 20°- 960μm - 1 | 4 | 12 | 3 | 3 | 0 |
| 20°- 960μm - 2 | 4 | 28 | 6 | 0 | 0 |
| 20°- 960μm - 3 | 0 | 6 | 0 | 0 | 0 |
| 55°- 1450μm - 1 | 10 | 37 | 5 | 14 | 0 |
| 55°- 1450μm - 2 | 4 | 20 | 0 | 6 | 0 |
| 55°- 1450μm - 3 | 0 | 20 | 4 | 10 | 0 |
| 55°- 480μm - 1 | 9 | 0 | 4 | 0 | 0 |
| 55°- 480μm - 2 | 0 | 6 | 0 | 0 | 0 |
| 55°- 480μm - 3 | 3 | 2 | 0 | 0 | 0 |
| 55°- 700μm - 1 | 0 | 0 | 6 | 5 | 0 |
| 55°- 700μm - 2 | 8 | 0 | 0 | 0 | 0 |
| 55°- 700μm - 3 | 10 | 0 | 0 | 5 | 0 |
| 55°- 960μm - 1 | 4 | 0 | 4 | 0 | 0 |
| 55°- 960μm - 2 | 5 | 41 | 0 | 0 | 0 |
| 55°- 960μm - 3 | 12 | 23 | 3 | 5 | 4 |
| 90°- 480μm - 1 | 2 | 4 | 4 | 0 | 0 |
| 90°- 480μm - 2 | 0 | 0 | 0 | 0 | 0 |
| 90°- 480μm - 3 | 0 | 0 | 6 | 0 | 0 |
| 90°- 960μm - 1 | 0 | 7 | 0 | 0 | 0 |
| 90°- 960μm - 2 | 5 | 11 | 3 | 0 | 0 |
| 90°- 960μm - 3 | 10 | 9 | 3 | 0 | 0 |
| Hypodermic - 1 | 35 | 84 | 10 | 15 | 20 |
| Hypodermic - 2 | 72 | 75 | 5 | 28 | 36 |
| Hypodermic - 3 | 52 | 30 | 11 | 35 | 8 |
| Teflon rod - 1 | 0 | 0 | 0 | 0 | 0 |
| Teflon rod - 2 | 0 | 0 | 0 | 0 | 0 |
| Teflon rod - 3 | 0 | 0 | 0 | 0 | 0 |

*Note: Dimension pairs refer to microneedle 'tip-angle in degrees'-'length in microns'. The trailing numbers -1,-2 and -3 refer to triplicates for each insertion. Use Table 3.1 to determine the remaining microneedle dimensions and the appropriate groups for 'Length study' and 'Tip angle study'.*

**Table A.2.A.** Triplicate raw VAS pain scores for stage – II of the pain study (Volunteers 1 to 5).

| Skin insertion treatment | Raw VAS pain scores | | | | |
|---|---|---|---|---|---|
| | Subject 1B | Subject 2B | Subject 3B | Subject 4B | Subject 5B |
| Array 5 - 1 | 2 | 0 | 0 | 2 | 0 |
| Array 5 - 2 | 4 | 0 | 0 | 4 | 12 |
| Array 5 - 3 | 3 | 0 | 0 | 2 | 0 |
| Array 50 - 1 | 3 | 0 | 0 | 2 | 11 |
| Array 50 - 2 | 4 | 0 | 9 | 6 | 15 |
| Array 50 - 3 | 7 | 0 | 0 | 7 | 17 |
| Thick-100μm - 1 | 0 | 3 | 0 | 6 | 14 |
| Thick-100μm - 2 | 3 | 3 | 8 | 39 | 9 |
| Thick-100μm - 3 | 2 | 3 | 22 | 33 | 22 |
| Thick-30μm - 1 | 2 | 4 | 0 | 35 | 40 |
| Thick-30μm - 2 | 3 | 2 | 10 | 5 | 15 |
| Thick-30μm - 3 | 0 | 3 | 28 | 19 | 15 |
| Wide-160μm/Thick-45μm - 1 | 0 | 3 | 17 | 6 | 12 |
| Wide-160μm/Thick-45μm - 2 | 2 | 3 | 0 | 4 | 0 |
| Wide-160μm/Thick-45μm - 3 | 7 | 0 | 12 | 40 | 9 |
| Wide-245μm - 1 | 0 | 3 | 35 | 6 | 27 |
| Wide-245μm - 2 | 3 | 3 | 16 | 4 | 10 |
| Wide-245μm - 3 | 2 | 0 | 6 | 39 | 10 |
| Wide-465μm - 1 | 5 | 4 | 0 | 9 | 0 |
| Wide-465μm - 2 | 2 | 4 | 0 | 0 | 9 |
| Wide-465μm - 3 | 0 | 3 | 19 | 4 | 12 |
| Hypodermic - 1 | 4 | 10 | 34 | 51 | 24 |
| Hypodermic - 2 | 8 | 7 | 21 | 48 | 30 |
| Hypodermic - 3 | 8 | 10 | 11 | 55 | 20 |
| Teflon rod - 1 | 0 | 0 | 0 | 0 | 0 |
| Teflon rod - 2 | 0 | 0 | 0 | 0 | 0 |
| Teflon rod - 3 | 0 | 0 | 0 | 0 | 0 |

*Note: The trailing numbers -1,-2 and -3 refer to triplicates for each insertion. Use Table 3.1 to determine the remaining microneedle dimensions and the appropriate groups for 'Number study', 'Thickness study' and 'Width study'.*

**Table A.2.B.** Triplicate raw VAS pain scores for stage – II of the pain study (Volunteers 6 to 10).

| Skin insertion treatment | Raw VAS pain scores | | | | |
|---|---|---|---|---|---|
| | Subject 6B | Subject 7B | Subject 8B | Subject 9B | Subject 10B |
| Array 5 - 1 | 0 | 4 | 4 | 0 | 0 |
| Array 5 - 2 | 0 | 4 | 6 | 0 | 0 |
| Array 5 - 3 | 8 | 0 | 0 | 0 | 0 |
| Array 50 - 1 | 10 | 7 | 4 | 0 | 11 |
| Array 50 - 2 | 19 | 8 | 6 | 0 | 0 |
| Array 50 - 3 | 6 | 3 | 7 | 0 | 14 |
| Thick-100μm - 1 | 0 | 9 | 6 | 0 | 15 |
| Thick-100μm - 2 | 17 | 16 | 0 | 0 | 36 |
| Thick-100μm - 3 | 12 | 3 | 8 | 6 | 0 |
| Thick-30μm - 1 | 14 | 5 | 7 | 0 | 14 |
| Thick-30μm - 2 | 6 | 0 | 6 | 3 | 15 |
| Thick-30μm - 3 | 0 | 4 | 6 | 0 | 5 |
| Wide-160μm/Thick-45μm - 1 | 0 | 7 | 0 | 5 | 18 |
| Wide-160μm/Thick-45μm - 2 | 16 | 5 | 14 | 0 | 8 |
| Wide-160μm/Thick-45μm - 3 | 0 | 14 | 6 | 0 | 15 |
| Wide-245μm - 1 | 18 | 10 | 6 | 0 | 29 |
| Wide-245μm - 2 | 7 | 9 | 6 | 0 | 19 |
| Wide-245μm - 3 | 0 | 7 | 4 | 4 | 0 |
| Wide-465μm - 1 | 0 | 9 | 8 | 0 | 9 |
| Wide-465μm - 2 | 8 | 5 | 8 | 4 | 14 |
| Wide-465μm - 3 | 9 | 9 | 8 | 0 | 9 |
| Hypodermic - 1 | 26 | 28 | 22 | 6 | 74 |
| Hypodermic - 2 | 27 | 20 | 16 | 11 | 58 |
| Hypodermic - 3 | 31 | 29 | 8 | 0 | 15 |
| Teflon rod - 1 | 0 | 0 | 0 | 0 | 0 |
| Teflon rod - 2 | 0 | 0 | 0 | 0 | 0 |
| Teflon rod - 3 | 0 | 0 | 0 | 0 | 0 |

*Note: The trailing numbers -1,-2 and -3 refer to triplicates for each insertion. Use Table 3.1 to determine the remaining microneedle dimensions and the appropriate groups for 'Number study', 'Thickness study' and 'Width study'.*

**Table A.3.** Typical calculation to determine mean normalized pain scores.

| | Subject 1A | | |
|---|---|---|---|
| **'Length study' group in triplicates** | **Raw VAS pain score** | **Mean of triplicates** | **Normalized pain score** |
| **55°- 480μm - 1** | 0 | | |
| **55°- 480μm - 2** | 0 | | |
| **55°- 480μm - 3** | 0 | 0.0 | 0.0 |
| **55°- 700μm - 1** | 0 | | |
| **55°- 700μm - 2** | 0 | | |
| **55°- 700μm - 3** | 0 | 0.0 | 0.0 |
| **55°- 960μm - 1** | 6 | | |
| **55°- 960μm - 2** | 4 | | |
| **55°- 960μm - 3** | 2 | *Eg. (6+4+2)/3 = 4.0* | *Eg. (4/7.3 x 100) = 54.8* |
| **55°- 1450μm - 1** | 4 | | |
| **55°- 1450μm - 2** | 8 | | |
| **55°- 1450μm - 3** | 4 | 5.3 | 72.7 |
| **Hypodermic - 1** | 6 | | |
| **Hypodermic - 2** | 7 | | |
| **Hypodermic - 3** | 9 | 7.3 | 100.0 |
| **Teflon rod - 1** | 0 | | |
| **Teflon rod - 2** | 0 | | |
| **Teflon rod - 3** | 0 | 0.0 | 0.0 |

**Table A.4.** Raw and normalized pain scores for 'Length study' group.

*Rounded off to the nearest integer*

| | 55°- 480μm | | 55°- 700μm | | 55°- 960μm | | 55°- 1450μm | | Hypodermic | | Teflon rod | |
|---|---|---|---|---|---|---|---|---|---|---|---|---|
| **Subjects** | Raw VAS pain score | Normalized VAS pain score | Raw VAS pain score | Normalized VAS pain score | Raw VAS pain score | Normalized VAS pain score | Raw VAS pain score | Normalized VAS pain score | Raw VAS pain score | Normalized VAS pain score | Raw VAS pain score | Normalized VAS pain score |
| Subject 1A | 0 | 0 | 0 | 0 | 4 | 55 | 5 | 73 | 7 | 100 | 0 | 0 |
| Subject 2A | 6 | 10 | 15 | 25 | 28 | 47 | 45 | 76 | 59 | 100 | 0 | 0 |
| Subject 3A | 3 | 6 | 5 | 9 | 6 | 10 | 12 | 22 | 56 | 100 | 0 | 0 |
| Subject 4A | 3 | 5 | 8 | 14 | 20 | 36 | 42 | 77 | 55 | 100 | 0 | 0 |
| Subject 5A | 1 | 4 | 2 | 6 | 11 | 29 | 1 | 3 | 37 | 100 | 0 | 0 |
| Subject 6A | 4 | 8 | 6 | 11 | 7 | 13 | 5 | 9 | 53 | 100 | 0 | 0 |
| Subject 7A | 3 | 4 | 0 | 0 | 21 | 34 | 26 | 41 | 63 | 100 | 0 | 0 |
| Subject 8A | 1 | 15 | 2 | 23 | 2 | 27 | 3 | 35 | 9 | 100 | 0 | 0 |
| Subject 9A | 0 | 0 | 3 | 13 | 2 | 6 | 10 | 38 | 26 | 100 | 0 | 0 |
| Subject 10A | 0 | 0 | 0 | 0 | 1 | 6 | 0 | 0 | 21 | 100 | 0 | 0 |

# APPENDIX B: ELECTROPOLISHING PROTOCOL AND APPARATUS

Laser-cut microneedles were electropolished to remove slag and to sharpen the tips. The electropolishing apparatus for this purpose was designed and built in the laboratory, and the complete apparatus is shown in Figure B.1.

## Electropolishing protocol

Briefly, the protocol to electropolish an out-of-plane microneedle array is:

1. Fill 250 ml of electropolishing solution in a 300 ml glass beaker by adding 150 ml glycerine, 25 ml DI water and filling with phosphoric acid up to the 250 ml mark.
2. Place the beaker on the hot plate with the thermocouple dipped into the electropolishing solution and program the hot plate to heat the electropolishing solution temperature to 70 °C (Figure B.2)
3. Place the copper cathode holder (Figure B.3 A) into the beaker by resting the cathode holder on the rails and screwing it in place (Figure B.2 and B.5).
4. Clean the stainless steel sheet containing the laser-cut microneedles with powdered soap and water.
5. Bend the microneedles out of the plane of the stainless steel sheet.
6. Trim extra metal surrounding the arrays.
7. Clamp the edge of the stainless steel sheet to the screw-and-plate clamp of the microneedle array holder as shown in Figure B.3 B and B.4.
8. Place the microneedle array holder in the beaker filled with electropolishing solution, let the holder surface rest onto the rails as shown in Figure B.5, and withdraw the holder out. Measure the length and width of the stainless steel sheet wetted by the solution.

9. Find the wetted area by multiplying the wetted length and width in $mm^2$. The current density required for electropolishing is 1.8 $mA/mm^2$. Multiply the current density and the wetted area to determine the constant current required for electropolishing.
10. Now place the microneedle array holder back into the beaker by letting its surface to rest on the rails. Attach the threaded connection between the microneedle array holder and the linear oscillator as shown in Figure B.5. Once both the cathode holder and the microneedle array holder are placed securely on the rails, they will be in close proximity as shown in Figure B.4.
11. Start the linear oscillator by turning the power on to the power supply for linear oscillator (Figure B.1).
12. Attach the positive lead of the electropolishing power supply (Figure B.1) to the microneedle array holder lead, and the negative lead to the cathode holder lead.
13. Turn on the power supply for electropolishing and match the ammeter current reading to the current value required from step 9.
14. Perform electropolishing for 15 min.
15. Stop all power supplies, remove the microneedle array holder from the beaker and the rails, wash the microneedles thrice alternatively in 25% nitric acid and DI water stored in beakers, wash the microneedles under running hot water and DI water, dry the microneedles with pressurized air or nitrogen and store in air-tight containers.
16. Repeat electropolishing for other arrays if required. A 250 ml beaker of electropolishing solution once prepared is good for electropolishing 4-5 stainless steel sheets, each containing two arrays of microneedles.

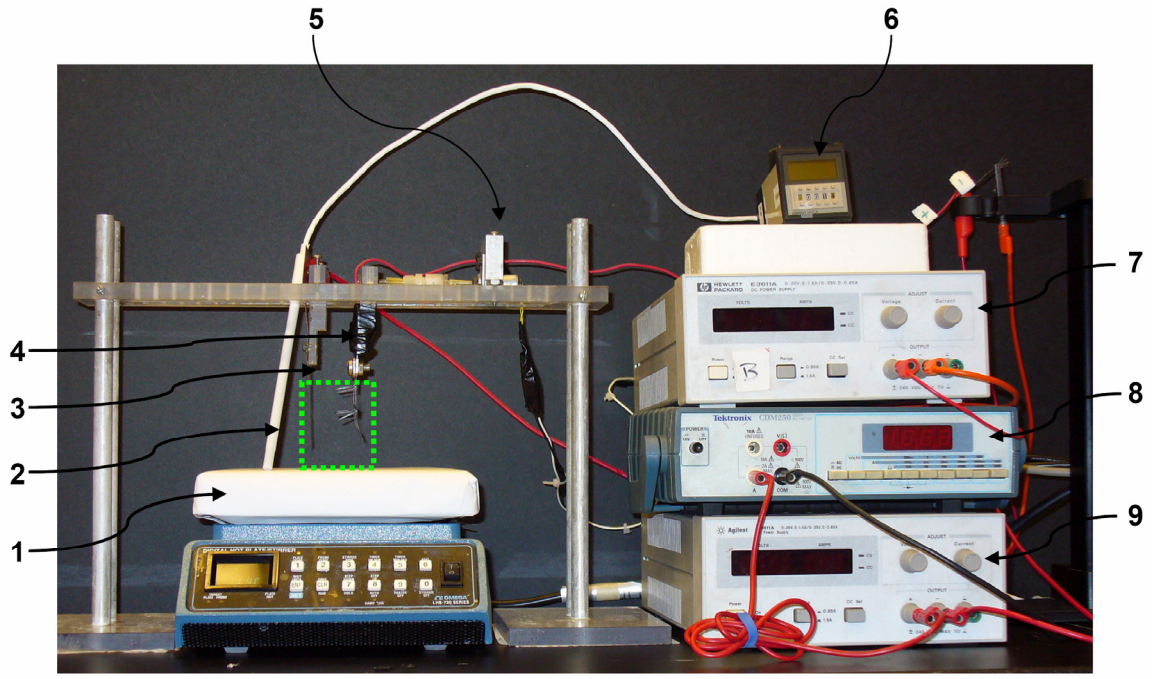


1. Hot plate
2. Thermocouple
3. Copper cathode holder (- ve)
4. Microneedle array holder (+ ve)
5. Linear oscillator
6. Frequency timer for oscillator
7. Power supply for oscillator
8. Multimeter
9. Constant current power supply for electropolising

**Figure B.1. Electropolishing apparatus**. Photograph of the electropolishing apparatus showing all the components required for electropolishing. The beaker with the electropolishing solution is not shown but its expected location is marked with the dotted rectangle. Refer Figure B.2 for a close-up photograph of the beaker on the hot-plate.

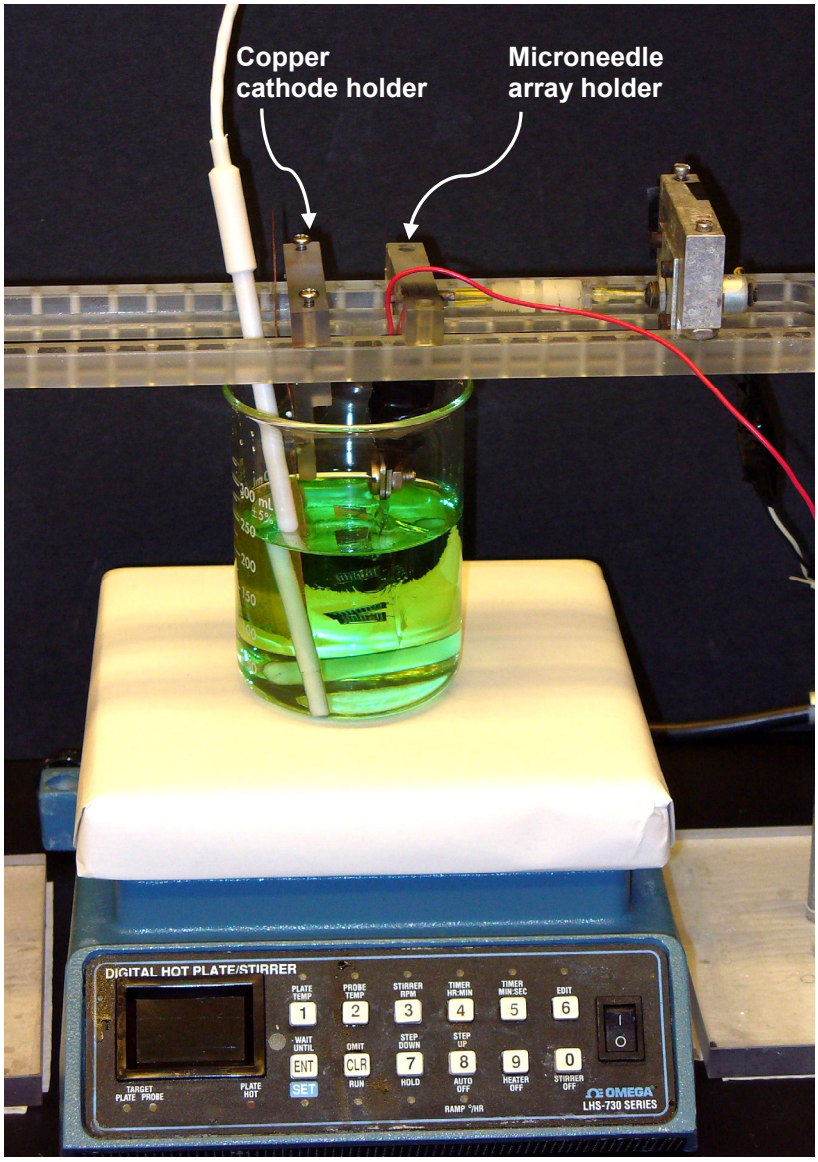


**Figure B.2. Electropolishing beaker on the hot plate**. Photograph of the glass beaker containing electropolishing solution and resting on the hot plate. Thermocouple, cathode holder and the microneedle holder are shown resting on the rails and immersed in the electropolishing solution. The electropolishing solution is initially colorless and starts turning green after electropolishing is performed.

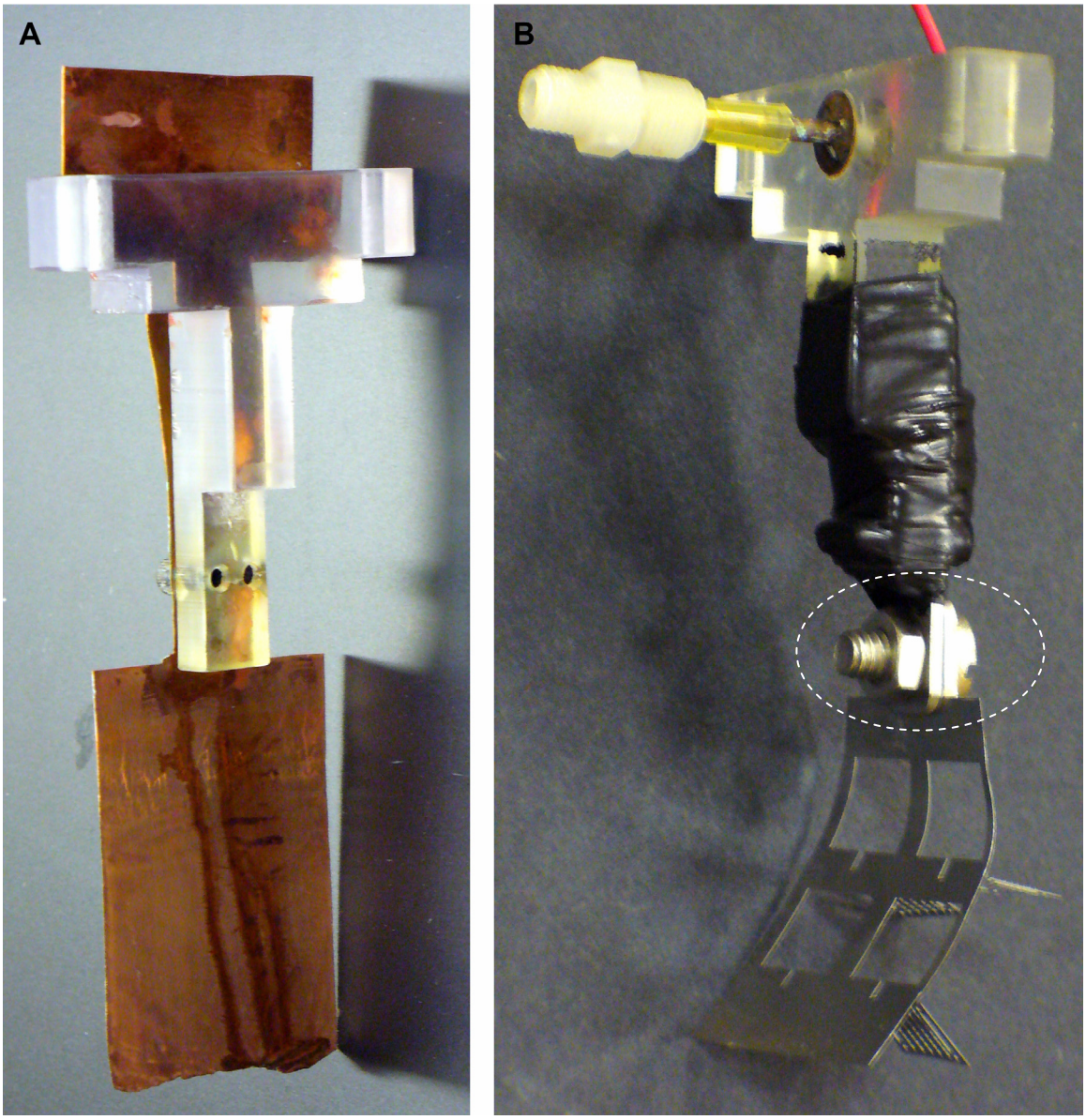


**Figure B.3. Cathode and microneedle holders**. Photographs of (A) cathode holder and (B) microneedle holder. Dotted ellipse is shown surrounding the screw-and-plate clamp.

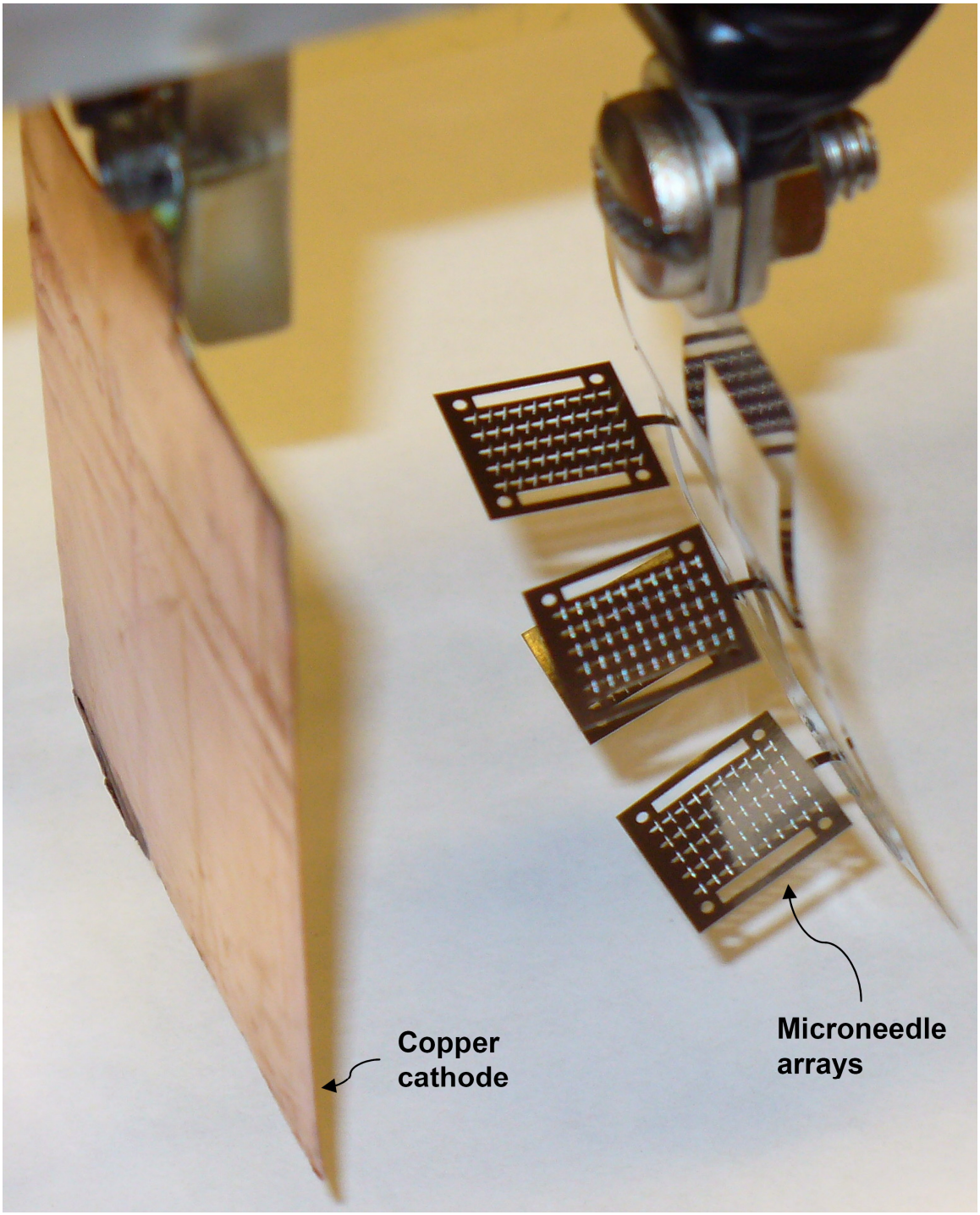


**Figure B.4. Orientation of microneedle arrays in the holder**. Photograph showing the proper orientation of microneedle arrays after clamping to the microneedle-array holder. Microneedle arrays face the copper cathode and the arrays are bent at their flexible joint with the stainless steel sheet such that the microneedles point up.

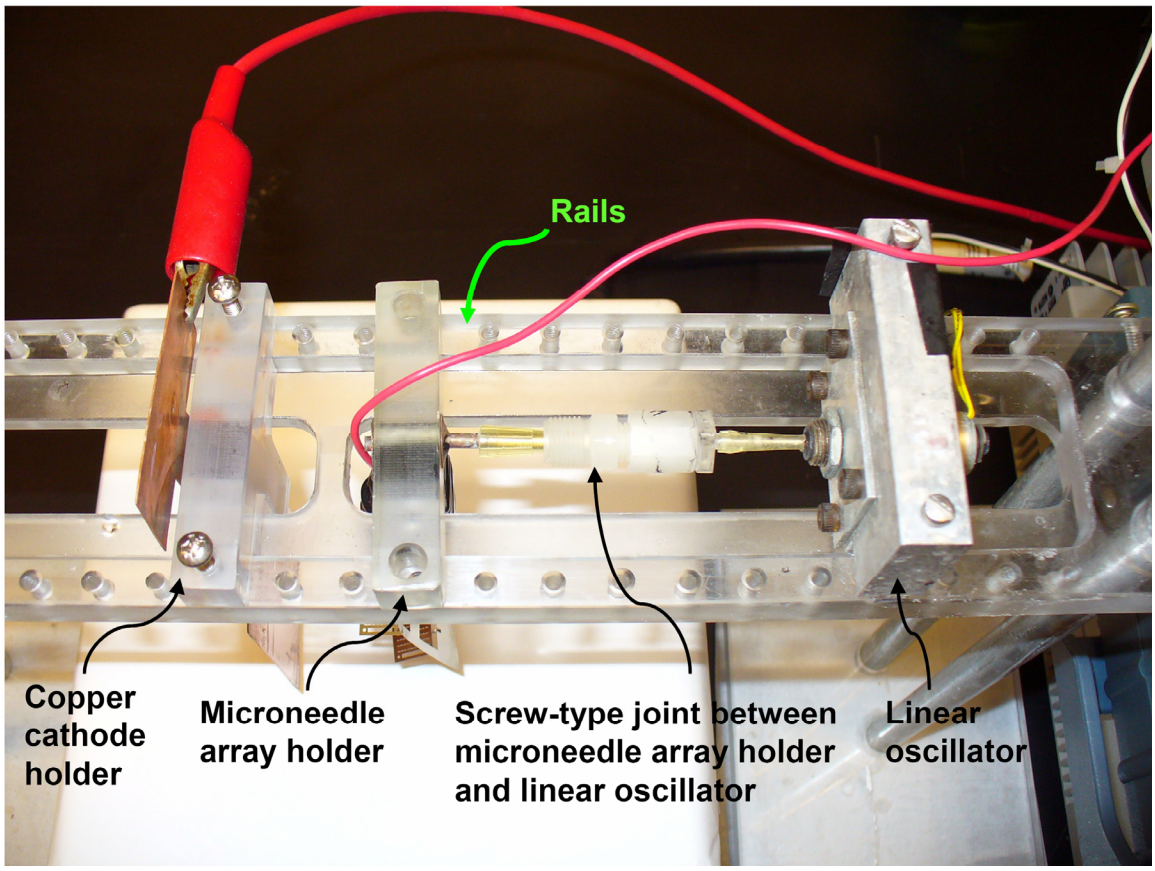


**Figure B.5. Joint between microneedle array holder and linear oscillator**. Top view of the rails showing the cathode holder and the microneedle holder resting on the rails; and the screw joint between the microneedle holder and the linear oscillator.

# APPENDIX C: DIP-COATING DEVICES

Novel dip-coating devices were designed and fabricated to form uniform and spatially controlled coatings on microneedles. Three different dip-coating devices were fabricated, the first to coat single microneedles (Figure C.1), the second to coat in-plane rows of microneedles (Figure C.2) and the third to coat out-of-plane microneedles arrays (Figure C.3).

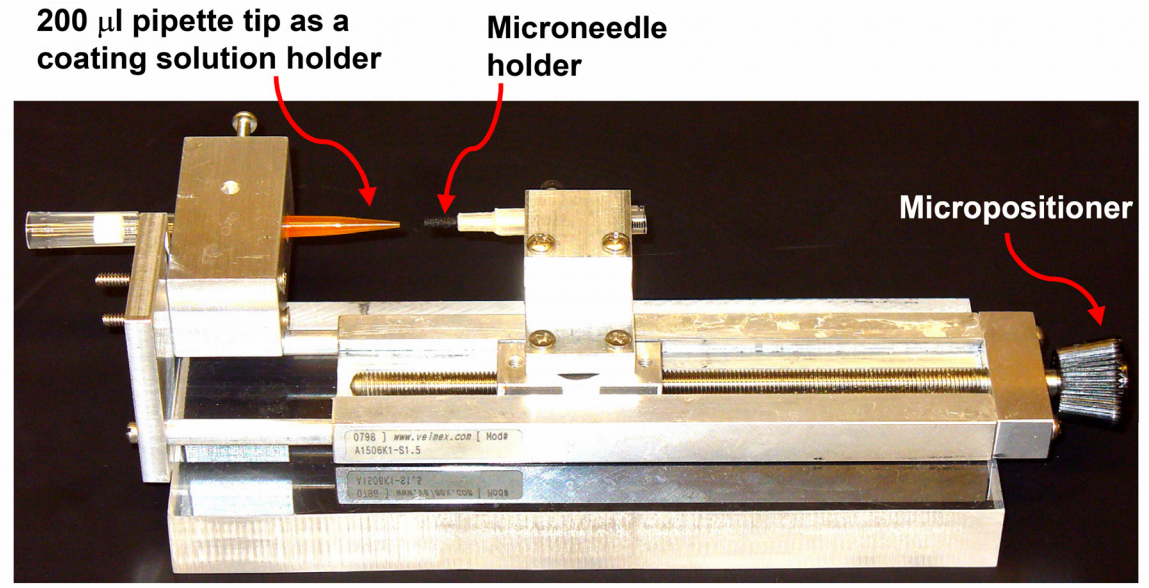


**Figure C.1. Dip-coating device to coat single microneedles.** Photograph of a dip-coating device to form coatings on single microneedles. A single microneedle is held on the sticky end of the cylindrical microneedle holder. The sticky end is formed by wrapping a double sided adhesive tape on one end of the cylindrical holder. At the opposite end of the device, a pipette tip filled with the coating solution is secured. The microneedle is then dipped in and out of the pipette tip while visually monitoring the movement under a stereomicroscope. Micron-scale control in the movement is achieved by the use of a micropositioner on which the microneedle holder is mounted.

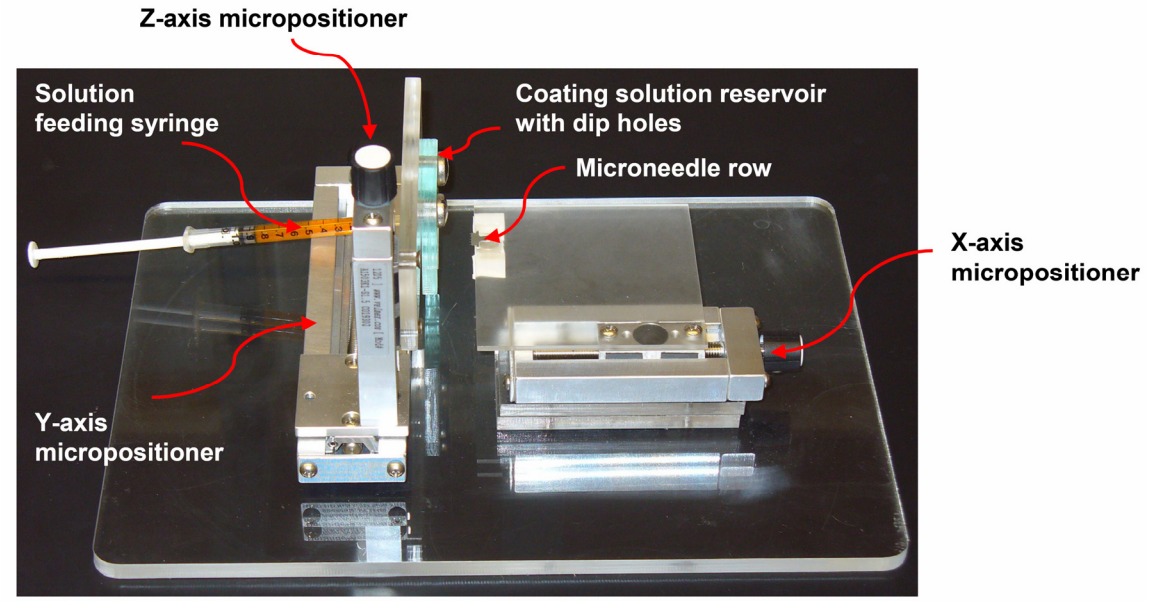


**Figure C.2. Dip-coating device to coat in-plane rows of microneedles**. Photograph of a dip-coating device to coat in-plane rows. A row of microneedles is placed in a grove in the acrylic sheet and held in place with the aid of a tiny magnet located on the underside of the sheet. A 1-ml syringe is filled with the coating solution and attached to the dip-coating device to fill the coating solution reservoir. X, Y and Z micropositioners are next used to align the microneedles in the in-plane row to the dip holes in the coating reservoir. After alignment is achieved, the microneedle row is dipped in and out of the dip holes using the X-axis micropositioner. The coating is monitored by performing it under a stereomicroscope.

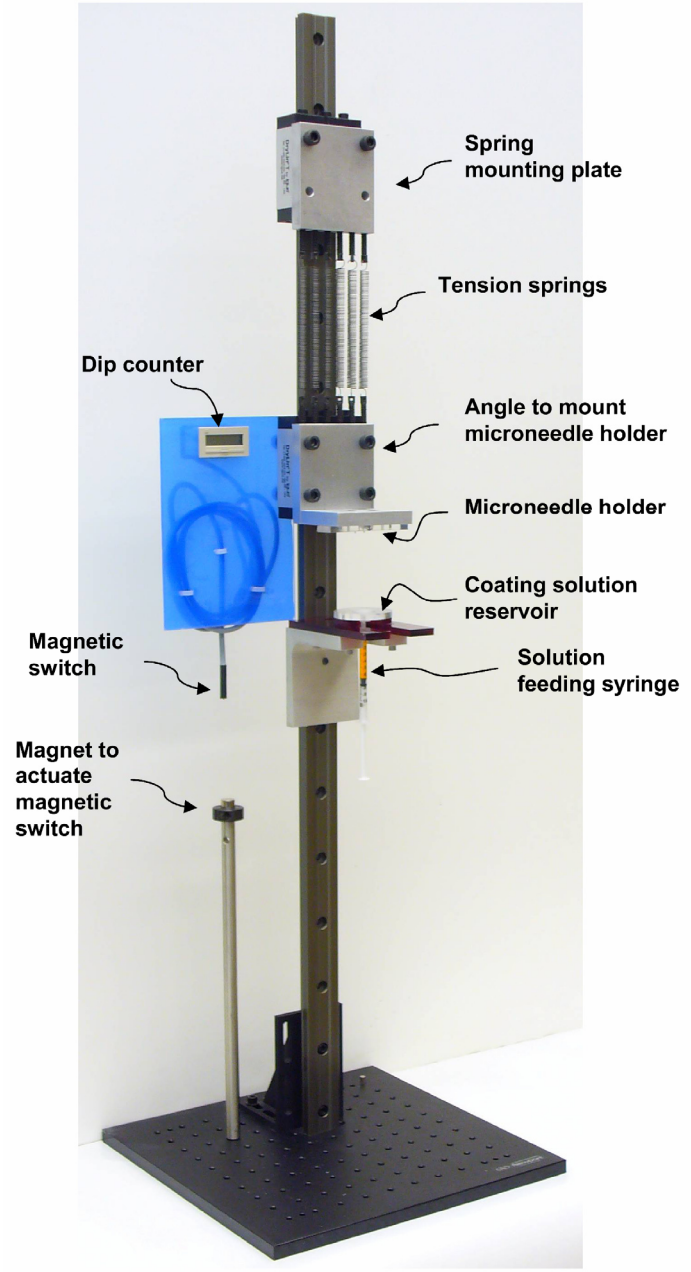


**Figure C.3 Dip-coating device to coat out-of-plane microneedle array** . Photograph of a dip-coating device to coat out-of-plane arrays. Dip holes and the microneedle array holder are pre-aligned. A 1ml syringe is filled with the coating solution and attached to the coating solution reservoir to fill the reservoir. A microneedle array is placed on the microneedle holder where a magnet helps to keep the array secure. The angle plate on which the microneedle holder is mounted is then pulled down to dip the microneedles into the dip holes. Upon release of pressure to the angle plate, it moves up due to tension of the springs. The motion is repeated if multiple dips are required. The dip counter gets actuated each time the angle plate moves down because the magnetic switch gets actuated in the presence of the magnetic field generated by the magnet attached to the small cylindrical post fixed on the bread-board. This allows keeping track of the number of dips of the array.

# REFERENCES


Draft Guidance for Industry on Powder Blends and Finished Dosage Units - Stratified In-Process Dosage Unit Sampling and Assessment, Docket No. 2003D-0493, Federal Drug Adminstration, Rockville, MD, 2003.

(2006). "Centers for Disease Control and Prevention. General recommendations on immunization." MMWR **55 (No. RR-15)**.

Alarcon, J. B., A. W. Hartley, et al. (2007). "Preclinical Evaluation of Microneedle Technology for Intradermal Delivery of Influenza Vaccines." Clin. Vaccine Immunol. **14**(4): 375-381.

Ansel, H. C., L. V. Allen, Jr., et al. (1999). Pharmaceutical Dosage Forms and Drug Delivery Systems, Lippincott Williams & Wilkins Publishers.

Arendt-Nielsen, L., H. Egekvist, et al. (2006). "Pain following controlled cutaneous insertion of needles with different diameters." Somatosens Mot Res **23**(1-2): 37-43.

Babiuk, S., M. Baca-Estrada, et al. (2000). "Cutaneous vaccination: the skin as an immunologically active tissue and the challenge of antigen delivery." J Control Release **66**(2-3): 199-214.

Banga, A. K. and M. R. Prausnitz (1998). "Assessing the potential of skin electroporation for the delivery of protein- and gene-based drugs." Trends Biotechnol **16**(10): 408-412.

Barry, B. W. (2004). "Breaching the skin's barrier to drugs." Nat Biotech **22**(2): 165-167.

Beebe, D. J., G. A. Mensing, et al. (2002). "Physics and applications of microfluidics in biology." Annu Rev Biomed Eng **4**(1): 261-286.

Bierwagen, G. P. (1992). "Film coating technologies and adhesion." Electrochim Acta **37**(9): 1471-1478.

Birchall, J., S. Coulman, et al. (2006). "Cutaneous gene expression of plasmid DNA in excised human skin following delivery via microchannels created by radio frequency ablation." Int J Pharm **312**(1-2): 15-23.

Birchall, J., S. Coulman, et al. (2005). "Cutaneous DNA delivery and gene expression in ex vivo human skin explants via wet-etch micro-fabricated micro-needles." J Drug Target **13**(7): 415-421.

Blake, T. D. and K. J. Ruschak (1997). Wetting: static and dynamic contact lines. Liquid Film Coating : Scientific Principles and Their Technological Implications. S. F. Kistler and P. M. Schweizer. London, Chapman and Hall**:** 63-97.

Bos, J. D. (2005). Skin Immune System: Cutaneous Immunology and Clinical Immunodermatology. Boca Raton, Florida, CRC Press.

Braverman, I. M. (1997). "The cutaneous microcirculation: ultrastructure and microanatomical organization." Microcirculation **4**(3): 329-340.

Braverman, I. M. (2000). "The cutaneous microcirculation." J Investig Dermatol Symp Proc **5**(1): 3-9.

Center for Drug Evaluation and Research (2007). Electronic orange book data files, FDA.

Cevc, G. and U. Vierl (2007). "Spatial distribution of cutaneous microvasculature and local drug clearance after drug application on the skin." J Control Release **118**(1): 18-26.

Chabri, F., K. Bouris, et al. (2004). "Microfabricated silicon microneedles for nonviral cutaneous gene delivery." Br J Dermatol **150**(5): 869-877.

Cheboyina, S., J. O'Haver, et al. (2006). "A mathematical model to predict the size of the pellets formed in freeze pelletization techniques: parameters affecting pellet size." J Pharm Sci **95**(1): 167-180.

Chisari, F. V. (1997). "Cytotoxic T Cells and Viral Hepatitis." J Clin Invest **99**(7): 1472-1477.

Cormier, M., B. Johnson, et al. (2004). "Transdermal delivery of desmopressin using a coated microneedle array patch system." J Control Release **97**(3): 503-511.

Datta, M., L. F. Vega, et al. (1992). "Mass transport effects during electropolishing of iron in phosphoric-sulfuric acid." Electrochim Acta **37**(13): 2469-2475.

Davis, S. P., B. J. Landis, et al. (2004). "Insertion of microneedles into skin: measurement and prediction of insertion force and needle fracture force." J Biomech **37**(8): 1155-1163.

Davis, S. P., W. Martanto, et al. (2005). "Hollow metal microneedles for insulin delivery to diabetic rats." IEEE Trans Biomed Eng **52**(5): 909-915.

Deacon, B. and J. Abramowitz (2006). "Fear of needles and vasovagal reactions among phlebotomy patients." J Anxiety Disord **20**(7): 946-960.

Dean, C. H., J. B. Alarcon, et al. (2005). "Cutaneous Delivery of a Live, Attenuated Chimeric Flavivirus Vaccines against Japanese Encephalitis (ChimeriVaxTM-JE) in Non-Human Primates." Hum Vaccin **1**(3): 106-111.

Degim, I. T. and N. Celebi (2007). "Controlled delivery of peptides and proteins." Curr Pharm Design **13**(1): 99-117.

Dexter, F. and D. H. Chestnut (1995). "Analysis of statistical tests to compare visual analog scale measurements among groups." Anesthesiology **82**(4): 896-902.

Donnelly, J., K. Berry, et al. (2003). "Technical and regulatory hurdles for DNA vaccines." Int J Parasitol **33**(5-6): 457-467.

Egekvist, H., P. Bjerring, et al. (1999a). "Pain and mechanical injury of human skin following needle insertions." Eur J Pain **3**(1): 41-49.

Egekvist, H., P. Bjerring, et al. (1999b). "Regional variations in pain to controlled mechanical skin traumas from automatic needle insertions and relations to ultrasonography." Skin Res Technol **5**(4): 247-254.

Encke, J., J. zu Putlitz, et al. (1998). "Genetic immunization generates cellular and humoral immune responses against the nonstructural proteins of the hepatitis C virus in a murine model." J Immunol **161**(9): 4917-4923.

Fang, J.-Y., W.-R. Lee, et al. (2004a). "Transdermal delivery of macromolecules by erbium:YAG laser." J Control Release **100**(1): 75-85.

Fang, J. Y., W. R. Lee, et al. (2004b). "Enhancement of topical 5-aminolaevulinic acid delivery by erbium:YAG laser and microdermabrasion: a comparison with iontophoresis and electroporation." Br J Dermatol **151**(1): 132-140.

Freedman, B. M., E. Rueda-Pedraza, et al. (2001). "The epidermal and dermal changes associated with microdermabrasion." Dermatol Surg **27**(12): 1031-1033; discussion 1033-1034.

Frelin, L., G. Ahlen, et al. (2004). "Codon optimization and mRNA amplification effectively enhances the immunogenicity of the hepatitis C virus nonstructural 3/4A gene." Gene Ther **11**(6): 522-533.

Frelin, L., M. Alheim, et al. (2003). "Low dose and gene gun immunization with a hepatitis C virus nonstructural (NS) 3 DNA-based vaccine containing NS4A inhibit NS3/4A-expressing tumors in vivo." Gene Ther **10**(8): 686-699.

Fruhstorfer, H., T. Müller, et al. (1995). "Capillary blood sampling: How much pain is necessary?. Part 2: Relation between penetration depth and puncture pain." Pract Diabetes Int **12**(4): 184-185.

Fruhstorfer, H., G. Schmelzeisen-Redeker, et al. (1999). "Capillary blood sampling: relation between lancet diameter, lancing pain and blood volume." Eur J Pain **3**(3): 283-286.

Fujimoto, T., K. Shirakami, et al. (2005). "Effect of microdermabrasion on barrier capacity of stratum corneum." Chem Pharm Bull (Tokyo) **53**(8): 1014-1016.

Fuller, D. H., P. Loudon, et al. (2006). "Preclinical and clinical progress of particle-mediated DNA vaccines for infectious diseases." Methods **40**(1): 86-97.

Gardeniers, H. J. G. E., R. Luttge, et al. (2003). "Silicon micromachined hollow microneedles for transdermal liquid transport." J MEMS **12**(6): 855-862.

Garmory, H. S., S. D. Perkins, et al. (2005). "DNA vaccines for biodefence." Adv Drug Deliver Rev **57**(9): 1343-1361.

Gill, H. S. and M. R. Prausnitz (2007a). "Coated microneedles for transdermal delivery." J Control Release **117**(2): 227-237. [6]

Gill, H. S. and M. R. Prausnitz (2007b). "Coating formulations for microneedles." Pharm Res **24**(7): 1369-1380.[7]

Graham, B. S., R. A. Koup, et al. (2006). "Phase 1 Safety and Immunogenicity Evaluation of a Multiclade HIV-1 DNA Candidate Vaccine." J Infect Dis **194**(12): 1650-1660.

[6] This journal publication is based on the study described in Chapter 4 of this thesis.
[7] This journal publication is based on the study described in Chapter 5 of this thesis.

Greenland, J. R. and N. L. Letvin (2007). "Chemical adjuvants for plasmid DNA vaccines." Vaccine **25**(19): 3731-3741.

Gupta, S. and B. Kumar (2000). "Suction blister induction time: 15 minutes or 150 minutes?" Dermatol Surg **26**(8): 754-756.

Hahn, T. S. and A. R. Marder (1988). "Effect of electropolishing variables on the current density-voltage relationship." Metallography **21**(4): 365-375.

Hamilton, J. G. (1995). "Needle phobia: a neglected diagnosis." J Fam Pract **41**(2): 169-175.

Hanas, R. (2004). "Reducing injection pain in children and adolescents with diabetes: a review of indwelling catheters." Pediatr Diabetes **5**(2): 102-111.

Hanas, R., L. Lytzen, et al. (2000). "Thinner needles do not influence injection pain, insulin leakage or bleeding in children and adolescents with type 1 diabetes." Pediatr Diabetes **1**(3): 142-149.

Harrop, R., M. G. Ryan, et al. (2004). Monitoring of human immunological responses to vaccinia virus. Methods in Molecular Biology - Vaccinia Virus and Poxvirology: Methods and Protocols. S. N. Isaccs. Clifton, New Jersey, USA, Humana Press. **269:** 243-266.

Hauri, A., G. Armstrong, et al. (2004). "The global burden of disease attributable to contaminated injections given in health care settings." Int J STD AIDS **15**(1): 7-16.

Henry, S., D. V. McAllister, et al. (1998). "Microfabricated microneedles: a novel approach to transdermal drug delivery." J Pharm Sci **87**(8): 922-925.

Herndon, T. O., S. Gonzalez, et al. (2004). "Transdermal microconduits by microscission for drug delivery and sample acquisition." BMC Med **2**: 12.

Ito, Y., E. Hagiwara, et al. (2006). "Feasibility of microneedles for percutaneous absorption of insulin." Eur J Pharm Sci **29**(1): 82-88.

Ito, Y., J. Yoshimitsu, et al. (2006). "Self-dissolving microneedles for the percutaneous absorption of EPO in mice." J Drug Target **14**(5): 255-261.

Jiang, J., H. Gill, et al. "Coated microneedles for drug delivery to the eye." Invest Ophthalmol Vis Sci in press.

Kane, A., J. Lloyd, et al. "Transmission of hepatitis B, hepatitis C and human immunodeficiency viruses through unsafe injections in the developing world: model-based regional estimates." B WHO **77**(10): 801-807.

Karande, P., A. Jain, et al. (2005). "Design principles of chemical penetration enhancers for transdermal drug delivery." Proc Natl Acad Sci U S A **102**(13): 4688-4693.

Karimipour, D. J., S. Kang, et al. (2005). "Microdermabrasion: a molecular analysis following a single treatment." J Am Acad Dermatol **52**(2): 215-223.

Kaushik, S., A. H. Hord, et al. (2001). "Lack of pain associated with microfabricated microneedles." Anesth Analg **92**(2): 502-504.

Kettwich, S. C., W. L. Sibbitt, Jr., et al. (2007). "Needle phobia and stress-reducing medical devices in pediatric and adult chemotherapy patients." J Pediatr Oncol Nurs **24**(1): 20-28.

Kheshgi, H. S. (1997). The fate of thin liquid films after coating. Liquid Film Coating : Scientific Principles and Their Technological Implications. S. F. Kistler and P. M. Schweizer. London, Chapman & Hall**:** 183-672.

Kibbe, A. H., Ed. (2000). Handbook of Pharmaceutical Excipients. Washington, D.C., American Pharmaceutical Association.

Landolt, D. (1987). "Fundamental aspects of electropolishing." Electrochimica Acta **32**(1): 1-11.

Lee, W.-R., S.-C. Shen, et al. (2003). "Lasers and microdermabrasion enhance and control topical delivery of vitamin C." J Invest Dermatol **121**(5): 1118-1125.

Leuner, C. and J. Dressman (2000). "Improving drug solubility for oral delivery using solid dispersions." Eur J Pharm and Biopharm **50**(1): 47-60.

Lide, D. R. (2006). CRC Handbook of Chemistry and Physics, 87th edition, CRC Press.

Lin, W., M. Cormier, et al. (2001). "Transdermal delivery of antisense oligonucleotides with microprojection patch (Macroflux) technology." Pharm Res **18**(12): 1789-1793.

Luckay, A., M. K. Sidhu, et al. (2007). "Effect of Plasmid DNA Vaccine Design and In Vivo Electroporation on the Resulting Vaccine-Specific Immune Responses in Rhesus Macaques." J. Virol. **81**(10): 5257-5269.

Martanto, W., S. M. Baisch, et al. (2005). "Fluid dynamics in conically tapered microneedles." AIChE Journal **51**(6): 1599-1607.

Martanto, W., S. P. Davis, et al. (2004). "Transdermal delivery of insulin using microneedles in vivo." Pharm Res **21**(6): 947-952.

Martanto, W., J. S. Moore, et al. (2006a). "Mechanism of fluid infusion during microneedle insertion and retraction." J Control Release.

Martanto, W., J. S. Moore, et al. (2006b). "Microinfusion using hollow microneedles." Pharm Res **23**(1): 104-113.

Matriano, J. A., M. Cormier, et al. (2002). "Macroflux microprojection array patch technology: a new and efficient approach for intracutaneous immunization." Pharm Res **19**(1): 63-70.

McAllister, D. V., P. M. Wang, et al. (2003). "Microfabricated needles for transdermal delivery of macromolecules and nanoparticles: fabrication methods and transport studies." Proc Natl Acad Sci U S A **100**(24): 13755-13760.

Mikszta, J. (2003). "Cutaneous or mucosal delivery of anthrax rPA provides protection against inhalational anthrax. Innovative Adminstration Systems for Vaccines Meeting, Rockville, MD." Retrieved July 9, 2007, from: http://www.hhs.gov/nvpo/meetings/dec2003/Contents/ThursdayAM/Mikszta/Mikszta.pdf.

Mikszta, J. A., J. B. Alarcon, et al. (2002). "Improved genetic immunization via micromechanical disruption of skin-barrier function and targeted epidermal delivery." Nat Med **8**(4): 415-419.

Mikszta, J. A., V. J. Sullivan, et al. (2005). "Protective immunization against inhalational anthrax: a comparison of minimally invasive delivery platforms." J Infect Dis **191**(2): 278-288.

Mitragotri, S. and J. Kost (2004). "Low-frequency sonophoresis: a review." Adv Drug Deliv Rev **56**(5): 589-601.

Miyano, T., Y. Tobinaga, et al. (2005). "Sugar micro needles as transdermic drug delivery system." Biomed Microdevices **7**(3): 185-188.

Naik, A., Y. N. Kalia, et al. (2000). "Transdermal drug delivery: overcoming the skin’s barrier function." Pharm Sci Technol To **3**(9): 318-326.

Nair, V., O. Pillai, et al. (1999). "Transdermal iontophoresis. Part I: Basic principles and considerations." Methods Find Exp Clin Pharmacol **21**(2): 139-151.

Neter, J., M. H. Kutner, et al. (1996). Applied Linear Statistical Models. Homewood, IL, McGraw Hill/Irwin.

Nir, Y., A. Paz, et al. (2003). "Fear of injections in young adults: prevalence and associations." Am J Trop Med Hyg **68**(3): 341-344.

Oaklander, A. L. and S. M. Siegel (2005). "Cutaneous innervation: Form and function." J Am Acad Dermatol **53**(6): 1027-1037.

Orive, G., R. M. Hernandez, et al. (2003). "Drug delivery in biotechnology: present and future." Curr Opin Biotechnol **14**(6): 659-664.

Park, J. H., M. G. Allen, et al. (2005). "Biodegradable polymer microneedles: fabrication, mechanics and transdermal drug delivery." J Control Release **104**(1): 51-66.

Park, J. H., M. G. Allen, et al. (2006). "Polymer microneedles for controlled-release drug delivery." Pharm Res **23**(5): 1008-1019.

Partidos, C. D., A. S. Beignon, et al. (2002). "Applying peptide antigens onto bare skin: induction of humoral and cellular immune responses and potential for vaccination." J Control Release **85**(1-3): 27-34.

Partidos, C. D., A. S. Beignon, et al. (2003). "Immunity under the skin: potential application for topical delivery of vaccines." Vaccine **21**(7-8): 776-780.

Peachman, K. K., M. Rao, et al. (2003). "Immunization with DNA through the skin." Methods **31**(3): 232-242.

Pillai, O., V. Nair, et al. (1999). "Transdermal iontophoresis. Part II: Peptide and protein delivery." Methods Find Exp Clin Pharmacol **21**(3): 229-240.

Prausnitz, M., J. Mikszta, et al. (2005). Microneedles. Percutaneous Penetration Enhancers. E. W. Smith and H. I. Maibach, CRC Press, Boca Raton, FL**:** 239-255.

Prausnitz, M. R. (1999). "A practical assessment of transdermal drug delivery by skin electroporation." Adv Drug Deliv Rev **35**(1): 61-76.

Prausnitz, M. R. (2004). "Microneedles for transdermal drug delivery." Adv Drug Deliv Rev **56**(5): 581-587.

Prausnitz, M. R., E. R. Edelman, et al. (1995). "Transdermal delivery of heparin by skin electroporation." Biotechnology (N Y) **13**(11): 1205-1209.

Prausnitz, M. R., S. Mitragotri, et al. (2004). "Current status and future potential of transdermal drug delivery." Nat Rev Drug Discov **3**(2): 115-124.

Pruss-Ustun, A., E. Rapiti, et al. (2005). "Estimation of the global burden of disease attributable to contaminated sharps injuries among health-care workers." Am J Ind Med **48**: 482-490.

Rajan, P. and P. E. Grimes (2002). "Skin barrier changes induced by aluminum oxide and sodium chloride microdermabrasion." Dermatol Surg **28**(5): 390-393.

Raval, A., A. Choubey, et al. (2004). "Development and assessment of 316LVM cardiovascular stents." Mat Sci Eng A **386**(1-2): 331-343.

Reed, M. L. and W.-K. Lyev (2004). "Microsystems for drug and gene delivery." Proc IEEE **92**(1): 56-75.

Roy, M. J., M. S. Wu, et al. (2000). "Induction of antigen-specific CD8+ T cells, T helper cells, and protective levels of antibody in humans by particle-mediated administration of a hepatitis B virus DNA vaccine." Vaccine **19**(7-8): 764-778.

Schaefer, H. and T. Redelmeier (1996). Skin barrier: principles of percutaneous absorption, Karger AG, Switzerland,1996.

Schramm, J. and S. Mitragotri (2002). "Transdermal drug delivery by jet injectors: energetics of jet formation and penetration." Pharm Res **19**(11): 1673-1679.

Schunk, P. R., A. J. Hurd, et al. (1997). Free-meniscus coating processes. Liquid film coating : scientific principles and their technological implications S. F. Kistler and P. M. Schweizer, London : Chapman & Hall**:** 673-708.

Scriven, L. E. (1988). Physics and applications of dip coating and spin coating. Mat Res Soc Symp Proc. C. J. Brinker, D. E. Clark and D. R. Ulrich, Materials Research Society. **121:** 717-729.

Shim, E. K., D. Barnette, et al. (2001). "Microdermabrasion: a clinical and histopathologic study." Dermatol Surg **27**(6): 524-530.

Shirkhanzadeh, M. (2005). "Microneedles coated with porous calcium phosphate ceramics: effective vehicles for transdermal delivery of solid trehalose." J Mater Sci Mater Med **16**(1): 37-45.

Simonsen, L., A. Kane, et al. (1999). "Unsafe injections in the developing world and transmission of bloodborne pathogens: a review." Bull World Health Organ **77**(10): 789-800.

Sintov, A. C., I. Krymberk, et al. (2003). "Radiofrequency-driven skin microchanneling as a new way for electrically assisted transdermal delivery of hydrophilic drugs." J Control Release **89**(2): 311-320.

Sivamani, R. K., B. Stoeber, et al. (2005). "Clinical microneedle injection of methyl nicotinate: stratum corneum penetration." Skin Res Technol **11**(2): 152-156.

Smart, W. H. and K. Subramanian (2000). "The use of silicon microfabrication technology in painless blood glucose monitoring." Diabetes Technol Ther **2**(4): 549-559.

Song, J. Y., H. A. Kang, et al. (2004). "Damage and recovery of skin barrier function after glycolic acid chemical peeling and crystal microdermabrasion." Dermatol Surg **30**(3): 390-394.

Spencer, J. M. (2005). "Microdermabrasion." Am J Clin Dermatol **6**(2): 89-92.

Stokes, R. J., D. F. Evans, et al. (1997). Liquid coating processes. Fundamentals of Interfacial Engineering. R. J. Stokes and D. F. Evans, Wiley-VCH**:** 399-456.

Tan, M. H., J. M. Spencer, et al. (2001). "The evaluation of aluminum oxide crystal microdermabrasion for photodamage." Dermatol Surg **27**(11): 943-949.

Tatsis, N., S. W. Lin, et al. (2007). "Multiple immunizations with adenovirus and MVA vectors improve CD8(+) T cell functionality and mucosal homing." Virology **doi:10.1016/j.virol.2007.05.028**.

Teo, M. A., C. Shearwood, et al. (2005). "In vitro and in vivo characterization of MEMS microneedles." Biomed Microdevices **7**(1): 47-52.

Titeux, M. and A. Hovnanian (2006). "Gene therapeutic strategies for blistering skin diseases." Drug Discovery Today: Therapeutic Strategies **3**(1): 87-92.

Tsuchiya, K., N. Nakanishi, et al. (2005). "Development of blood extraction system for health monitoring system." Biomed Microdevices **7**(4): 347-353.

Walsh, G. (2005). "Biopharmaceuticals: recent approvals and likely directions." Trends Biotechnol **23**(11): 553-558.

Wang, P. M., M. Cornwell, et al. (2006). "Precise microinjection into skin using hollow microneedles." J Invest Dermatol **126**(5): 1080-1087.

Weinstein, S. J. and K. J. Ruschak (2004). "Coating flows." Annu Rev Fluid Mech **36**(1): 29-53.

Widera, G., J. Johnson, et al. (2006). "Effect of delivery parameters on immunization to ovalbumin following intracutaneous administration by a coated microneedle array patch system." Vaccine **24**(10): 1653-1664.

Xie, Y., B. Xu, et al. (2005). "Controlled transdermal delivery of model drug compounds by MEMS microneedle array." Nanomedicine **1**(2): 184-190.

Yoshioka, S. and V. J. Stella (2002). Stability of Drugs and Dosage Forms. New York, Kluwer Academic Publishers.

Zahn, J. D., N. H. Talbot, et al. (2000). "Microfabricated polysilicon microneedles for minimally invasive biomedical devices." Biomed Microdevices **2**: 295-303

Zahn, J. D., D. Trebotich, et al. (2005). "Microdialysis microneedles for continuous medical monitoring." Biomed Microdevices **7**(1): 59-69.

Zhao, Q., C. Wang, et al. (2007). "Bacterial adhesion on the metal-polymer composite coatings." Int J Adhes Adhes **27**(2): 85-91.

# VITA

Harvinder Singh Gill was born in Chandigarh, India, in 1973. He attended the Panjab University in India from where he graduated with honors at the top of his class with a Bachelor of Engineering degree in Chemical Engineering in 1994. He was awarded a gold medal, two silver medals and a University medal for academic excellence during his undergraduate studies. From 1994-97 he worked as a professional plant operations and safety engineer at Engineers India Limited - one of Asia's leading engineering design and consulting firms; where he was primarily engaged with commissioning and start-up of petroleum refineries, and risk and hazard assessment of petroleum refineries and pipelines. From 1997-2001 he worked as an entrepreneur establishing a chemical plant in India. In 2001, he entered graduate school at Georgia Institute of Technology, Atlanta, GA, to pursue his doctorate in Bioengineering. He defended his doctoral thesis titled "Coated Microneedles and Microdermabrasion for Transdermal Delivery" on May 22, 2007. He was awarded his Ph.D. in Bioengineering with a minor in Immunology on August 4, 2007.